Regional mapping and frequency-magnitude analysis of debris avalanches and debris flows in Hordaland, Norway

Kamilla Skåre Sandboe

Master thesis in Geosciences GEO5960
Geohazards
60 credits

Department of Geosciences
The Faculty of Mathematics and Natural Sciences

UNIVERSITY OF OSLO

June 2019

2019

Regional mapping and frequency-magnitude analysis of debris avalanches and debris flows in Hordaland, Norway

Kamilla Skåre Sandboe

http://www.duo.uio.no/

Trykk: Reprosentralen, Universitetet i Oslo

Summary

With its large topographic differences and location at the west coast of Norway, Hordaland county is susceptible to weather-induced landslides such as debris flows and debris avalanches. The temporal and spatial occurrence of these landslides are predicted by the landslide warning system established by the Norwegian Water Resources and Energy Directorate (NVE). The warnings are disseminated to the public as text messages and in the form of four color-coded levels. Each level describes the number of landslides that are expected from a meteorological event within an area with a 10.000-15.000 km^2 extension.

However, the warnings do not include expected landslide size, except a general assumption as "large landslides that disturb infrastructure and roads may occur" for the orange level 3. The observations, however, show that the same warning level might cause several smaller slides instead, causing widespread damage. Although the Norwegian landslide database (NLDB) is quite extensive and with a large number of historical and recent landslides recorded the information of landslide magnitude is lacking. This is a consequence of a lack of systematic mapping of landslides in Norway.

This study aimed to prepare event-inventory maps for rain- and snowmelt episodes, that have triggered landslides in the Hordaland county in the period 2011-2017 by controlling the quality of landslides registered in the database, mapping their extension and by performing frequency-magnitude (FM) analyses, resulting in FM-curves. A list of 20 weather events that caused landslides were prepared, and six weather events were investigated further. 78 of 205 landslides caused by these weather events were then mapped with polygons in ArcMap. The mapping was conducted using different sources of information like aerial photos, lidar imagery, photos, and written descriptions. Frequency-magnitude curves were prepared for the different event-inventories, resulting in a cumulative distribution with a power-law relationship and rollover point. The mapped landslides in Hordaland varied greatly, between 206 m^2 to 140.359 m^2, with most confirmed landslides between 4600 m^2 and 56000 m^2. A threshold analysis was also performed and confirmed that the thresholds did not perform well during the weather events. Results from the adjacent county Sogn og Fjordane were also compared, due to their proximity and similarities in weather and topography.

This thesis is part of a project by the Norwegian scientific community that aims to improve the quality of the landslide database and improve the thresholds used in the warning system.

Prologue

This thesis is part of an internal project at NVE lead by senior geologist Graziella Devoli, with work done by MSc students and summer students. The project has the aim of improving the quality of the landslide database to improve the landslide thresholds used in Norway. It was introduced to me through conversations with Graziella Devoli and piqued my interest due to my interest in landslides and the landslide warning system at NVE. Karianne Staalesen Lilleøren also joined as a supervisor for the project.

I want to give a big thank you to both of my supervisors Graziella Devoli and Karianne Staalesen Lilleøren. Thank you, Graziella for the idea for the thesis, and the guidance, ideas, and feedback during the work. Thank you to Karianne for your help with using GIS, understanding the results I got, and the encouragement and honest feedback during the past year. Thank you both for motivating me to attend both the "Geofaredagen" conference in Lillestrøm and the "EGU" conference in Vienna to present my thesis. They were both great experiences I am happy to have.

I also want to thank Michel Heeremans for his help with accessing and use of data needed for the work. A big thank you as well to Søren Boje at NVE for excellent assistance with data for the threshold analysis, and informative conversations about the thresholds used in Norway. Thank you to Jess Joar Andersen as well, for quick and helpful access to the data. And finally, thank you to my parents for help and encouragement during the past year and their understanding of my constant preoccupation.

Kamilla Skåre Sandboe

Table of contents

1 Introduction

1.1 Background

Climate change with increased temperatures and more intense rainfall is expected to increase, also in countries like Norway, where the frequency of weather-induced landslides is expected to be higher in the future (Schwarze et al., 2018). Based on a hundred years of statistical data, the Geoextreme project found that Norway can expect a landslide event with every 5-10-year interval killing 20-100 people (Amundsen, 2009). Mountains cover about 30% of the country, and 6,7% of the country has a slope angle above 30 degrees (Jaedicke et al., 2009), especially along the western coastline where the study area of Hordaland county is located. The western coastline experiences high amounts of precipitation along the west side of the Scandinavian mountain chain (Jaedicke et al., 2009). Landslides in Norway are often triggered by extreme weather events (EWEs) (Gregersen and Sandersen, 1989; Furseth, 2006). The amount of precipitation falling on either one or several days is, according to Førland et al. (2007) an important factor in triggering of landslides in Norway. Particularly strong storms with heavy precipitation as rain and snowfall initiate landslides and snow avalanches frequently (Sandersen et al., 1996). Due to the marine climate along the west coast, most landslides occur during fall and winter as a result of large amounts of precipitation.

In the last 150 years, around 125 people have been killed in debris avalanches, and debris flows in Norway (Solheim, 2017). Recent analysis has revisited the number of fatalities caused by landslides, in the period 1995-2019 (Schwarze et al., 2018; Haque et al., 2019). This currently shows that 42 fatalities, caused by in particular rock falls and landslides in soil, occurred in 10 different counties between 1995-2019 and 25 of these fatalities were caused by weather-induced landslides. Every year the Norwegian highways are hit by about 200 landslides in soil, and the railways by about 30 debris avalanches, debris flows, and slush flows (Hisdal et al., 2017). These types of landslides also cause major difficulties with accessibility and emergency response on road and railway. Insurance payments provide a certain estimate of economic losses but do not include costs associated with public infrastructure (Myrabø et al., 2016). The project "InfraRisk" was conducted between 2010 and 2013 to investigate the impacts of extreme weather events on infrastructure in Norway (Frauenfelder et al., 2013). The project found that landslides in Norway cost at least 100 million kroners yearly, and one fourth if these occur in

Hordaland county. Landslides can cause both economic loss and loss of human life, in addition to human health issues, social issues, environmental issues, and more (Morss et al., 2011). As rainfall events are getting more frequent and intense, the need for an early warning system increases (Jakob et al., 2012).

Due to urbanization, more people are put at risk moving into hazardous areas (Jakob et al., 2012; Smith, 2013; Piciullo et al., 2018). In many areas with older developments, no hazards assessment was done before settlement, and avoiding the hazard is no longer an option (Jakob et al., 2012). In Norway, after several landslides, like the "Hatlestad slide" in Hordaland in 2005, a new risk and vulnerability analysis (ROS) was put in place in 2011 (DSB, 2014). Every county was required to perform this, to reduce the risk and vulnerability to the population. This was not done yet when a landslide hit a house on Osterøy in Hordaland in 2017, and a woman was killed. The landslide is assumed to have been caused by a combination of the slope angle, precipitation, and human factors. After the landslide, the area was investigated, and ten properties were found to be exposed to landslides, and in addition, six more properties also needed mitigation measures in place.

A way to protect both older and new settlements is by better land-use planning to avoid building in high hazard areas. In order to do this, susceptibility maps[1] and hazard maps[2] are necessary, and a risk analysis must be performed. If the risk is high, mitigation measures must be put in place to reduce losses. Apart from land-use planning, physical mitigation measures like barriers, drainage or levees can be used to deflect or stop a landslide, or an early warning system that allows the evacuation of people from high-risk areas before the event (Morss et al., 2011).

According to UNISDR (2009) the definition of an early warning system (EWS) is "the set of capacities needed to generate and disseminate timely and meaningful warning information to enable individuals, communities and organizations threatened by a hazard to prepare and to act appropriately and in sufficient time to reduce the possibility of harm or loss". An EWS is a cost-effective measure, compared to physical measures (Glade and Nadim, 2013; Piciullo et al., 2018). In some cases, it is also the only suitable option. In Norway physical mitigation measures have been deemed both impossible and too costly to protect all hazardous areas due to climate

[1] A susceptibility map shows potential initiation areas and runout areas for landslides, with their likelihood of occurrence (Bargel et al., 2011).
[2] A hazard map combines the susceptibility map with the magnitude of the potential landslide (Corominas et al., 2013).

and topography, making an EWS a much better solution to reduce consequences of landslide events (Hisdal et al., 2017; Krøgli et al., 2018). The Norwegian landslide forecasting and warning service (NLFWS) was established to provide a prediction of future landslide events, and to give helpful advice to local authorities, making them take action in an appropriate time. Actions can be: to inform their population, closing roads, evacuation, and other measures necessary to keep the population safe. The NLFWS has been operating since 2013 at the Norwegian Water and Energy Directorate (NVE).

1.2 Motivation for the thesis

This thesis aims to improve the quality of historical landslide data, in terms of spatial and temporal distribution, that are used to improve the landslide thresholds in the warning system. The thesis is part of an internal project at NVE realized through a series of work done by other MSc students (Bugge, 2016; Mongstad, 2018).

There is a lack of systematical mapping of landslides in Norway. Systematic mapping of landslides is crucial to create a database for statistical and spatial analysis. The collection of data in Norway is biased, as most landslide events are reported along roads or near population and infrastructure (Jaedicke et al., 2009). The project "InfraRisk" concluded that the national landslide database is a useful tool for analyses of landslide risk, but needs improvement by also including landslides not resulting in damages (Frauenfelder et al., 2013). A lack in the mapping causes a low basis for a good analysis, as the effectiveness of the threshold model depends on the test site characteristics, meaning the quality and quantity of data (Lagomarsino et al., 2015). Several studies have shown that having an increased landslide sample might lead to an improvement in the performance of a warning system (Lagomarsino et al., 2013; Gariano et al., 2015; Rosi et al., 2015). The correctness of the landslide database is also crucial for a correct analysis, and evaluating this is also important when using the database. Performing a quality control, by correcting wrong input like location, landslide type and time of occurrence, and removing double registrations is necessary before any analysis is performed (Guzzetti et al., 2012; Krøgli et al., 2018).

The Norwegian forecasting and warning service uses hydrometeorological thresholds to predict weather-induced landslides (Colleuille et al., 2017) and aims always to improve its models and

warnings (Boje et al., 2014). The hydrometeorological threshold values used in Norway have been adjusted for different regions (Boje, 2017). The warning is in constant evaluations. Even with continuous evaluations and tests, the system can always be improved. One way of achieving this is to include the magnitude (area or volume of a landslide) of the landslide event expected. Currently, the landslide warning includes the expected number of landslides resulting from a weather event, but it does not include the expected size of the landslides. Including the size of the expected event in landslide hazard assessment is a common international approach (Guthrie and Evans, 2004; Hungr et al., 2008; Dahl et al., 2013), and results in producing a frequency-magnitude curve. The curve will provide the system with the expected magnitude, which will give a clearer picture of the expected damage from the event. A large landslide will potentially cause much greater damage than a smaller landslide. In addition to the importance of providing the correct warning about a future landslide event, it is also of great importance that the population have trust in the system (Maskrey, 1997; Bazin, 2012; Michoud et al., 2013; Thiebes and Glade, 2016). A warning system must lead to proper action, or it is useless (Maskrey, 1997; Thiebes and Glade, 2016; Hisdal et al., 2017; Piciullo et al., 2018). Continuously correcting thresholds, improving the system, and communicating well with the population is therefore also very important for the effectiveness of the system.

1.3 Objectives

The general objective of this thesis is to map and analyze the occurrence of weather-induced landslides in Hordaland between 2011 and 2017. By performing a quality control and characterizing landslide parameters of events recorded in the national mass movement database, this thesis will result in a new, improved dataset of mapped landslides. The new dataset will put the magnitude of the landslides in the context with the warning levels disseminated, to enable a more precise warning in the region, and further on a national level. To achieve the general objective, the following specific objectives are considered.

- **Rainfall analysis.** Identifying rainfall events that triggered landslides in the study area and during the period of interest and analyze their temporal occurrence. Considering the expected increase of extreme meteorological events in the future, an analysis of extreme events was considered interesting to perform. As an extreme event can cause damages

to infrastructure, and put human life at risk, it is important to perform a landslide hazard assessment and issue a proper warning to the public to avoid serious consequences.

- **Mapping landslides**. Performing a rainfall analysis will identify weather events resulting in many landslides. These landslides can then be mapped, finding their spatial occurrence and magnitudes. By performing a quality control of the available data, a new, improved dataset will be made, resulting in an event inventory for the rainfall events. The landslides in the new dataset will be characterized in terms of their geological and topographical features.

- **Frequency-magnitude analysis.** A frequency-magnitude analysis will show the typical magnitude of the landslides caused by extreme events, and their relationship to the frequency. This relationship can help to locate areas exposed to landslides and further assess their vulnerability (Flentje et al., 2011; Corominas et al., 2013). A frequency-magnitude curve will, therefore, be prepared for Hordaland county.

- **Threshold analysis.** A threshold analysis will show how the landslides are placed according to the warning levels disseminated by the NVE, and if this is within the expected level. Regions in different parts of the country may have quite different threshold limits. It is therefore important to look at specific areas to get a proper warning level for the area in question.

- **Comparison of results.** Finally, the results from the frequency-magnitude analysis and threshold analysis will be compared to results from previous work in the adjacent county Sogn og Fjordane (Mongstad, 2018). As the counties are both situated at the west coast experiencing similar weather and topographical conditions, similarities and differences between the counties are of interest.

- **Evaluate disseminated warnings.** As the western coastline is highly susceptible to weather-induced landslides, it poses a great risk to the population to issue an incorrect warning. The warnings disseminated during the period of interest will, therefore, be analyzed to show if the warnings were correct or not.

2 Theory

2.1 Landslides

The term “landslide” is generic, having variable classification schemes over the last decades (Calvello, 2017). Landslides can be characterized in different ways. The most frequently used are triggering causes, material type[3], and kinematics[4]. The scheme proposed by Varnes (1978) is the most widely adopted classification worldwide. This scheme was further developed in the classification by Cruden and Varnes (1996). Hungr et al. (2001) combined the systems from Varnes (1978) and Hutchinson (1988) in an attempt to correlate the systems. A more recent contribution is the Hungr et al. (2014) classification, where the Varnes (1978) classification was revised, resulting in 32 landslide types, each with a formal definition.

2.1.1 Classification based on triggering causes and kinematics

Landslides can be classified based on the triggering mechanisms, which are an external stimulus causing an immediate response (Bazin, 2012). The main trigger of landslides is heavy or prolonged rainfall, such as an intense storm or long duration rainfall with lower intensity, or both (Johnson and Sitar, 1989; Cruden and Varnes, 1996; Hungr et al., 2001; Highland and Bobrowsky, 2008; Guzzetti et al., 2007b; Bazin, 2012; Corominas et al., 2013). Other natural triggering causes are earthquakes and volcanic processes. Some landslide debris slides, debris flows, debris avalanches can also be triggered by the sudden load from an impact of a rock fall or rock slide (Lacerda, 2007; Hungr et al., 2014). Different forms of human activities can also trigger landslides, like road cutting, head loading, changes of the water table or removal of vegetation (Smith, 2013). Any progress that disturbs vegetation can lead to lower root strength, leading to a more susceptible slope (Jakob et al., 2012).

Rainfall, or other increase of water content, causes a reduction in material strength because the water percolating into the soil increases the pore water pressure. Due to this increase, the shear

[3] Material types are split into two main types; rock and soil, soil being further divided into debris and earth, based on particle size. Rock is defined as a “hard or firm mass that was in its natural place before movement”, and soil as “an aggregate of solid particles” that was either transported or formed by weathering of rocks at the location. Debris is coarser than earth, with 20-80% of the particles being larger than 2mm. Earth has 80% or more fine particles smaller than 2mm (Cruden and Varnes, 1996).

[4] Kinematics, or movement classes, are fall, topple, slide, spread and flow (Cruden and Varnes, 1996).

stress exceeds the shear strength of the material (Smith, 2013). During an intense rainstorm, the water infiltrates the soil quickly, causing a rapid increase in pore water pressure. The triggering can also be influenced by antecedent rainfall, which is rainfall occurring in the period before the rainfall event that initiated the landslide. Though many studies agree on the significance of antecedent conditions (Wieczorek and Glade, 2005), different studies have different opinions on how long this period should be, ranging from days to months (Guzzetti et al., 2007a). If the soil is already saturated from antecedent rainfall, the following rainfall event needs less intensity to initiate a landslide. The antecedent moisture content in the soil determines how much water is needed before landslide initiation (Johnson and Sitar, 1989).

"Weather-induced landslides" are landslides initiated by rainfall and/or snowmelt, and they are sometimes divided into "rainfall-induced" and "snowmelt-induced" landslides depending on the triggering factor (Devoli et al., 2018). Sometimes landslides are triggered by a combination of both. Based on kinematics, these landslides are usually slide- or flow-type, following the classification of Hungr et al. (2014), like soil- and debris slides, debris flows, and debris avalanches (fact boxes).

A slide (figure 2.1A) is defined as material that fails from a more stable underlying material, along a distinct zone of weakness (Varnes, 1978). The material is either soil or rock mass (Cruden and Varnes, 1996). The movement does not start over the entire slide area but starts locally and spreads as the failure occurs (Cruden and Varnes, 1996). Slides can be separated into rotational and translational slides depending on the shape of the surface the mass moves on. Rotational slides move along a curved and concave surface of rupture and might have little internal deformation (Cruden and Varnes, 1996). These occur mostly in homogeneous materials. Translational slides, however, move along a planar surface of rupture, and the displaced mass may break up, especially if there is an increase in velocity or water content.
A flow is a spatially continuous movement, and the surfaces of shear are short-lived, closely spaced and usually not preserved (Cruden and Varnes, 1996). The distributions of velocities in the displaced mass are similar to a viscous liquid. There is often a gradation of change from slides to flows, which depends on water content, mobility and the evolution of the movement (Highland and Bobrowsky, 2008). Flows can be divided into several types, among them debris flows and debris avalanches.

Debris flows are usually triggered by heavy precipitation and snowmelt, eroding the material on steep slopes making all the three requirements available for the slide to occur. The increase of water content saturates the soil and increases the pore pressure, decreasing the shear strength holding it in place (Meyer et al., 2012). According to Meyer et al. (2012), nearly all debris flows are triggered by hydrometeorological events, such as storms or prolonged rainfall or snowmelt, which is also the most common trigger in Norway (Sandersen et al., 1996; Nadim et al., 2009). Sandersen et al. (1996) presented three major weather patterns which trigger debris flows;

intense snowmelt in the spring typically lasting one week, heavy rainfall in one day with a 1-4 hour concentration, and rainfall combined with snowmelt for typically 3-7 days. The two latter weather patterns are common landslide triggers on the west coast. The NPRA reported that one-third of all mass movements registered lead to partly or fully closed roads, among all these the debris flows were the largest culprit of damages on the roads (25%) (Meyer et al., 2012).

Snowmelt can also contribute to landslide initiation, especially in mountain areas. A sudden increase in temperature can lead to rapid melting of the snowpack, increasing the soil pore pressure in the ground below (Highland and Bobrowsky, 2008; Bazin, 2012). In combination with precipitation, this process is enhanced, and also accelerate thawing. A landslide can also be triggered by erosion by a river, especially during a flood. Stability is reduced due to undercutting and excavation because the gradient of the slope is increased and the weighting is removed. Debris flows can initiate in this way, by surface erosion in a channel (Bazin, 2012).

A debris flow (figure 2.1B) is defined as a "form of rapid mass movement in which a combination of loose soil, rock, organic matter, and water mobilize as a slurry that flows downslope" (Innes, 1983; Hungr et al., 2008). They are confined to channels where there is not usually a permanent water flow (Øydvin et al., 2011). They have three basic requirements; steep slopes, the availability of unconsolidated sediments and loose material, and a high supply of water (Innes, 1983). The material is deposited along the edge of the path as levees and sorted in a fan shape at the deposit. Coarse material will deposit first, and finer material will move further (Øydvin et al., 2011). They usually initiate in slopes above 25º (Innes, 1983; Hungr et al., 2008), and the typical slope angles found in Norway is 25º-45º (Devoli, 2017), but in debris flows following rivers and creeks this angle can be down to 10º (Schanche, 2014). Runout distances in Norway can be up to 500 meters -1 kilometer as they do not stop until the slope gradient is close to zero (Devoli, 2017). They are considered the most hazardous landslide type due to their long travel distances, the difficulty of forecasting time and location, and frequent occurrence in mountainous terrain Jakob et al. (2012). However, a travel distance above 3000 meters is unlikely (Hungr et al., 2008).

A debris avalanche (figure 2.1C) is a very to an extremely rapid shallow flow consisting partially or fully saturated debris moving down a steep slope (Hungr et al., 2001). A debris avalanche can, in contrast to debris flows, occur anywhere in an open slope as a unique event due to the removal of the material (Hungr et al., 2001; Hungr et al., 2014), making their exact location harder to predict. The rapid undrained loading continues as the material moves down the slope, entraining material on the way down, which causes initially small debris slides to evolve into large debris avalanches (Hungr et al., 2014). During this process, the path widens downslope, giving a characteristic triangle shape (Sandøy et al., 2017). Debris avalanches can also enter established channels and become debris flows. Debris avalanches in Norway usually initiate at slope angles above 25º-30º (Schanche, 2014). Their runout distances are shorter than debris flows, usually less than 500 meters. Debris avalanches with a high volume or high amount of water may reach longer distances, closer to 1 kilometer (Devoli, 2017).

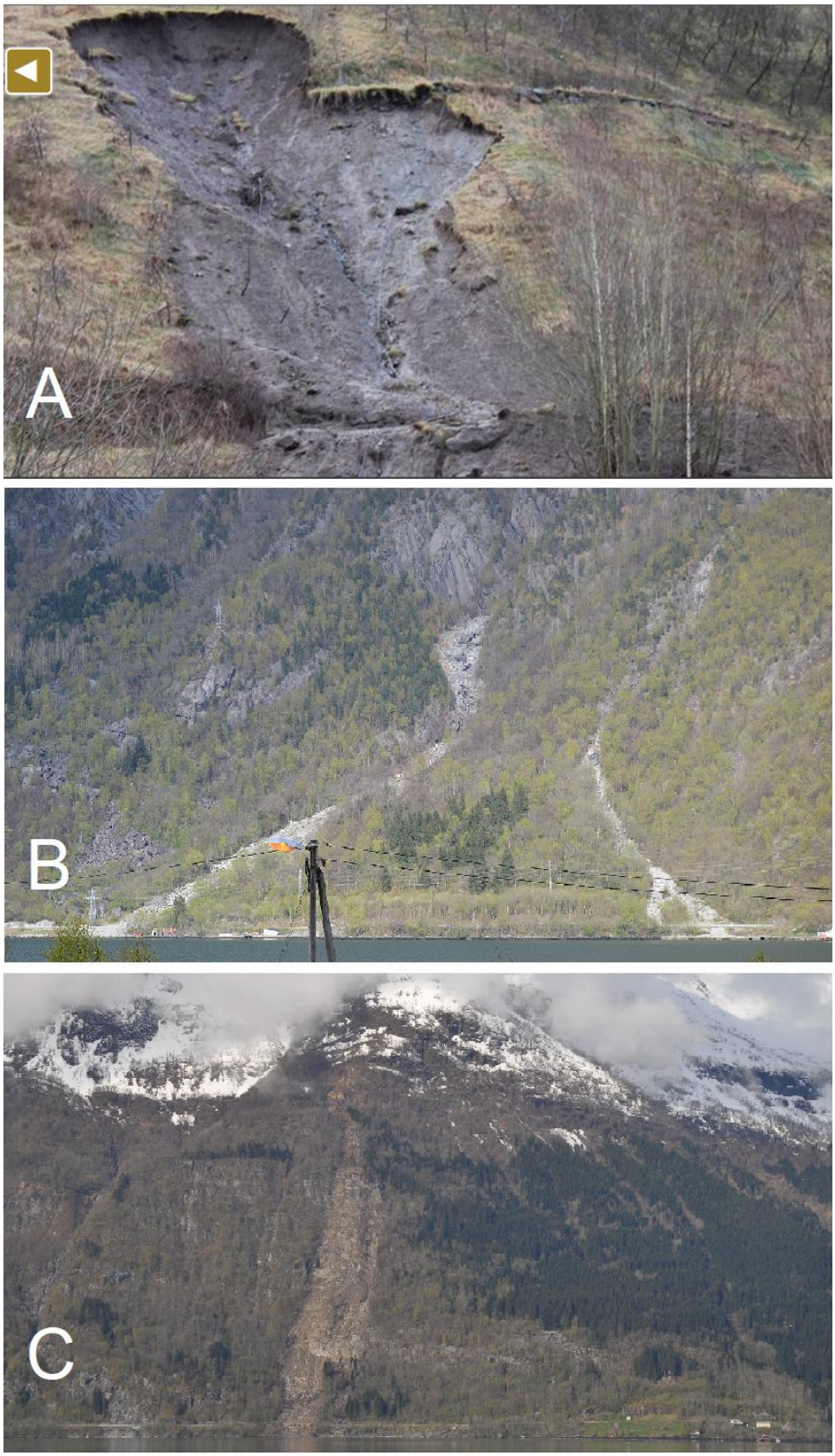

*Figure 2.1: Examples of weather-induced landslides in Hordaland. (**A**) Debris slide (Source: Bergens tidende), (**B**) two debris flows (Source: Odd-Arne Mikkelsen/NVE) and (**C**) a debris avalanche (Source: Aart Verhage/NVE) that all occurred during the storm "Dagmar" in December 2011.*

2.2 Assessment of landslide hazard

Landslides are natural processes, but when they occur close to buildings and infrastructure, they become a hazard with a potential of causing harm (Smith, 2013). A landslide hazard is, according to Corominas et al. (2013) characterized by its occurrence and intensity, and the intensity express the severity of the landslide hazard (Corominas et al., 2013). To assess the landslide hazard, the spatial and temporal probability of occurrence needs to be determined (Corominas et al., 2013), by the use of different maps, and the analysis of triggering frequency. To perform a good hazard assessment, and define the risk[5] in an area, these maps need to be of good quality.

Landslide zoning is, according to Corominas et al. (2013), dividing the land into homogeneous areas or domains and rank them based on their degree of potential or actual landslide susceptibility, hazard, or risk. To perform a landslide zoning, different maps can be prepared, as inventory maps, susceptibility zoning maps, hazard zoning maps, and risk zoning maps. To produce maps predicting hazard or risk in an area, a landslide inventory map needs to be complete with spatial and temporal frequencies (Corominas et al., 2013). A GIS (Geographical Information System) is often used in the production of these maps, as it allows the information to be separated into different layers while maintaining the geometrical consistency (Guzzetti et al., 2012).

An inventory map shows the extent of a landslide phenomenon in a region and includes information that can be used in analyses of landslide susceptibility, hazard, vulnerability[6] and risk (Guzzetti et al., 2012). This information can be shown in points, lines, or polygons, are given attributes to describe landslide typology, age, activity, estimated depth, or mapping certainty. The quality of the inventory depends on two things. Firstly, the accuracy, which further depends both on the completeness and correctness of the map. Secondly, it depends on the type and the certainty of the information on the map (Guzzetti et al., 2012).

A landslide susceptibility map shows potential initiation areas and runout areas for different kinds of landslides, based on topographic parameters and hydrological models (Bargel et al.,

[5] Risk is defined as the probability of an event multiplied by the consequences (Corominas et al., 2013), the latter being a combination of the element at risk and the vulnerability (Smith, 2013).
[6] Vulnerability can be defined as the degree of loss of an element in an area affected by a landslide hazard and can be divided into physical vulnerability and vulnerability of people (Smith, 2013; Corominas et al., 2013).

2011). The map subdivides an area into zones that show the different likelihoods that landslides of a certain type may occur (Corominas et al., 2013). It contains both information about the type of landslide and the spatial probability in terms of most likely initiation area and possible extension (Corominas et al., 2013). The susceptibility maps assume that areas and terrains that have experienced landslides in the past will also experience landslides in the future. It is therefore important that the analysis is based on an inventory map that is as complete and correct as possible both in time and space (Corominas et al., 2013). Susceptibility maps available for Hordaland are described further in chapter 3.4.

Landslide hazard maps include the spatial and temporal information of the susceptibility maps, along with the mode of propagation, size, and intensity. For this, the magnitude of a landslide, usually expressed as area or volume, is necessary for hazard assessment, (Corominas et al., 2013). Landslide risk maps include the losses that might be expected from a certain landslide type within a certain period. The landslide risk can be expressed either as expected losses in an area by a specific magnitude in a given year, recurrence interval for the losses of for example an area hit by a 100-year event, or the cumulative losses during a given time interval (Corominas et al., 2013).

2.2.1 Frequency-magnitude

According to Corominas and Moya (2008), two different approaches are used to assess a future occurrence of landslides. The first method is an analysis of slope failure, considering the present conditions of the slope (Corominas and Moya, 2008), which evaluates the potential of the instability of slopes and existing landslides. This method can be achieved by either stability analysis and numerical modeling, formal probability and reliability analyses, and event tree methods (Corominas and Moya, 2008). However, this only shows the potential initiation area and not the deposition or track of the landslide. The second method is a statistical analysis of the frequency of past landslides, using this to find the probability for future landslides (Corominas and Moya, 2008). This method assumes that landslides are recurrent events, and uses landslide inventories to perform a frequency-magnitude analysis, establishing a power-law used to predict future landslides (Hungr et al., 2008; Dahl et al., 2013). In order for a hazard or risk analysis to result in a reliable map, the landslide inventory used needs to be as complete as possible, both in space and time (Corominas et al., 2013).

Established frequency-magnitude relationships can be of great help with finding the location of exposed areas and their vulnerability to a landslide hazard (Flentje et al., 2011; Corominas et al., 2013). Frequency-magnitude curves have become a fundamental step in quantitative hazard assessment, due to the spatially distributed nature of the frequency of landslides (Hungr et al., 2008; Corominas and Moya, 2008). Using the relationship between magnitude and frequency, an area might be classified with a more accurate hazard level not only based on frequency alone. A frequency-magnitude analysis will provide a summary of the number and magnitudes of landslides, which have occurred in a specific area in a specific period (Brardinoni and Church, 2004). This analysis will give a typical landslide magnitude, or range of magnitudes, that is most frequent in that specific area. The relationship found cannot however be directly applied for other regions with differences in size and relief, as it will under- or overestimate the magnitudes due to these being influenced by the local scale of the slope (Hungr et al., 2008).

Several definitions have been used in terms of defining the magnitude, such as scar area, total area, or volume (Brardinoni and Church, 2004). Regardless of the chosen type of magnitude when performing a frequency-magnitude analysis, the resulting logarithmic frequency-magnitude plot appears to have a linear power-law relationship (Brardinoni and Church, 2004; Hungr et al., 2008; Dahl et al., 2013; Corominas et al., 2013). At lower magnitudes, this linear relationship is no longer valid, as the curve flattens at a point called the "roll-over" (Guthrie and Evans, 2004; Dahl et al., 2013). This rollover point has been found in several studies, including in British Colombia (Guthrie and Evans, 2004) and the northern Faroe Islands (Dahl et al., 2013) shown in figure 2.2.

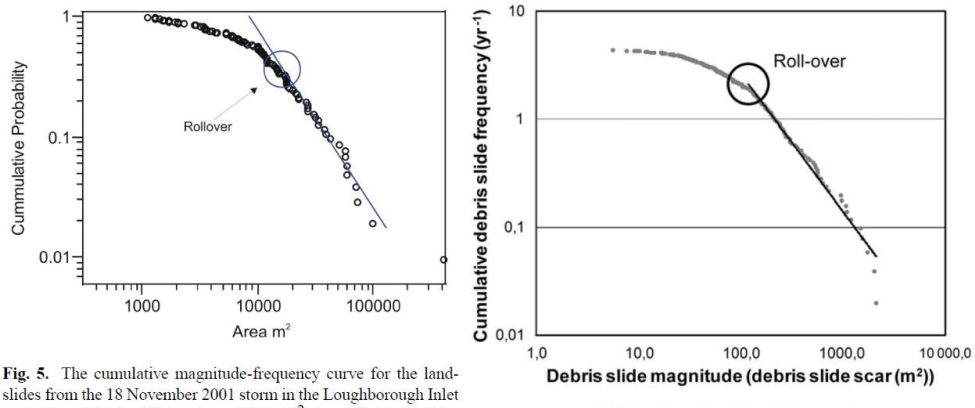

Fig. 5. The cumulative magnitude-frequency curve for the landslides from the 18 November 2001 storm in the Loughborough Inlet study area. The landslides above 10 000 m^2 are well described by a power law with a slope of about −1.24. Several curves would fit the remainder of the data.

Fig. 4. MCF relationship of the 219 debris-slides.

*Figure 2.2: Examples of the roll-over point in cumulative frequency-magnitude curves. **Left**: Frequency-magnitude curve with power-law relationship and roll-over point from British Colombia by Guthrie and Evans (2004). **Right**: Frequency-magnitude curve with power-law relationship and roll-over point from the northern Faroe Islands by Dahl et al. (2013).*

There are several possible reasons for the roll-over point suggested both geomorphological explanations and explanations related to the collection of data during the mapping. Two possible explanations were proposed by Pelletier et al. (1997), one being the role of gullying associated with stream and river networks influencing climatically induced landslides. The other possible explanation was the difference in failure criteria of smaller and larger landslides, larger landslides being more controlled by the force of friction, and smaller landslides being more controlled by the cohesion in the material. Due to this cohesion in the shallow smaller landslides, the occurrence of these will be prevented (Guzzetti et al., 2002). The third possible reason for the lower frequencies for the magnitudes below the roll-over point is the lack of registration of the smaller events (Corominas and Moya, 2008). There can be several reasons for this to occur, and this lack of mapping of smaller landslides is used as a possible explanation in several studies (Stark and Hovius, 2001; Brardinoni and Church, 2004). A problem with using aerial photos to map landslides of variable magnitudes is that the smaller landslides might be hidden below the vegetation (Brardinoni and Church, 2004). This leads to an underestimation of landslides of smaller size, creating an error in the database further used in the analysis. Both Brardinoni and Church (2004) and Stark and Hovius (2001) determined that the reason for the deviation from the power-law was due to the limitations of the resolution of aerial photos. Another problem related to mapping is the cleanup by rescue or repair workers and the quick erosion of smaller landslide deposits, both leading to a short life span. With aerial photos taken long after the event, the traces of the smaller landslides might be long gone (Corominas and Moya, 2008). Different studies have come to different conclusions of the reasons for the roll-over point. The physical explanations have been accepted by several studies, including Guthrie and Evans (2004) and Dahl et al. (2013). Other studies determine the cause to be the problems surrounding aerial photos (Stark and Hovius, 2001), while some studies find both types of issues as a combined reason for the roll-over point (Guzzetti et al., 2002; Brardinoni and Church, 2004).

2.2.2 Landslides in a changing climate

The stability of slopes is influenced by different factors, like precipitation, snow melting, temperature changes, among others (Gariano and Guzzetti, 2016). Climate change may alter some of these factors, influencing slope stability (Seneviratne et al., 2012). Stoffel et al. (2014) investigated the frequency, magnitude, and seasonal variations in shallow landslides in the

Alps, the latter possibly revealing how a changing climate may influence landslides. The changes were observed to be impacted by a change in seasonal precipitation distribution and a decrease in snowpack depth and duration. Crozier (2010) and others found that climate changes affect stable slopes and unstable slopes differently. For stable slopes, the preparatory factors may be influenced by climate changes, like antecedent rainfall, weathering, land cover, forestation, and deforestation, making the slope less stable. For slopes that are already less stable, the triggers for landslides are the ones that are affected by climate change, like precipitation, water table rise, and temperature-induced fractures (Crozier, 2010). Different landslide types also react differently to rainfall. While the total precipitation seems to influence mostly rock slides, mudflows and earthflows, the intensity of rainfall influence rock falls, debris flows, and debris avalanches (Gariano and Guzzetti, 2016). An increase in total precipitation will lead to wetter antecedent conditions, which will affect slope instability in several ways. Not only will wetter conditions reduce the necessary precipitation to reach the threshold for slope failure, but it will also contribute to a reduction of shear strength, soil suction, and cohesion, and an increase in the weight of the material on the slope (Tacher and Bonnard, 2007).

According to Hov et al. (2013), studies suggest higher precipitation for Northern Europe, and in the next 70 years, both high intensity and extreme precipitation are expected to become more frequent. There is also an expected change in the seasonality and structure of precipitation. The precipitation in Northern Europe depends largely on moisture transported along the storm track over the Atlantic Ocean, compared to Southern Europe. These occur most frequently in winter months and are accompanied by wind (Hov et al., 2013). An increase in both count and lifespan of storms during winter and autumn in Northern Europe was found by Wang et al. (2012). This was consistent with reported changes in precipitation frequency, intensity, and duration (Hov et al., 2013). Climate models indicate a decrease in the total number of cyclones, but an increase in the number of severe storms in Northwestern and Central Europe. The Cyclones are, however, expected to have a higher intensity, with increased wind speeds (Hov et al., 2013).

2.2.3 Thresholds

A threshold was defined by White et al. (1996) to be “the minimum or maximum level of some quantity needed for a process to take place or a state to change.” The minimum threshold defines when landslides are unlikely to occur (Guzzetti et al., 2007a; Baum and Godt, 2009), and the

maximum threshold defines when landslides almost always occur (Guzzetti et al., 2007a). Lagomarsino et al. (2015) define two kinds of thresholds. The first is the "minimum threshold", which is a lower threshold based on past data. Any conditions surpassing this threshold is expected to result in landslides. The second kind of threshold defined in Lagomarsino et al. (2015), is the "early warning threshold". This threshold attempts to find a compromise between two scenarios. One side is the effectiveness in recognizing triggering conditions, in which a low threshold would have good results. The other side is the effectiveness of committing a low number of false alarms, in which a high threshold would have good results (Segoni et al., 2014; Staley et al., 2012). The early warning threshold will then have to be placed somewhere in between, so both missed alarms and false alarms are avoided at best effort (Lagomarsino et al., 2015). An illustration of these two types of thresholds is proposed in figure 2.3. Both of these lead to distrust in the system, especially if recurring (Staley et al., 2012). Guzzetti et al. (2007a) describe several categories of thresholds, grouped in physical and empirical models. The thresholds are divided into categories based on the different goals of use, size of the study area, and choice of data used for the decision for the threshold. One of the most commonly used empirical thresholds is the intensity-duration (ID) thresholds (Guzzetti et al., 2007b; Piciullo et al., 2018; Segoni et al., 2018). The first ID-threshold was established by Caine (1980), using worldwide data to plot intensity (mm/hour) against duration (hours). Several works have observed that wetter regions have a higher intensity-duration threshold for initiation of landslides (Innes, 1983; Guzzetti et al., 2007a; Nadim et al., 2009), and that this shows an adjustment of the slopes according to the common rainfall regime (Sandersen et al., 1996; Wilson and Jayco, 1997; Nadim et al., 2009).

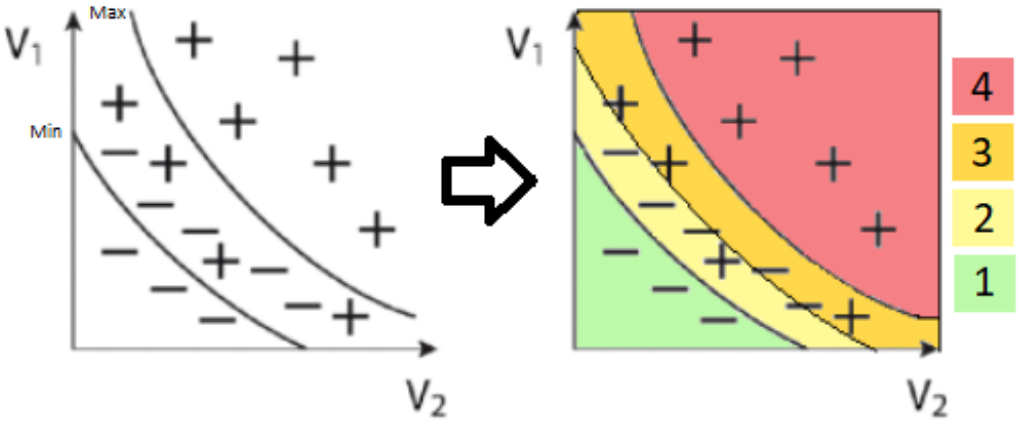

Figure 2.3: Illustration showing the classical threshold and the early warning threshold. Inspired by Cepeda and Devoli (2008).

Three different thresholds have been proposed in Norway (figure 2.4), two of them based on the ID-threshold established by Caine (1980). The first was proposed Sandersen et al. (1996), establishing a threshold using critical water supply (P) expressed as a percentage of mean annual precipitation, instead of intensity. The threshold was based on 30 debris flow events. This threshold takes snowmelt into account, as the water supply in Norway has two main sources; rainfall and snowmelt. The second threshold based on the ID-relationship was established by Meyer et al. (2012), and used 502 debris flows with daily meteorological information available. Approximately at the same time as Meyer et al. (2012) worked with the ID-threshold, Colleuille et al. (2010) worked on another type of threshold. This threshold was found combining available interpolated hydrometeorological parameters from the HBV-model, and 206 landslide events in southern Norway. The threshold performed best with a combination of the parameters relative water supply and relative soil water saturation (Boje et al., 2014).

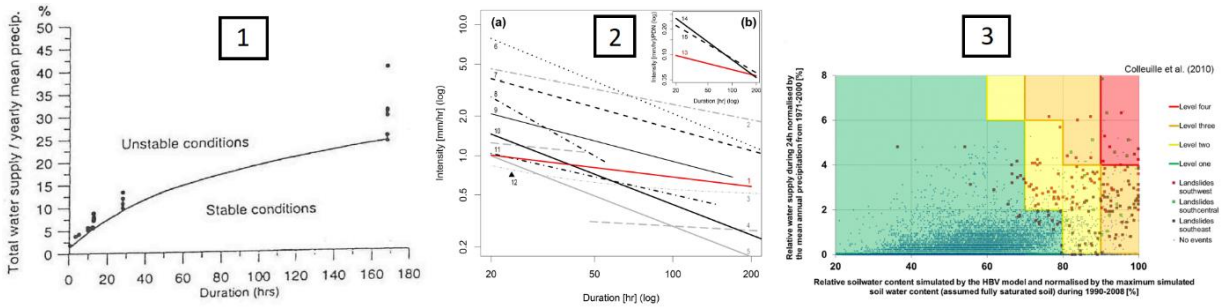

*Figure 2.4: The three thresholds attempted in Norway. **1**: The PD-threshold from Sandersen et al. (1996). **2**: The ID-threshold from Meyer et al. (2012). **3**: The threshold from Colleuille et al. (2010),*

2.3 Landslide Early Warning Service

Hazard mitigation can be done in several ways depending on the landslide types, by using structural and non-structural measures (Morss et al., 2011). Structural protective measures can be a deflecting wall, gallery/shed (Frauenfelder et al., 2013), drainage to remove water from the slope, plant vegetation to provide stability in the soil (Smith, 2013). Non-structural mitigation is also useful, like land-use planning to protect existing communities and steer new developments away from dangerous areas (Smith, 2013). However, since it is not possible to avoid all extreme events and their impacts, early warning systems are useful to detect the event in a timely fashion so the people at risk can take the proper measures to protect themselves (Di Biagio and Kjekstad, 2007; Morss et al., 2011; Devoli et al., 2018). There are four main elements of early warning systems (UNISDR, 2006); risk knowledge, monitoring and warning

services, dissemination and communication, and lastly response capability. Weakness or failure in one of these elements will affect the entire system (Calvello, 2017; Piciullo et al., 2018). Landside early warning systems have been classified in several studies recently (Thiebes et al., 2012; Bazin, 2012; Stähli et al., 2015; Calvello, 2017). Though many countries have spent years understanding landslide processes, define thresholds, and organize monitoring, few of these LEWSs have become operational. The potential for landslide early warning systems is not fully exploited by the government and the decision makers (Baum and Godt, 2009; Intrieri et al., 2013; Glade and Nadim, 2013; Segoni et al., 2015). Some countries that have operational early warning systems are summarized in Calvello (2017), such as USA (Baum and Godt, 2009), Rio de Janeiro in Brazil (D'Orsi, 2012; Calvello et al., 2015; Piciullo et al., 2018), as well as in several Asian countries like Japan, Taiwan, Malesia, Bangladesh and China. In Europe, two systems are in operation, in Italy and Norway.

2.3.1 Norwegian landslide forecasting and warning service (NLFWS)

The creation of the NLFWS was based on a study from Colleuille and Engen (2009) that evaluated the need for a regional warning system for snow avalanches and landslides. From January 1th 2009, NVE got responsibility to coordinate national efforts for snow avalanches and landslides prediction, and a warning was one of these tasks. This was considered a good choice, due to the synergy already in work with the other tasks like flood warning and monitoring of water and ice conditions and climate change effects (Colleuille and Engen, 2009). From June 2011, the Hydrology department in the NVE got the responsibility to establish a section to operate and further develop the flood warning and establish a section for landslide warning. In 2015, they were combined as one service (Colleuille et al., 2017). This synergy gives an effective use of resources, and cooperation with other agencies like MET, NPRA, and BaneNOR.

The NLFWS uses daily meteorological quantitative gridded forecasts of precipitation and temperature from the Meteorological Institute (MET) (Krøgli et al., 2018). The warning service uses forecasted hydrometeorological variables to describe water and energy balances due to the sparse station network and short measurement periods (Krøgli et al., 2018). The variables are forecasted with two different models, the HBV-model (Beldring et al., 2003) and the S-Flow model. For more information about these two models, see Krøgli et al., 2018) The service also

uses data from meteorological station networks, operated by MET, NPRA, and BaneNOR. NVE also operate hydrological stations measuring discharge in rivers, snow depth and coverage, and hydrological networks measuring groundwater level (Krøgli et al., 2018). The daily landslide assessment uses real-time observations of rainfall, air temperature, water discharge, and groundwater levels to evaluate the performance of the models (Krøgli et al., 2018).

As mentioned in chapter 2.2.3, three thresholds have been proposed for Norway; of these, the one proposed by Colleuille et al. (2010) is used in the prediction of landslides. The other two are at the moment, not in use. The PD-threshold proposed by Sandersen et al. (1996) was on a research level and considered too high to be used in the warning service (Meyer et al., 2012). The ID-threshold proposed by Meyer et al. (2012) was overestimated for very wet regions, and this could, therefore, not be used either. The threshold in use is based on the relationship between hydrometeorological events and occurred landslides. The threshold is based on the original work by Colleuille et al. (2010), further adjusted for different regions in Norway due to regional physiographic and climatic differences (Colleuille et al., 2010; Cepeda et al., 2012; Cepeda, 2013a; Cepeda, 2013b; Boje et al., 2014) shown in figure 2.5. The relative water supply is the sum of rain and snowmelt as a percentage of yearly mean precipitation in the period of 1981-2010. Relative soil water saturation is the sum of water in the HBV-model normalized by a maximum value for the same period (Boje et al., 2014).

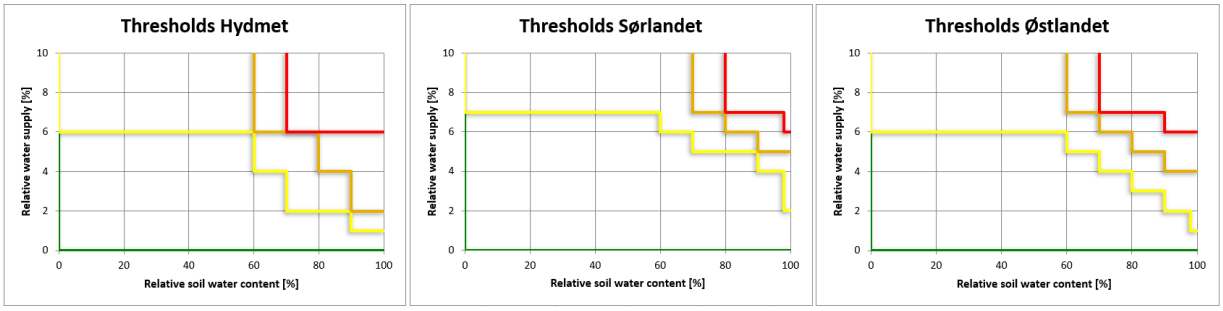

Figure 2.5: The hydrometeorological thresholds currently used in Norway. The original version used for Western Norway (left), adjusted Southern Norway (middle), and adjusted Eastern Norway (right). Limits showed for green (level 1), yellow (level 2), orange (level 3), and red (level 4). In comparison with the original thresholds above, several differences can be seen in which values the thresholds change to a new level (Boje et al., 2014; Boje, 2017).

The warning levels used are similar to the ones used for the flood forecasting service and uses four levels with associated colors. The colors represent different levels of landslide hazard and recommended awareness, information on what to expect, the severity of the hazard and recommended actions or measures to reduce potential damage (Krøgli et al., 2018). The levels

go from red (highest level) to orange, yellow and green (lowest level). The red level occurs much less frequent than the green level, which expects no landslide occurrence (Krøgli et al., 2018). The levels are shown in figure 2.6.

Table 1. Criteria for evaluating daily warning levels in the Norwegian EWS.

Warning level	Classification criteria
4 (red)	> 14 landslide (per 10–15 000 km^2) Hazard signs: several road blocks due to landslides or flooding Extreme situation that occurs very rarely, which requires immediate action and may cause severe damages within a large extent of the warning area. This level corresponds to a > 50-year return period flood warning.
3 (orange)	6–10 landslides (per 10–15 000 km^2) Hazard signs: several road blocks due to landslides or flooding Severe situation that occurs rarely, which requires contingency preparedness and may cause severe damages within some extent of the warning area. This level corresponds to 5–50-year return period flood warning.
2 (yellow)	1–4 landslides (per 10–15 000 km^2) Hazard signs: flooding/erosion in streams Situation that requires monitoring and may cause local damages within the warning area. Expected some landslide events; certain large events may occur.
1 (green)	No landslides 1–2 landslide caused by local rain showers One small debris slide if in area with no signs of elevated warning level Man-made events (from e.g. leakage, deposition, construction work or explosion)

Figure 2.6: Warning levels used in Norway (from Piciullo et al., 2017).

Bulletins for the warning service are available on the web page varsom.no (Johnsen, 2013). The dissemination of warnings is done through a "family" of different tools. These are all available to the public, as a part of the systems open data policy. Anyone can, therefore, contribute to the warning system by adding observations of either occurred landslides of different kinds, or landslide signs. The tools are further explained in chapter 4.4. For more information, see Krøgli et al. (2018).

An important part of an early warning system is to have a reliable warning to the authorities and population. The usefulness of a warning system is not only that the warning itself is correct, but if the warning resulted in appropriate and timely decision-making by the people at risk (Maskrey, 1997; Baum and Godt, 2009; Hisdal et al., 2017). The system needs to be able to give correct predictions but also lead to the proper action to mitigate loss and damage (Maskrey, 1997). It is crucial that the system meets the expectations of the users (Thiebes and Glade, 2016). The Norwegian landslide warning system has been evaluated (Hisdal et al., 2017; Piciullo et al., 2017) both on the technical performance and the user perception of the warning system (Krøgli et al., 2018). To test the technical performance, the daily hazard assessment is evaluated every week. The test quantifies how well the warning performs, meaning if the warning levels were correct or not. The evaluation is based on a comparison between the

warning levels that were issued, and the number of events that occurred, in addition to hazard signs recorded (Krøgli et al., 2018). The evaluation then has another quality control several weeks after the first evaluation, as new information about the landslide events may be available. This weekly technical performance test continuously improves the landslide warning service, and the thresholds for different regions have been adjusted based on these evaluations (Cepeda et al., 2012; Cepeda, 2013a; Cepeda, 2013b; Boje, 2017). The performance of the Norwegian early warning service was also tested with the EDuMaP method by Piciullo et al. (2017). For evaluation in Norway, the method was slightly modified as the original method uses fixed warning zones, and the Norwegian EWS uses variable size warning zones (Piciullo et al., 2017).

2.4 Extreme weather events

The term "extreme weather event" (EWE) is not very well defined in literature. The definition used in this document is taken from the Norwegian meteorological institute (MET). An extreme weather event is then defined as either strong winds, heavy rainfall, high water level, or a combination of weather elements that pose a danger combined. It is likely that such an event will cause serious damage or extraordinary danger to life and values in a significant area (Meteorologisk Institutt 2018a). An extreme weather warning is a weather event within a red warning level that have been named. Events like these get names as a good aid for the authorities, to get people's attention and awareness of the hazardous event. The names are chosen from a list in alphabetical order, switching between male and female names, except royal names and names containing letters æ, ø, å or begin with q, w, x, or z (Meteorologisk Institutt 2018b). The purpose is to facilitate communication between authorities, the public, the media, and meteorologists, so there is no misunderstanding about which event the warning is about (Meteorologisk Institutt 2018b). This system was set in place due to a hurricane in 1991 which were warned in the media but did not receive proper attention by the public, and no action was prepared, which lead to major damages.

3 Study area

Hordaland county is located at the west coast of Norway, bordering the counties Sogn og Fjordane in the north, Rogaland in the south and Buskerud and Telemark in the east (figure 3.1). As of January 1st, 2018, the population had reached 522 539 people (Statistisk sentralbyrå, 2018), with 255 464 people living in the city of Bergen (Statistisk sentralbyrå, 2018). The county has a spatial extension of 15 437 km^2 including bodies of water (14 522 km^2 this being land area). The highest terrains in Hordaland are Folgefonna (1662 m.a.s.l.), Hårteigen (1690 m.a.s.l.) and Hardangerjøkulen (1863 m.a.s.l). Hordaland county is divided into five districts; Nordhordland, Midthordland, Sunnhordland, Hardanger, and Voss shown in the bottom right figure 3.1. Hardanger, marked in green, is well known for its fruit cultivation, especially apple production.

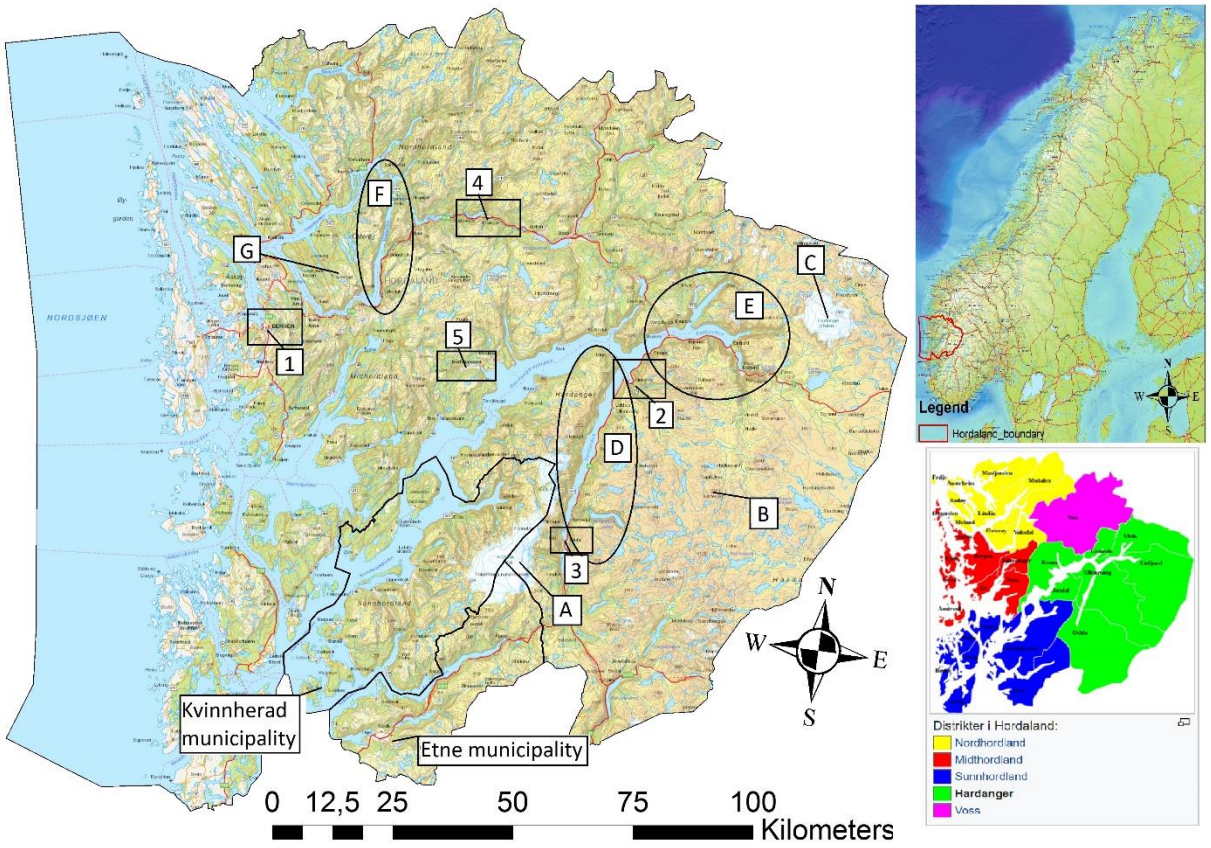

Figure 3.1: Study area: Map of Hordaland with outer borders (left), location of Hordaland county in Norway (top right), and the five districts (bottom right). Location names mentioned throughout the work is marked. Highest terrains: A: Folgefonna; B: Hårteigen; C: Hardangerjøkulen. Fjords (circles): D: Sørfjorden; E: Inner Hardangerfjorden; F: Veafjorden. Island: G: Osterøy. Cities/towns (squares): 1: Bergen; 2: Kinsarvik; 3: Odda; 4: Evanger; 5: Nordheimsund. Etne and Kvinnherad municipalities are seen in the bottom of the map, marked with their borders.

The county is home to two of Norway's largest glaciers, Folgefonna and Hardangerjøkulen. Folgefonna is divided into three parts, the north Folgefonna 26 km^2, central Folgefonna 10,4 km^2 (NVE, 2017b) and southern Folgefonna 164 km^2. Hardangerjøkulen is 71 km^2 (NVE, 2017a). Both glaciers in Hordaland are located close to the coast, and therefore they are classified as maritime glaciers. In Andreassen et al. (2005), it was found that the maritime glaciers had a much higher mass turnover than the continental glaciers further inland. The two glaciers are both dominated by the winter balance as the most important parameter in the mass balance.

The landscape in Hordaland is largely dominated by several fjords. All of them are parts of the major Hardanger fjord, which is the country's longest and Norway's second longest fjord (Thorsnæs, 2015). The fjords were created by repeated glaciations. During the uplift of the land occurring during Paleogene and Neogene, the rivers eroded the flattened surface following weakened zones (Vorren and Mangerud, 2007). The glaciers then followed these same paths, eroding these into steeper valleys. The fjords were created where glaciers eroded below the sea level (Vorren and Mangerud, 2007), while the u-shaped valleys visible today did not go as deep (Erikstad et al., 2009).

About half of the Hardangervidda national park is located within the Hordaland county. In the elevation map obtained from a DTM (digital elevation model) shown in figure 3.2, the two glaciers, Hardangerjøkulen and Folgefonna are both noticeable in solid dark red colors. The plateaux Hardangervidda in the east is shown to be quite high above sea level, and the fjords have steep declines towards the sea level in blue. The elevation map shows how the topography changes from high lying and steep mountains in the east, to lower height above sea level and gentler slopes towards the coast.

A slope map was made from the elevation map and is shown in figure 3.3. It shows the steep slopes in the fjords and valleys, visible in dark red. Both glaciers are also visible here, along with the plateaux Hardangervidda in the east, due to their flat surfaces. The green color scheme covers a big part of the county, showing that slope angles of 15-30 degrees are quite common. The county also inhibits some of the country's highest and most knows waterfalls, several with a vertical drop of 300 meters (Bryhni & Thorsnæs, 2014). These rivers with steep slopes are often much shorter than rivers in mountain plateaux, which have longer paths. The county has

a great variety of topography and inhibits both of these river types. Along the fjords, the shorter and steep rivers are more common due to the slope angles.

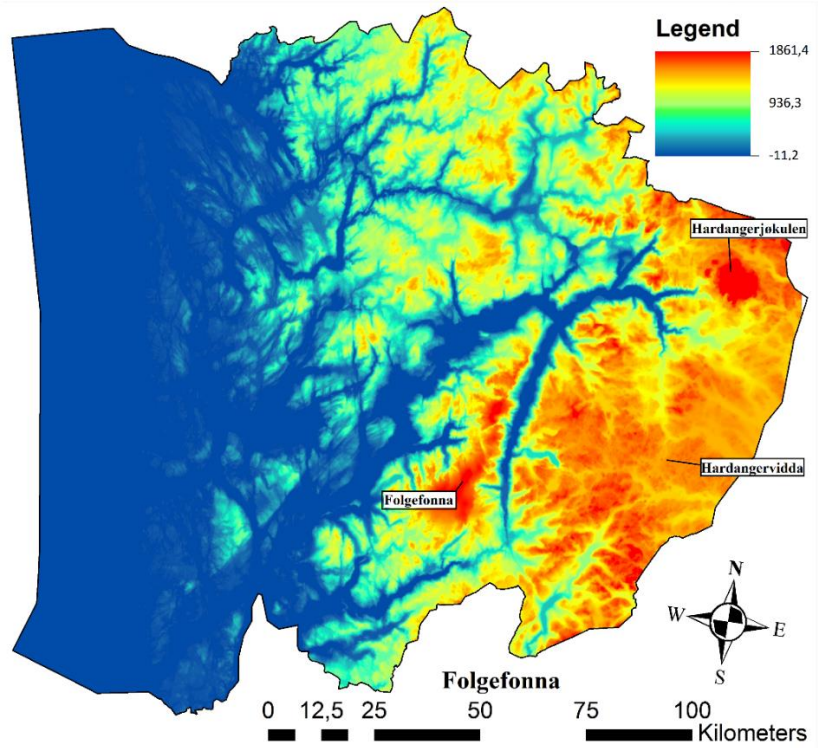

Figure 3.2: Elevation map of Hordaland county. The plateaux Hardangervidda is visible on the right, and the two glaciers Folgefonna and Hardangerjøkulen are visible in the darkest red colors.

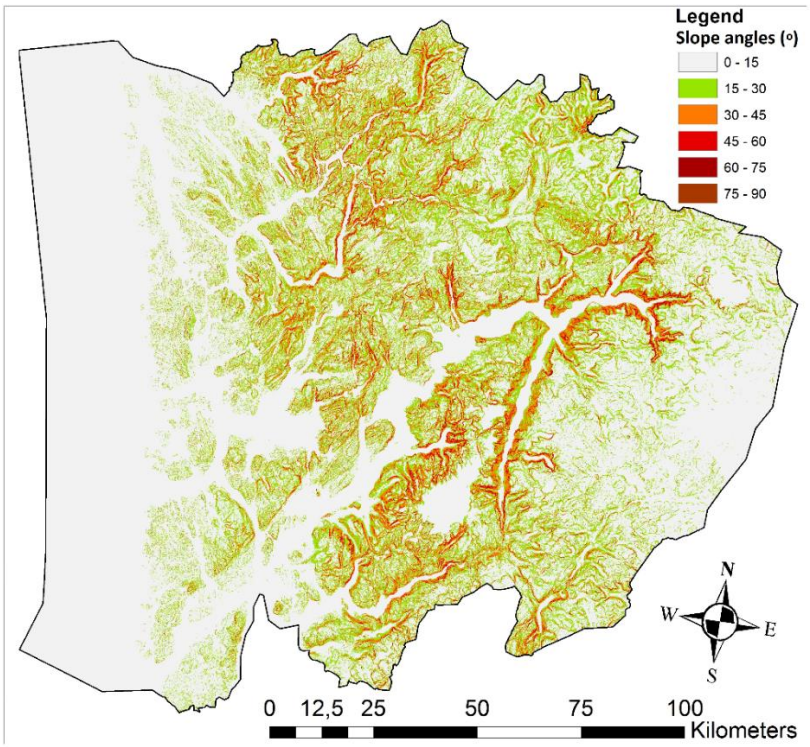

Figure 3.3: Slope map of Hordaland county. The steep slopes of the fjords are visible in the darker colors.

3.1 Meteorological conditions

Hordaland has a temperate climate, with winds coming in from west and south-west (Dannevig, 2009). The moist air coming in from the Atlantic Ocean carries most of the precipitation falling in Norway, and the mountain range in the south part of the country greatly influence the geographical distribution (Barstad and Grønås, 2005; Dyrrdal et al., 2011). Due to this orographic effect, the west side of the mountain range receives heavy long duration precipitation, and the areas in the east lie in the rain shadow receiving less precipitation (Barstad and Grønås, 2005; Dyrrdal et al., 2011). The west coast experiences frequent mild weather in the winter months, leading to a discontinuous snow cover close to sea level (Sandersen et al., 1996). The maximum amount falls within a "maximum zone" about 50 km from the coast, with annual precipitation of above 3000 mm. The annual precipitation at the coastline is about 1500 mm, and in the innermost areas decreasing to about 1000 mm (Dannevig, 2009). This great variation of precipitation over short distances is seen by example in Haukeland in Masfjorden and Vively in Eidsfjord, which are just 100 km apart, and receives 3537 mm and 840 mm yearly respectively (Uni Research klima, 2017). The precipitation pattern is clear in figure 3.4, showing the highest amount of precipitation in purple and pink slightly inland in the "maximum zone", and a decrease in the innermost areas towards the plateaux Hardangervidda.

To visualize the temporal pattern in precipitation in the stations, the data from the ten selected gauge stations (figure 3.5) are plotted in figure 3.6. To differentiate better between the stations, the data was split in half based on latitude, the top figure 3.6 representing the northern part of the county and the middle figure 3.6 represents the southern part, both covering spatial distribution from coast to inland. The bottom figure 3.6 shows the temperature variations at five of the gauge stations.

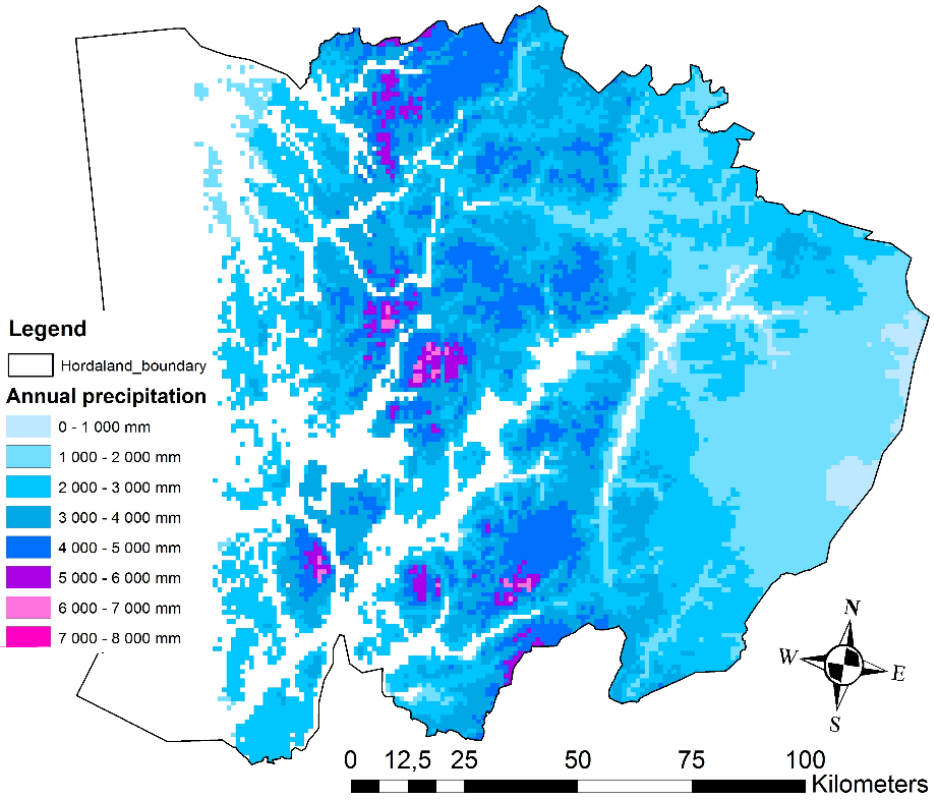

Figure 3.4: Annual precipitation in Hordaland, showing the typical precipitation pattern in the county, by normalized values in the period 1961-1990 (senorge.no).

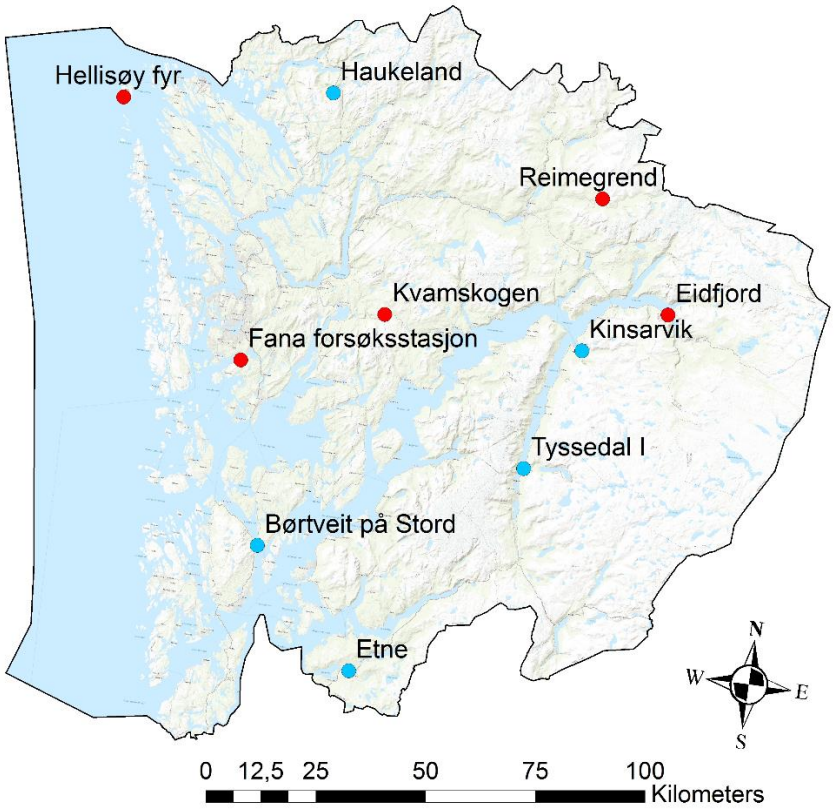

Figure 3.5: Spatial distribution of the selected gauge stations, blue measuring precipitation, and red measuring both precipitation and temperature.

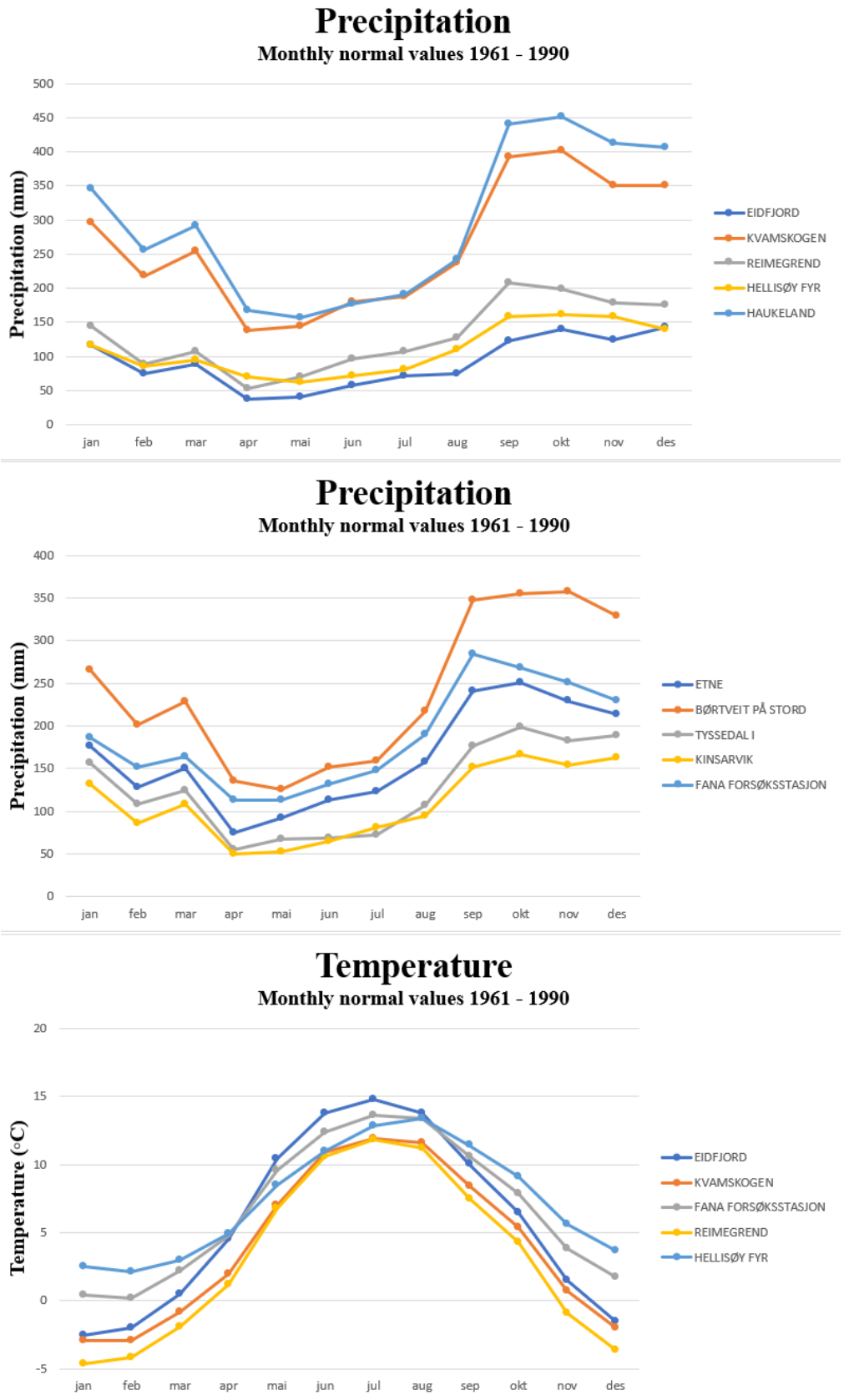

*Figure 3.6: Normal monthly values of precipitation levels in the northern part (**top**) and southern part (**middle**), and temperatures (**bottom**) measured at the selected gauge stations in Hordaland, covering the spatial distribution from coast to inland. Downloaded from eklima.no.*

The northern part is represented by gauge stations Hellisøy fyr, Haukeland, Reimegrend, Kvamskogen, and Eidfjord. Precipitation values are significantly higher in Haukeland and Kvamskogen located in the north and central part of the county, especially in fall months. The three other stations show both lower total precipitation and an evener distribution throughout the year, in contrast to Haukeland and Kvamskogen, which also have larger differences in precipitation between the spring-summer months and fall-winter months. Haukeland has the highest measured yearly precipitation at 3537 mm. Lowest yearly precipitation is measured at Eidfjord at 1088 mm.

The southern part of the county is represented by gauge stations Fana forsøksstasjon, Børtveit på Stord, Etne, Tyssedal I and Kinsarvik. The differences here are smaller between the stations, and the stations in the south-west have higher precipitation values. The other gauge stations are located more inland, and precipitation levels here are therefore lower. The pattern throughout the year is similar to the north, the stations receiving most precipitation also have the largest variations through the year, with highest levels in fall-winter months. Highest precipitation is measured at Børtveit på Stord, at 2871 mm, and the lowest value of 1302 mm is measured in Kinsarvik.

Temperatures are variable according to location, the coastline and lower areas in the fjords having temperature averages around 0-2ºC. The in-land has an average of -5ºC, and the highlands inland has an average down to -10ºC (Dannevig, 2009). Minimum temperatures measured is -10 to -15ºC at the coast and -25 to -35ºC in the valleys and highlands. Maximum temperatures measured is 32ºC in the lowlands and 20-25ºC in the highlands. The bottom graph in figure 3.6 shows the two stations closest to the coast, Hellisøy fyr and Fana forsøksstasjon, having the evenest temperature changes year around among the selected stations. Hellisøy fyr has the smallest variations with a maximum and minimum temperature of 13,4 ºC and 2,1ºC, respectively. The largest variations through the year are measured in Eidfjord, with a maximum and minimum temperatures 14,8ºC and -2,5ºC respectively.

3.2 Landforms and landscape

A regional classification of landforms and topography was proposed by Etzelmüller et al. (2007), dividing the country into ten major landforms. As shown in figure 3.7, the county of Hordaland consists of nine out of the ten major landform types. The variations of the landforms follow both the longitudinal direction and height above sea level. The outer coastline is mainly coastal plains and strandflats (1), followed by hills with moderate slopes (3), and glacially scoured low mountains and valleys (7). The central part of the county consists of Alpine relief (9/10), with steeper slopes along the Sørfjorden and further inland. Some smaller areas of lower mountain plateaux (5) are visible in the northern-central area. The innermost areas of the county are dominated by high paleic mountains (8) and higher mountain plateaux (6). A very small area is classified as elevated hills/tablelands (4) at the very south end of the county.

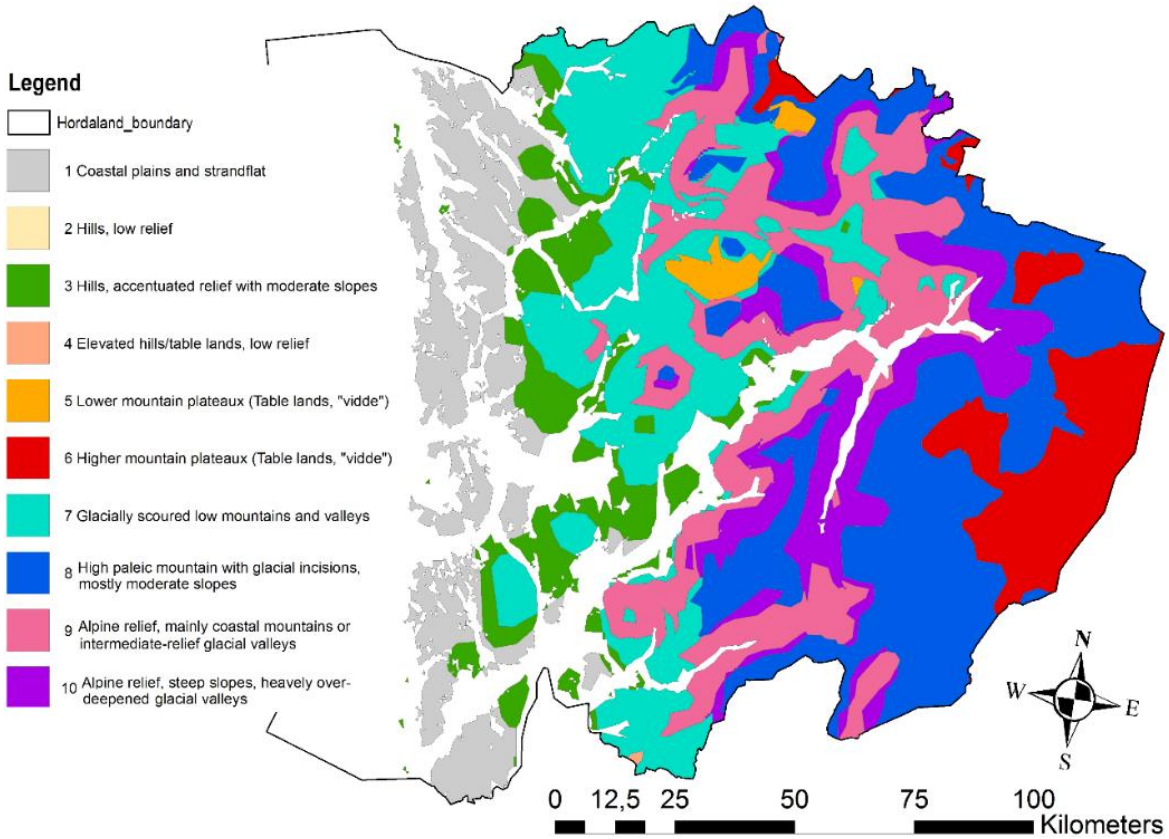

Figure 3.7: Landform subdivision for Hordaland county (from Etzelmüller et al. (2007) obtained from NVE).

Vegetation

Hordaland consists of seven different landscape regions based on the hierarchy from Puschmann (2005), which have 45 landscape region classifications in total. From west to east, the county consists of regions 20-23 with a gradual shift inland, and the higher lying areas consist of landforms 15-17 (figure 3.8). The seven regions are shown in table 3.1, with translations to the right. Some examples of landforms are shown in figure 3.9.

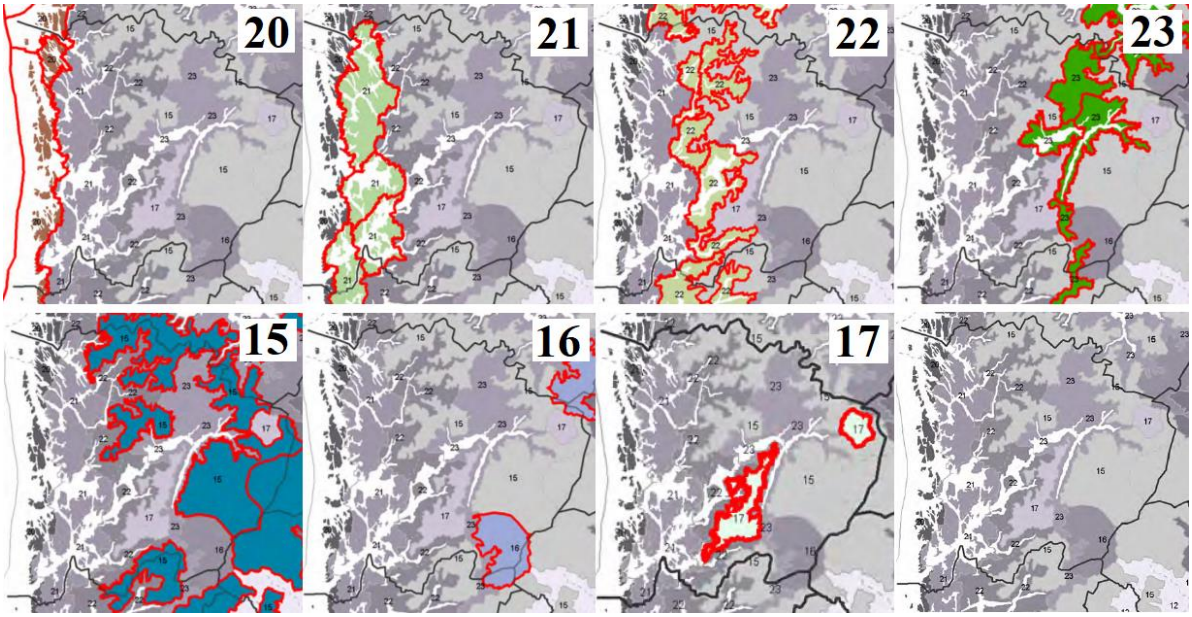

Figure 3.8: Landscape regions in Hordaland county (Puschmann, 2005).

Table 3.1: Landscape regions in Hordaland county.

Region number	Norwegian classification	Translation
15	Lågfjellet i Sør-Norge	The low mountains in Southern Norway
16	Høgfjellet i Sør-Norge	The high mountains in Southern Norway
17	Breene	The glaciers
20	Kystbygdene på Vestlandet	The coastal settlements in Western Norway
21	Ytre fjordbygder på Vestlandet	Outer fjord settlements in Western Norway
22	Midtre bygder på Vestlandet	Central settlements in Western Norway
23	Indre bygder på Vestlandet	Inner settlements in Western Norway

The areas along the coast (20) have scarce vegetation on the outermost areas, and nutritious soil gives lush vegetation in some places (21). The oceanic climate decreases towards the east, and in the inland areas, it changes to more variable vegetation, and more forested areas consisting of deciduous forests, especially birch forest, and mixed forests (22). Oceanic pine forests are also common, especially in Hardanger (23). Artificially planted spruce is widespread in the fjord- and valley sides. The marshes more common on the coastline still occur further inland but in decreased amount.

The two next landscape regions in Hordaland are regions 15 and 16, which represent the low-lying and high-lying mountain areas (Puschmann, 2005). In the lower-lying areas of region 15, most of the region is above the tree line, but also include scattered areas of mountain forests. The mountain plateaux Hardangervidda covers large parts of this region. The higher mountains in region 16 above 1500 meters above sea level are characterized by almost no higher-standing vegetation, and the main feature bare rock and a variety of species of crustaceans. Moss can also be widespread. Lastly, region 17 describes the glaciers. The variety in vegetation is small in the harsh conditions, and all higher-standing vegetation by the glacier edge are herbs, except for the dwarf willow. The vegetation changes over time, due to the glacier withdrawal, and reclaims the terrain (Puschmann, 2005).

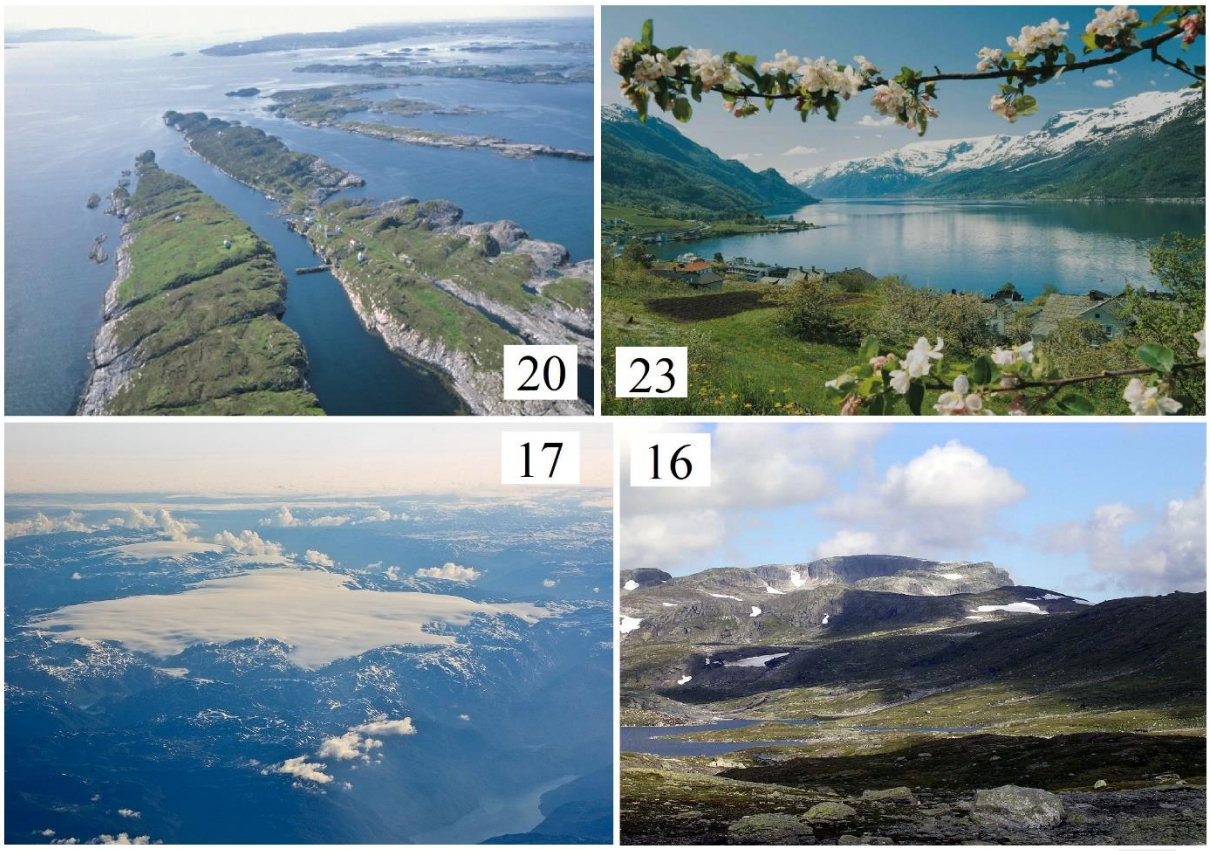

Figure 3.9: Examples of landscape types in Hordaland. ***Top****: Landscape pictures for regions 20 on the left (Source: Helge Sunde/Grind, downloaded on 07.05.19) and 23 on the right (Source: Per Eide/Visit Norway, downloaded on 15.11.18).* ***Bottom****: Glacier Folgefonna on the left (Source: Wikipedia, downloaded on 15.11.18). The mountain Sandfloegga in Hardangervidda on the right (Source: Wikipedia, downloaded on 01.04.19).*

3.3 Geology

The geological structure of Hordaland county can be split into three parts, which are from top to bottom:

- **Allochthonous hard rock:** The top layer consists of allochthonous hard rocks from the Caledonian orogeny, originating from the Precambrian period. A wide belt of other allochthonous rocks, mostly gneiss, quartzite, and old metamorphic volcanic rocks along the north side of the Hardanger fjord and in isolated remains in Hardangervidda (Bryhni & Thorsnæs, 2014).
- **Sediment rock/Cambrian Silurian:** Sedimentary rocks from the Cambro Silurian period, some of these metamorphic sedimentary rocks like phyllite and limestone, and some volcanic rocks from the Caledonian mountain range. The phyllite makes for good soil well used for the fruit cultivation in Hardanger (Bryhni & Thorsnæs, 2014).
- **Lower bedrock/Precambrian:** Consisting of Precambrian gneiss and granite, with elements of metamorphic sedimentary and volcanic rocks. The upper part is influenced by the Caledonian orogeny, especially in the north-northwest areas, among them "Bergensbuene" (Bryhni & Thorsnæs, 2014).

The bedrock was assumingly worn down to a peneplain, due to erosion and weathering during Precambrian (Bryhni & Thorsnæs, 2014). During Cambrian, the ocean deposited clay and calcareous ooze, which were later transformed into sandstone, shale, limestone, and phyllite during the Caledonian mountain range folding (Bryhni & Thorsnæs, 2014). In some areas, the upper part of the bedrock was influenced by the Caledonian mountain range folding, where it was heated up, creating a new structure. One part of the bedrock is called "Bergensfeltet" or "Bergensbuene", due to its proximity to the city of Bergen. After the Caledonian mountain range was created, it was worn down again to a plane surface, and volcanic melts penetrated cracks in Sunnhordland which are visible today. Most of the county is seen to be covered in the quaternary deposits "thin layer above bedrock" seen in pink in figure 3.10. Several fields of moraine material are also seen in green and light colors (thick and thin layer). Other sediments present in the county are different glacial deposits, marine deposits, weathered material, and previous landslide deposits. The detrital sediments covering most of the county is almost exclusively from the last ice age or after (Mangerud, 1976).

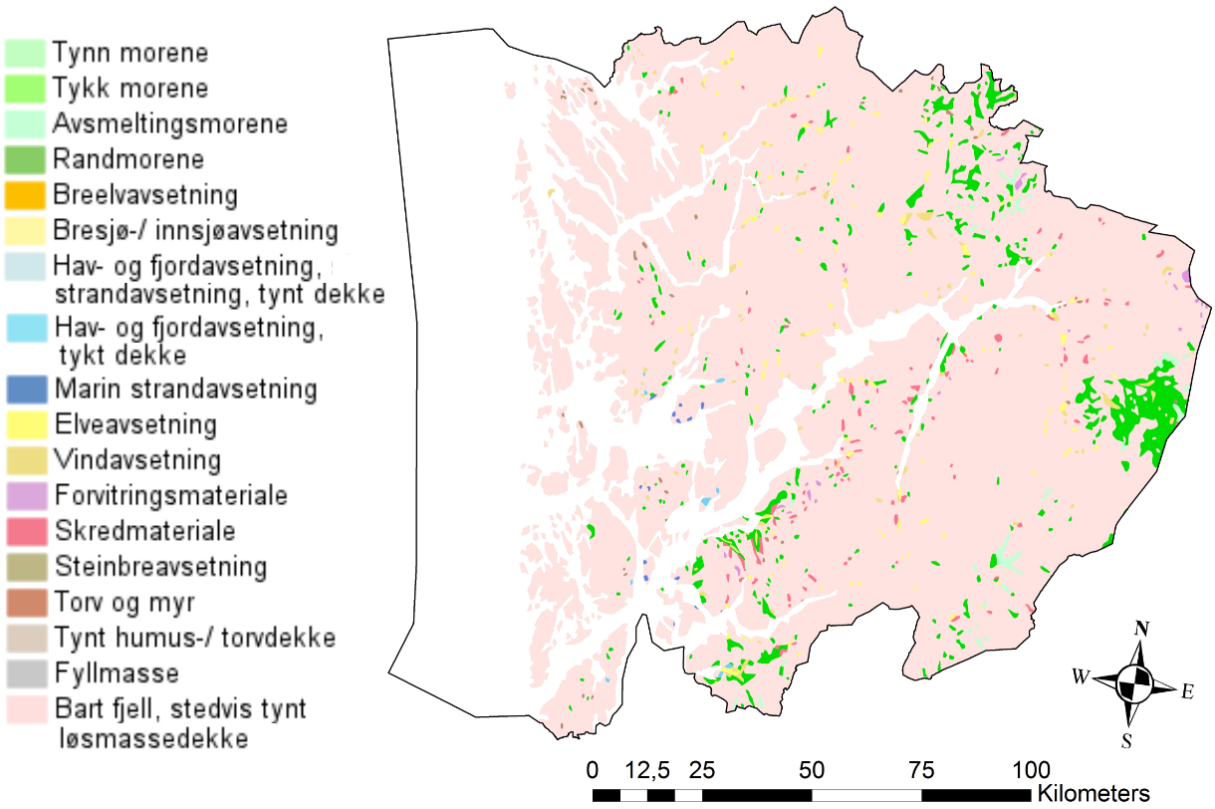

Figure 3.10: Map of quaternary deposits in Hordaland. The source of the map is shown in chapter 4.5.

The Hardanger fjord follows the strike direction of the Caledonian mountain range (Bryhni & Thorsnæs, 2014). The sides of the fjords are gentler and more comprehensive, where the bedrock is dominated by Cambro Silurian deposits (Bryhni & Thorsnæs, 2014). The fjords and valleys around "Bergensbuene" are completely dominated by this structure, creating concentric arches. The county has two eye-catching fjords that stand out in the general landscape. Largest is the Sørfjorden, a sidearm of the Hardanger fjord between Kinsarvik and Odda. The smaller one is Veafjorden east of Osterøy. Both fjords have a north-south direction (Mangerud, 1976). The different direction in contrast to the general west-east direction of the other fjords is due to these being joint valleys (Erikstad et al., 2009). A joint valley is a long and quite straight valley or gorge created due to cracks and weaknesses in the bedrock. The weakened zone has then been eroded by rivers and glaciers, making deep and sharp valleys which cross independently through the general terrain (Erikstad et al., 2009). This landform exists in several sizes, the smaller ones referred to as depressions, and the large ones like Sørfjorden fall under the term valley or fjord.

3.4 Landslides and climate change scenarios in Hordaland

Meyer et al. (2012) state that the western face of the mountain ranges is regarded as the most debris flow prone area of Norway. The intense and long-duration water supply caused by both rainfall and snowmelt increases the water content in the soil, making the area prone to landslides, not only on steep slopes but also gentle slopes and modified slopes and filling along roads and railways (Krøgli et al., 2018). Hordaland county is prone to all mass movements occurring in steep terrain due to its location on the west coast of Norway and its topography. These mass movements can be snow avalanches, rock falls, rock avalanches, slush flows, debris slides, debris avalanches, and debris flows. As the thesis focus on weather-induced landslides, this summary includes only the last three types mentioned. According to Sandersen et al. (1996) the months August to December experience most heavy rainfall in the marine climate region, as well as most frequent debris flows. Many landslides also correspond with periods of heavy snowmelt (Sandersen et al.,1996). Previous studies in western Norway have found that landslide peaks occur in spring and late autumn (Jørandli, 2016; Devoli et al., 2017; Bugge, 2017; Mongstad, 2018). All studies found peaks in November and December, and some of the studies also found March to have a high landslide occurrence, followed by October, May, and January.

Two different susceptibility maps are available for Hordaland county and are presented shortly below. They are both used to predict the spatial occurrence of weather-induced landslides. The first one is a catchment-based approach showing the catchments that are susceptible to landslides in soil (Cepeda and Bell, 2014; Bell et al., 2014; Devoli et al., 2019) in particular debris avalanches, debris flows, shallow soil slides, and clay slides (top in figure 3.11). The other (bottom in figure 3.11) is a pixel-based approach, showing specifically the possible occurrence of debris avalanches and small debris flows (Fischer et al., 2012, 2014). Since debris flows and debris avalanches are two different processes, the model was separated into two customized parts, allowing a higher accuracy (Fisher et al., 2014). For more information about the maps, see Devoli et al. (2019) and Fischer et al. (2014).

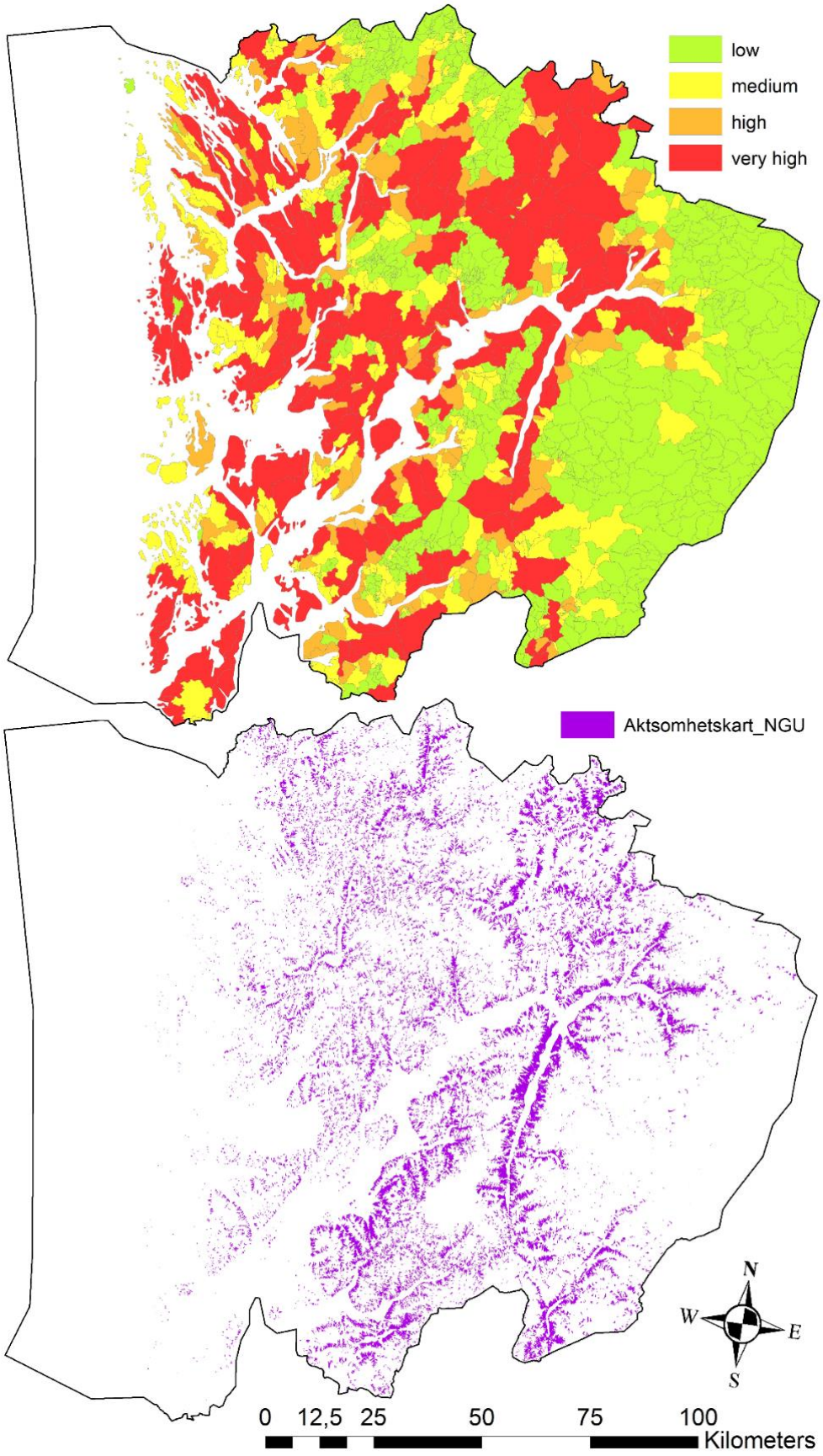

*Figure 3.11: Susceptibility map from Cepeda and Bell, 2014 (**top**) and Fisher et al., 2012,2014 (**bottom**).*

There is limited information about human and economic losses due to landslide hazards in Norway (Krøgli et al., 2018). For the impacts on main roads in terms of costs, Hordaland was found to have the highest costs, with almost 22,5 million kroners every year. The costs are the combined costs of repairs of damages, clearing of roads, and closing of roads which leads to increased travel time and delays in the transportation of goods (Frauenfelder et al., 2013). Damages to railways also cause significant economic losses, due to both clearing the tracks, repairs, and delays in traffic.

In addition, landslides also cause great damage to private properties, among them apple cultivation farms in Hardanger. The pictures in figure 3.12 show examples of damages caused by landslides in Hordaland. Top left picture show damages to the railway near Evanger. The top right picture shows damages to an apple farm caused by the storm "Dagmar" in 2011, leading to great economic loss for the farmers. Norway has the world's most comprehensive compensation scheme, "Statens naturskadeordning", which pay out compensation for damage caused by natural disasters. Statens naturskadeordning process around 1500 cases a year, each with a typical compensation sum of 85.000 kroners. The bottom pictures in figure 3.12 show damage to a private property on the left, and damage to a public road on the right. As precipitation and extreme weather are expected to increase in the future, Hordaland will likely experience more damages due to landslides.

Furseth (2006) found that at least 11 people had been killed by landslides in soil, and 24 people killed by rock falls, in Hordaland county between 1822 and 2005. However, the number of fatalities caused by both typologies are likely higher. Many of the mass movements have unclear typologies in their descriptions, and the exact number of people killed is in many cases unknown (Furseth, 2006). A new revision of fatalities due to landslides in Norway was done for the period 1995 to 2019, as part of analyses presented in Haque et al. (2019). The analysis shows that six fatalities occurred in Hordaland caused by debris slides or debris flows, and one by a rock fall (Haque et al., 2019), during the same investigated period. Five of these fatalities are in both Furseth and Haque datasets; all occurred in 2005. In total, at least 12 people have been killed by weather-induced landslides in Hordaland between 1822 and 2017. Six of the fatalities occurred between 2005 and 2017, and all of these landslides were caused by heavy precipitation. Five was caused by extreme weather events. The storm "Kristin" in 2005 caused a landslide hitting a terraced house, killing three people in Hatlestad Terrasse in Bergen. The

storm “Loke” just two months later killed one person working on a house in Nyborg in Åsane. One fatality occurred on January 16th, 2011 in Kvitingen in Samnanger, due to intense rainfall and mild weather. Lastly, the storm “Aina” in December 2017 caused a landslide that hit a house, killing one person in Votlo on Osterøy (figure 3.13).

*Figure 3.12: Economic damages in Hordaland. **Top**: Damaged railway after a landslide during “Dagmar” in 2011 on the left (Source: NRK). One of many apple farms, destroyed by a debris flow during “Dagmar” in 2011 (Source: Hardanger Folkeblad). **Bottom**: Destruction on private property after “Dagmar” in 2011 on the left (Source: Odd-Arne Mikkelsen/NVE). A blocked road after a debris flow occurred during the storm “Synne” in 2015 (Source: Bergens Tidende).*

*Figure 3.13: Lethal weather-induced landslides in Hordaland since 2000. **Top left**: Hatlestad Terrasse in Bergen night before September 14th killed three people in the residences, caused by storm Kristin (Source: Nettavisen). **Top right**: Nyborg in Åsane November 14th killed one person working in the house, caused by storm Loke (Source: Dagbladet). **Bottom**: Votlo on Osterøy December 7th killed one person living in the house, caused by storm Aina (Source: NRK).*

3.4.1 Climate change scenarios

Some studies have been performed in the past to analyze the changes in future climate in Norway, an how this will influence the occurrence of landslides. The “Geoextreme project” focused on investigation coupling between meteorological factors and landslides and snow avalanches (Jaedicke et al., 2008). The main objective was to predict future geohazards in a changing climate, by extrapolating this coupling, and estimating socioeconomic implications. Results from the “GeoExtreme project” shows how the landslide hazard might change over the next 50 years. It is likely that the thresholds for landslides will change. While the processes remain the same, the areas with increased precipitation will have an increased pore water pressure in the ground, and therefore need less additional rainfall to initiate landslides. Climate change can also change forest growth, and an increase in temperature in Norway will increase the tree line (Kronholm and Stalsberg, 2009).

The main processes leading to landslides are the weather, climate, and slope, and the main factor leading to shallow debris avalanches is high pore water pressure caused mainly by precipitation, but also in some instances snowmelt (Kronholm and Stalsberg, 2009). The critical amount of precipitation needed to initiate landslides can be either reached on one day with intense precipitation or over a longer period with lower intensity. There are also big differences between different regions in how much precipitation the soil cover can handle before initiation (Kronholm and Stalsberg, 2009).

The report “Climate in Norway 2100” provided an updated basis for future climate scenarios and is mainly based on IPCC's fifth assessment report (Hanssen-Bauer et al., 2017a). Both temperature and precipitation are expected to increase, with 4.5^{o} (3.3 - 6.4^{o}) and 18% (7 - 23%) respectively. For precipitation, there is an expected increase in the annual precipitation, and events with heavy rainfall will increase in both magnitude and frequency (Hov et al., 2013; Hanssen-Bauer et al., 2017a). The increase in temperature will also increase runoff in winter and spring, leading to earlier snowmelt. Because of the link between weather conditions and landslides, the report concludes it might lead to an increase in the frequency of landslides associated with heavy rainfall in areas with steep terrain (Hanssen-Bauer et al., 2017a). However, no specific landslide studies have been done to confirm the possible increase in these processes in the future due to climate change.

The Norwegian version of the "Climate in Norway 2100" report also includes scenarios for different regions in Norway (Hanssen-Bauer et al., 2017b). The scenario for Hordaland expects an increase in temperature of 4.0°, with the increase being largest in fall and winter (Hanssen-Bauer et al., 2017b). The increase in precipitation is expected to be largest for the areas along the coast, where precipitation is already common, and an increase of heavy rainfall episodes both in intensity and frequency (Hanssen-Bauer et al., 2017b). The increased rainfall and snowmelt will also likely cause more floods, especially in fall and winter. The steep rivers with small watersheds typical in Hordaland have strong reactions to heavy rainfall, which leads to increased discharge and problems for the infrastructure. Due to the steep terrain in Hordaland combined with the expected increase of precipitation, an increase of weather-induced landslides like debris avalanches and debris flows are expected based on this report (Hanssen-Bauer et al., 2017b).

4 Data and source of data

Rainfall data, landslide data, information about warning and thresholds, as well as geological and topographical information have been collected from several sources, to be used in this work.

4.1 Rainfall data

The spatial extent of rainfall data (24h) have been obtained from xgeo.no and was used to identify rainfall events that caused landslides. "Xgeo" is a decision-making tool which consists of different data sets like precipitation, air temperature and snow characteristics with a spatial distribution of 1 km and temporal resolution of 24 hours (Engeset, 2016). The precipitation data are visualized in a raster ($1km^2$ grid) map showing the spatial extent between 07:00 and 07:00 every day. The website also features other types of information, like the temperature, type of precipitation, and amount of snowmelt in the county. The spatial extent of the annual rainfall in Hordaland in the form of an ASCII-file was accessed on 15.12.2018, and the spatial extent of rainfall for each day of interest in the same data format was accessed on 15.05.2019, obtained directly from NVE. These are presented in chapter 3.1 and chapter 6.1.1.

A preliminary table of known significant rainfall events was also used as an additional source to find rainfall events for the analysis. The table was obtained from supervisor Graziella Devoli on 26.06.2018 and contained a preliminary list of significant weather events in Western Norway, which is known to have caused landslides.

Precipitation data was downloaded from eklima.no on 19.01.2019. Monthly normal values from the gauge stations consist of normalized values in the period 1961-1990. The ten selected stations (figure 3.5) are evenly distributed in the county and were all operative in the entire study period 2011-2017.

4.2 Landslide data

Landslide location was obtained in the form of point data, and landslide extension was obtained in the form of polygons. Points, polygons, and additional landslide data have been collected from several sources.

To locate landslide occurrence, landslide data represented by points were extracted on 20.07.2018 from the Norwegian mass movement database (www.skredregistrering.no), herein called database or NLDB. The database contains all registered mass movements that have occurred in Norway. The database includes several typologies like rock falls, rock avalanches, debris flows, debris slides/debris avalanches, shallow soil slides in artificial slopes, landslides in clay, but also snow avalanches, slush flows, and ice falls (Krøgli et al., 2018). For the period of interest 2011-2017, the database included 2824 mass movements of all typologies in point format in Hordaland county.

As pointed out by previous works (Bakken, 2017; Bugge, 2017; Mongstad, 2018) the mass movement database is made up by point data, supported by different sources of confirmation of the landslide occurrence. These sources are, for example, field observations, technical reports, news articles, historical documents, and church books. NVE has had the responsibility for the development of the database since January 2014 (Sokalska et al., 2015). Registrations come from many different contributors, such as the Norwegian Public Road Administration (NPRA), and the Norwegian Railway Administration (BaneNOR) (Krøgli et al., 2018), in addition to the landslide forecasters and local geologists. The NPRA has the responsibility for registering landslides along the roads they are responsible for and update their data every month. BaneNOR has the same responsibility for rail tracks, but do not have a regular update of data.

In previous years, the Geological Survey of Norway (NGU) and the Norwegian Geotechnical Institute (NGI) both contributed with registrations to the database. NGU registered, through local historian Astor Furseth, a lot of historical landslides in the database, using all sorts of resources, focusing on landslides having caused damages and loss of life. NGI has also registered some information to the database in connection to their work with landslide hazard assessment (NVE, 2017c). As the responsibility of the registration of the landslides is split between different institutions, the NVE works with registering the landslides occurring outside the roads and railways. Most landslides that are registered in the database, however, have occurred near inhabited places due to these getting more attention. There is, therefore, a lack in the registration of landslides occurring in more sparsely inhabited areas (Boje, 2017; Krøgli et al., 2018).

Landslide data can also be registered and accessed by everyone through the tool RegObs (www.regobs.no). The tool "RegObs", short for "register observations", is a real-time registration tool for observations, danger signs, and events (Ekker et al., 2013). The registrations are used by forecasters and emergency personnel. RegObs was originally created to collect observations for the Norwegian Avalanche Center. Later the database was extended to include other natural hazards like landslides, floods, and ice conditions (Krøgli et al., 2018). The tool is publicly available as both an app and a web page, enabling anyone to make registrations out in the field shortly after an event. The observations registered at RegObs are uploaded to the NLDB every 48 hours. The NLDB can be visualized in the web portals www.skrednett.no and www.skredatlas.nve.no and xgeo.no.

The landslide point data is often placed in the area of deposit, or where the landslide has caused damage to infrastructure or people (Sokalska et al., 2015). In addition to the location of the point, the database also includes other forms of information (figure 4.1). For example, the date, time of day, the accuracy of both time and location, typology of the landslide, area name, occasionally size or volume, and damages to roads, railway, infrastructure or people and more (Sokalska et al., 2015). The quality and amount of the data depend on the institution or person doing the registration of the event.

Dagmar 2011

OBJECTID *	SHAPE *	skredID	skredType	skredNavn	stedsnavn	skredTidspunkt
22	Point	5FA58E3F-E663-4C99-BEE5-894366A0B530	140	Fadnestreet	Fadnestreet	26.12.2011 19:00:00
131	Point	06A0980D-AFDB-4DC1-A6A1-B3770439F47D	140	Langeland	Langeland	26.12.2011 18:00:00
480	Point	8238D1EF-72F7-499A-9109-BF047CCABA3F	110	Krossdalen	Krossdalen	26.12.2011 18:30:00
518	Point	F9519313-7F1E-42EC-AB19-8317E864B4C0	140	Haukanesberget	Haukanesberget	26.12.2011 02:00:00
535	Point	2A58D9A8-2B52-4B06-A674-A69838C23178	140	Urheim	Urheim	26.12.2011 01:32:00
678	Point	8193DEA7-10EE-41A3-87D4-5335017B7C71	140	Måge	Måge	26.12.2011 01:54:50
1222	Point	05AE43C8-1405-4B71-8B77-FA62554A2915	140	Tveito rasteplass	Tveito rasteplass	26.12.2011
1242	Point	68CFA818-0A92-4810-84EF-CB31C7791ED7	140	Skjelvik 3	Skjelvik 3	26.12.2011 02:00:00
1280	Point	AC62129F-8FE7-428C-867E-E1210B87F7C2	140	Brimnes	Brimnes	26.12.2011
1312	Point	4A1B73CA-E936-46FB-B566-1767C253F1AB	142	2330-00003 Evanger - Bolstadøyri	Evanger - Bolstadøyri	27.12.2011
1368	Point	A3153539-7077-4F30-9537-A7CA7FC94FF5	142	2312-23260 Mjølfjell stasjon	Mjølfjell stasjon	26.12.2011
1649	Point	20B29679-1359-47AA-8D83-328A2C0143CA	142	2330-00003 Evanger - Bolstadøyri	Evanger - Bolstadøyri	27.12.2011
1815	Point	BD662DBE-1E0E-4AE0-9DAB-79E168C1D6BD	140	Mestad	Mestad	26.12.2011 19:00:00
1865	Point	D075792E-75AB-49F8-B694-38DA687159DC	140	Berget	Berget	26.12.2011 01:05:50
2006	Point	3FD8582C-2073-4BEA-BE62-59775A259FC0	110	Svartaberget	Svartaberget	26.12.2011
2304	Point	35BA4FA4-5586-47F6-BF09-062C81186F1B	142	Aga/ULLENSVANG (flaum 2011)	<Null>	26.12.2011
2467	Point	D89B492A-DD53-4999-9F09-656F219BAF20	140	Aga	Aga	26.12.2011 18:00:00
2517	Point	50AAC445-26B8-4DE6-934B-9C14CCC37D2F	140	Aga	Aga	26.12.2011 18:00:00
2620	Point	ECEBF2CC-EC29-41BA-B34E-69B2960D0256	110	Lindvik	Lindvik	26.12.2011 08:42:00
2632	Point	A2E23722-D1F7-4824-BB7B-E8B5F1FD4BA4	140	2330-00002 Bulken - Evanger	Bulken - Evanger	26.12.2011
2647	Point	E97B7BD9-31C5-4723-81AE-2A917D4A984F	140	Myrkdalstunnelen	Myrkdalstunnelen	26.12.2011
2661	Point	4F1217BB-B449-4C80-AE14-CDB8035CD09F	140	Sekse/ULLENSVANG (flaum)	<Null>	26.12.2011
2868	Point	C83199B2-857C-4CFB-AB9A-D107B72926F5	140	Kyskredo	Kyskredo	26.12.2011 09:51:00

Figure 4.1: Attribute table for "Dagmar" 2011, showing some of the attributes for the registered landslides. Here shown ID's, typology, location, and time.

In this work, a dataset of landslide polygons has been used as a supportive source during the mapping of landslide extension. This dataset was obtained from supervisor Graziella Devoli on 06.06.2018. The dataset contained 317 polygons drawn by two other students during their master thesis (Bakken, 2017; Bugge, 2017) representing landslide occurred between 1966 and 2015.

4.2.1 Additional information about landslides

Photos were used as an additional source to map the landslides. The photos were obtained directly from NVE (11.10.2018), from newspaper articles, and RegObs, the two latter sources also included written information on location and time of occurrence. The pictures were useful to identify landslide typology, location, and defining the extension. Other online sources used were newspaper articles, google street view, which was used together with google earth, and reports from the NVE and road authorities during the mapping of the landslides. How the sources were used together is explained further in chapter 5.2.3.

Weekly summaries from the Norwegian landslide forecasting and warning service were obtained from NVE on 14.06.2018. These contained weather forecasts, warning messages issued from NVE, number of landslides registered, evaluations of whether the warnings were considered correct or not, and photos of landslide events in the period of interest.

4.3 Aerial photos and lidar imagery

Aerial photos were accessed from www.norgeibilder.no through a WMS (Web Mapping Service). Fourteen aerial photos taken between 2006 and 2016 were used. However, only seven photos were available for the areas of interest after 2011. Lidar imagery was accessed from www.hoydedata.no through a WMS (Web Mapping Service). Thirteen lidar images were used in the mapping, taken between 2009 and 2016. Only five images were available after 2011. The lidar images are dated with the year, but the exact date of the image is unknown. The Norwegian Mapping Authority (Kartverket) could not provide the dates, Satellite imagery from several sources was also attempted, like planet labs (planetlabs.com) and Sentinel (hoydedata.no), but the images available had low resolution and were therefore not useful for this work.

4.4 Information about landslide warning and thresholds

Warning messages and warning levels issued between 2011-2017 were obtained from xgeo.no and varsom.no. Varsom.no shows warning messages, geographical information, weather forecasts, precipitation radar images, in addition to educational material to change awareness and behavior.

The previously mentioned webpage xgeo also contains a map of the warning area and the warning levels that are disseminated each day.

The landslide warning thresholds (Hydmet, figure 2.5), and the separate values for relative water supply and relative soil water saturation were accessed directly from NVE for the dates of interest. The dataset consisted of ASCII-files and was obtained on 04.03.2019.

4.5 Geological and topographical information

Several maps showing geological and topographical information were downloaded or accessed through web portals.

Geological maps of bedrock and quaternary deposits were downloaded from Kartverket.

- The bedrock map was accessed on 24.10.2018 from:
    - https://kartkatalog.geonorge.no/metadata/norges-geologiske-undersokelse/berggrunn-n250/7c39be66-77b6-4b74-b58d-53b6bee90067
- The quaternary deposits map was accessed on 24.10.2018 from:
    - https://kartkatalog.geonorge.no/metadata/norges-geologiske-undersokelse/losmasser/3de4ddf6-d6b8-4398-8222-f5c47791a757

Other maps were accessed directly through the University of Oslo and NVE.

- A digital terrain model (DTM) for the county were downloaded from an all-access folder available to students of the University of Oslo on 14.11.2018.

- Maps of landforms were accessed on 15.12.2018 directly from NVE.

- Susceptibility maps were obtained on 06.02.2018 directly from NVE.

5 Method

The method is split into several parts, all of which are included in the flow chart (figure 5.1). Because this thesis is part of the same NVE project as the thesis from Mongstad (2018), similarities can be observed in the approaches used in this analysis.

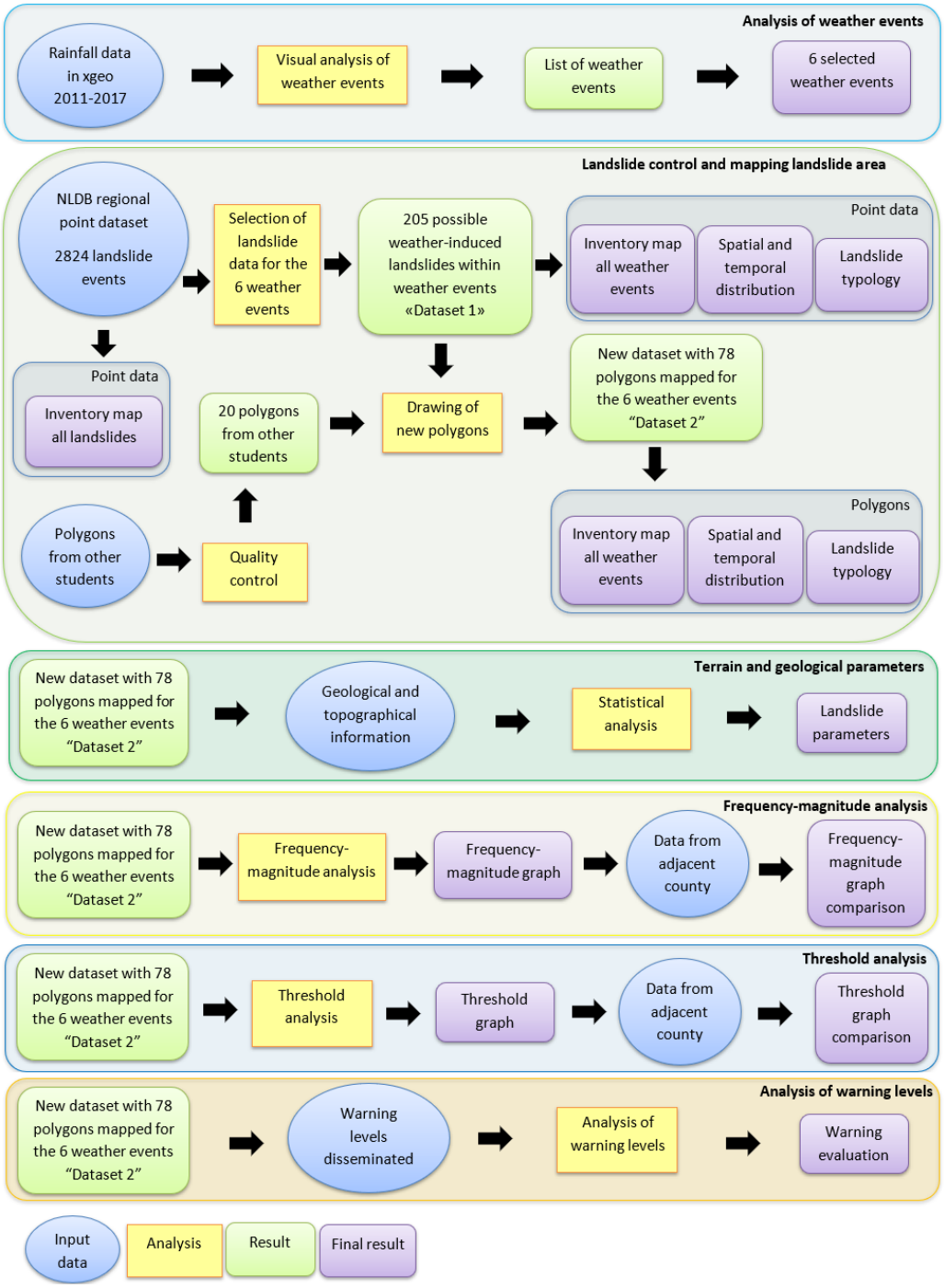

Figure 5.1: Flow chart showing the data used, the method, and the results from the analyses performed.

5.1 Analysis of weather events

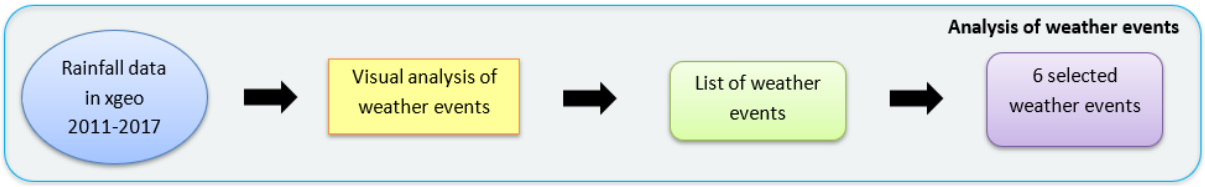

Figure 5.2: The methodology of the analysis of rainfall events.

The first task was to identify specific rainfall events that triggered landslides that could be mapped. This was done by looking at the raster map of interpolated daily rainfall available at xgeo.no for those days when it was raining more than 20 mm somewhere in Hordaland. For each of these events, it was analyzed if they triggered landslides. Because of time restriction, a precipitation level above 40-60 mm per day was considered to obtain more severe weather events. These were herein defined as a "rainfall day". Figure 5.3 shows the spatial distribution of two examples of a rainfall event, one above 20 mm and the other above 40 mm. Each event was listed in a table for an overview of interesting dates within the chosen period 2011-2017 (figure 5.3). Weeks with precipitation above the threshold were marked in green as interesting weeks, and all those above the 40-60 mm threshold were marked specifying the geographical location of the most intense rainfall. The threshold was then increased further to above 100 mm of precipitation, for more extreme events. One or more days above this threshold is herein called a "weather event".

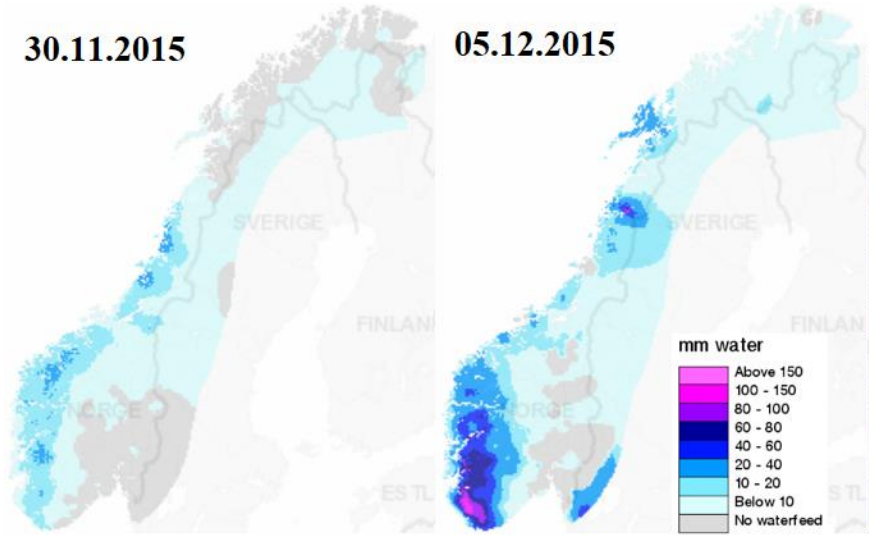

Interessante datoer

Uke	Dato	Nedbør i mm (max)	Område
Uke 47	16.11.2015	60-80	NW
	17.11.2015	40-60	NW+S
Uke 48	23.11.2015	20-40	NW
	24.11.2015	20-40	W
	26.11.2015	80-100	NW
	27.11.2015	60-80	NW (+S)
	28.11.2015	40-60	S (+C)
	29.11.2015	40-60	SE
Uke 49	30.11.2015	20-40	NE+SE
	02.12.2015	40-60	NW+C+S
	03.12.2015	40-60	S
	04.12.2015	100-150	S (+C+N)
	05.12.2015	100-150	NE (+C+S)
	06.12.2015	40-60	NE
Uke 50	08.12.2015	40-60	NE+C+S
	09.12.2015	80-100	S (+N-C)
	10.12.2015	40-60	NE
	11.12.2015	20-40	N+C

Figure 5.3: Example of visual inspection in xgeo and information transformed into a table on the right. The maps show examples of low and high precipitation on the west coast before and during the weather event "Synne" in 2015. The dates of the weather event are marked in orange in the table. The maximum intensity precipitation (mm) in the table is marked with the representative color used for the map in xgeo.

A qualitative description of the precipitation was also done by distinguishing if the precipitation fell as either rain, snow, sleet or a mix of these. The list of weather events was then combined with warning messages sent by NVE, and the number of landslides registered in the NLDB during the same day. Weekly summaries were provided by NVE, which also include whether the warning sent out was considered correct or not. Because of the large number of weather events on the list, it was decided during the process to focus the analysis only on specific extreme events which have resulted in a high number of landslides.

The list weather events were also compared with a preliminary list of known significant weather-induced landslide events in Western Norway obtained through my supervisor Graziella Devoli to check that all were included. The events chosen for further analysis in this thesis were the extreme weathers on 26-27th November 2011 ("Berit"), 26-27th December 2011 ("Dagmar"), and 15-16th November 2013 ("Hilde"), snowmelt and rainfall on March 20th, 2014, rainfall and flood on 26-29th October 2014 and extreme weather on 4-6th December 2015 ("Synne"). The events are described in detail in chapter 6.1.1. The events were especially interesting due to work performed in the adjacent county Sogn og Fjordane, in a previous master thesis by Håvard Mongstad (Mongstad, 2018). It was therefore of interest to investigate any similarities or differences of results between the two counties.

5.2 Landslide control and mapping landslide area

The landslide control and mapping were done in several steps using two sources of data, both point data, and polygons. These are shown in blue circles in figure 5.4.

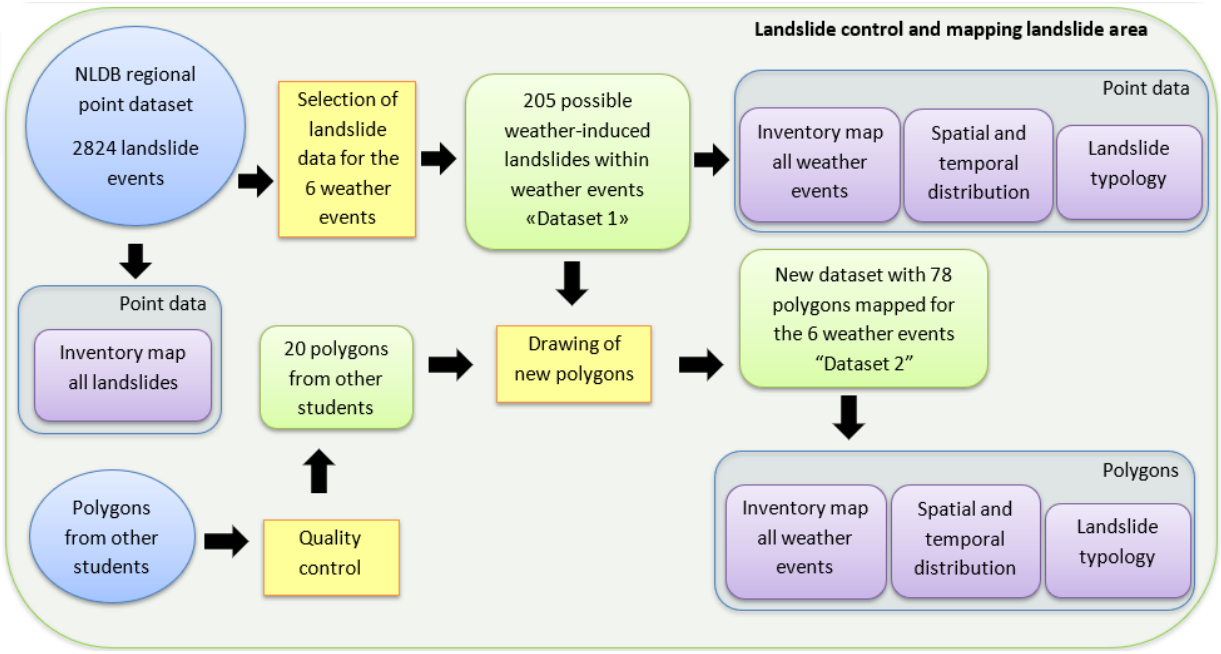

Figure 5.4: The methodology of the landslide control and mapping landslide area.

5.2.1 Collection and selection of landslide data: "Dataset 1"

To perform the mapping of the region of interest, point data from the national landslide database (NLDB) were downloaded from NVE on 20.07.2018. It was then loaded into the application ArcMap in the program ArcGIS for spatial analysis. This database includes a geographic point at the location of the event, along with other information registered about the event such as date, topologies, and descriptions. The data set included a total of 2824 mass movements of different typologies for Hordaland county within the selected time frame 2011-2017 (figure 5.5). For the analysis of rainfall-induced landslides, only some typologies were of interest, and the others were therefore removed from the data set. These excluded typologies included snow avalanche types, ice fall, and rock fall. All typologies in the dataset are shown in table 5.1, both in Norwegian and with English translation. The English translations are retrieved from Jensen et al. (2015).

After the landslides were sorted by typology, they were sorted by date. Because of all the possible errors in the database, Krøgli et al. (2018) recommended to always perform a quality

control before an analysis is done. The landslide events recorded in the database present several possible errors similar to the ones indicated by Sokalska et al. (2015):

- The same event registered twice by the same person or institution, in two different locations.
- The same event registered twice by two different people or institutions, in different locations, with different level of details and usually different landslide typologies.
- Events registered by different people, in the same place, but as different landslide typologies.

The name of the area might be wrong, or to general. The location of the point can also be wrong, being placed far away from the landslide itself. Sometimes the attribute table has included the accuracy of the location, and this can be resolved. The point is, as mentioned, often located at the place of damage, therefore not where the landslide initiated (Sokalska et al., 2015). The time of the event can also be wrong but do often include accuracy as well. For example, some landslides have an accuracy of 5 years, and some do not have a date at all. Landslide data like this is not accurate enough for analysis, especially if in connection with hydrometeorological data and analysis of the occurrence of events (Sokalska et al., 2015). For the analysis presented herein, the dates are assumed to be correct, to have a basis for the selection of the landslides that will be mapped. The typology of the landslide is also a possible error, as several landslides may be registered with the wrong typology. As this is a possibility, several typologies are included in the data set, and then excluded by further analysis.

The polygons and the point data from NLDB were all combined into one functioning data set. The coordinate system of the polygons was changed, so all datasets have the same (ETRS 1989 UTM Zone 33N). The polygons were sorted by typology and date and used as an initial guide to see which areas in Hordaland have been mapped before. The initial objective was to include the existing polygons in the new dataset, but new polygons were drawn instead on top of the old.

As mentioned, several point data might be representing the same landslide, leading to a double registration. All points are included in “dataset 1”, to investigate if this could be the case for any of the landslides. After sorting by date, a dataset consisting of 205 landslides was made (“dataset 1”). The dataset contains:

- 28 landslides occurring during 26-27 December 2011 (“Berit”)
- 85 landslides occurring during 26-27 December 2011 (“Dagmar”)
- 5 landslides occurring during 15-16 November 2013 (“Hilde”)
- 35 landslides occurring on March 20th, 2014
- 35 landslides occurring during 26-29 October 2014
- 17 landslides occurring during 4-6 December 2015 (“Synne”).

The different weather events of interest were put into separate feature layers, separating the different point data from each other. The separation gave an easy overview of the data available for the different events, and also helped work on the events separately while still keeping the results systematic.

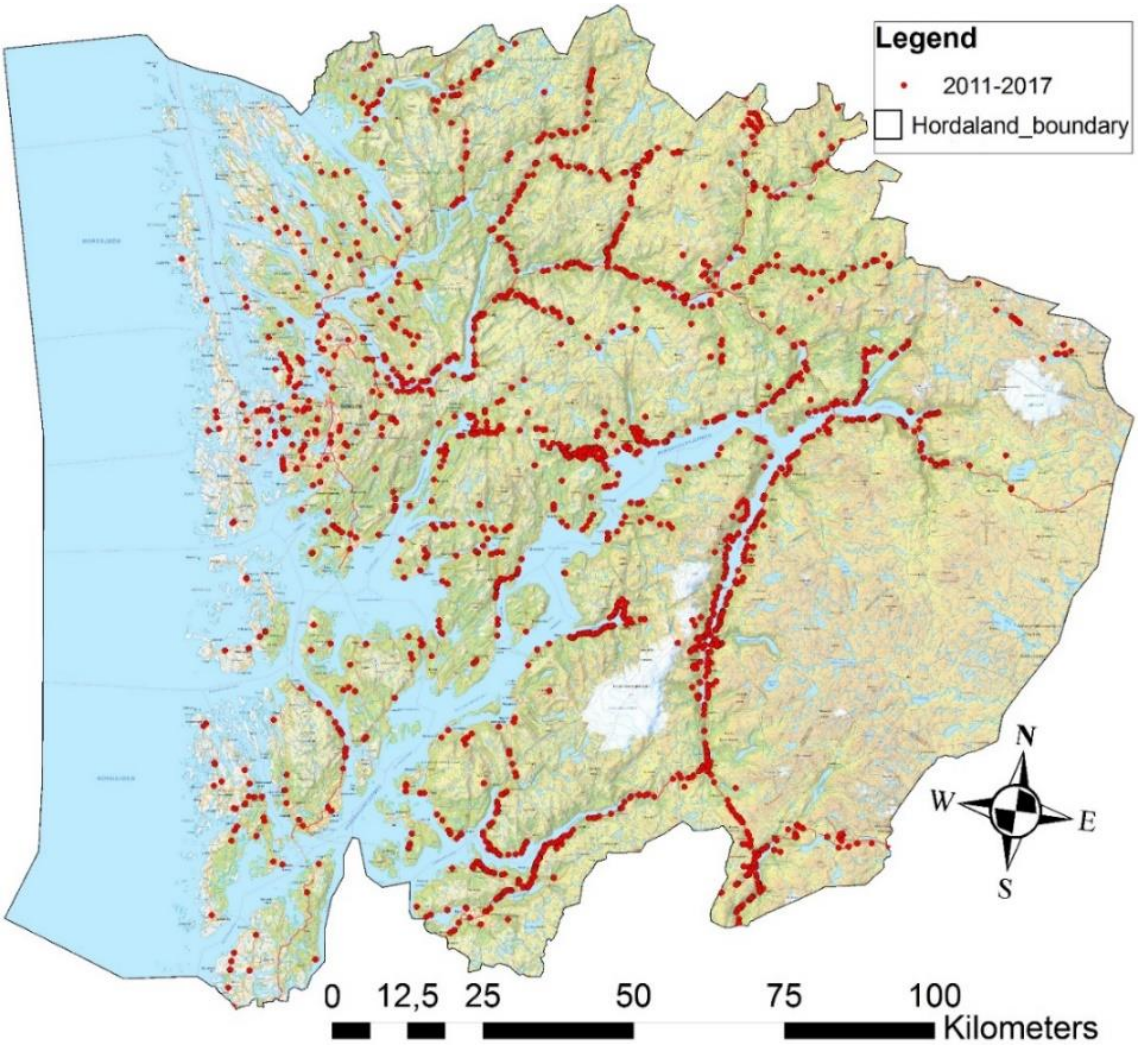

Figure 5.5: Mass movements registered in Hordaland during the period 2011-2017. The total number of mass movements is 2824.

*Table 5.1: Number of rainfall-induced landslides from the original dataset of 2824 mass movements, and translations of the relevant typologies in the Norwegian landslide database from Jensen et al. (2015). All typologies marked in grey were excluded, and the white rows were included in the dataset. *No translation found.*

Code	Number	Typology in Norwegian	Typology in English
110	420	Steinskred uspesifisert	Unspecified, rock fall, rock block topple or rock slide
111	1287	Steinsprang, uspesifisert	Rock fall, unspecified
112	20	Lite fjellskred	Small rock avalanche
130	355	Snøskred, uspesifisert	Snow avalanche, unspecified
131	1	Vått løssnøskred, uspesifisert	Wet, loose snow avalanche, unspecified
133	57	Sørpeskred	Slush flow
134	1	Løssnøskred, uspesifisert	Loose snow avalanche, unspecified
135	16	Vått løssnøskred	Wet loose snow avalanche
136	8	Tørt løssnøskred	Dry loose snow avalanche
137	13	Flakskred, uspesifisert	Slab avalanche, unspecified
138	23	Vått flakskred	Wet slab avalanche
139	43	Tørt flakskred	Dry slab avalanche
140	297	Løsmasseskred uspesifisert	Landslide in soil, unspecified
142	45	Flomskred	Debris flow
144	117	Jordskred	Debris slide or debris avalanche
145	2	Jordskred, uspesifisert	Debris slide or debris avalanche, unspecified
150	75	Isnedfall, uspesifisert	Ice fall
151	3	Skavlfall	Snow-dune fall*
160	37	Utglidning av vei	Shallow planar soil slide or shallow rotational soil slide
190	4	Ikke angitt	Not specified

5.2.2 Quality control: received polygons

In previous years, students and NVE personnel have mapped landslide area in the form of polygons. These polygons were received on 06.06.18 and loaded into ArcMap. The polygons received from NVE personnel were, however outside the period of interest and were therefore excluded. The polygons received from the other student's thesis work (Bakken, 2017; Bugge, 2017) were sorted by location and time. Some of the polygons drawn by Bakken (2017) were outside of Hordaland county and were therefore removed from the data set. Many of the polygons were dated as approximate intervals of years, and these were kept in the data set to investigate if any of these occurred within the chosen weather events. The polygons drawn by Bugge (2017) were then sorted by the dates of the weather events. Both polygon data sets were then placed into the previously made feature layer groups in ArcMap for the weather events.

These polygons were used as an initial guide to which areas contained sufficient sources to map landslides. It was of interest to include the polygons in the new dataset, but the sources and criteria of these polygons are not known, and the interpretation of the landslide tracks was slightly different. It was decided to draw new polygons in the new "dataset 2". Some of the new polygons, therefore, correspond to the polygons made by other students. This is marked in the

attribute table and is shown in appendix 1. The polygons were located mostly along the steep sides of Sørfjorden, as well as inner Hardangerfjorden and Nordheimsund.

5.2.3 Drawing of the new polygons: "Dataset 2"

The new polygons were drawn using different sources available. The locations of the received polygons were investigated first, then the rest of the point data in the database on the dates of the weather events. The new polygons in "dataset 2" were mostly mapped in map scale 1:5000, after recommendation through supervisor Graziella Devoli. The reason being that this is the map scale used by consultants when performing hazard mapping. By using the different available sources, a polygon is drawn around the traces of the landslides, as shown in figure 5.6. Several sources were used for drawing the polygons, these are described separately, and the sources used for each polygon is listed in appendix 2.

Out of the 205 point registrations in the database ("dataset 1"), 75 polygons could be mapped with a polygon ("dataset 2"). 110 points could not be mapped, and 20 points were possible double registrations in the database. These points could not be verified, and it is difficult to confirm if they are doubles or not. Three additional landslides not registered in the database were mapped based on other sources like news and pictures taken by NVE. An example is shown in figure 5.7, where the bottom polygon does not have a point registration in the database.

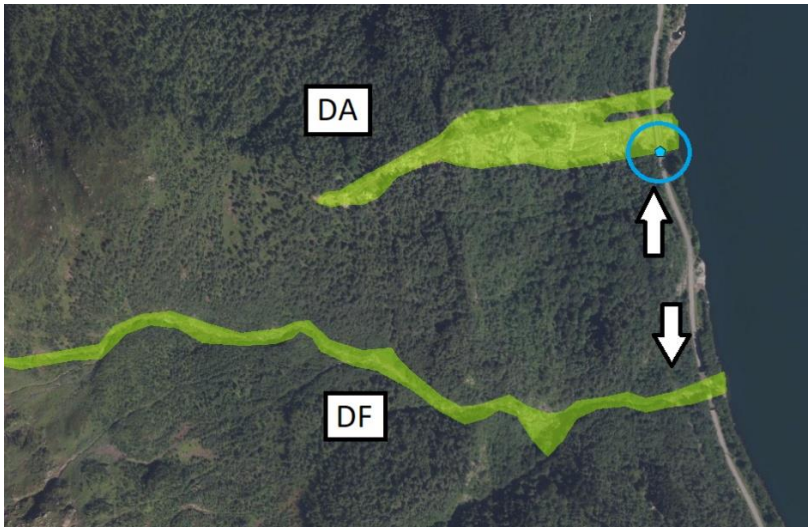

Figure 5.6: Example of two polygons drawn on top of an aerial photo. The debris avalanche (DA) is registered in the database; the point registration is shown in blue. The debris flow (DF) was not registered in the database but was featured in the news.

Aerial photos

Photogrammetry is the most useful method to map landslide extension where either there is little or no vegetation, or when the debris flow has removed the vegetation on the slope (Jakob, 2005). The mechanism of the slide can also be confirmed by looking at the aerial photos if the geometrical shape is distinctive enough. The first source used to map the landslides were aerial photos of the area from norgeibilder.no, with the coordinate system Euref89 UTM33 (appendix 3). The photos were added to ArcMap through a WMS-server, and photos from before and after the events were used to spot differences such as soil discoloration and disturbed vegetation (Sokalska et al., 2015). An example is shown in figure 5.7, with a debris avalanche (top) and the deposit of a debris flow (bottom).

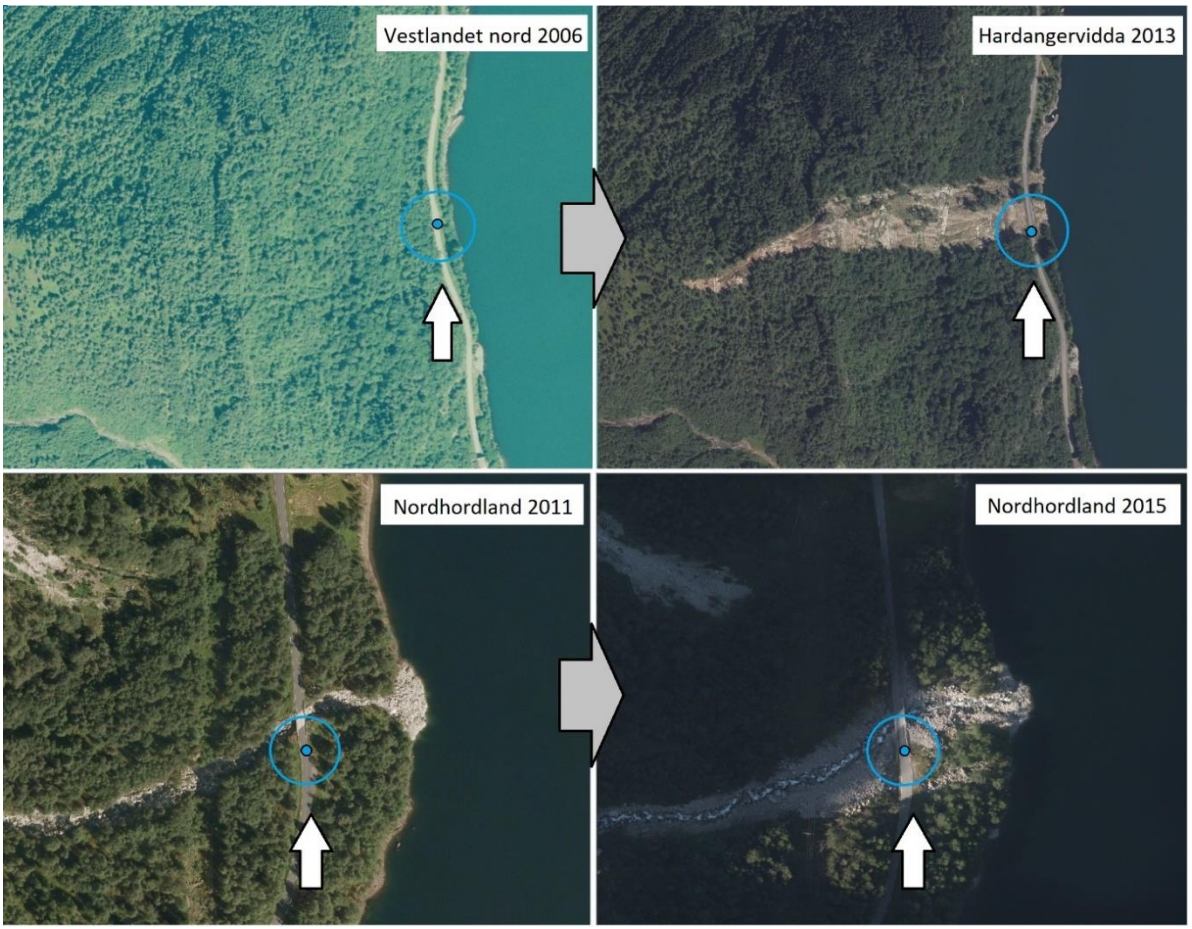

Figure 5.7: Examples of aerial photos before (left) and after (right) a landslide occurred, showing the traces visible after the event. A debris avalanche (top) and the deposit of a debris flow (bottom). The point registrations from the database are marked in blue circles.

For some slide occurrences, however, aerial photos alone were not enough to fully confirm the total area of the landslides. In these situations, several aerial photos were used, as these varied in quality. Since the aerial photos were taken in different years, they were compared to be sure that they show the same landslide and not an earlier or later one. Figure 5.8 shows the temporal distribution of the aerial photos used, together with the dates of the events. It shows clearly a lack of aerial photos taken between the different weather events herein analyzed, and as well as the lack of aerial photos in later years.

Weather event	Aerial photo date	Aerial photo name
	19.07.2006	«Vestlandet Nord 2006»
	22.08.2007	«Indre Sogn 2007»
	11.06.2008	«Voss og Vaksdal 2008»
	18.08.2008	«Hardangerjøkulen 2008»
	02.09.2010	«Kvam 2010»
	05.09.2010	«Odda 2010»
	13.07.2011	«Nordhordland 2011»
26.11.2011 - 27.11.2011 ("Berit") 26.12.2011 - 27.12.2011 ("Dagmar")		
	21.07.2012	«Hardanger-Voss 2012»
	02.09.2013	«Etne-Kvinnherad 2013»
	27.09.2013	«Hardangervidda 2013»
	28.09.2013	«Vestlandet 2013»
15.11.2013 - 16.11.2013 ("Hilde") 20.03.2014		
	10.09.2014	«Eidfjord-Ulvik-Granvin 2014»
26.10.2014 - 28.10.2014		
	09.09.2015	«Nordhordland 2015»
04.10.2014 - 06.10.2015 ("Synne")		
	02.10.2016	«Voss Fusa Samnanger 2016»

Figure 5.8: The dates the available aerial photos were taken, combined with the dates of the weather events investigated.

In some instances, the registered landslide was not visible, or there was a doubt that the visible landslide was the right one, being far away from the point registration. In these situations, the point data from the entire NLDB within the time frame were turned on in ArcMap, to see whether other registered landslides have occurred at the same location. In some cases, there were no other points registered, and the landslide visible in the aerial photo was assumed to be the registered one. In other cases, another point (or more) were registered in the database within the dates of the aerial photos, and the landslide could not, therefore, be confirmed. However, if the landslides were of different typologies, and the visible landslide was identifiable in the aerial photo, the typology was assigned and the landslide mapped with a polygon. In other instances, the typology registered did not fit the geometrical shape of the visible landslide, and it was then assumed that the track belonged to the other registered event. As some landslides of other typologies were included during this step, these typologies were assumed to be correct.

Lidar images

Lidar images were also used as a supportive source also accessed through a WMS-server from hoydedata.no (appendix 4). In several instances, an area had lidar images both before and after an event, and the landslide was therefore visible. Lidar images were useful to find the track, especially when landslides were in a shadow area or under vegetation in the available aerial photos (figure 5.9). Several debris flows followed rivers or gully's downstream, and as these are visible in a lidar photo, the polygon could be drawn even though the landslide were not visible in the aerial photo. In a few cases, the lidar image was the main source of the drawn polygon, as the aerial photos were not very useful.

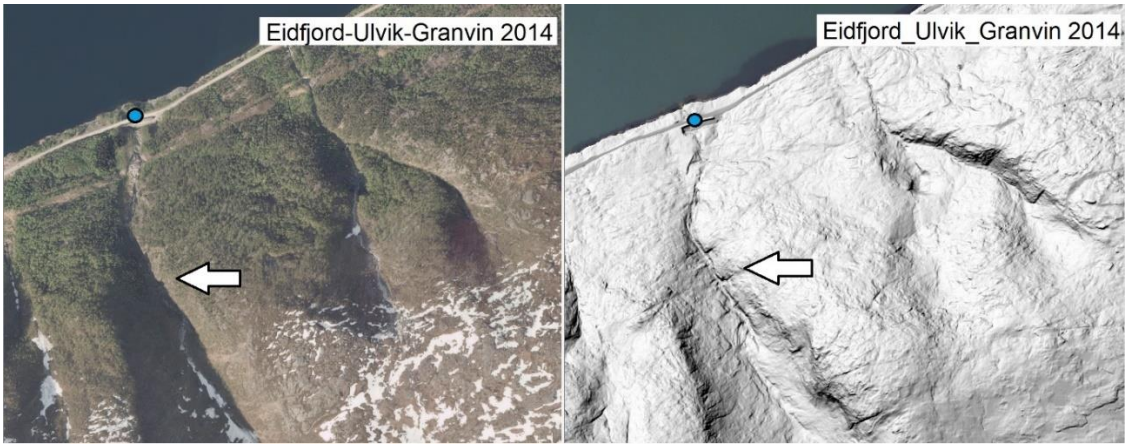

Figure 5.9: Example of how lidar images were useful when challenges with aerial photos occurred. The area is covered by forest and shadows in the aerial photo (left), the track is easier to spot with lidar imagery (right). White arrows show the gully, and the blue point is the registration from the database, where the landslide hit the road.

Newspaper articles

Newspaper articles can also be useful for locating and properly map landslides. Newspapers can give information on (a): landslides that occurred close to infrastructure and are reported many times and are registered in the landslide database, (b): also on landslides that are not registered in the database. The landslides reported in the media are often the ones affecting the population. Landslides that do not cause damage might not be registered in the landslide database (Sokalska et al., 2015). The focus of this thesis was mapping landslides caused by extreme weather events, and because of that, several landslides were reported in the newspapers. The landslides making headlines were the ones affecting roads and buildings, and this was only a useful source for some of these landslides like the ones shown in figure 5.10, and also the debris avalanche in figure 2.1C.

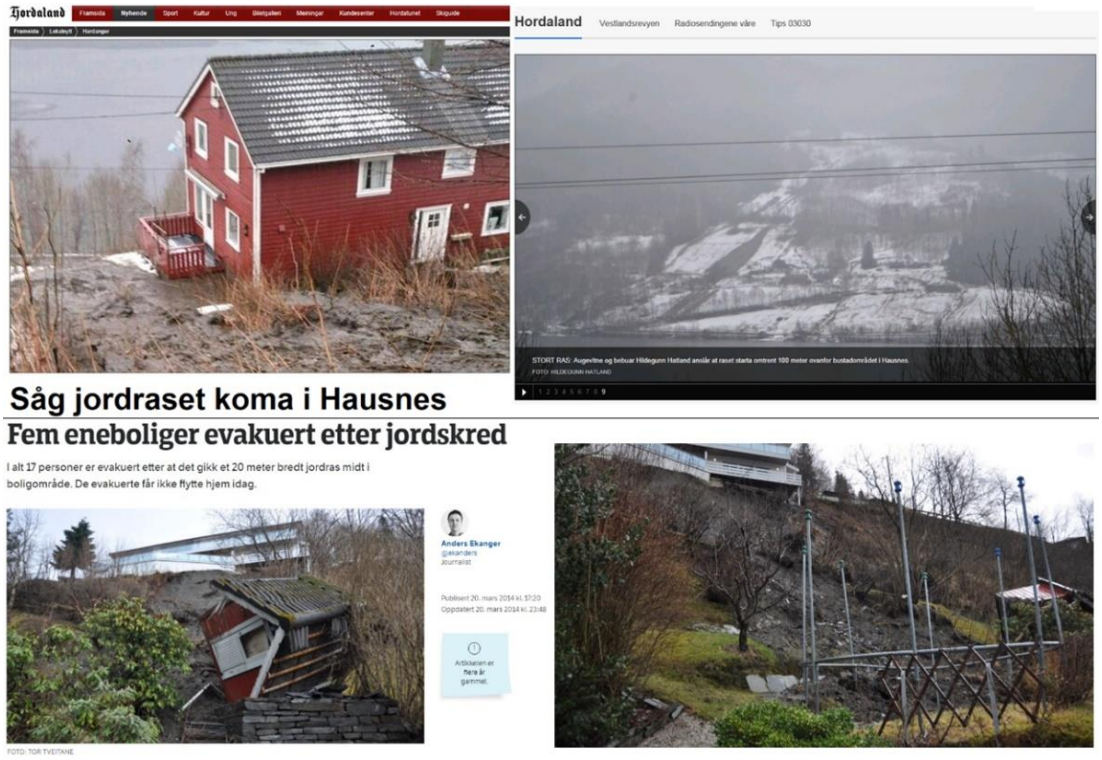

Figure 5.10: Examples of landslides reported by newspapers. ***Top****: News covering debris avalanche hitting a house, with several pictures of the extent of the landslide (Sources; Fjordaland avis and NRK).* ***Bottom****: News covering a debris slide in the middle of a neighborhood. There were not any aerial photos or lidar images available of the event, but eight pictures of the landslide in the media from different angles (Sources; NRK).*

The left picture in figure 5.11 shows an example of a landslide that was featured in the media repeatedly but not registered in the landslide database. It is possible that this was because it was caught by a gallery (mitigation measure) above the road. The landslide was in the media due to the drivers seeking shelter beneath the structure, because of other landslides in the area. As the NPRA is responsible for registering landslides along the roads, it is assumed that the landslide was not registered because the road was not damaged.

Another landslide that was mapped is shown in the right picture in figure 5.11. The landslide was not registered as a part of the event "Dagmar" in 2011 but was registered as occurring one month before, during the storm "Berit". A picture of the landslide was however used in a report from NPRA (NPRA, 2012) about landslides occurring during "Dagmar" and was therefore assumed to possibly be registered with the wrong date and included in the "Dagmar" data set.

Figure 5.11: Examples of the use of photographs. ***Left****: Picture of a landslide hitting a mitigation measure along Sørfjorden. The news coverage focused on the trailers trapped below it, as the road on both sides was blocked by other landslides, but this landslide was not registered in the database. Deposit material is shown with a red circle (Source; NRK).* ***Right****: Example of a landslide that might have the wrong date in the database, because of contradicting sources. The picture shows a debris flow after "Dagmar" 2011 from the NPRA, with the red line showing where the track is.*

Other photos

Several pictures were obtained from NVE, taken during a field trip in Sørfjorden in May 2012 after "Dagmar" 2011. These were used to confirm and check some of the mapped landslides. Some pictures taken by civilians were also obtained from RegObs. Figure 5.12 shows a few of the pictures used to confirm landslides registered in the NLDB.

Figure 5.12: Examples of pictures of landslides taken by NVE personnel and available at RegObs. The two pictures on top that was taken by Aart Verhage, and the lower left that was taken by Odd-Arne Mikkelsen, all three pictures taken in the field after "Dagmar" 2011. The lower right is a registration from the RegObs platform of a landslide occurring March 20th, 2014, taken by Øystein S. Lohne.

Google earth pro

The program Google earth pro was also used as a supportive source, mostly to get a three-dimensional visual impression of the terrain around the landslide, since classical stereoscopic interpretation was not used. An example is shown in figure 5.13, where two landslides have their source areas near each other but have propagated in different directions due to the topography in the area.

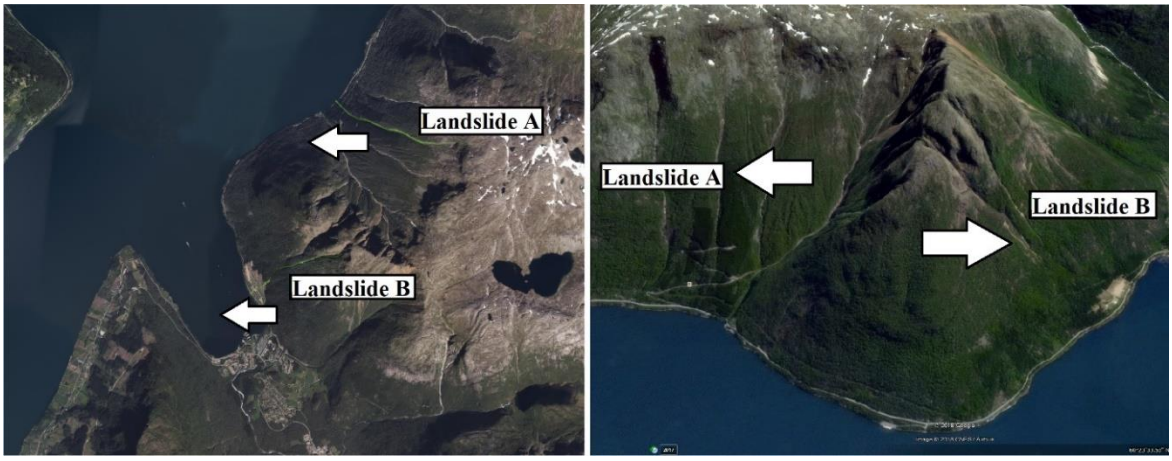

Figure 5.13: Example of how Google earth pro was used as a supportive source, The polygons and aerial photo on the left, and the same area in google earth pro on the right. It is clear in the right picture that the landslides have very different slope aspects of their slopes.

Google street view

Google street view was used to find the right location of some landslides. Photos that were obtained from the Norwegian Public Road Administration (NPRA, 2012) were used together with aerial photos to map the polygon. An example is shown in figure 5.14. The location of the landslide pictured on the left was found in google street view (middle). The same landslide pictured in an aerial photo is shown in the right. The pictures obtained from google street view were from 2009 and did therefore not show the landslide, but the buildings in the area coincide with photos and aerial photos.

Figure 5.14: Example of how google street view was used to find the right location of landslides. Picture taken by the NPRA, the location on google maps and the aerial photo of the same area.

5.3 Terrain and geological parameters

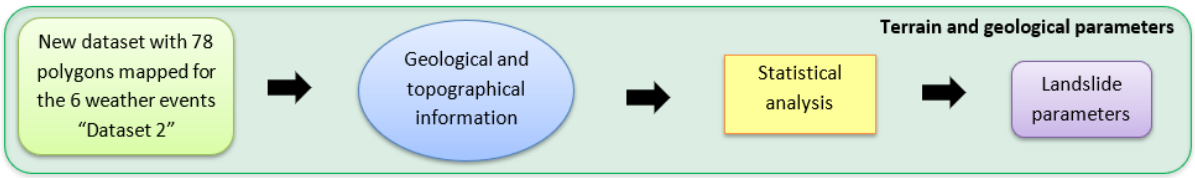

Figure 5.15: The methodology of the statistical analysis.

After the quality control and drawing of the new polygons, a DTM for the entire county was downloaded from an internal folder "lagringshotell vann" at UIO. The relevant raster files for Hordaland county were copied and loaded into ArcMap. The raster files were cut to the county borders and merged to one DTM raster file. Some adjustments were made in scale and color for practical and visual reasons. The DTM was used to find parameters and characteristics of the mapped landslides. The runout distances were found using the measuring tool manually, and zonal statistics were used to find other parameters like the maximum and minimum elevation for the landslides, the ranges in elevation, mean elevation and standard deviation. The H/L relationship of the landslides was calculated from these results.

The DTM was then used to make a slope gradient map over the county, with a cell size of 10 meters. The scale and colors were adjusted for practical and visual reasons. The slope angles at the initiation point of the landslides were found manually by the use of this map. Zonal statistics were also used on the slope map, acquiring minimum and maximum slope value, along with slope range, mean and standard deviation.

To investigate the geology close to the landslide locations, two WMS-servers were accessed from Kartverket (kartkatalog geoNorge) 24.10.18. The first WMS-server show the bedrock mapped in the area, and the other WMS-server show the quaternary deposits. The type of bedrock and Quaternary deposits in the source area of the landslides mapped was identified by zooming in on each polygon and visually inspecting the maps individually for each landslide. The quaternary map is shown in chapter 3.3.

To find any typical orientation of the landslides, the aspect was calculated using the approach from Davis (2002). The vector resultant R is calculated to find a dominant direction in the set of vectors, by summing up the sines and cosines of the individual vectors. From this result, the

mean vector direction is calculated (equation 1). The mean vector direction is the angular average of all of the vectors in a sample (Davis, 2002).

$$\bar{\Theta} = tan^{-1}\left(\frac{Y_r}{X_r}\right) = tan^{-1}\left(\frac{\sum_{i=1}^{n}\sin\Theta_i}{\sum_{i=1}^{n}\cos\Theta_i}\right) \quad (1)$$

The magnitude or length of the resultant R depends on both the amount of dispersion and the number of vectors. Therefore, the resultant is divided on the number of observations n. The result of this is the vector strength, or mean resultant length, is calculated with equation 2. The result will range from zero to one. A vector strength close to one shows that the values are tightly bunched together with a small dispersion, and a vector strength close to zero indicates that the vectors are widely dispersed (Davis, 2002).

$$\bar{R} = \frac{R}{n} = \frac{\sqrt{\sum_{i=1}^{n}\cos\Theta_{ir}^2 + \sum_{i=1}^{n}\sin\Theta_{ir}^2}}{n} \quad (2)$$

5.4 Frequency-magnitude analysis

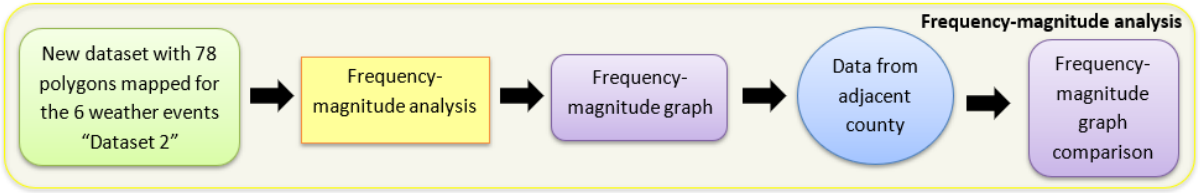

Figure 5.16: Methodology of the frequency-magnitude analysis.

To perform a frequency-magnitude analysis, the magnitudes expressed by area in m^2 and automatically calculated during the mapping of the polygon were used. A frequency-magnitude analysis can use either cumulative or non-cumulative statistics (Guzzetti, 2005). For this work, a cumulative distribution was chosen, and the method follows the methodology in Hungr et al. (2008) and Dahl et al. (2013). The landslide magnitudes were ranked from largest to smallest magnitude, and the individual landslide frequency (f_i) was calculated using equation 3. As the period investigated is 2011-2017, the T is set to 7 years.

$$f_i = \frac{1}{T} \tag{3}$$

The annual landslide frequency (F_i) is then calculated by summing up all the individual landslide frequencies using equation 4.

$$F_i = \sum_{i=1}^{n} f_i \tag{4}$$

The magnitudes of the landslides were then plotted against the annual landslide frequency, on a log-log scale. A frequency-magnitude plot was made with the data divided into the six weather events, to see how these influenced the data. A plot was also made with only data from the weather event "Dagmar", and the results were compared with similar plots from Sogn og Fjordane (Mongstad, 2018), which were also made using cumulative statistics.

5.5 Threshold analysis

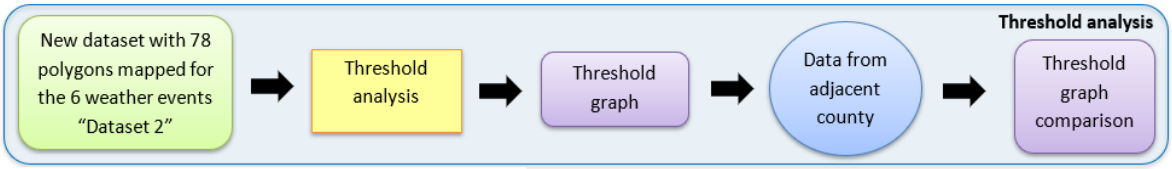

Figure 5.17: The methodology of the threshold analysis.

For the threshold analysis, daily data of relative water supply and relative soil water saturation from xgeo.no were acquired through NVE and entered into ArcMap in the form of a raster map ($1km^2$). Individual values of relative water supply and relative soil water content were manually extracted from the dataset by zooming into the initiation point of the polygons (figure 5.18). Since the daily data ranges from 07:00 one day to 07:00 the next day, an attempt to find an accurate time of the landslides were done.

The data were then extracted according to the time of day registered in the landslide database, as the mean value is representative until 07:00 the next morning. As several landslides occurred during the night, or in the early morning, the data were therefore extracted from the day before. The values extracted were then plotted in the Hydmet threshold plot (figure 2.5), to see how these fit with the proposed thresholds. The result is shown in chapter 6.5. The results were also compared to the plots from Sogn og Fjordane (Mongstad, 2018).

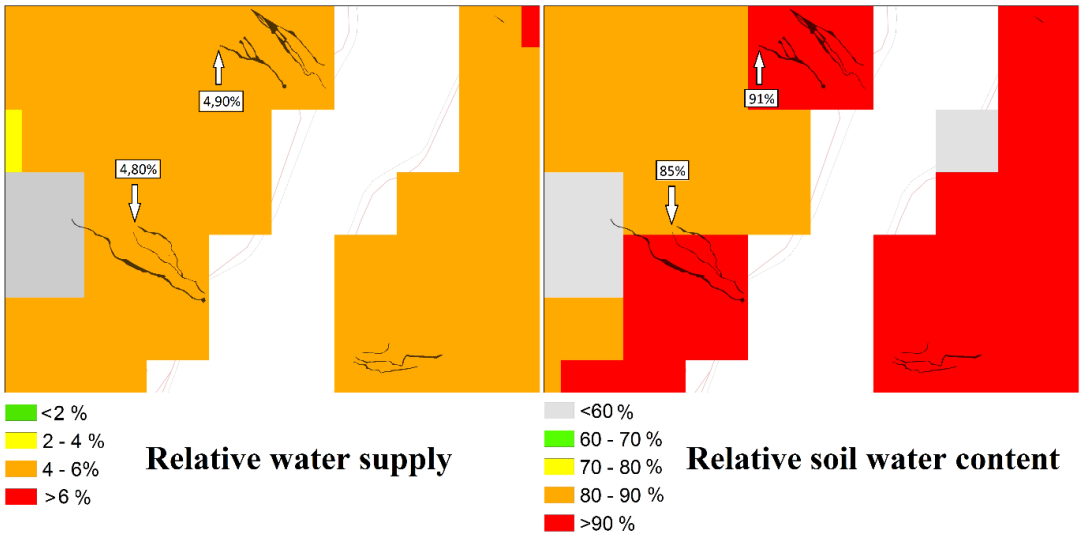

Figure 5.18: Example of the method of extracting data from the xgeo data in ArcMap, here shown data for landslides occurring between 07:00 on December 26th – 07:00 December 27th, 2011 in Sørfjorden during weather event "Dagmar". Relative water supply is shown on the left, and relative soil water content on the right. The data was extracted from the pixel of the initiation area of the polygons. Two examples are shown with white arrows. The white and grey areas are grid cells with "No data".

5.6 Analysis of warning levels

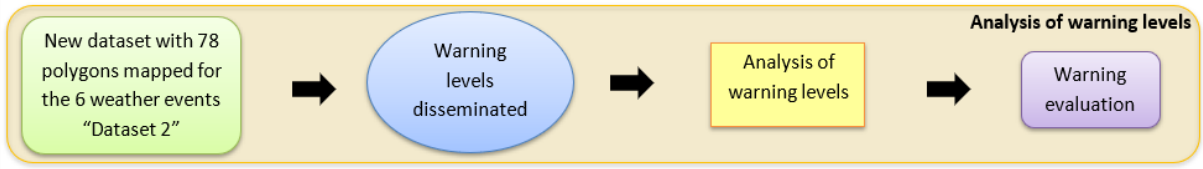

Figure 5.19: Methodology of the analysis of warning levels.

The warnings issued each day during the period 2011-2017 were found by going through all dates, the selected period, on the website Varsom.no. Since the warning service became public in 2013, the years during testing of the service 2011 and 2012 were not included here. Usually, one warning level was sent for most of the studied weather events. However, more than one levels can be issued in one day. An example is shown in figure 5.20, showing the second day of the event "Synne" on December 5th, 2015. The county is shown to have three different levels of warnings on this day, green, yellow, and orange (right in figure 5.20). The warning levels issued for the events are shown in table 6.4 in chapter 6.6. The maximum warning level was noted in an excel table, which was used to make the graph in figure 6.32 shown in chapter 6.6.

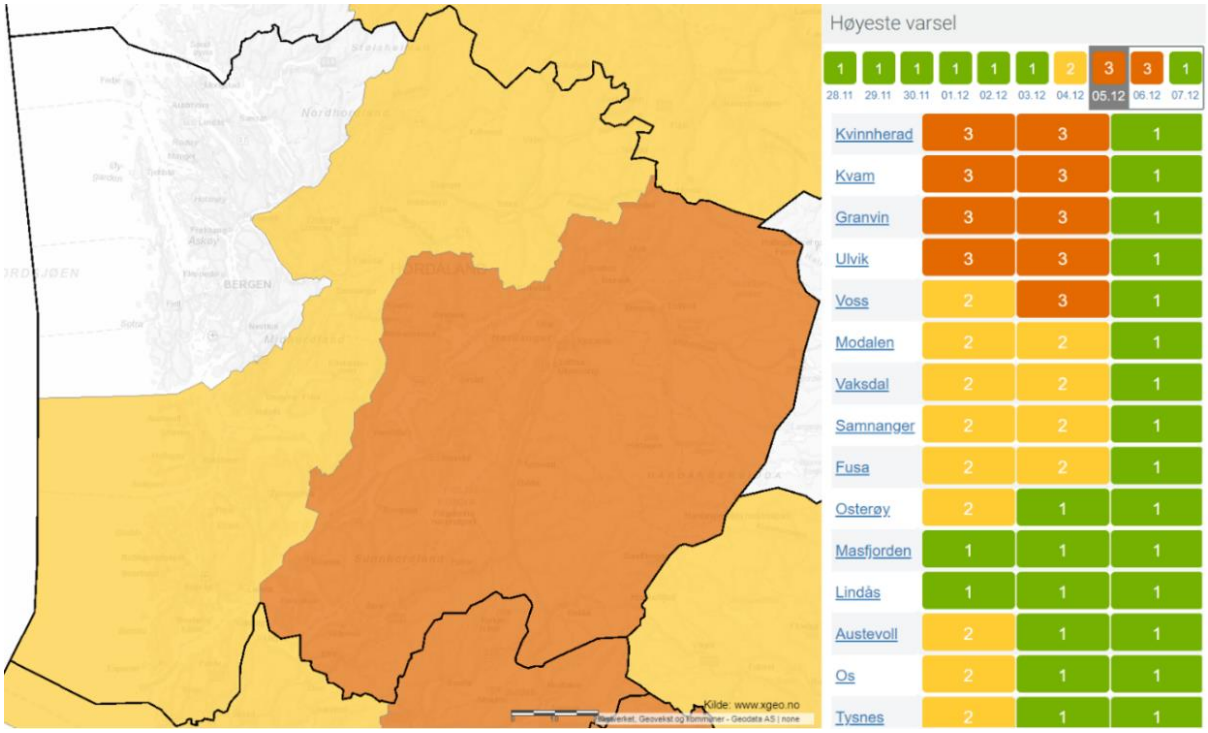

Figure 5.20: Example of warning levels issued in Hordaland. Here an example from December 5th, 2015, showing green, yellow, and orange level in the same county.

6 Results

In this work, landslide events occurring in Hordaland county in the period 2011-2017 were studied. A preliminary rainfall analysis was done, to find landslides triggered by rainfall events. The focus was on extreme rainfall events, and six extreme weather events were analyzed. The landslides occurring during these weather events were mapped in the program ArcMap. The mapped landslides were then characterized in relation to their topography, geology, and landslide parameters. Lastly, the warning disseminated during these extreme weather event was analyzed in relation to the occurred landslides.

6.1 Weather events that triggered landslides in the period 2011-2017

The weather events occurring in Hordaland from 2011 to 2017 were analyzed. In particular, weather events with precipitation above 40 mm were considered for further analysis (figure 6.1). The maximum precipitation in the county exceeded 40 mm in 361 days over the seven years investigated. Twenty-five days had maximum precipitation above 100 mm (figure 6.2), which are combined as 20 weather events lasting 1-4 days. Seven of them received names, being characterized as "extreme weather events". Of these, two occurred in 2011 (Berit and Dagmar), one in 2013 (Hilde), one in 2015 (Synne), and three in 2017 (Ylva, Aina and Birk). They were all characterized by strong winds and heavy precipitation. While the majority of the extreme weather events occurred in November and December, for the other weather events, the monthly distribution is spread out throughout the year. This was not unexpected, as frequent and heavy rainfall is a common occurrence in this part of the country (figure 3.4). The year with most weather events with precipitation above 100 mm was 2015, with four events. It was then investigated how many landslides occurred during these events (figure 6.3). The extreme weather event "Dagmar 2011" seems to have the highest number of landslides (85) registered in the database, followed by six weather events which have around 30 landslides registered each. Two weather events have between 10-15 landslides registered, and ten weather events have between one and six landslides. Two weather events did not cause any landslides. Six extreme weather events were later studied in detail; these are marked in green in figure 6.2 and the table in figure 6.3. These are herein called "Berit 2011", "Dagmar 2011", "Hilde 2013", "March 2014", "October 2014", and "Synne 2015". The exact period the event lasted is shown

in the figures above. The monthly distribution of the six weather events selected is shown in figure 6.4.

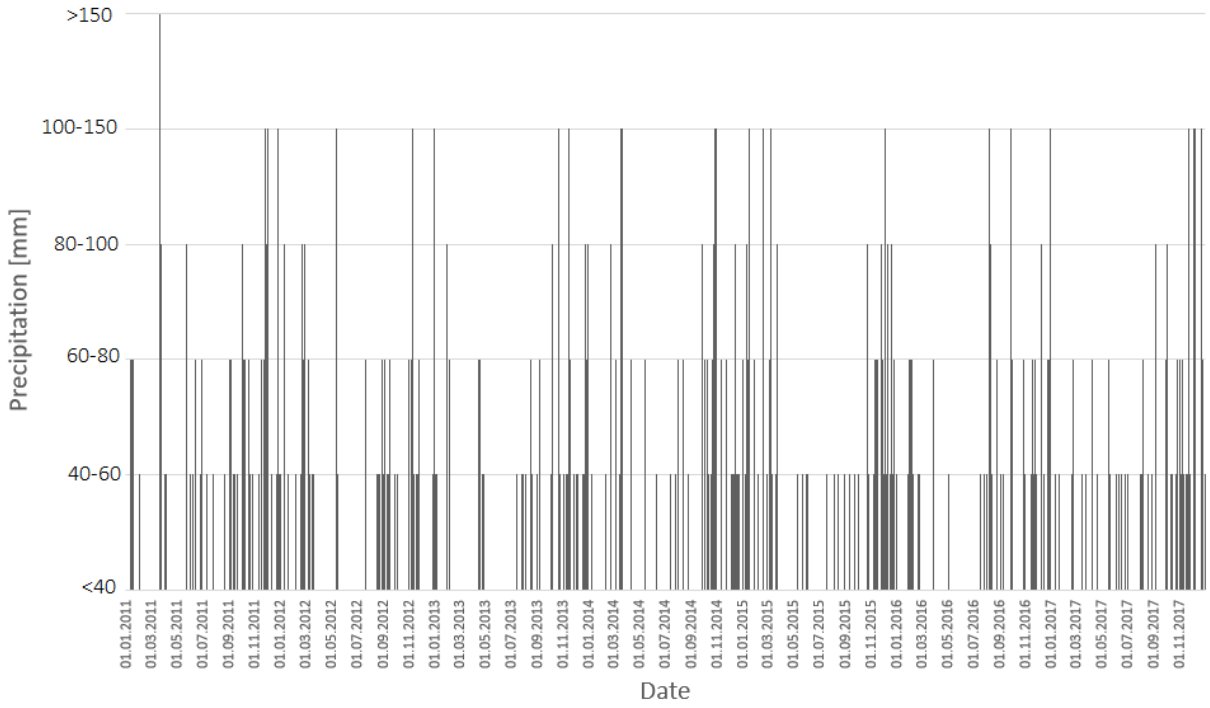

Figure 6.1: Yearly distribution of weather events above the threshold of 40 mm in the period of 2011-2017. Maximum precipitation visually extracted from xgeo during the rainfall analysis.

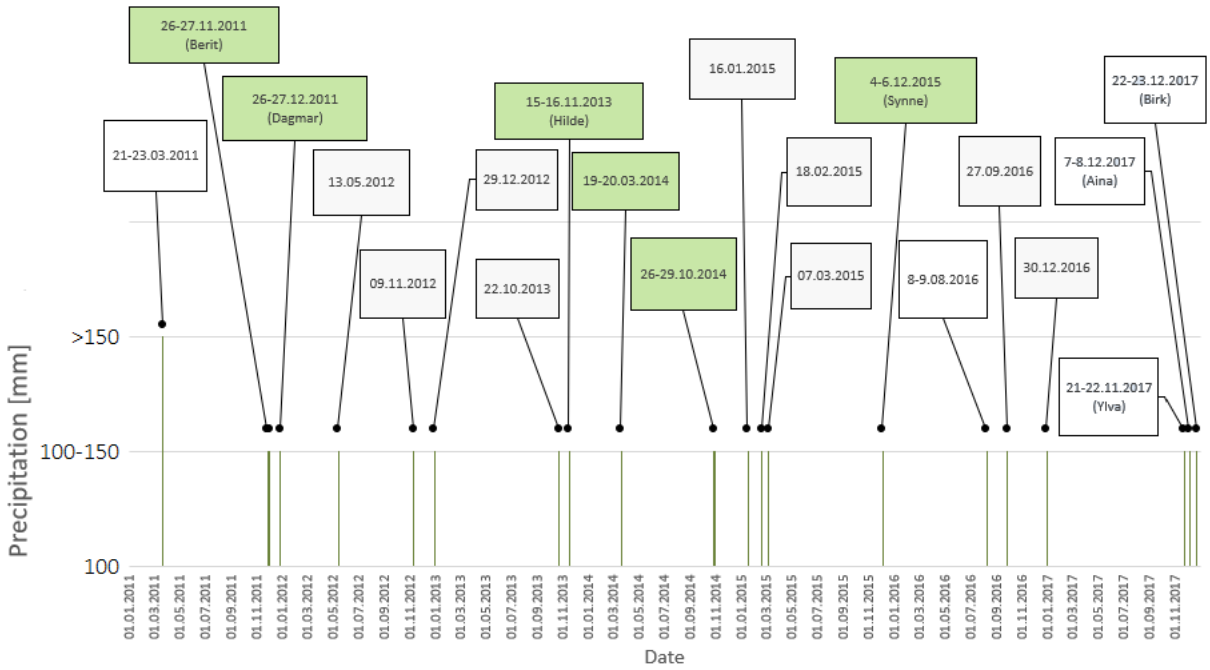

Figure 6.2: Yearly distribution of weather events above 100 mm in the period of 2011-2017. The weather events that are marked in green were further analyzed in this study.

Date	Description of rainfall	Number of landslides registered
21.03.2011 – 23.03.2011	Heavy precipitation	31
26.11.2011 – 27.11.2011	Berit extreme weather	28
26.12.2011 – 27.12.2011	Dagmar extreme weather	85
13.05.2012	Heavy precipitation	0
09.11.2012	Heavy precipitation	0
29.12.2012	Heavy precipitation	6
22.10.2013	Heavy precipitation	1
15.11.2013 – 16.11.2013	Hilde extreme weather	5
20.03.2014	Heavy precipitation	35
26.10.2014 – 29.10.2014	Heavy precipitation	35
16.01.2015	Heavy precipitation	2
18.02.2015	Heavy precipitation	4
07.03.2015	Heavy precipitation	3
04.12.2015 – 06.12.2015	Synne extreme weather	17
08.08.2016 – 09.08.2016	Heavy precipitation	10
27.09.2016	Heavy precipitation	2
30.09.2016	Heavy precipitation	3
21.11.2017 – 22.11.2017	Ylva extreme weather	5
07.12.2017 – 08.12.2017	Aina extreme weather	31
22.12.2017 – 23.12.2017	Birk extreme weather	35

Figure 6.3: List of weather events analyzed. The events marked in green were taken further into the analysis. The number of landslides registered is collected from the landslide database and include all typologies in the category of weather-induced landslides.

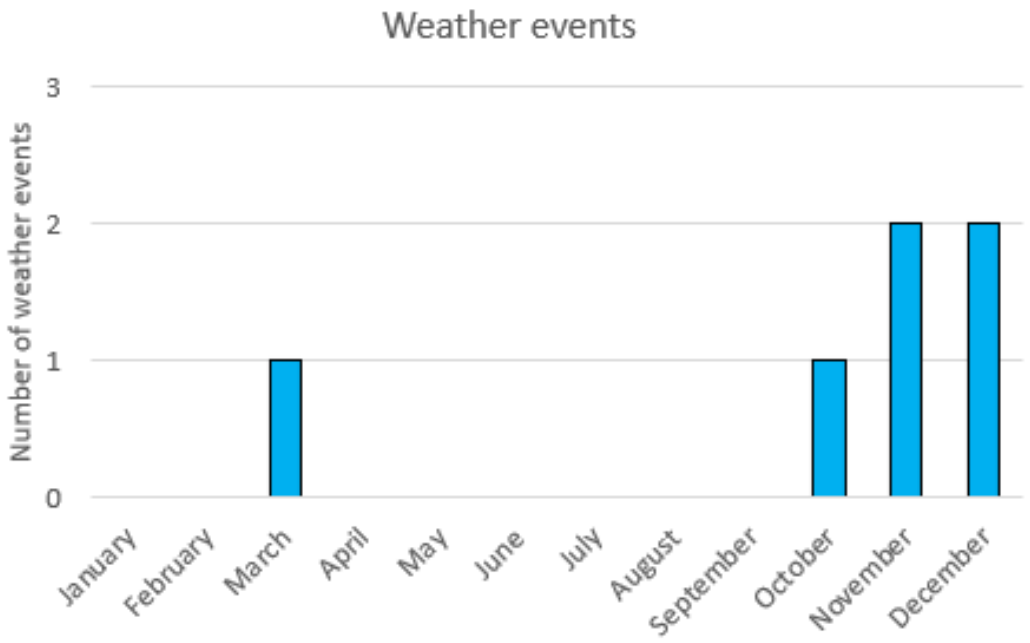

Figure 6.4: Monthly distribution of the six weather events analyzed.

6.1.1 Spatial pattern and characteristics of the selected weather events

26-27th November 2011 ("Berit")

The extreme weather "Berit" occurred on the 26th - 27th of November 2011. The storm was caused by a heavy low pressure moving in from the Atlantic Ocean, causing high precipitation levels, high waves, and strong winds (figure 6.5C). Twenty-eight landslides, mostly occurring on the 27th of November, were found registered in the database, triggered by this storm. The precipitation pattern and amount for "Berit" are shown in figure 6.5A. Precipitation above 40 mm is seen covering large amounts of the county, with clusters of 80 up to 150 mm north of Veafjorden and in the south along Sørfjorden, and a large cluster of with more than 150 mm in Etne and Kvinnherad municipalities in the south of the county. The county experienced some snowmelt in high-lying areas (figure 6.5B). The majority of the precipitation fell as rain, with some of the innermost areas receiving sleet or snow (figure 6.5D). The precipitation pattern is seen in figure 6.5E, showing most precipitation along the south-western coast, and another cluster further north.

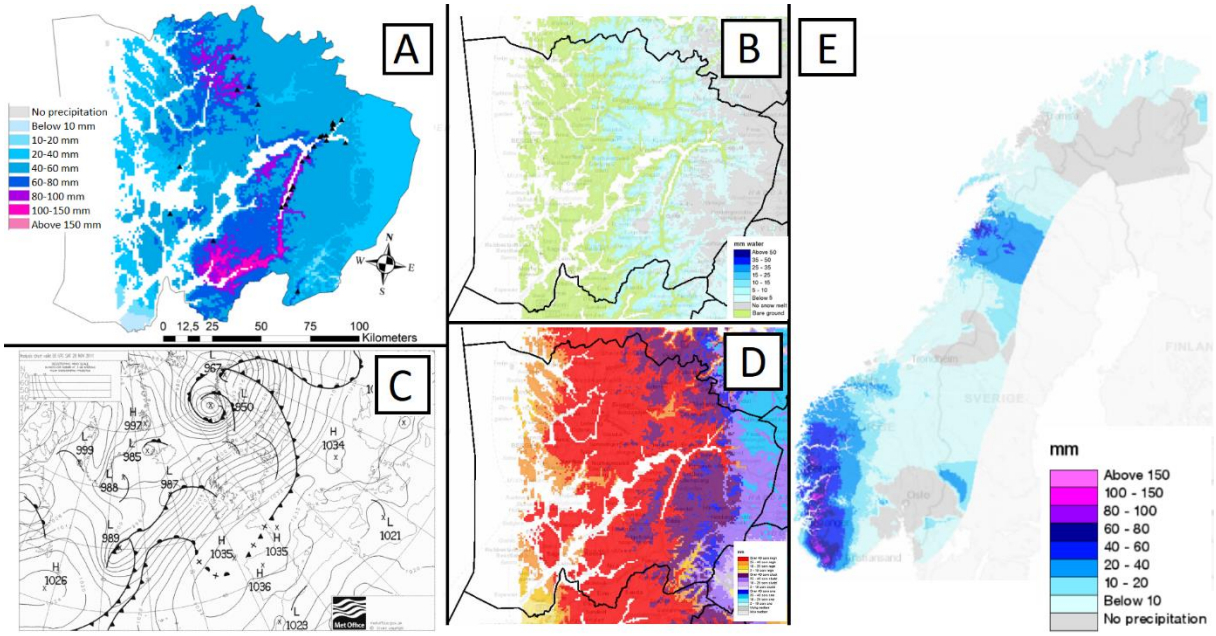

Figure 6.5: Spatial pattern and characteristics of the weather event "Berit" in 2011. ***A****: Rainfall and landslide point data (black).* ***B****: Snowmelt.* ***C****: Pressure system.* ***D****: Type of precipitation.* ***E****: Precipitation pattern for the whole of Norway. (Maps from 27.11.2011).*

26-27th December 2011 ("Dagmar")

The extreme weather "Dagmar" arrived only a month after "Berit", the 26th – 27th of December 2011. An additional attribute of "Dagmar" was snowmelt and the strong wind, well over hurricane strength (pressure system shown in figure 6.6C). This wind led to trees falling over power lines, causing loss of electricity for large parts of the population in the area. The event has 85 landslides registered in the national landslide database on the dates of occurrence, with most of the landslides occurring on the 26th of December. The precipitation was distributed over the entire county (figure 6.6A), with the highest intensity in Sørfjorden and Etne municipality in the south, both with values above 100 mm. Some areas of Sørfjorden received above 150 mm. The snowmelt is seen in figure 6.6B, showing higher levels than Berit the month before. Most of the precipitation fell like rain, and some as snow and sleep in the higher lying areas and Hardangervidda (figure 6.6D). Figure 6.6E shows the distribution slightly further north compared to Berit, but with most precipitation still on the south-western coast.

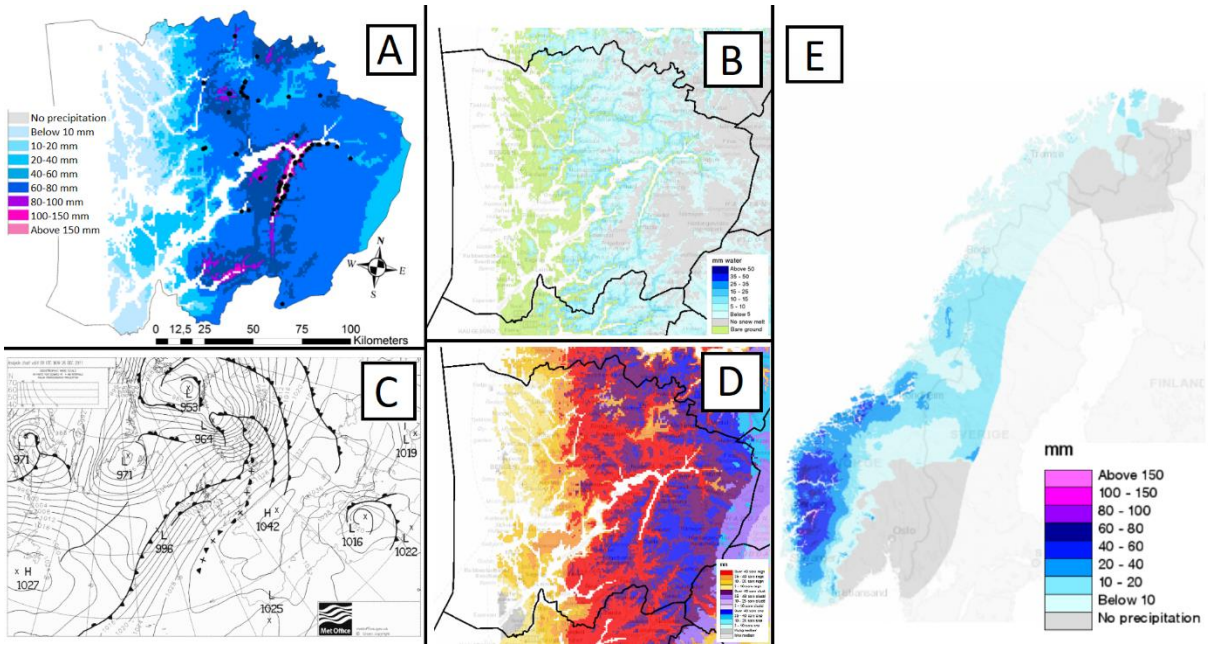

Figure 6.6: Spatial pattern and characteristics of the weather event "Dagmar" in 2011. ***A****: Rainfall and landslide point data (black).* ***B****: Snowmelt.* ***C****: Pressure system.* ***D****: Type of precipitation.* ***E****: Precipitation pattern for the whole of Norway. (Maps from 26.12.2011).*

15-16th November 2013 ("Hilde")

Extreme weather "Hilde" was caused by a low pressure moving in from the Atlantic Ocean, developing into a storm center south-west of Iceland hitting the Norwegian coast with full force 15th – 16th of November 2013 (figure 6.7C). The event has five landslides registered in the

national landslide database on the dates of occurrence, with most of the landslides occurring on the 15th of November. The storm "Hilde" led to precipitation falling over the entire county (figure 6.7A), but most fell in a cluster north-west of Veafjorden, with up to above 100 mm. The event only caused some snowmelt in the higher-lying areas in the east and south (figure 6.7B). Most precipitation fell as rain, also along the fjords, while some as sleet in the higher lying and innermost areas (figure 6.7D). Figure 6.7E shows how the low pressure hit further north than the other weather events in the analysis, and therefore had less impact in terms of both precipitation and number of landslides in Hordaland.

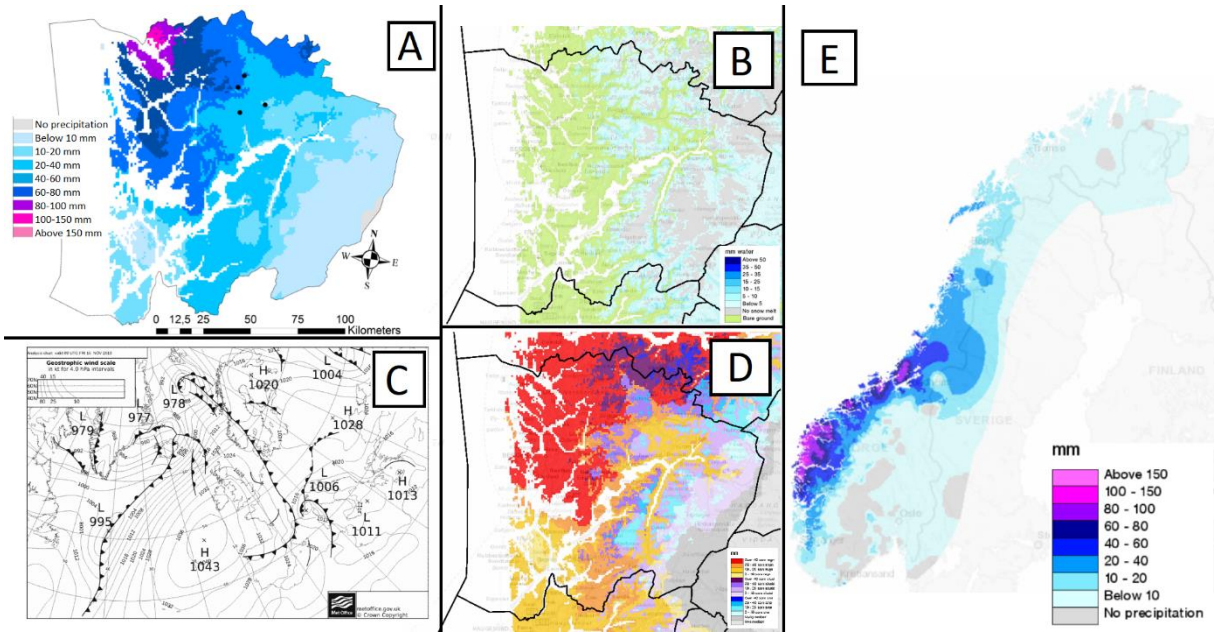

Figure 6.7: Spatial pattern and characteristics of the weather event "Hilde" in 2013. ***A****: Rainfall and landslide point data (black).* ***B****: Snowmelt.* ***C****: Pressure system.* ***D****: Type of precipitation.* ***E****: Precipitation pattern for the whole of Norway. (Maps from 15.11.2013).*

20th March 2014

The weather event on 20th of March 2014 was caused by heavy, short term precipitation on the 19th and 20th of March. In combination with snowmelt, the sudden rainfall led to many landslides. The wind was not a significant factor in this event (pressure system is seen in figure 6.8C). The event has 35 landslides registered in the national landslide database on the date of occurrence, with all of the landslides occurring on the 20th of March. The precipitation pattern on March 20th can be seen in figure 6.8A, showing several high-intensity areas up to above 100 mm north of Veafjorden, and in Etne and Kvinnherad municipalities, and above 80 mm around Nordheimsund in the center of the county. The snowmelt is seen in figure 6.8B, most values

between 5 and 10 mm water. The strongest snowmelt occurred on the day before, with values above 10 mm. The precipitation fell as rain along the fjords, and lower lying coastal areas. In the highlands and innermost areas, the precipitation fell as snow and some sleet (figure 6.8D). The precipitation pattern is seen to reside mostly on the south coast (figure 6.8E).

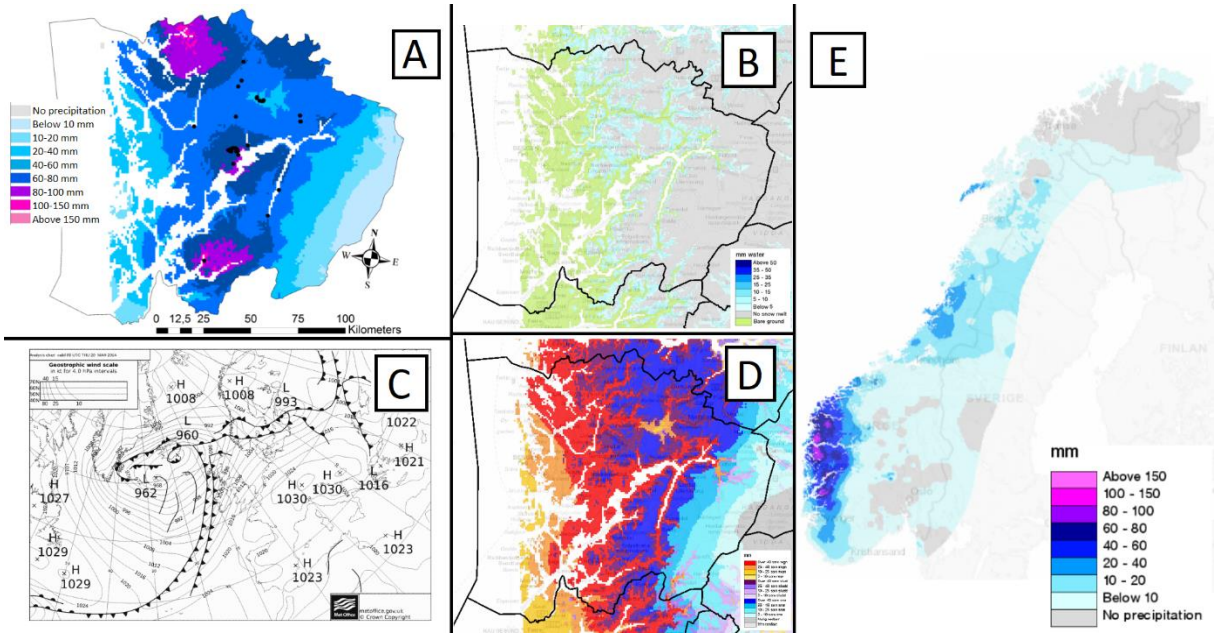

*Figure 6.8: Spatial pattern and characteristics of the weather event in March in 2014. **A**: Rainfall and landslide point data (black). **B**: Snowmelt. **C**: Pressure system. **D**: Type of precipitation. **E**: Precipitation pattern for the whole of Norway. (Maps from 20.03.2014).*

26-29th October 2014

The weather event of 26th – 29th of October 2014 caused major flooding at the western coast of Norway and causing significant damage to infrastructure (Müller et al., 2017). The rainfall intensity was not extreme, but the precipitation fell over several days in significant amounts, leading to great damages. It originated from a tropical cyclone "Gonzalo" in the Caribbean Sea and moved on to hit the west coast of Norway 26-29 October (Müller et al., 2017) (figure 6.9C). The wind was, however, not a significant factor in this event. The event has 35 landslides registered in the national landslide database on the dates of occurrence, with most of the landslides occurring on the 28th of October. Figure 6.9A shows that the weather event caused high amounts of precipitation over the entire county, with the highest intensity of up to above 80 mm north of Veafjorden, and up to above 100 mm around Nordheimsund, and in Etne and Kvinnherad municipalities in the south. No significant snowmelt occurred due to the time of

year (figure 6.9B). All precipitation fell as rain (figure 6.9D). The precipitation pattern on the west coast is seen to be relatively similar to the March event earlier the same year (figure 6.9E).

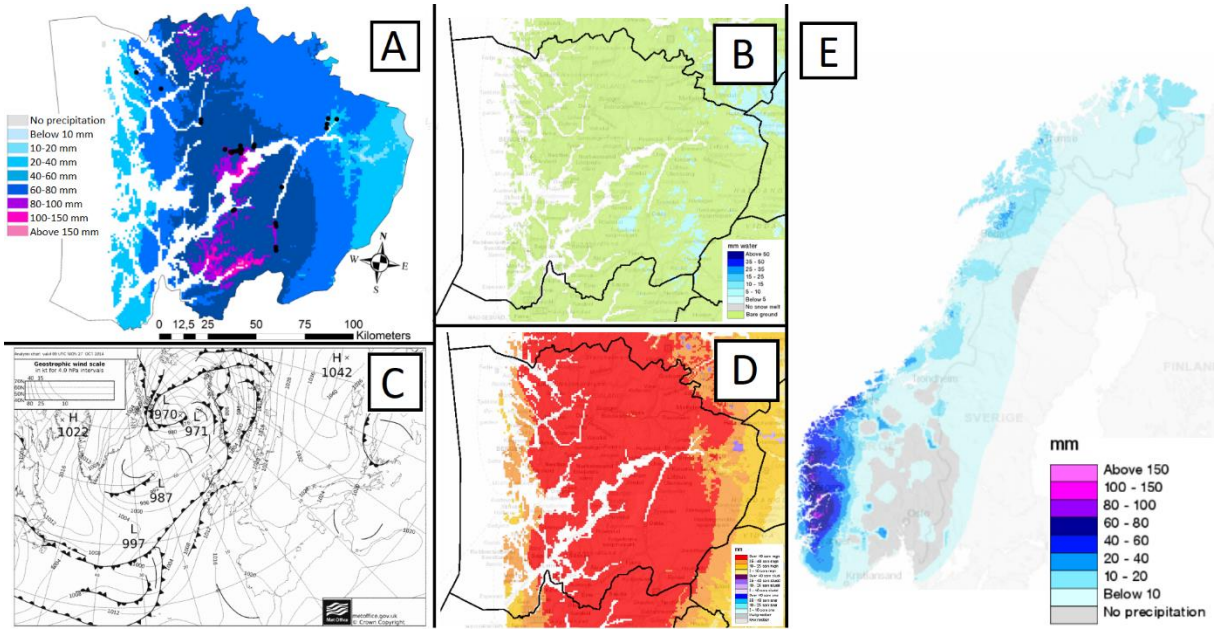

*Figure 6.9: Spatial pattern and characteristics of the weather event in October in 2014. **A**: Rainfall and landslide point data (black). **B**: Snowmelt. **C**: Pressure system. **D**: Type of precipitation. **E**: Precipitation pattern for the whole of Norway. (Maps from 28.10.2014).*

4-6th 2015 ("Synne")

The extreme weather "Synne" hit 4th – 6th of December 2015, and originated from extratropical cyclone "Desmond" (figure 6.10C). The low pressure caused heavy precipitation, in a short amount of time. Due to snowfall in previous days, this was combined with snowmelt leading to both floods and landslides. The event has 17 landslides registered in the national landslide database on the dates of occurrence, with most of the landslides occurring on the 5th of December. Figure 6.10A shows the precipitation distribution in the county. The snowmelt is shown in figure 6.10B, varying between 5 and 10 mm, with 10 mm snowmelt in the south in Etne and Kvinnherad municipalities. The type of precipitation (figure 6.10D) shows that a lot of the precipitation fell as rain, most along the steep fjords and the central lower lying areas, and the coast. Some precipitation fell as sleet, and in the highland most fell as snow or sleet. The precipitation pattern shown in figure 6.10E shows similarities to Berit in 2011, for the southern part of the country.

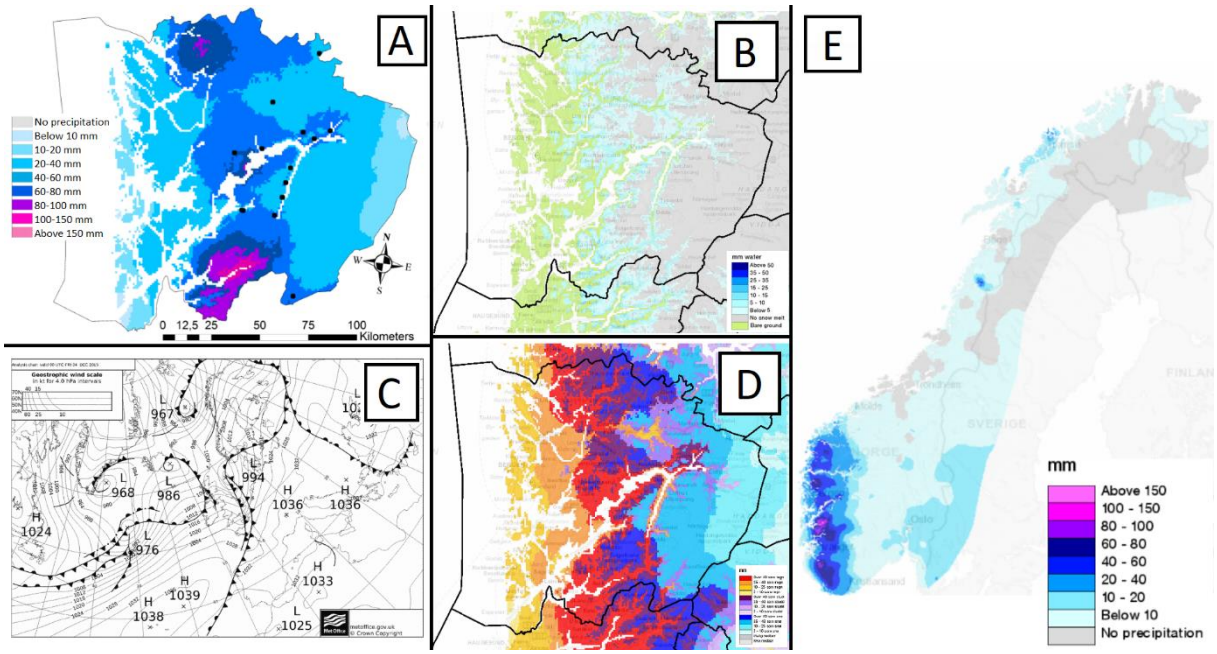

Figure 6.10: Spatial pattern and characteristics of the weather event "Synne" in 2015. ***A****: Rainfall and landslide point data (black).* ***B****: Snowmelt.* ***C****: Pressure system.* ***D****: Type of precipitation.* ***E****: Precipitation pattern for the whole of Norway. (Maps from 04.12.2015).*

6.2 Spatial and temporal distribution of landslide events

To define the spatial distribution of the landslide events occurred during these weather events, point data from the national landslide database were extracted. The analysis of the landslide points registered during the years 2011-2017 shows that 205 points (dataset 1) occurred during the six weather events. Out of the total 205 point registrations in "dataset 1", 28 occurred during "Berit" (2011), 85 during "Dagmar" (2011), 5 during "Hilde" (2013), 35 on March 20th, 2014, 35 during the October event in 2014 and 17 during "Synne" (2015). The spatial distribution is shown in figure 6.11. The point data are for each weather event separately shown in appendix 5.

The landslides are spread out in the county, but with clusters together in the steep valley sides, especially along Sørfjorden, and the innermost parts of Hardangerfjorden. Many landslides have also clustered in Nordheimsund (center), and Evanger (north). The landslides do not seem to correlate with the most intense precipitation during the events, but rather the topography in the county. Landslides that occurred during "Berit" (2011) are registered mostly along Sørfjorden and the inner parts of Hardangerfjorden (figure 6.5A), but also a few in other locations. Many landslides registered for "Dagmar" (2011) occurred in Sørfjorden and the inner

Hardangerfjorden as well (figure 6.6A). Landslides from this event are also registered in proximity to Evanger, and some sporadically around the county. The landslides triggered during "Hilde" (2013) occurred near Evanger in the northern part of the county (figure 6.7A). The landslides reported on March 20th, 2014 occurred mostly in Nordheimsund, and around Evanger, with also some sporadically in other areas (figure 6.8A). Nordheimsund also inhibits most of the landslides registered in October 2014. This event has also landslides south in Sørfjorden, the inner parts of Hardangerfjorden, as well as a few in the north-western part of the county (figure 6.9A). Lastly, landslides triggered during "Synne" (2015) occurred in the steep valley sides of Sørfjorden, and most landslides are located in the central part of the county (figure 6.10A).

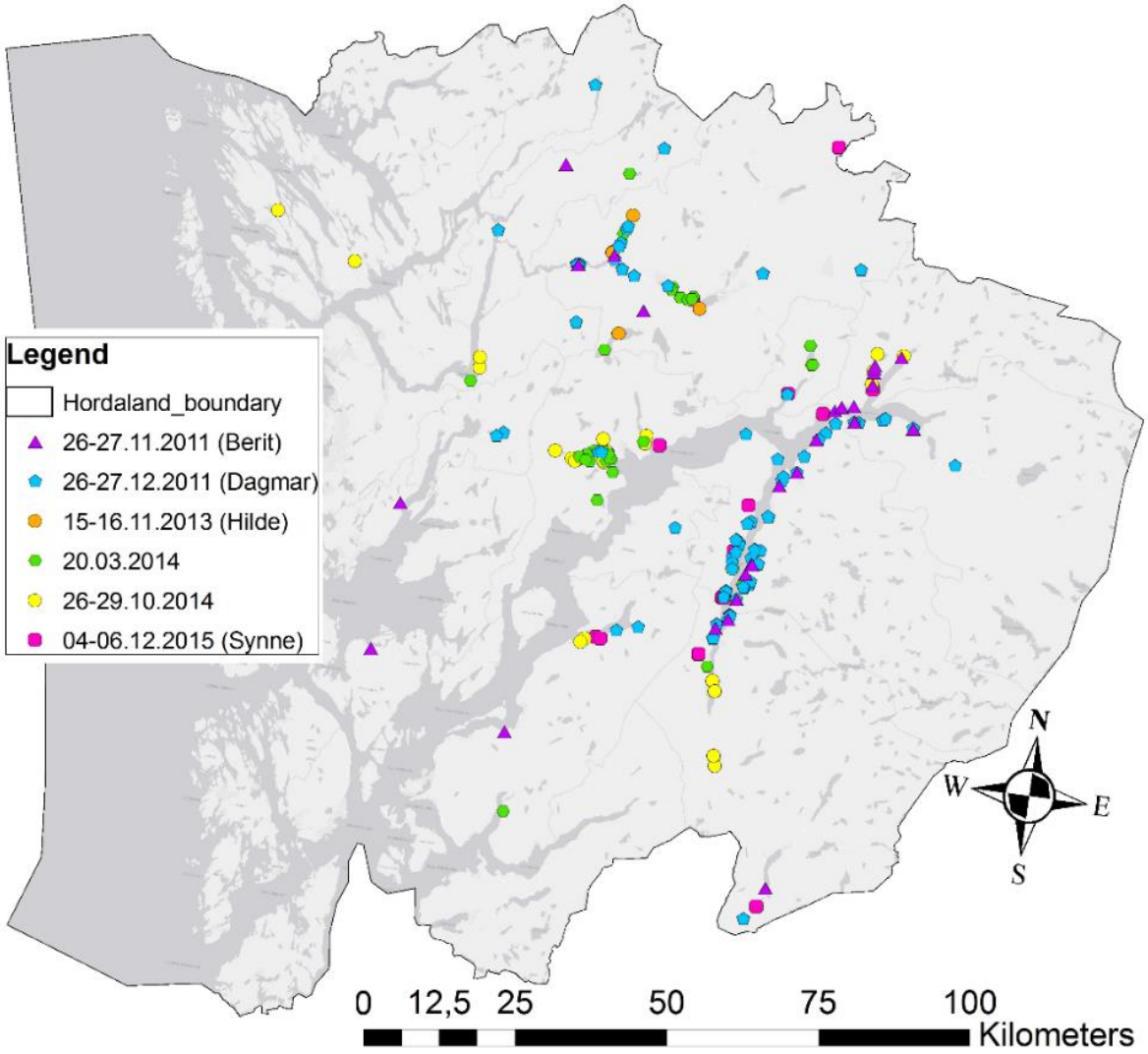

Figure 6.11: Spatial distribution of landslides registered during the six weather events, ("dataset 1").

In addition to the point data extracted from the database, polygons were drawn for the landslides registered on the dates of these weather events. Out of the 205 point registrations ("dataset 1"), 20 were possible double registrations, 110 registrations could not be mapped due to lack of aerial photos and other sources necessary to see the extent of the landslide. Finally, 75 could be mapped. By analyzing other sources like news and pictures taken by NVE, it was possible to map three other landslides that were not in the database, occurring in 2011 during "Dagmar". A "dataset 2" was made with a total of 78 polygons. Table 6.1 shows an overview of the number of points and polygons in each weather event.

Table 6.1: Overview of the number of points and polygons in the data set.

Weather event	Number of point registrations in the NLDB	Number of polygons drawn for the point registrations	Percent mapped	Number of points not mapped with a polygon	Number of possible double point registrations in the NLDB
Berit 2011	28	8	28%	16	2
Dagmar 2011	85	54	63%	25	11
Hilde 2013	5	5	100%	0	0
March 2014	35	5	14%	26	4
October 2014	35	2	5%	33	0
Synne 2015	17	4	23%	10	3

The polygons mapped can be seen in figure 6.12, together with the landslide point data investigated ("dataset 1", in black). The size of the polygons has been significantly increased to be visible in the county map. Even though the number of polygons is lower compared to the point data, the polygons are still well distributed around the county. Figure 6.13 shows how many landslides from "dataset 1" could be mapped in "dataset 2", for each weather event. The histogram shows that all landslides could be mapped for only one weather event ("Hilde"). The highest number of landslides could be mapped for Dagmar (63%), Berit (28%) and Synne (23%). For the event in March 2014, only 14% of the landslides could be mapped, and for the event occurring in October the same year, only 5% could be mapped.

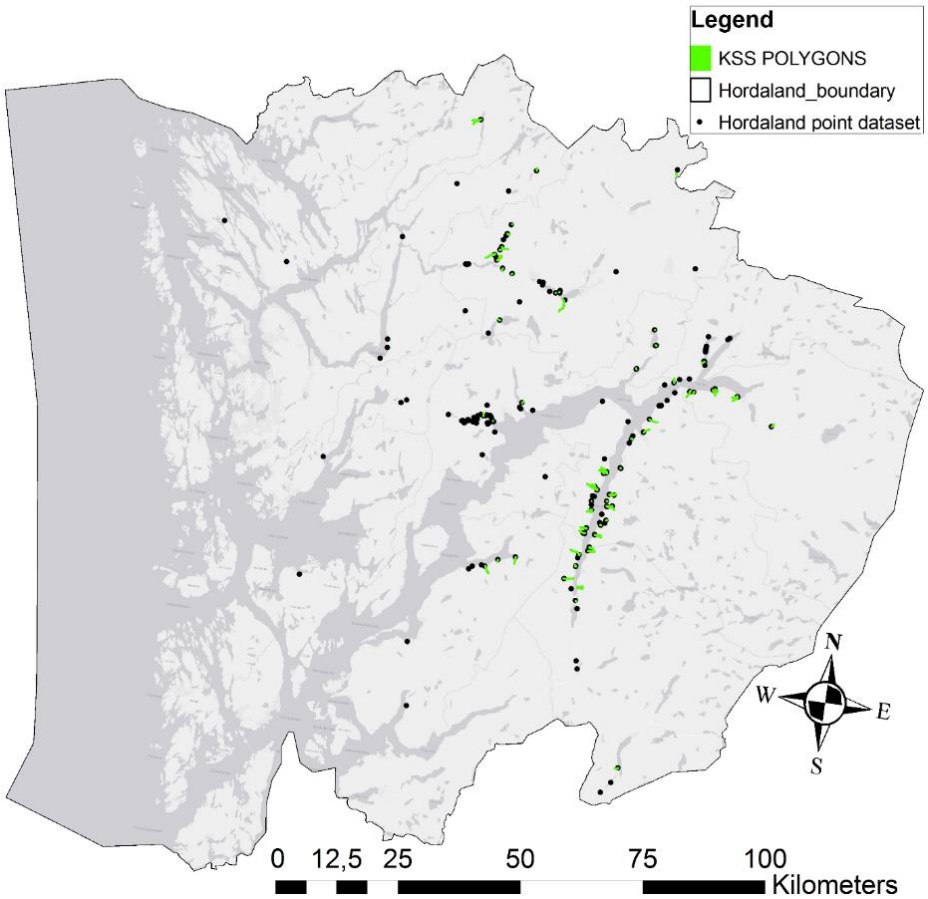

Figure 6.12: The investigated landslides for the six weather events in "dataset 1", and the mapped polygons in "dataset 2".

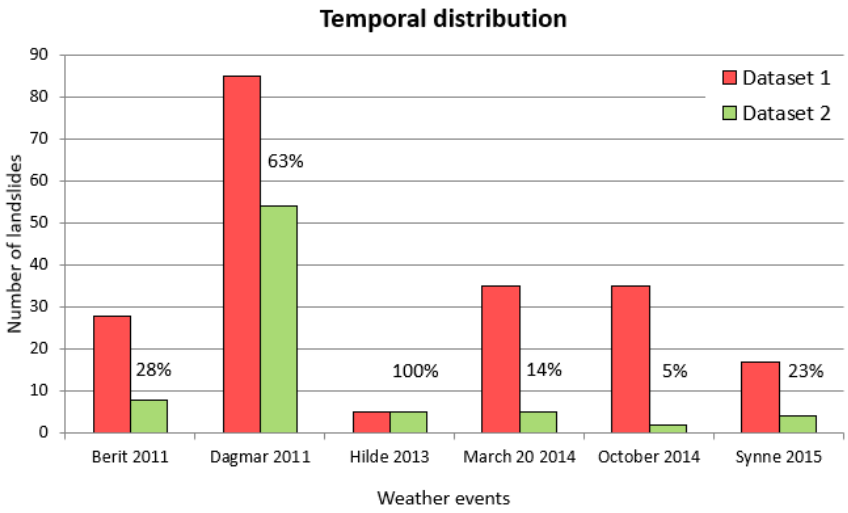

Figure 6.13: The number and percentage of landslides mapped for each event in "dataset 2" compared to "dataset 1". "Dataset 1" is shown in red, and "Dataset 2" shown in green.

Figure 6.14 shows how the 78 landslide events are distributed within the six weather events and show the large contribution from the extreme event "Dagmar 2011" (69%). Due to this, most landslides mapped in "dataset 2" (74%) occurred in December (including the landslides triggered by the event "Synne").

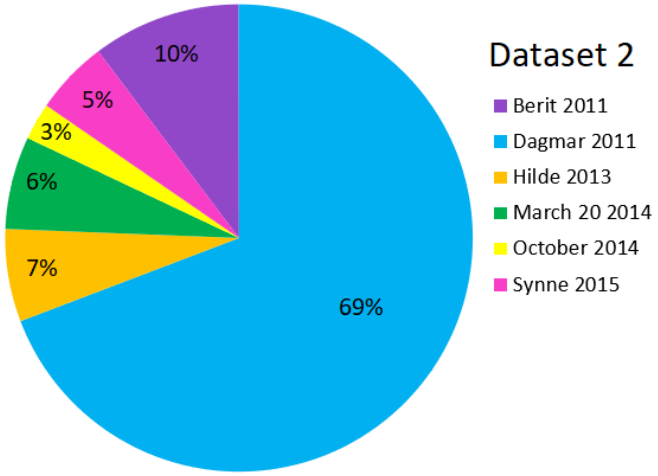

Figure 6.14: The influence of the different weather events on "dataset 2". The weather event "Dagmar" (2011) dominates the data strongly.

The analysis of the 78 mapped landslides shows that 81% were debris flows occurring along the steep slopes of the fjords (figure 6.15). The debris avalanches are sporadic, representing 9% of the total, also occurring in steep slopes. Debris slides are also sporadic (10%), but often following gentler slopes.

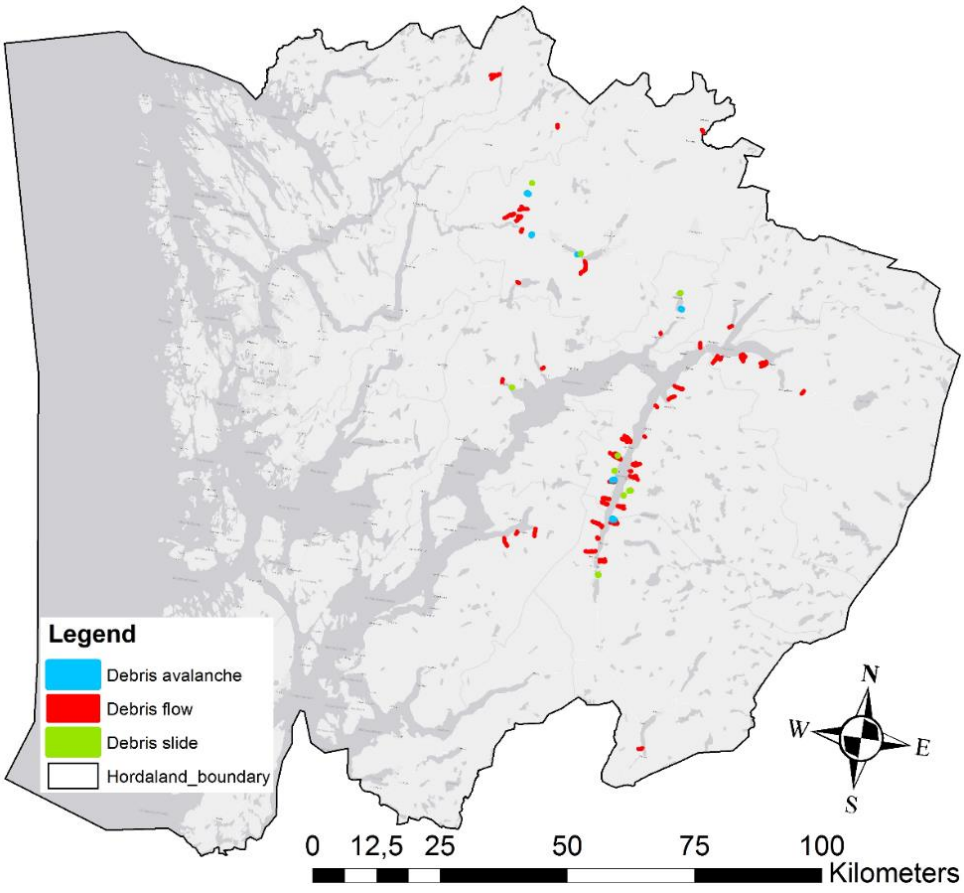

Figure 6.15: Map showing the spatial distribution of the different landslide typologies.

6.3 Landslide characterization

6.3.1 Landforms and susceptibility

Plotting the landslide distribution against landforms in the county (figure 3.7), it can be observed that the majority of the landslides in "dataset 1" occur within the landform types 9 (31%) and 10 (33%), which are alpine relief with either coastal mountains and intermediate-relief glacial slopes, or steep slopes and over-deepened glacial valleys, followed by landform 7 (30%) represented by glacially scoured low mountains and valleys (figure 6.16).

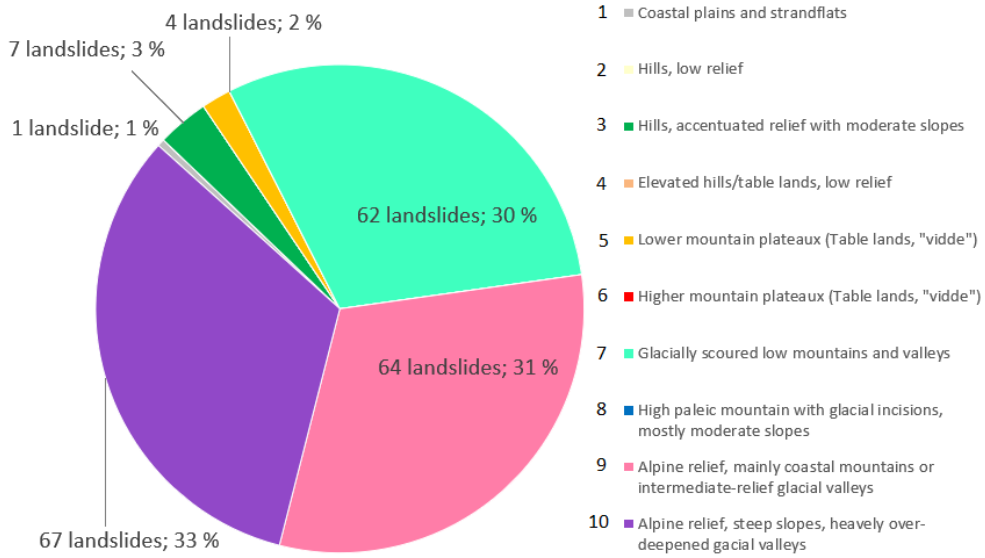

Figure 6.16: Distribution of the landslides in the landform classes.

The landslides in "dataset 1" were also plotted against the two susceptibility maps available for Norway, to evaluate their performance. In respect to the susceptibility map at catchment level (Cepeda and Bell, 2014; Devoli et al., 2019), the quantitative analysis shows that landslides occurred in areas with very high susceptibility, high susceptibility, and a few in medium susceptibility (top figure 6.17). However, these results were obtained only with 180 of 205 landslide events, since the map had a problem with its coordinate system that could not be fixed. An attempt was made to fix the issue, but the problem could not be solved. NVE was made aware of the issue, and it was found not to be solvable in time for another analysis. In respect to the national susceptibility map for debris avalanches and small debris flows from Fischer et al. (2014) (bottom figure 6.17) the quantitative analysis shows that 113 of 205 landslides fall within the modeled zones.

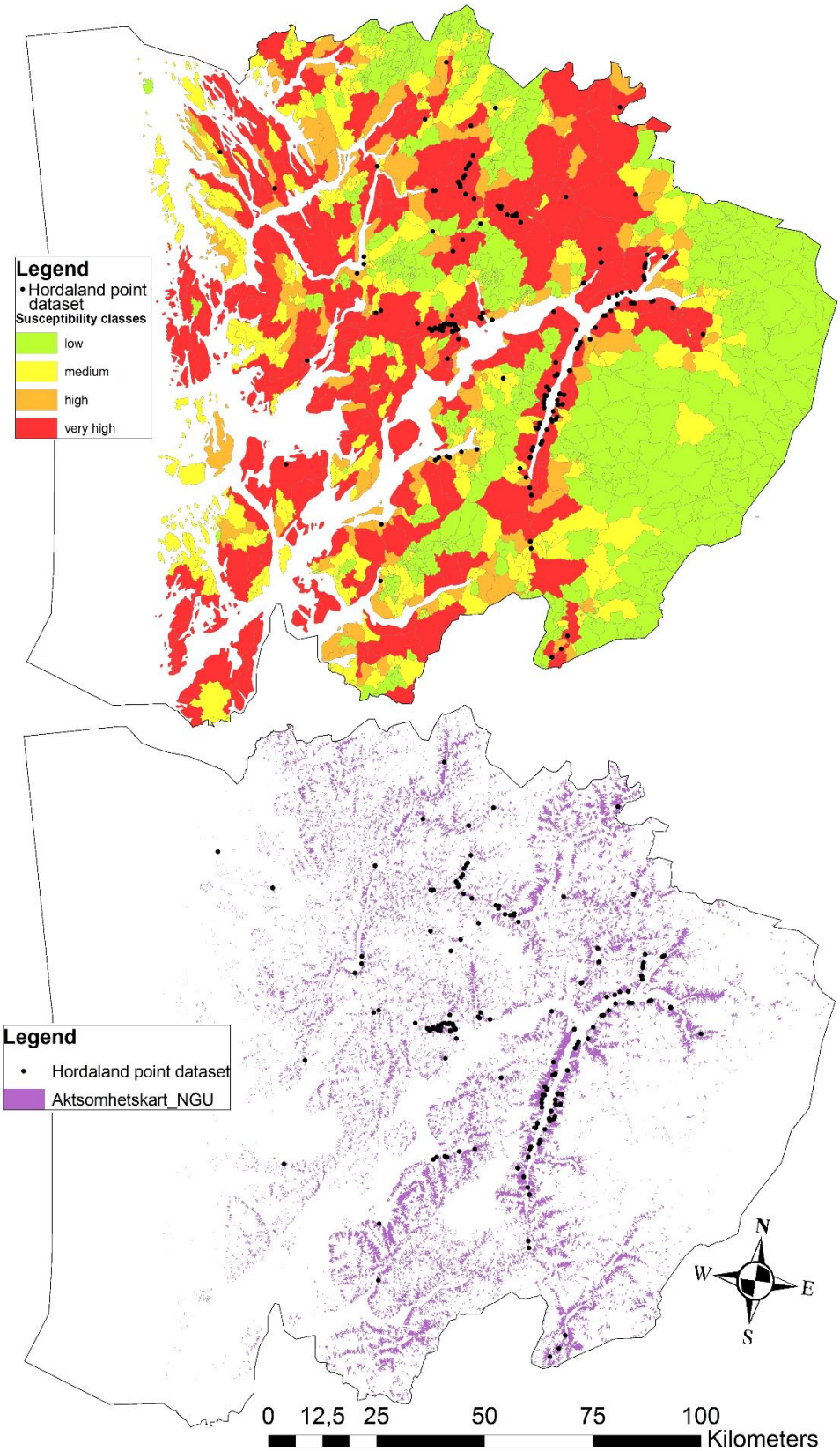

Figure 6.17: Distribution of landslides against susceptibility maps. ***Top****: Point data of the landslides that occurred during the six weather events, plotted together with susceptibility map from Cepeda and Bell, 2014.* ***Bottom****: Point data of the landslides that occurred during the six weather events, plotted together with susceptibility map from Fisher et al., 2014. "Hordaland point dataset" is equivalent to "dataset 1".*

Like for the point data for "dataset 1", the polygons in "dataset 2" were checked to see how they fit with the susceptibility maps. The polygons were therefore plotted against the two susceptibility maps, and evaluated with a qualitative analysis. As the susceptibility map at catchment level had an issue with the coordinate system, the fit was evaluated qualitatively. Figure 6.18A from the susceptibility map at catchment level (Cepeda and Bell, 2014; Devoli et al., 2019) show that 69 out of 78 landslides occurred in catchments with very high susceptibility (red level). Five landslides initiated in catchments with high susceptibility (orange level), and four landslides in catchments with medium susceptibility (yellow level). No landslides initiated in catchments with low susceptibility (green level).

Comparing landslide occurrence with the national susceptibility map for debris avalanches and small debris flows from Fischer et al. (2014), it can be observed that 62 polygons fit completely within the modeled susceptibility area, and 16 polygons were outside the area (figure 6.18B). All three typologies are present both within and outside the susceptible areas. The example in figure 6.18C shows one debris flow inside the susceptible area (bottom) and one debris avalanche outside (top). The susceptible areas are marked in purple.

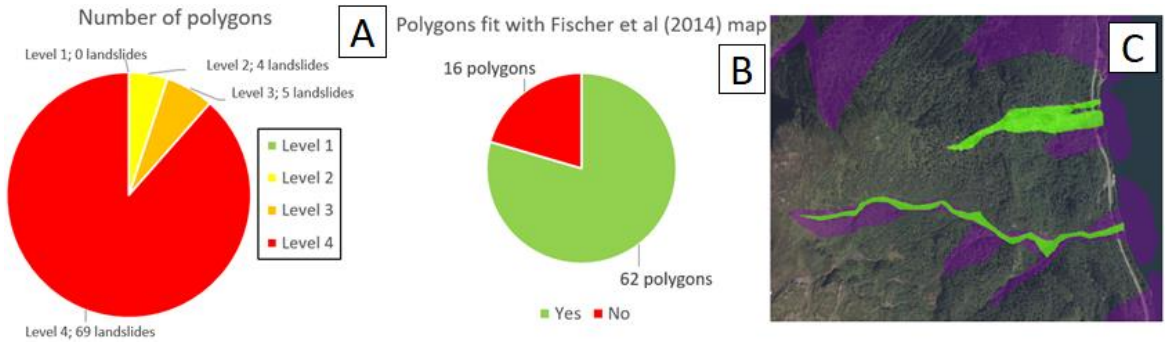

*Figure 6.18: Landslides vs. susceptibility maps. **A**: The number of polygons in each level of susceptibility from Cepeda and Bell (2014). **B**: Distribution of fit and non-fit of the Fischer et al. (2014) map. **C**: Example of fit a non-fit with the polygons in "dataset 2".*

6.3.2 Topography and geology

The "dataset 2" was used for further analysis in relation to topography and geology (figure 6.19 and appendix 6). The mean slope angles at the initiation point for all typologies is seen to be around 20^{o} - 45^{o}, with some outliers. Debris flows mostly occurred in 30-45^{o} slopes, with peaks at 30-35^{o} and 40-45^{o}. Debris avalanches range mostly between 25-35^{o} slopes, with a peak at 30-35^{o}. Debris slides range between 20-40^{o} slopes with one at 45-50^{o}.

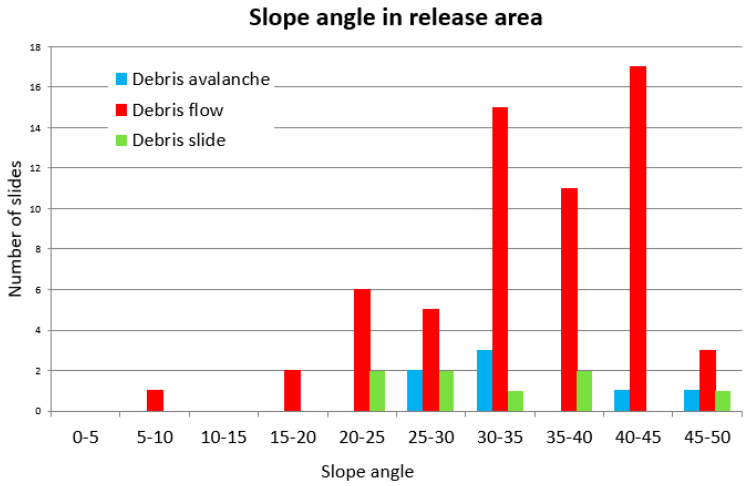

Figure 6.19: Slope angles in the initiation point of the landslides in "dataset 2", divided in typologies.

An attempt to find any typical slope orientation of the landslides mapped was done. The calculation was done in excel, and a simplified table 6.2 is shown below. The mean aspect, also called mean vector direction, was calculated to be 228,96 degrees. The vector strength is calculated to be 0,071, which indicate almost no trend in the aspect of the slopes.

Table 6.2: Mean aspect and vector strength calculation for the polygons mapped, in a simplified version, showing the results in bold writing.

	Mean sin aspect	Mean cos aspect	Sinaspdeg	Cosaspdeg	Mean aspect $\bar{\theta}$	Length of resultant R	Vector strength $\bar{R}$
Calculated for each polygon	Individual mean value of sin of aspect	Individual mean value of cos of aspect	Changing rad to sin	Changing rad to cos			
Final results			Mean sin (used for eq 1)	Mean cos (used for eq 1)	**228,9609529 (eq 1)**	5,42618415 (used for eq 2)	**0,071161434 (eq 2)**

The analysis of landslide initiation and geology shows that the majority of landslides occurred in correspondence of "diorite- to granite gneiss and migmatite", and "unspecified volcanic rocks" (figure 6.20). Debris flows occur in all bedrock types. Comparing to quaternary deposits (figure 6.21) it can be observed that the majority of the events occurred in the category "thin or no cover", followed by a thin cover of "moraine material" (till), "weathered material" and "previous landslide deposits" (talus). Debris flows occur in all classes, especially dominated in "thin or no cover" with 46 landslides. No debris flows are observed in "glaciofluvial deposit". Debris avalanches seem to occur mostly in "thin or no cover" and "weathered material". (The class of both bedrock and quaternary deposit at the initiation point of the mapped landslides in "dataset 2" are shown in appendix 7.)

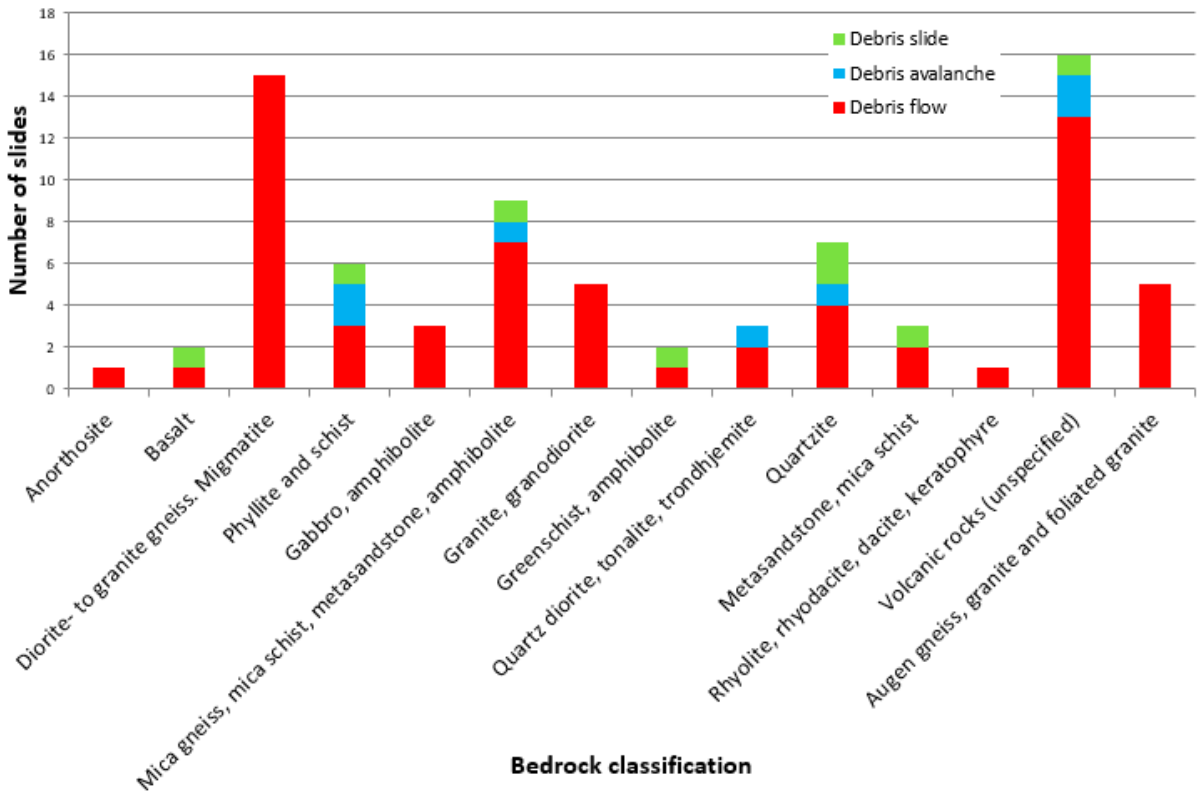

Figure 6.20: Distribution of landslide occurrence within bedrock lithology ("Dataset2").

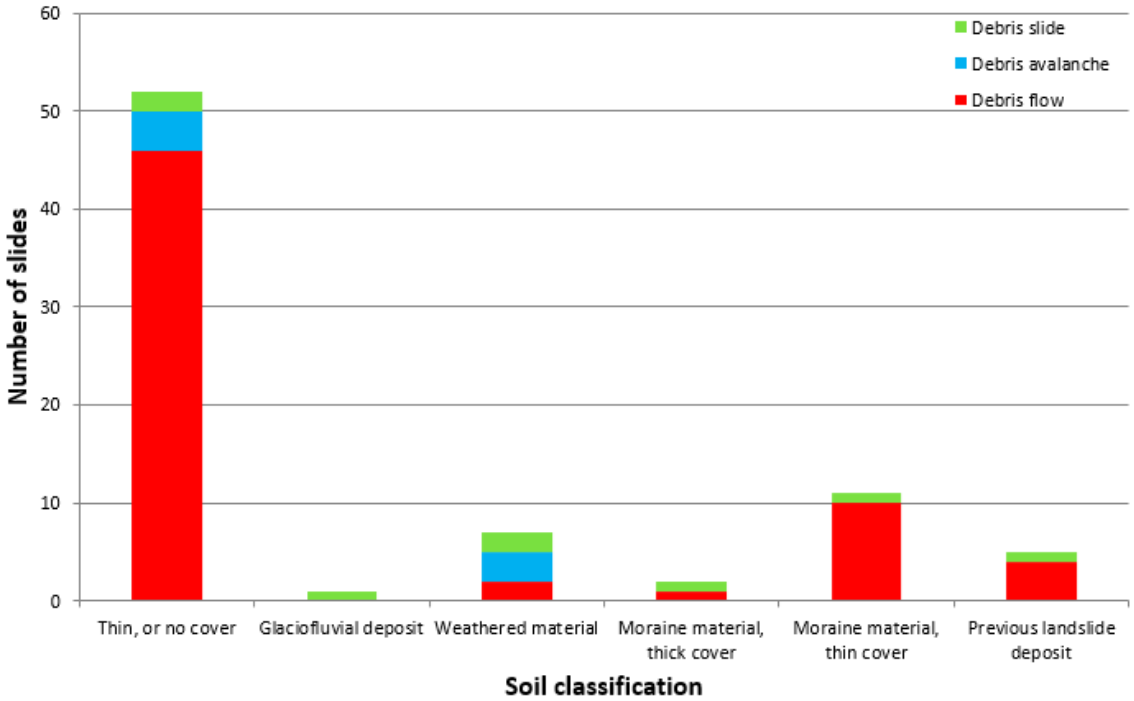

Figure 6.21: Distribution of landslide occurrence within quaternary deposits ("Dataset 2").

6.3.3 Landslide parameters

The mapped landslides were analyzed against terrain parameters (more details can be found in appendix 6). From the 78 polygons, it was found that the landslide area range between 200 and 140.400 m^2. The approximate area values ranges differ between landslide typologies. Debris slides range in area between 206 and 8245 m^2, debris flows range between 1085 and 140.359 m^2, and debris avalanches range between 558 and 35.889 m^2. The elevation of the initiation point ranges between 36 masl and 1291 masl, all typologies included. Debris slides occur between 36 and 295 masl, debris flows occur between 79 and 1291 masl, and debris avalanches occur between 113 and 902 masl. In terms of runout length, all landslides range between 29 and 3225 meters. Debris slides range between 29 and 77 meters, debris flows between 185 and 3225 meters, and debris avalanches range between 59 and 582 meters. The mean values are all presented in table 6.3. As known, the analysis confirmed that debris flows can initiate at higher elevations (H), have the highest mean range of elevation, and have the longest runouts (L). Debris avalanches initiate at the lowest elevation (H), and debris slides have the shortest runouts (L).

Table 6.3: Some of the parameters and mean values for the 78 polygons in "dataset 2".

	Mean area (m^2)	Maximum elevation H (m.a.s.l.)	Mean range of elevation (m)	Mean runout distance L (m)	Mean H/L	Mean slope angle (°)	Number of landslides
All landslides	24921	1291	511	980	0,55	34	78
Debris flows	29065	1291	603	1169	0,55	34	63
Debris avalanches	14385	565	235	338	0,61	33	7
Debris slides	1512	902	26	50	0,52	32	8

The relationship between the range of elevation (fall height H) and runout length (L) is shown in figure 6.22. The debris flows are shown to have large variability in both fall height and runout length, with some outliers present. These four outliers have been marked in the figure with their values. Debris slides have a very short runout and very low fall heights. They are all clustered in the lower left corner. The linear relationship for debris slides is $y = 0{,}3655x + 7{,}507$ with an r^2 of 0,4474. Runouts between 1200 and 1500 meter runout seem to have a variety of fall height within 500 meters. The linear relationship is shown to be $y = 0{,}3656x + 175{,}86$ with an r^2 of 0,6218. As expected, debris avalanches have very short runout lengths and relatively low fall height. The linear relationship is shown to be $y = 0{,}9309x - 79{,}751$ with an r^2 of 0,8298.

The relationship between the fall height (H) and the previous relationship (H/L) is shown in figure 6.23 and show the fall height compared to slide mobility. Again debris flows have a large variability, although most values are within a range of 0,2 and 0,96 H/L. Debris avalanches seem to follow almost a linear relationship between fall height and mobility and have most values within a range of 0,3 and 0,8, with one value of 0,9673. Debris slides all have a fall height below 40 meters, and a range between 0,2988 and 0,7738 in H/L values. One outlier (marked in figure 6.23) is seen having a higher H/L value (low mobility) of 1,2835.

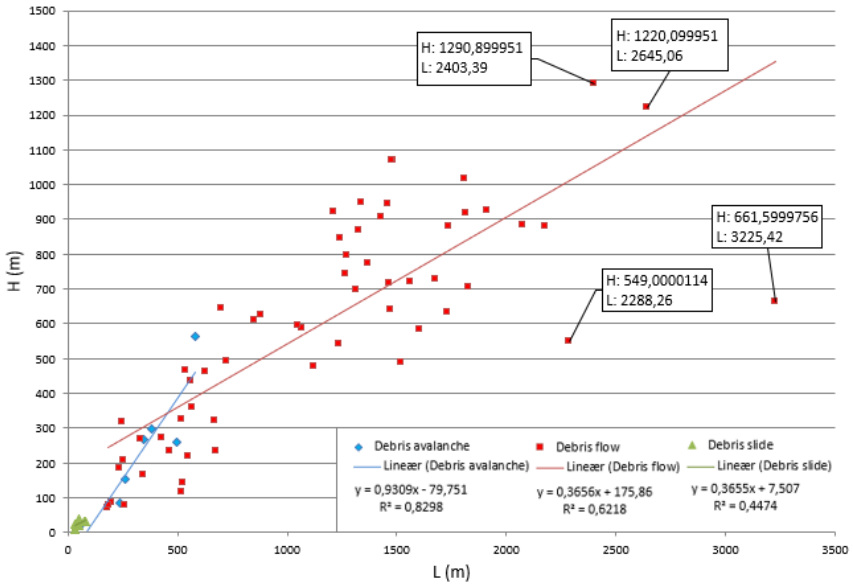

Figure 6.22: Relationships in terms of height (H) and runout length (L). Top: Relationship of H/L; height (H) over runout length (L). The plot is based on "dataset 2", with 78 polygons with typologies debris flows, debris avalanches, and debris slides.

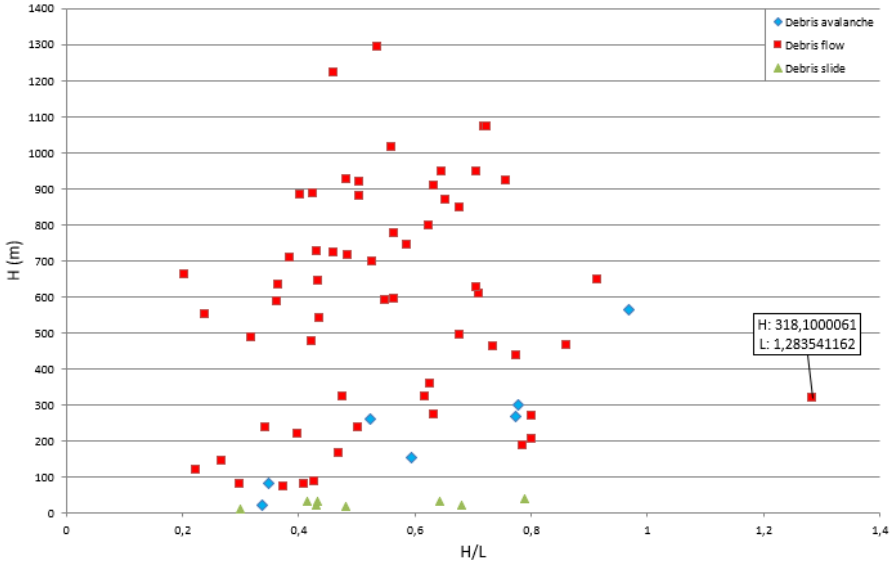

Figure 6.23: Relationship of height (H) over the relationship H/L; height (H) divided by runout distance (L). The plot is based on "dataset 2", with 78 polygons with typologies debris flows, debris avalanches, and debris slides.

6.4 Frequency-magnitude analysis

A frequency-magnitude analysis was performed using the landslides in "dataset 2", to find the typical magnitudes and their frequencies in the county. The result is shown in figure 6.24 and listed in appendix 8. The graph shows a great variety in landslide magnitudes, ranging from 206 m^2 to 140.359 m^2. However, most of the mapped landslides have an area between 4600 m^2 and 56000 m^2. The data shows that the county can expect ten landslides a year with a magnitude above 1000 m^2, about 7-8 landslides above 10 000 m^2 and ten landslides with a magnitude above 60 000 m^2. The curve follows the expected form, with a nearly linear relationship towards higher magnitudes, and a flattening of the curve at smaller magnitudes. The curve starts to decline around the magnitude of 5000 m^2 and steepens around 30 000 m^2.

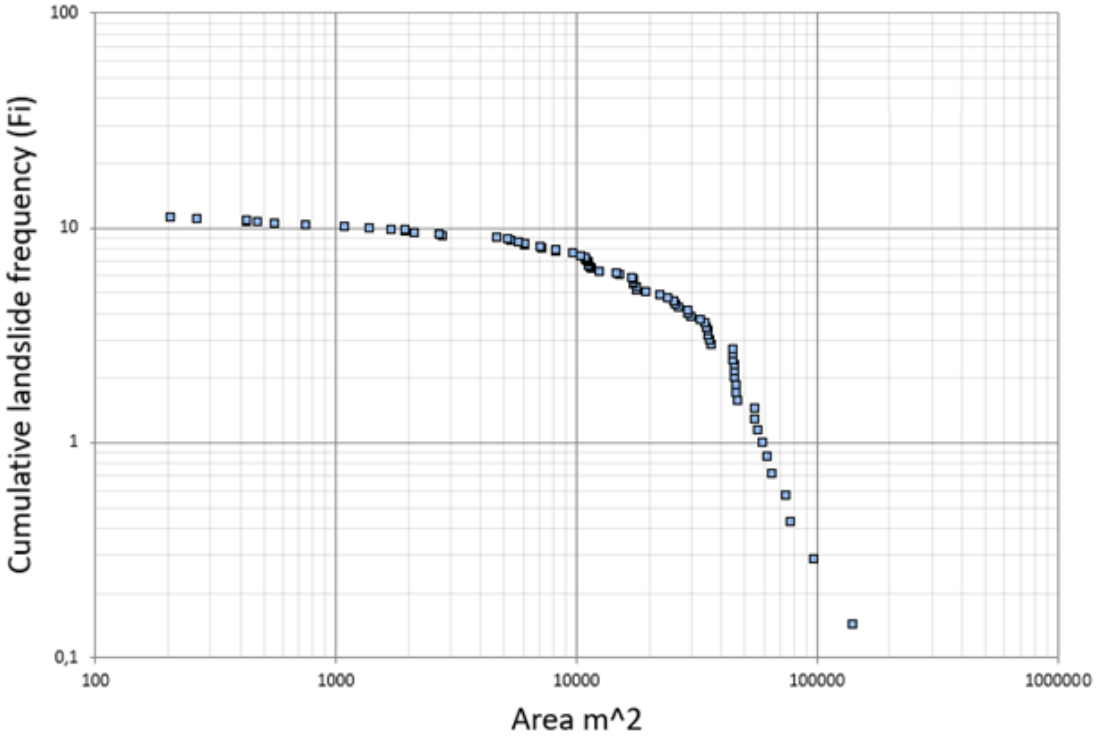

Figure 6.24: Frequency-magnitude curve.

Figure 6.25 shows the magnitudes related to different typologies. The debris slides are shown to represent the smallest magnitude, but with some at higher values. Debris avalanches are seen to be placed around the intermediate values. Debris flows are seen to represent a large range of values. The debris flows dominate the data, and therefore, controls much of the shape of the curve.

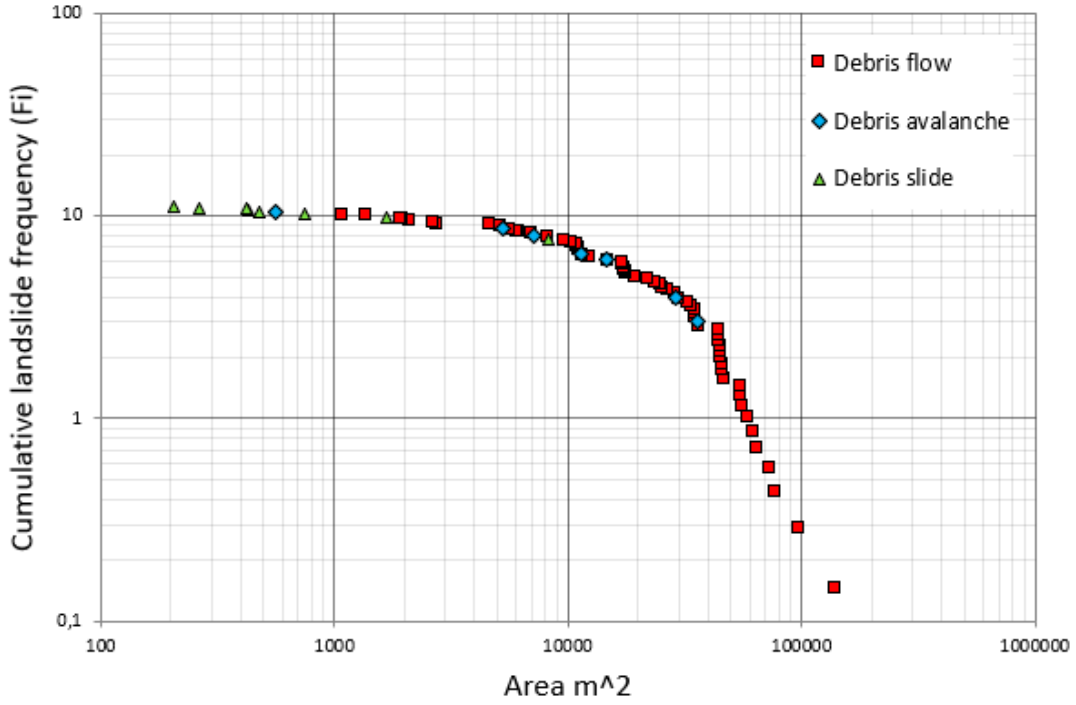

Figure 6.25: Frequency-magnitude curve for "dataset 2", divided into the landslide typologies.

The frequency-magnitude curve was also visualized by distinguishing the landslides triggered by the different weather events, to be later compared with the results from previous studies (Mongstad, 2018). Figure 6.26 shows that during "Dagmar," landslides with all magnitudes are seen to dominate the data strongly. The magnitudes of the landslides occurring during the different events are listed below:

- "Dagmar" (2011): Landslide areas have great variability, 206 m^2 - 140 359 m^2, and represent both the smallest and largest magnitudes on the curve.
- "Berit" (2011): Landslides are seen to range between 11 016 m^2 and 46 057 m^2.
- "Hilde" (2013): Landslide area ranges between 474 m^2 to 74 036 m^2.
- The event on March 20th, 2014: represents several of the smaller magnitudes, between 425 m^2 and 5 326 m^2.
- The event in October 2014: Landslides range between 6 153 m^2 and 8 245 m^2, but only two landslides have been mapped for this event.
- "Synne" (2015): Landslides from this event represent some of the larger magnitudes, between 10 924 m^2 and 56 619 m^2.

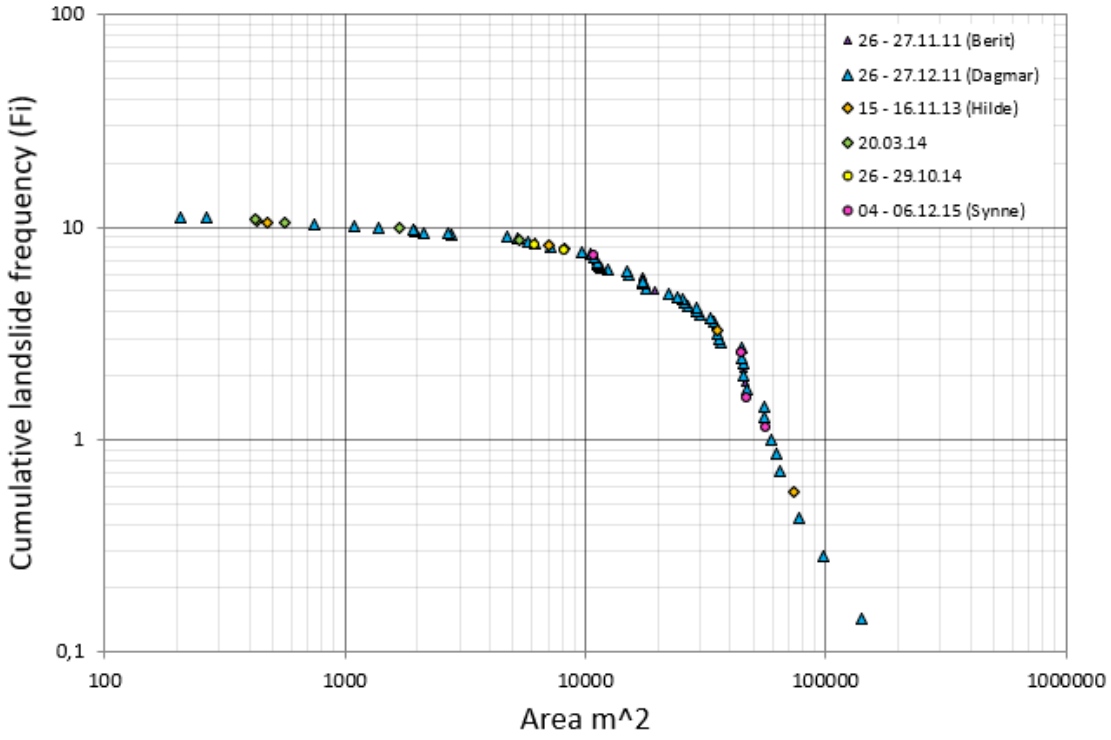

Figure 6.26: Frequency-magnitude curve divided into the six different weather events. The curve consists of 8 landslides for "Berit" (2011), 54 landslides for "Dagmar" (2011), five landslides for "Hilde" (2013), five landslides for March 20th, 2014, two landslides for October 2014, and four landslides for "Synne" (2015).

6.5 Time of occurrence and threshold analysis

In order to perform a threshold analysis, the time of occurrence of mapped landslides ("dataset 2") was necessary. This was obtained from the attribute table in the national landslide database. As mentioned in chapter 5.2, the time of occurrence registered in the database is assumed to be correct. The daily distribution is shown in figure 6.27, where 30 % of the landslides have an unknown time of occurrence. Another 30% occurred between 01:00 and 07:00, 15% occurred between 07:00 and 13:00, and 15% between 13:00 and 19:00. The last 10% occurred between 19:00 and 01:00. This confirmed what was already observed by landslide forecasters, that the majority (40 %) of landslides occur during the night (between 19:00 and 07:00).

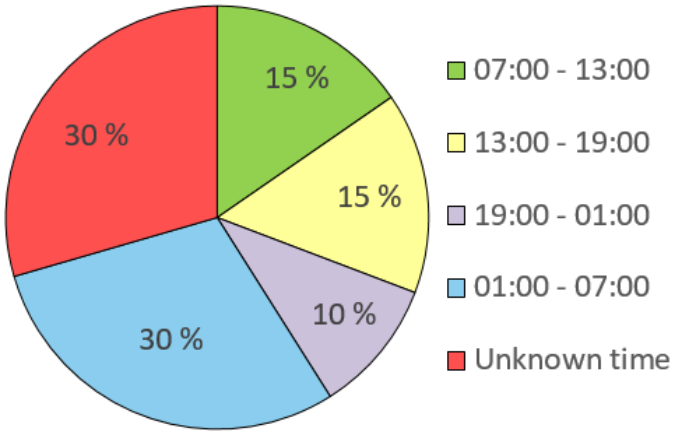

Figure 6.27: Time of occurrence for the landslide registrations in "dataset 2".

The time of occurrence and location of the initiation point of the landslides (“dataset 2”) were plotted against existing thresholds to evaluate the performance (figure 6.28). All values for relative water supply and relative soil water saturation are listed in appendix 9. The mapped polygons in “dataset 2” is here plotted as green squares, together with the Hydmet thresholds used in Western Norway (figure 2.5). The graphic shows a visual representation of the four thresholds used, in terms of relative water supply (%) and relative soil water content (%). Most of the data are located within the green level (1), with thirty landslides within this threshold (38%). Eighteen landslides (23%) falls within the yellow level (2), and twenty-seven landslides (34%) are within the orange level (3). No landslides are within the red level (3), and three landslides (3%) had the value “No Data” in the pixel of the initiation point and is placed in the left lower corner.

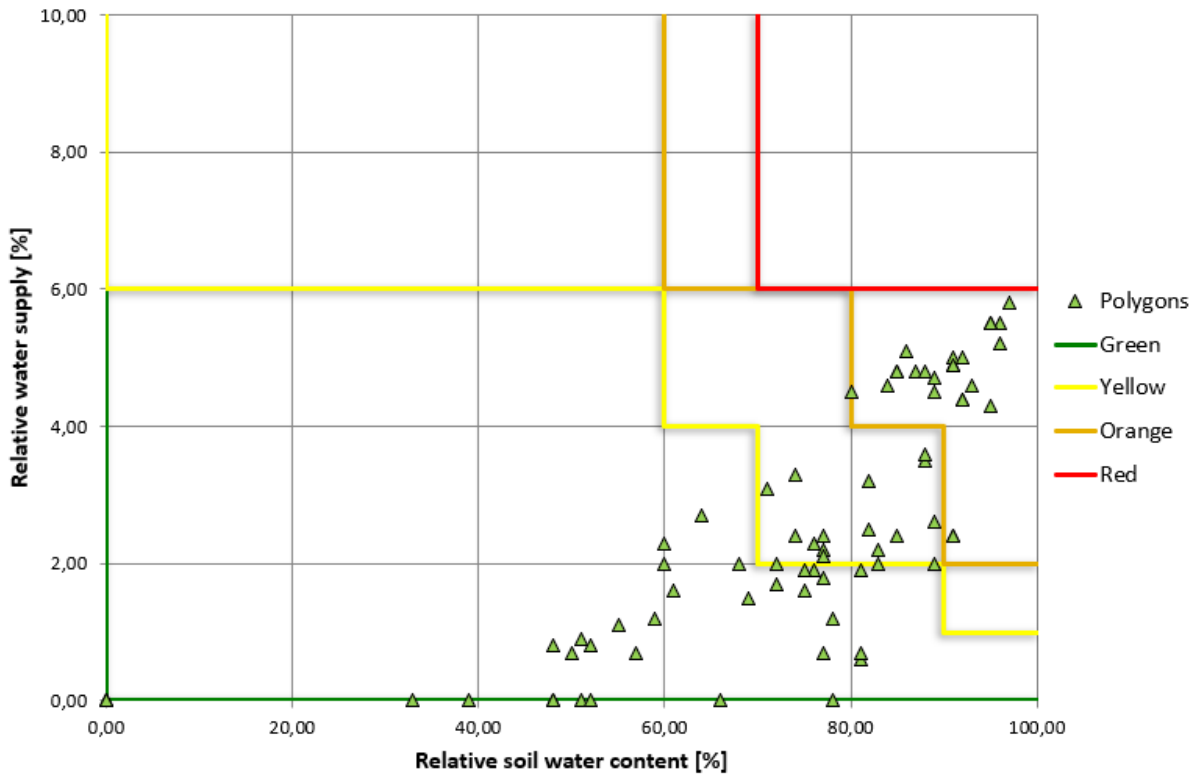

Figure 6.28: Landslides in "dataset 2" plotted on the Hydmet graph showing the corresponding warning levels.

In figure 6.29, the mapped landslides in "dataset 2" plotted distinguished into the weather events with their representative colors. This was done to see how the threshold performed during the different weather events. "Dagmar" (2011) landslide events seems to be spread out over several warning levels but also dominates the green level of warning (1). Events "Berit" (2011), "Hilde" (2013) and "Synne" (2015) is also present within the green level. All of the weather events represent the yellow level (2), but the events March 20th, 2014 and October 2014 is both only within this level of warning. The orange level (3) is only represented by "Berit" (2011) and "Dagmar" (2011). As mentioned above, none of the events reached a red warning level (4).

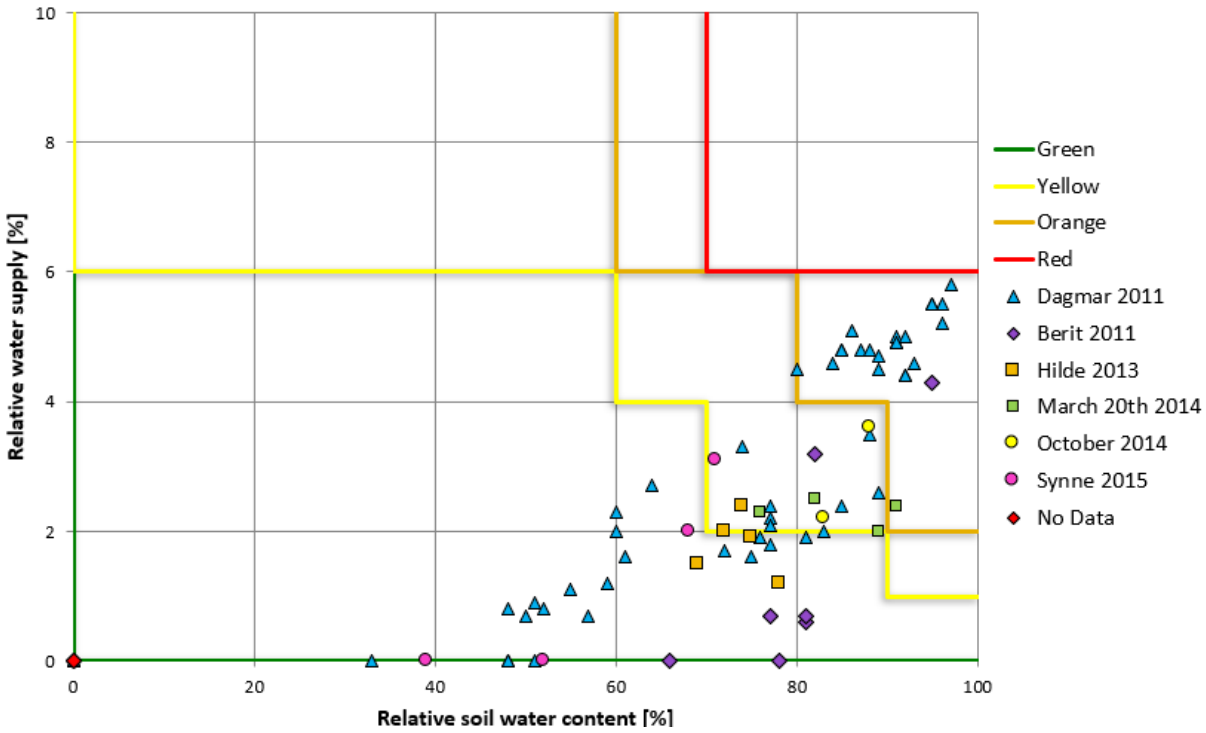

Figure 6.29: The landslides displayed with the weather-event color codes. The storms "Berit" (2011), "Dagmar" (2011), "Hilde" (2013) and "Synne" (2015) is all seen within the green level of warning.

The landslide events were plotted against the threshold map (Hydmet). Figure 6.30 show the Hydmet index map for each of the weather events investigated, for the day most landslides occurred. The landslide point registrations ("dataset 1") is shown in black for each of the weather events. The landslides are seen to cluster around the red, orange, and yellow areas. Some points are located in green areas.

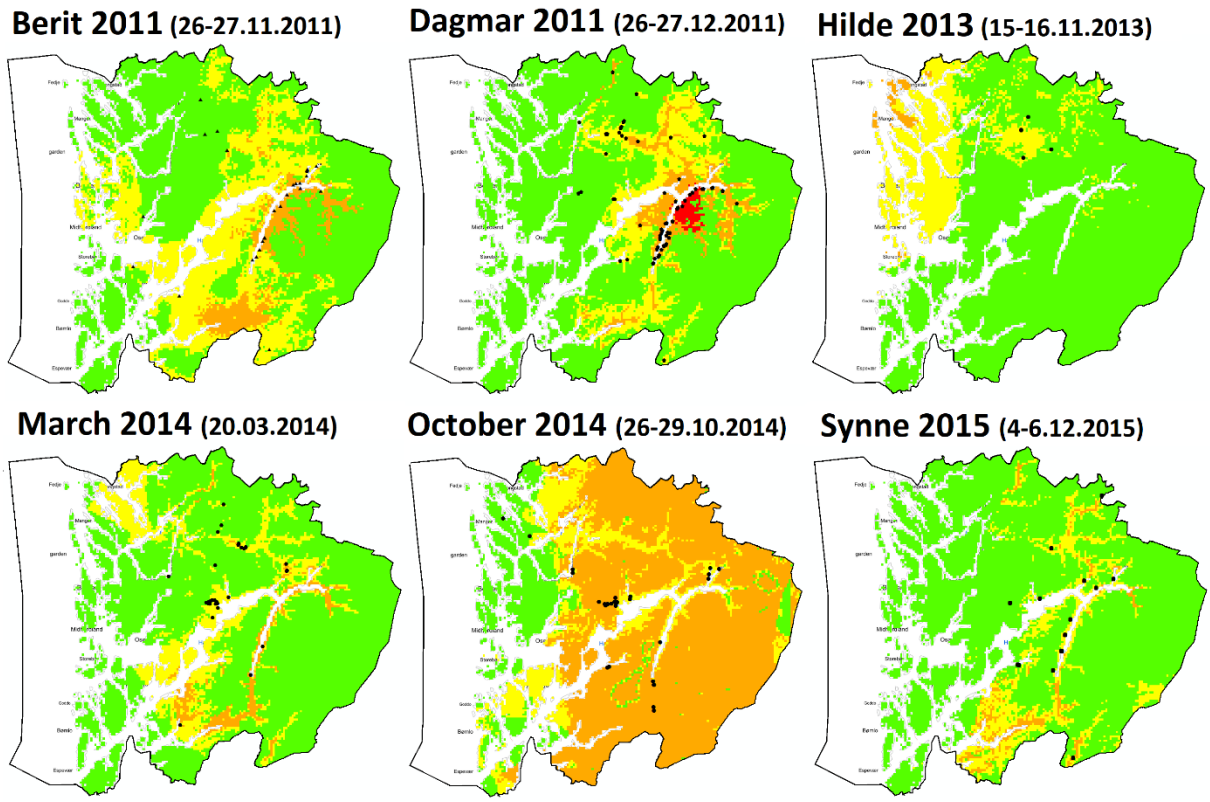

Figure 6.30: The Hydmet index map on the day most landslides occurred during the events. The landslide point data from the weather events are shown in black ("dataset 1"). (The dates of the maps are: 27.11.2011, 26.11.2011, 15.11.2013, 20.03.2014, 28.10.2014, and 05.12.2015.)

During the threshold analysis, the Hydmet index in the initiation point of the polygons in "dataset 2" was also found. The result is shown in figure 6.31, showing 30 landslides in the green level (1), 18 landslides in the yellow level (2), and 27 landslides in the orange level (3). No mapped landslides occurred in the red level (4). Three landslides started in a pixel with no data.

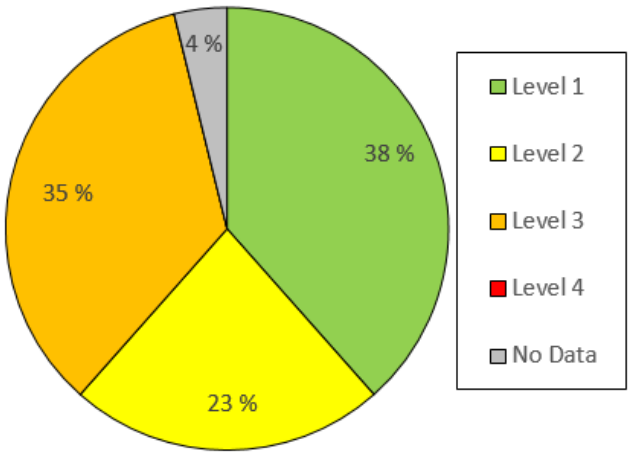

Figure 6.31: Percentage of polygons within the different levels in Hydmet. None of the mapped landslides occurred within the red level (4).

6.6 Warning levels

Since the landslide warning started to operate at NVE in 2013, 68 daily warnings have been issued in Hordaland in the investigated period, among them 61 yellow and 9 orange. No red level was issued in this period. Two of the warnings issued had both yellow and orange warning within the county. These two occurred during the event "Synne" in December 2015. The maximum warning levels disseminated each day can be seen in the graph in figure 6.32. The six weather events analyzed are all marked as well, showing their temporal distribution.

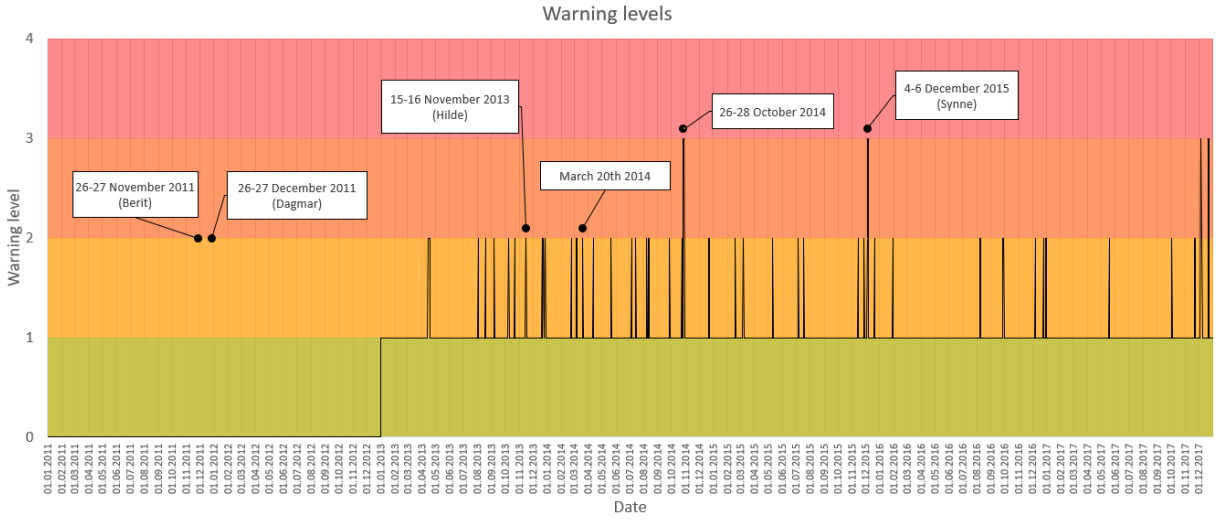

Figure 6.32: Maximum warning levels disseminated for all years 2011-2017 in the county. As the service was being tested in 2011 and 2012, there is no warning for these years.

A detailed overview of the warning levels issued each day for the events is shown in table 6.4, which also include the flood warnings issued for the events. The first two weather events in November 2011 "Berit" and December 2011 "Dagmar" occurred while the warning service was in a test-phase, and therefore no warning level was issued. Both events, however, had a flood warning issued, which indicated the possibility of landslides as well. The weather event in November 2013 "Hilde" was warned with a yellow level (2) in the entire county due to the high expected precipitation levels. The weather event on March 20th, 2014 caused a yellow warning (2) in the county, due to the heavy precipitation. Strong winds and high temperatures leading to higher snowmelt was also expected. The weather event in October 2014 was forecasted, and local authorities and the public were warned with an orange level (3). High soil water saturation and intense precipitation over several days led to the warning. The last weather event in December 2015 "Synne" was warned with two different warning levels, yellow (2) and orange (3). The orange level in the inner half of the county expected high levels of precipitation, in

addition to strong winds. High levels of soil saturation along with high temperatures, led to the expectation of a high level of snowmelt. For the yellow warning, the expected precipitation level was also high, with a high level of soil saturation. The spatial distribution of all warnings for the four events can be seen in figure 6.33.

Table 6.4: The different warning levels for all the weather events. For the weather event "Synne" in 2015, two warning levels were issued, yellow and orange.

Date	Landslide warning	Flood warning
26.11.2011 27.11.2011		Yellow (melding) Yellow (melding)
26.12.2011 27.12.2011		Yellow (melding) Yellow (melding)
15.11.2013 16.11.2013	Yellow Yellow	Yellow Yellow
20.03.2014	Yellow	Green
26.10.2014 27.10.2014 28.10.2014 29.10.2014	Orange Orange Orange Yellow	Yellow and orange Yellow and orange Yellow and orange Yellow and orange
04.12.2015 05.12.2015 06.12.2015	Yellow Yellow and orange Yellow and orange	Yellow Yellow and orange Yellow and orange

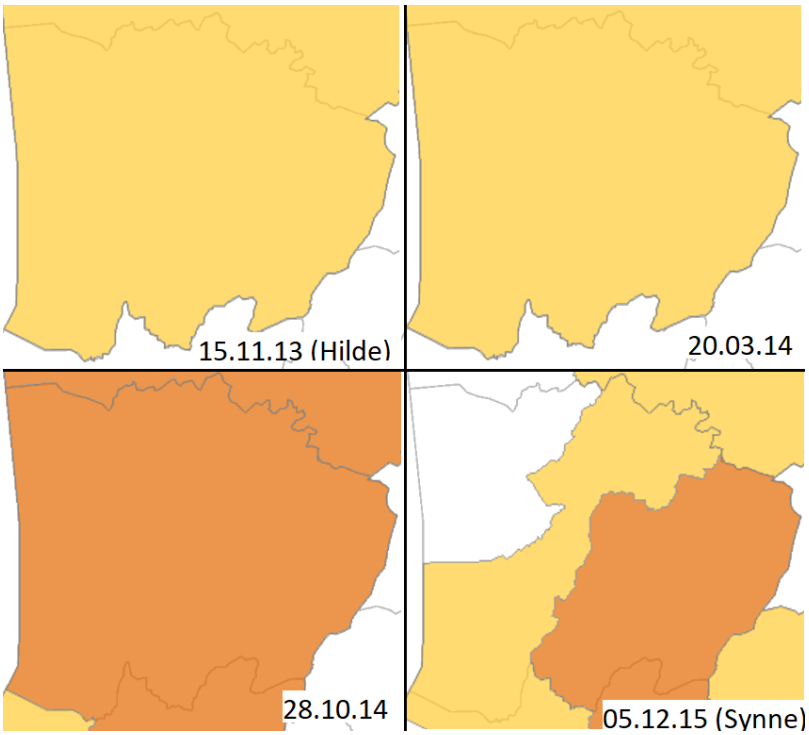

*Figure 6.33: Warning levels issued on the day most landslides occurred during the weather events. "Hilde" (2013) **(top left)** and March 20th, 2014 **(top right)**, both with yellow levels of warning in the entire county. October 2014 **(bottom left)** with an orange level of warning in the entire county. "Synne" (2015) **(bottom right)** with both a yellow and an orange level of warning on the same day.*

A quantitative evaluation in ArcMap of the warning levels issued during the weather events was attempted but was not successful due to technical issues. Therefore a qualitative evaluation was attempted, by counting the point data ("dataset 1") and noting the warning level (table 6.5). All events except "Synne" in 2015 had only one level of warning, and all landslide registrations were therefore within the same level. For "Synne", the registrations were split between the yellow level and orange level.

Table 6.5: Number of point data from "dataset 1" registered in the different warning levels issued.

Event	Date	Warning level	Landslides "dataset 1"
Berit 2011	26.11.2011	No warning issued	1
	27.11.2011	No warning issued	27
Dagmar 2011	26.12.2011	No warning issued	74
	27.12.2011	No warning issued	10
Hilde 2013	15.11.2013	Yellow	4 in yellow
	16.11.2013	Yellow	1 in yellow
March 2014	20.03.2014	Yellow	35 in yellow
October 2014	26.10.2014	Orange	4 in orange
	27.10.2014	Orange	4 in orange
	28.10.2014	Orange	24 in orange
	29.10.2014	Green	3 in green
Synne 2015	04.12.2015	Yellow	0 in yellow
	05.12.2015	Yellow and orange	1 in yellow and 13 in orange
	06.12.2015	Yellow and orange	2 in orange

7 Discussion

This thesis is part of an ongoing effort by the scientific community aiming to characterize rainfall-induced landslides in Norway better. This study analyzed landslides in Hordaland in the period 2011-2017, occurring during six weather events. Due to the expected increase in the frequency of extreme weather and landslide events, a better understanding of these landslides is necessary. This thesis analyzed rainfall events known to have caused several landslides, and the aim was to map as many of these landslides as possible in order to improve the knowledge on landslide magnitude (especially area, m^2). Although many landslides were mapped, challenges and limitations were encountered. The lack of aerial photos and lidar images in the region have been considered the main issue, as well as lack of satellite images. Not all investigated rainfall events initiating landslides were brought further into analysis due to this. Variable quality of landslide information in the national landslide database has influenced the analysis as well, and even with a quality control, several landslide events could not be confirmed.

7.1 Rainfall events and landslide distribution

During the analysis of rainfall, six extreme weather events were found to have enough supportive sources to map landslides. Fourteen other weather events were considered in the analysis, but these did not have enough aerial photos, lidar imagery, or other supportive data available, and were therefore not brought further into the analysis. These events occurred in 2011, 2015, 2016, and 2017, and included extreme events Aina (2017) and Birk (2017). All of the six selected weather events were present in the table obtained from supervisor Graziella Devoli, mentioned in chapter 5.1, and all caused several landslides.

As the mapping was based on the investigated rainfall events, the data is biased towards these dates. However, as mentioned in chapter 3.4, this selection is considered representative because previous studies have shown peaks for weather-induced landslides in Western Norway in November, December, followed by March, October, and January (Jørandli, 2016; Bugge, 2017; Devoli et al., 2017; Mongstad, 2018). The temporal distribution of the weather events selected from this analysis is therefore considered representative for the region. As mentioned in chapter 2.1.1, weather events as storms, intense rainfall, and rainfall combined with snowmelt are the

most common trigger of landslides in Norway (Sandersen et al., 1996; Nadim et al., 2009). Boje et al. (2014) also state that landslides in the regions along the coast are triggered especially in the fall, by long-lasting rainfalls and frontal precipitation. However, further analysis is needed both to improve the quality of the data and increase the number of landslides mapped, to create a better understanding of the typical landslides in the county. Especially landslides induced by snowmelt combined with rainfall, and landslides induced by general soil saturation, needs further investigation on the west coast (Boje et al., 2014).

The rainfall distributions during the selected rainfall events are shown in chapter 6.1.1, figure 6.5-6.10. All weather events have precipitation distributed over the entire county, with smaller clusters of higher intensity. The precipitation, however, is not the only factor that contributed to the landslides occurring during the events. As mentioned in chapter 6.1.1 were several of the events influenced by snowmelt. An example shown is "Dagmar" (2011) and "Synne" (2015) in figure 7.1. Both events occurred in December, and are seen to be heavily influenced by snowmelt (figure 7.1B). The precipitation pattern for "Dagmar" is clustered in Sørfjorden, and Etne and Kvinnherad municipalities (figure 7.1A). An increase in snowfall before "Dagmar" led to more snowmelt during this event, increasing the soil water input, especially along the fjords. The precipitation pattern for "Synne" is seen in one cluster in the same two municipalities, but only 20-40 mm in Sørfjorden. "Synne" in December 2015 experienced snowfall in the days prior, which caused increased snowmelt during the event.

Figure 7.2 shows a comparison of the two events in 2014, occurring in March and October, which have very different precipitation patterns (figure 7.2A). The event in October 2014 is seen to have both higher intensity and a larger area of precipitation above 60-80 mm. However, the snowmelt (figure 7.2B) is much higher during the event on March 20th, increasing the total amount of water supply to the soil. The duration of the events was also different, as the October event lasted four days. The two events resulted in the same amount of landslides, which shows the importance of including the influence of snowmelt as a landslide trigger.

The other two weather events both occurred in November in different years and were not significantly influenced by snowmelt. "Berit" in 2011 had little snowmelt, mostly in the higher plateaux. "Hilde" in 2013 was not influenced by snowmelt, as much of the county was not covered with snow.

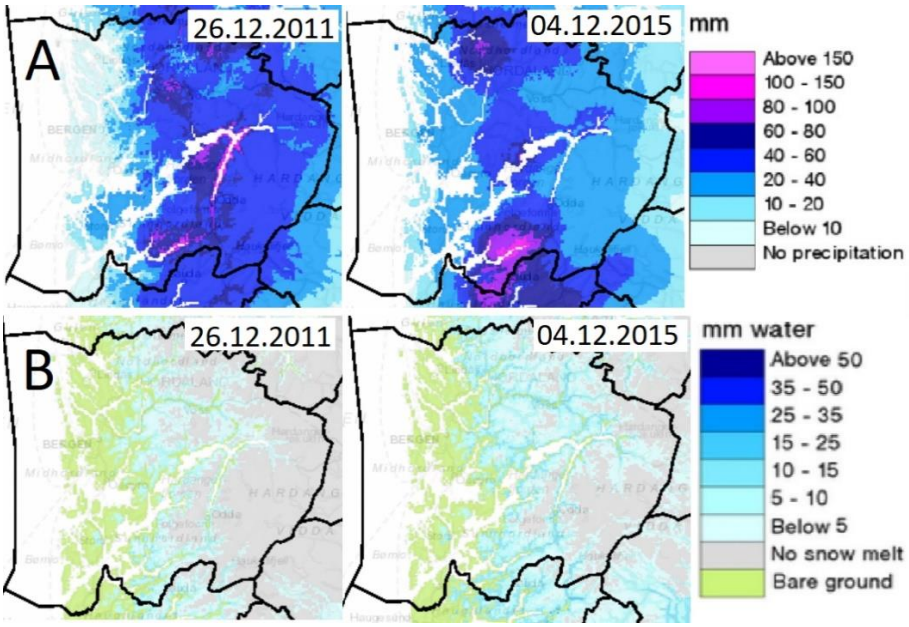

*Figure 7.1: Similarities in the influence of snowmelt for the two events "Dagmar" in 2011 and "Synne" in 2015".. **A**: Precipitation. **B**: Snowmelt. Both events were significantly influenced by snowmelt (from xgeo.no).*

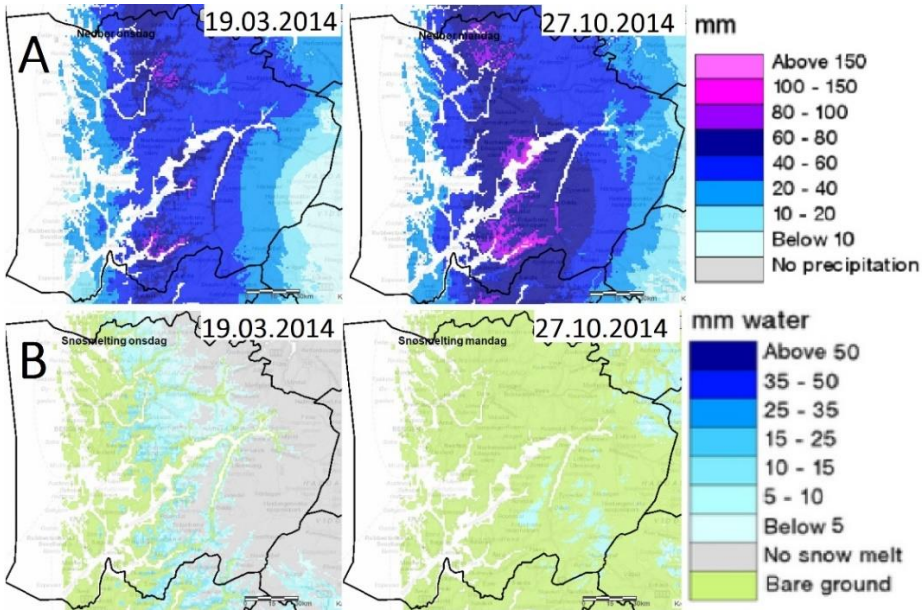

*Figure 7.2: Difference in the influence of snowmelt for the two events occurring in 2014, in March and October. **A**: Precipitation. **B**: Snowmelt. March is seen to have much higher snowmelt than October (from xgeo.no).*

Four of the selected rainfall events were winter storms, experiencing not only rainfall but also strong winds. Strong wind is found in several studies to influence the vegetation on slopes, which can further influence slope stability (Dai et al., 2003; Jakob et al., 2012; Smith, 2013; Antinao and Farfán, 2013; Schanche, 2014). Vegetation provides stability of slopes, in terms of hydrological and mechanical effects (Dai et al., 2003). When strong winds disturb the vegetation, the slope becomes more susceptible to landslides as the root strength is reduced,

and the runoff characteristics are changed (Jakob et al., 2012). As strong winds were a significant factor in several of the events, it is important to consider. The storm "Dagmar" (2011) was especially influenced by strong winds, as mentioned in chapter 6.1.1. "Berit" (2011) one month before was also influenced by wind, but to a less degree as it moved further north along the coastline (Bøyum, 2011). An example is shown in figure 7.3, showing fallen trees after the storm. Strong winds were also a factor during "Hilde" (2013), also with power outages due to wind, but not as strong as "Dagmar" (2011) (Gjengstø and Malvik, 2014). This storm also hit the coastline further north, reducing the damages in Hordaland. The storm "Synne" (2015) was less influenced by the wind and more by rainfall and snowmelt. An increase of snowfall before the event possibly led to the absorption of some of the rain during the event in some areas (Holmqvist, 2016). The two other weather events investigated occurred in March and October, and consisted of rainfall combined with snowmelt, and intense rainfall respectively, and was therefore not affected by wind to the same degree. Other effects of wind are further discussed in chapter 7.5.1.

Figure 7.3: Cleanup of fallen trees in Kismulvegen in Bergen after "Berit" (2011). Other trees were also cut as a preventive measure to avoid similar damages at future storms. (Source: Bergensavisen/Arne Ristesund)

The spatial distribution of "dataset 1" is influenced by many landslides having occurred along roads, railways and close to buildings and other infrastructure. The different spatial patterns between the different weather events could be partially explained by the spatial distribution of the rainfall and snowmelt. The landslide events during storms "Berit 2011", "Dagmar 2011" and "Synne 2015" mostly follow the steep sides of the fjords. The landslide events on March

20th and in October 2014 both have many landslides occurring in less steep areas, in Nordheimsund, and around Evanger. The October event seems to have landslides spread all over the county while the March event was more clustered. The landslides from "Hilde 2013" are spatially distributed in the northern part of the county because this weather event hit the Western coastline further north, and seemed to have less impact on Hordaland than the other weather events. Due to the different weather events having both different triggers and clusters, a quick comparison was made between the event on March 20th in 2014 and "Dagmar" in 2011 (figure 7.4). 15 out of 35 landslides during the "March 2014" event occurred in Nordheimsund, consisting of mostly weathered material. In contrast, 42 out of 85 landslide events during "Dagmar" occurred in Sørfjorden, consisting mostly of "thin or no cover" and "moraine material". The spatial distribution of the landslide events (appendix 5), confirms how the named extreme weathers (except Hilde) all trigger landslides in Sørfjorden, while the events on March 20th and in October 2014 mostly trigger landslides in Nordheimsund. The quaternary deposit is very different in the two areas. Nordheimsund consisting of finer materials might need more water input to trigger landslides. In comparison, Sørfjorden, with steep slopes and thin materials, might not need as much water input to trigger landslides. This implicates that Sørfjorden is more susceptible to landslides during winter storms, and Nordheimsund is more susceptible to heavy snowmelt and long-duration rainfall. It is also observed that most landslides registered in Sørfjorden are debris flows, while many landslides in Nordheimsund are smaller debris slides.

Figure 7.4: Example of landslide point data from "dataset 1" together with the quaternary deposit. "March 2014" event in Nordheimsund on the left and "Dagmar 2011" in Sørfjorden on the right (the right picture shows only 27 of the landslide points due to the resolution of the map).

The point data seems to follow the topography rather than the precipitation pattern. The landforms alpine relief and glacially scoured low mountains and valleys dominated the data with 94% of the landslides, showing the high susceptibility of these landforms. The point data are mostly placed at locations of very high susceptibility in the map from Cepeda and Bell (2014), but also some in high and medium susceptibility. Due to the point often being placed at the deposit, the actual initiation point might be placed at a different level. For the map from Fischer et al. (2014) the point data seems to follow the susceptible area for the most part, but some are also registered outside.

7.2 Mapping and landslide characterization

7.2.1 Selection and quality control of landslide data

As visible in the map (figure 6.11 in results) many of the landslides are registered along Sørfjorden. This pattern is assumed to be both because of the steep sides of the fjord being prone to landslides, but also because of the important roads on each side, causing the population to be isolated when blocked by landslides. They will, therefore, have a larger probability to be registered and mapped by NPRA. The same applies to the landslides along the train tracks further north, being registered by BaneNOR. These landslides will have good media coverage, as they cause a big impact on the population (Krøgli et al., 2018). Landslides occurring in remote areas will likely not be mapped due to not causing damage or disturbance to the infrastructure or population (Guzzetti, 2005; Jaedicke et al., 2009; Boje, 2017).

As the work began, an assumption was made together with supervisor Karianne Staalesen Lilleøren that the date and time in the database were correct. This assumption was made to have a basis for the mapping, as it was difficult to check the accuracy of this. The registrations were still evaluated critically, and a few were later assumed to have the wrong date, based on other sources found. After the first selection with the national database was done, the quality control was conducted. The polygons received from other students were investigated, and several of the landslides mapped were interpreted slightly different from these. A reason for this could be the choice of map scale, which aerial photos used and other possible sources available. Figure 7.5 shows an example with two polygons from “dataset 2” and from Bakken (2017). As the

interpretation of aerial photos and other sources during mapping is subjective, this is likely to affect results of an analysis.

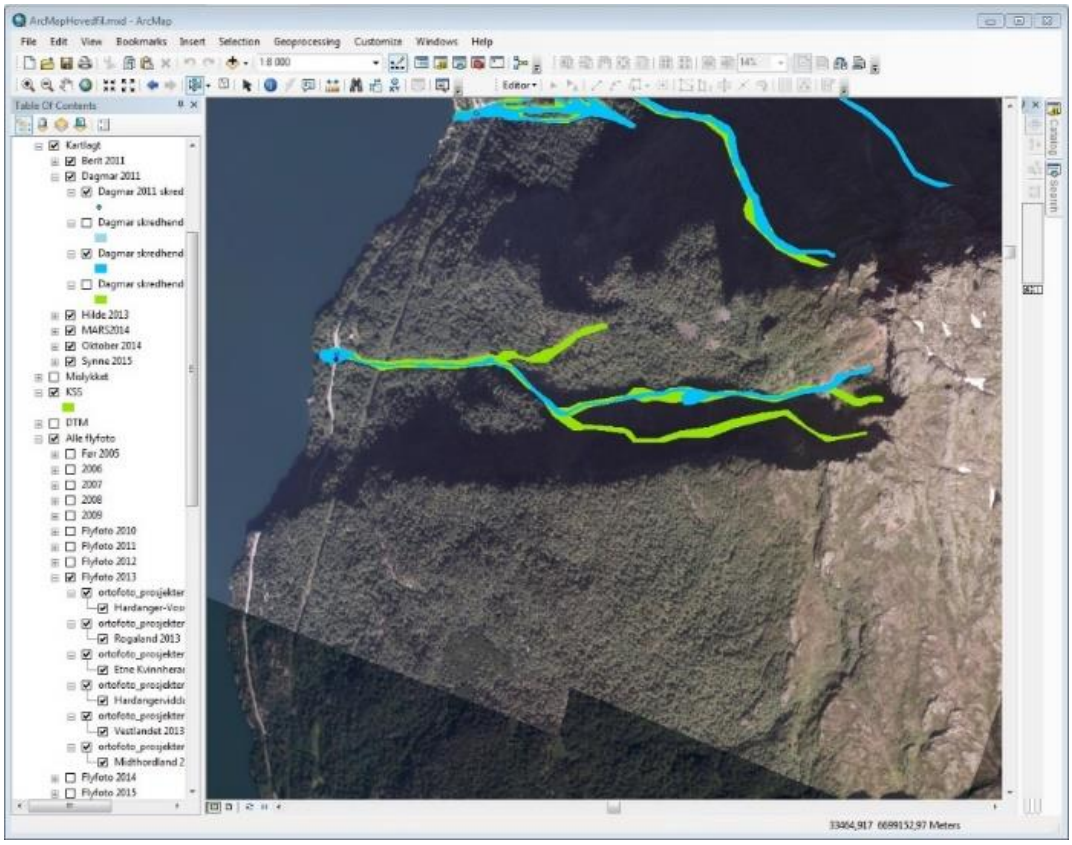

Figure 7.5: Example difference between Bakken (2017) polygon and new polygon. It is possible that two different aerial photos were used, as there was spotted minor differences between some images taken at similar times.

7.2.2 The mapped polygons: Dataset 2

A total of 205 events were investigated, but only 75 of these could be mapped. Some of the events had more sources available, most photos were available for the storms "Dagmar" in 2011 and "Synne" (2015), but some photos were available for other events as well. It is likely that a media focus has influenced the sharing of pictures and information. Several of the photos that were used during the mapping was of roads, railways, and infrastructure, showing the bias towards these landslides (Krøgli et al., 2018). Most of the landslides mapped were characterized as debris flows. As a result of this, the basis for drawing any definite conclusion based on the debris slides or debris avalanches is too weak. The interpretation done during the mapping must also be considered, as this is also a possible source of error.

7.2.3 Challenges during mapping

Different challenges appeared during the mapping process, many of which were expected. These are explained in detail separately below.

Aerial photos and lidar images

The lack of aerial photos and lidar images taken after the events were considered the main limitation during mapping. There were quite a few aerial photos available, making the use of them limited, as shown in figure 7.6. Some aerial photos were available after 2014, but these did not cover the areas with registered landslides. In these cases, the other sources were used as primary sources, like news, reports, and photos taken of the events. Often photos are taken at the deposit, making it difficult to draw the source area and path precisely. The event "Dagmar" in 2011 has quite good aerial photo coverage after the event. Other events have very limited aerial photo coverage. There was also a lack of lidar images; an example of the coverage is also shown in figure 7.6. All years had few lidar images available, making the use on them limited. All aerial photos and lidar images available the years after all the events are shown in appendix 3 and 4.

In some cases, the lidar images were a good supporting source. Especially when aerial photos like "Vestlandet 2013" had many shadowed areas, making it difficult to spot differences such as soil discoloration and disturbed vegetation, as explained in chapter 5.2.3. In these cases, other aerial photos were used, as well as lidar images to see the changes done by the landslides. Many of the debris flows occurred in steep streams and gully's, and these were easily located on lidar images. Some of the older aerial photos were of lower quality, with either bad resolution or distortion in the image, making it hard to define precisely the path of the slide.

During mapping, other landslides registered in the NLDB were compared to make sure the landslide visible was indeed the one on the date in question. Several areas in Hordaland are especially prone to landslides, and therefore have many registrations in the same areas. Some landslides occurred in the same path during different events but were in the same aerial photo. In these cases, individual evaluations were done in discussions with supervisor Graziella Devoli whether or not to include both landslides, and these were included as "uncertain", as they may have had different tracks for each event. This issue was the case for four landslides registered

both for “Berit” (2011) and “Dagmar” (2011), but both visible in the same aerial photo taken in 2013. There is no way to differentiate between the two events one month apart, as no other sources are picturing or explaining the “Berit” landslides. These landslides from “Berit” are therefore considered having a higher level of uncertainty.

Another limitation was represented by the fact that landslides were not visible in the available aerial photos; there were several reasons for this. Some debris flows were less visible in the aerial photos, either due to channelization or the presence of vegetation like indicated in Jakob et al. (2012). As mentioned in chapter 2.2.1, a problem with using aerial photos is the vegetation hiding the smaller landslides (Brardinoni and Church, 2004). Guzzetti (2005) also pointed out the problem of landslides being obscured or canceled in aerial photos by erosion, vegetation, urbanization, and human action. Another common problem in Norway is that landslides affecting roads and railways are often cleared quickly to get traffic moving again after the event. Examples of this are shown in figure 7.7. In cases where a debris flow track was covered by vegetation, lidar images could be of help, but a certain level of interpretation of the initiation point had to be made. Another possible cause of errors was the time passed between the landslide occurrence and the aerial photo capture. The landslide trace might be erased with time. These changes could be either human activities, or other landslides that have occurred in the area, as was the case for “Berit” and “Dagmar” in 2011.

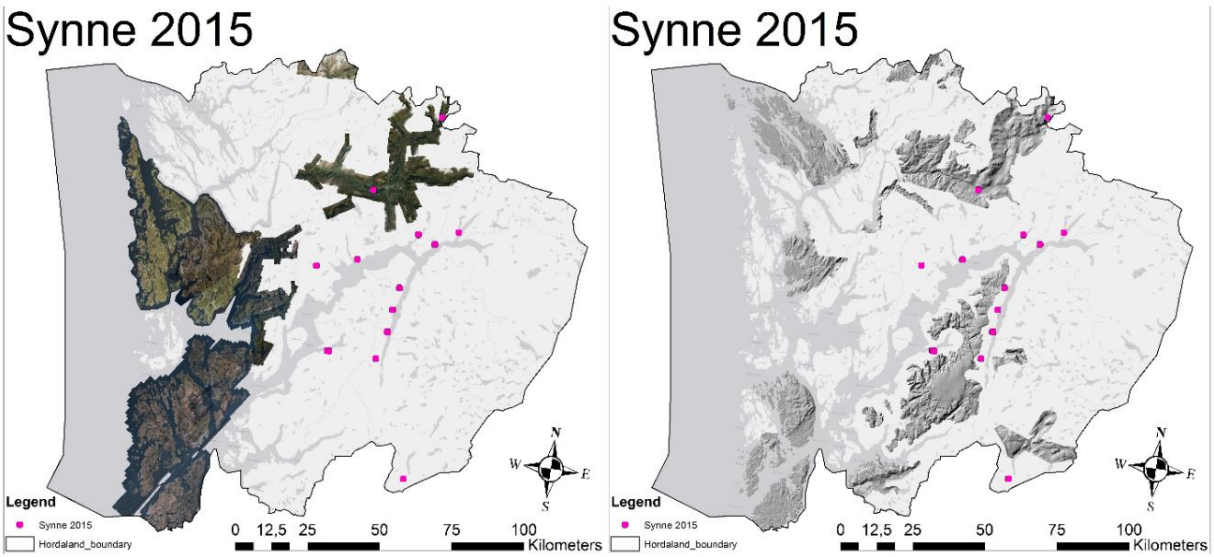

Figure 7.6: Example of data imagery available for the event “Synne”. ***Left to right****: Available aerial photos, and available lidar images. All aerial photos and lidar images available the years after all the events are shown in appendix 3 and 4.*

News and media

Using media as a source had a good outcome during the mapping, as they contained both descriptions and pictures. These were most useful for large events affecting roads and infrastructure, as expected. Media sources often used dramatic headlines and kept the focus on people affected, and when the situation would be resolved. Articles had variable descriptions of the landslides and could have the wrong typology. Several of the pictures used in media did not show the entire extent of the slide, but rather either a picture of the deposit, clearing of the streets or railways (figure 7.7), damages caused by the landslide, or people inspecting the damages to their property. Smaller landslides were often, if mentioned at all, commented briefly. Pictures taken of smaller landslides were often taken at close range and was therefore not much help in mapping the extent and precise location. For instance, several debris slides occurring during the event on March 20th, 2014 were mentioned in an article describing the evacuation of the inhabitants in the area, but no pictures or descriptions of the landslides were available (figure 7.8).

Figure 7.7: Roads (top) and railways (bottom) getting cleared quickly after landslides. All pictures were taken during "Dagmar" in 2011, except the top left, from "Hilde" (2013) top left.

Figure 7.8: Example of a newspaper mentioning landslides in the area, but not giving any useful information for mapping the landslide extent and location (red square, source: NRK).

The national landslide database (NLDB)

The mapping was based on the available data in the national landslide database, and this is contributed to by several different authors. Several landslides were registered by civilians and unknown contributors. As Jakob (2005) explains, the human memory can be highly selective, and they might be biased towards more recent events. People can also favor larger events and events with great consequences for the affected. Some landslides had several registrations for the same landslide, or a registration mentioning several landslides. One example of this was seen for three landslides occurring in Rogdo in Ullensvang during "Dagmar" in 2011 (figure 7.9). The three landslides had four registrations, some mentioning more than one landslide. Two of the landslides combined into one track and hit the main road together. The NPRA made two registrations of these two landslides, while NGU made one registration for both landslides and placed the point further up the slope. An unknown contributor made a registration mentioning all three, but with a focus on the smaller landslide occurring further upslope in between other two. It is important to have a common and clear system for registrations in the NLDB to avoid problems like this. The accuracy of time and location of the landslide was also variable. Time accuracy varied from exact to 5 years, and location accuracy varied from exact to 5000 meters.

Figure 7.9: Example of double registration. Three landslides, with four registrations. The registrations varied in the description, some mentioning more than one slide, and the points were in different locations.

7.3 Landslide characteristics in Hordaland

7.3.1 Evaluating the performance of susceptibility maps

The point data from "dataset 1" and polygons from "dataset 2" were both plotted against the two available susceptibility maps in the county. The susceptibility map from Fischer et al. (2012) seemed to fit well both the point data in "dataset 1" and polygons in "dataset 2". The Cepeda and Bell (2014) susceptibility map seemed to fit well with most landslides, the landslides outside the red areas (very high susceptibility) occurred during storms "Dagmar" (2011) and "Synne" (2015) and could have been influenced by other factors as well. A problem was discovered with the map, and this could not be fixed in time to run another analysis in this work. Discovering this problem, however, will lead to this being fixed in the future. The polygons were analyzed with a qualitative assessment and found to be a good fit with the map.

7.3.2 Characterization of landslides in terms of topography and geology

About 85% of the landslides are within a range of 24,13 - 45,28°. The debris avalanches range between 25 and 50° slopes. Based on the NVE guide for mapping of landslides in steep terrain (Schanche, 2014), debris avalanches in Norway typically initiate above 25-30°. The results from Sandøy et al. (2017) show slope angles between 22° and 53°. Both of these findings fit well with the debris avalanches in "dataset 2". For debris slides the typical slope angle is also 25-30° and above, which fit most of the debris slides in "dataset 2", except two initiated at 23,5746 and 23,6813 degrees. These two landslides are however very close to this criterion, also considering the possible errors concerning the interpretation of initiation point and other weather factors. A wrong interpretation of initiation point will further give errors in other characteristics collected in the map, such as the height of initiation, slope angle, and runout length. Interpretation of typology can also be a factor, especially with landslide events with few sources available. The debris flows occurring at lower slope angles could have been interpreted as a wrong typology, or be a mix of several typologies, therefore not being within the expected range of 25-45° (Fischer et al., 2012). The landslide events were marked with a level of certainty, and additional quality control might be beneficial for the lower certainty landslide events. 76,2% of the mapped debris flows were within the expected range.

The mean aspect of the landslides mapped was 228 degrees. The vector strength was calculated to be 0,071161434, which is very small. As mentioned in chapter 5.3, a value close to zero indicates that the vectors are widely dispersed (Davis, 2002). Given the differences in topography and direction of the valleys, this might explain the result. The main direction of the topography is west-east, but two joint valleys also occur in the north-south direction. One of these, Sørfjorden, represent a significant amount of the data. The lack of trend in the aspect of the landslides occurring in the county will, therefore, be affected by these great differences of slope aspects.

In terms of bedrock, two classes were strongly represented; "diorite- to granite gneiss, migmatite" and "volcanic rocks (unspecified)". According to Fischer et al. (2012), the bedrock type largely defines the intensity and type of weathering. This further influence the loose sediment availability, type, and grain size, which influence the possibility of debris flows. The study from Fischer et al. (2012) found that areas prone to debris flows consisted of gneissic rocks rather than granitic. This fit with some of the dominating classes being "diorite- to granite

gneiss, migmatite" and "mica gneiss, mica schist, metasandstone, amphibolite", but "granite, granodiorite" is also represented, as well as one class "augen gneiss, granite and foliated granite", which is mixed. The quaternary deposit dominating the landslide is "thin or no cover", but not specifying what kind of " thin cover" this is, followed by "moraine material, thin cover". Fischer et al. (2012) found that the lithology, type, and distribution of the quaternary deposits on a slope are decisive for the slope's sensitivity to debris slope activity. Aside from the "thin cover", the other sediment classes representing debris flows in "dataset 2" are "moraine material" (till) and "previous landslides deposits" (talus), which was also the sediments in the investigated areas in Fischer et al. (2012). However, both of the geological datasets are on a 1:250.000 scale and are not of the same quality in all areas, limiting the potential of making a geological distinction between areas susceptible to debris flows (Fischer et al., 2012).

7.3.3 Typical landslide parameters

The landslide areas were found during the drawing of polygons for "dataset 2". Debris slides were found to represent the smallest magnitudes, which was not surprising. However, the transition between debris slides and debris avalanches is seen to overlap. The largest debris slide is mapped as 8245m^2, and the smallest debris avalanche is mapped as 558 m^2. There is no official area limit between the two landslide typologies, and therefore some might have the wrong typology. This is difficult to determine during mapping before the area is found. Some debris flows are very large, up to 140.359m^2. These might have either been drawn too long, or been classified wrong, and in reality, be slush flows.

The great variety seen in the maximum elevation between the landslides can be explained by the vast difference in topography in the county. Many landslides occurred on steep slopes, with the upper parts at high elevation. Others occurred in lower lying areas. The values representing debris flows are, however, very high. This can be due to errors during mapping, as interpretation was done.

Comparing the runout lengths of "dataset 2" with typical runout lengths in Norway, the results are variable. Debris flows have the longest runout distance, of typically up to 500-1000 meters, but this is based on few data (Devoli, 2017). The debris flows in "dataset 2" is seen to have run out lengths of around 185 – 3225,42 meters. However, this includes possible outliers. These long runouts might indicate that these debris flows might be slush flows. Without the outliers,

the maximum runout length is 2179,84 meters. As debris flows normally do not stop until the slope is equal to zero (Devoli, 2017), this might explain the long runouts for some mapped debris flows as they often stop at a road or in the fjord. Sandøy et al. (2017) found that the runout length of 5 studied debris avalanches were 0,8-1,6 km. The debris avalanches mapped have a runout length of 59,36 to 582,63 meters, which is far below the results in Sandøy et al. (2017). However, the study is based on only five mapped debris avalanches, which all occurred in a different county. The typical debris avalanche for Hordaland might have different typical characteristics. Also, "dataset 2" consists of only seven debris avalanches, making it difficult to draw a definite conclusion on typical runout lengths. Debris slides have runout lengths between 29,78 and 77,65 meters.

The fall heights and runout lengths of the mapped landslides were plotted to investigate their relationship. This relationship between the height of fall and runout length (H/L), which together creates the angle of reach (α), is a well-known expression of mobility (Corominas, 1996). Figure 7.10 shows their relationship on a slope. Many researchers agree that a greater height of fall leads to longer runout (Corominas, 1996; Dai et al., 2003; Devoli et al., 2008; Qarinur, 2015). However, the H/L relationship alone is not sufficient to properly describe mobility (Devoli et al., 2008), and other factors influencing landslide mobility needs to be taken into account. According to Corominas (1996), mobility also depends on several factors like material properties, the slope geometry, the slope inclination, and any topographic obstacles and constraints in the path. Topographic constraints and obstacles will affect the runout distance of a landslide, and this will cause scattering in the data (Corominas, 1996). Some clustering was seen in the H/L plot (top figure 6.12), showing a variety of runout length for similar fall height. Similar results were also found in Devoli et al. (2008) and Qarinur (2015), for longer runout distances. Devoli et al. (2008) considered high-intensity rainfall as a possible reason for the longer runout distances, and that the runout distance was likely sensitive to the amount of water during the event, but this could however not be proven due to limited data. The landslides mapped in this thesis all occurred during different extreme weather events, which included large amounts of water. It is, therefore, possible that this is an explanatory factor for the scattering in the plot.

Devoli et al. (2008) also found that the material properties influenced runout distances of landslides with similar fall height and topography. The fall height is also dependent on both the

volume (Corominas, 1996; Devoli et al., 2008) and the slope angle (Corominas, 1996). The volume has not been calculated during this thesis. As the county has great variations in slope angles at initiation, in addition to large variations in height above sea level, it might be a good approach to divide it into smaller areas of similar traits to compare the different influencing factors of mobility.

Two outliers can be seen on the lower right (figure 6.22) with long runouts compared to their heights; these are marked with low qualities and unknown starting points. As they may have initiated further downslope, the subjective interpretation of this could, therefore, be a cause for these outliers. Both landslides had limited information available, limitations in both aerial photos and lidar imagery, and was registered as "unspecified landslide in soil". Both are drawn in the location of the location name, but it is unsure how precise this is in the database. They might also be slush flows but mapped with the wrong typology. The location of one of the outliers has been influenced by human activity, and this may lead to other changes in the area and further misinterpretation. Two other outliers are also seen on the top right (figure 6.22) and are seen to have very high fall heights compared to the rest of the data. In figure 6.23, one outlier can be seen with a very high H/L value (low mobility) in comparison with fall height, meaning the runout length is surprisingly short. The slide has a very steep initiation angle, which increases downslope, and stops at a road with a sudden slope reduction. The slide possibly went further into the fjord. The slide seems to have a small volume and occurred in an old path, which may have influenced the mobility as well. It is important to note that the dataset is dominated by landslides hitting roads, railways or buildings, often ending their paths in a body of water. This factor can influence the natural runout lengths expected from the fall height.

The r^2 for the landslide events indicate that the debris avalanches are best described by their empirical relationship, with an R^2 of 0,8298, but only seven debris avalanches contribute to the plot. The R^2 for debris flows of 0,6218 was improved to 0,7319 when excluding the five outliers, but there is still a spread in the data for longer runouts. For debris slides, the low R^2 values of 0,4474 represent only eight debris slides. It is, therefore, a need for more data to produce an accurate plot of the empirical relationship for these landslide types.

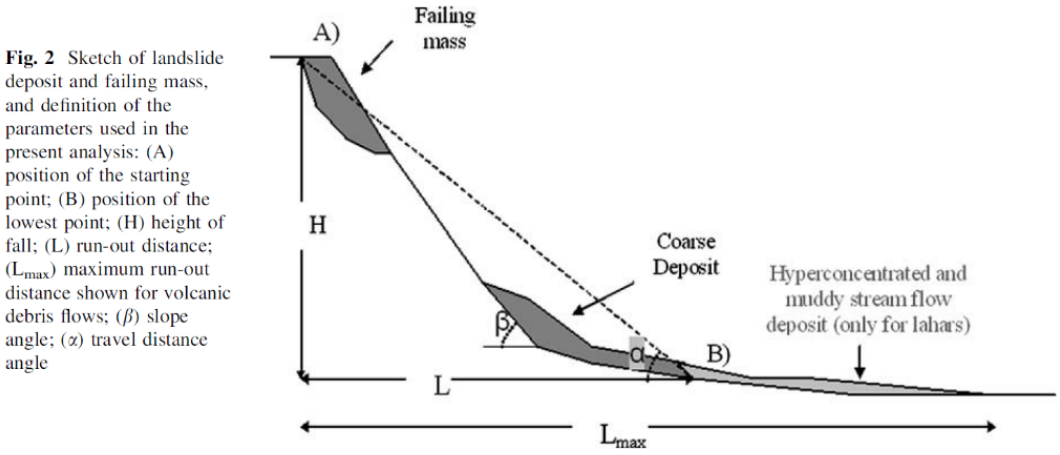

Fig. 2 Sketch of landslide deposit and failing mass, and definition of the parameters used in the present analysis: (A) position of the starting point; (B) position of the lowest point; (H) height of fall; (L) run-out distance; (L_{max}) maximum run-out distance shown for volcanic debris flows; (β) slope angle; (α) travel distance angle

Figure 7.10: The relationship between the height of fall (H) and run-out distance (L) of a landslide. Travel distance angle (α), also called the angle of reach, is marked in grey. Figure modified from Devoli et al., 2008.

7.4 Frequency-magnitude analysis

A frequency-magnitude analysis was performed using the areas calculated from the 78 mapped polygons and plotting them against the cumulative landslide frequency. The magnitudes ranged from 206 to 140359 m^2, with about 75% of the data ranging between 4685 and 64 787 m^2. This range is, however, not necessarily the most frequent magnitudes. As mentioned in chapter 2.2.1, to do a hazard or risk analysis, the landslide inventory needs to be as complete as possible (Corominas et al., 2013). "Dataset 2" is not a complete inventory, as several landslides could not be mapped, which will influence the analysis performed with the data. Many of the landslides not mapped were of smaller magnitudes, which is seen in the plot. An underestimation of lower magnitudes is seen in several studies (Stark and Hovius, 2001; Brardinoni and Church, 2004; Dahl et al., 2013). The assumption that missing data is likely smaller magnitudes were also suggested by Hungr et al. (1999). However, some of the landslides not mapped was also registered as unknown or larger magnitudes, and several variable magnitudes are likely to be included in the missing data.

The reasons for this underestimation are explained in chapter 7.2.3. The main problem influencing the smaller magnitudes was the lack of aerial photos and the variable quality of those available. The lack of aerial photos after 2013 was considered a major limitation, and the mapping relied on other available sources and pictures. Several landslides could not be mapped because they were covered by vegetation, and were not visible in aerial photos. A lack of media attention for smaller landslides was also observed. The smaller landslides are not usually

reported, while the larger landslides got most of the attention. Landslides blocking roads and railways were quickly cleared (figure 7.4), and this also influenced the lack of visibility in aerial photos taken years later. Similar causes for lack of smaller magnitudes are also found in other works, as Stark and Hovius (2001), Brardinoni and Church (2004), Jakob (2005), Guzzetti (2005) and Corominas and Moya (2008). The choice of basing the analysis of extreme weather events might have also influenced the number of smaller registered landslides. It is also vital to include other possible explanations for the lack of smaller magnitudes, besides lack of data. As mentioned in chapter 2.2.1, geomorphological explanations are also possible; both the significance of water and groundwater and the different influence of cohesion and friction on small and large landslides, respectively. The county might be more prone to larger landslides due to the topography, while smaller magnitudes are prevented by vegetation as proposed by Dahl et al. (2013).

The plot (figure 6.15) has a typical shape similar to other works (Guthrie and Evans, 2004; Guzzetti, 2005; Dahl et al., 2013), with a lower frequency for smaller magnitudes and a near-linear relationship for the larger magnitudes. The point of rollover, where the data moves away from the power-law, is gradual, and not easily placed. The reason for this might be the low sample size, but Stark an Hovius (2001) also stated that a cumulative distribution hides the rollover as it causes a smoothing of the curve. A mathematical power-law based on the curve shape is still suggested below in equation 5 (figure 7.11):

$$Y = 5\mathrm{E} + 09x^{-1,02,021} \qquad R^2 = 0,9443 \tag{5}$$

This equation, however, only describes 43% of the data and describe landslides with magnitudes above 20 000m^2. A power-law describing around 70% of the data was attempted, but had an R^2 of 0,8509, and was, therefore, a less good fit (but still good). This second power-law describes landslides with magnitudes above 7100m^2. Due to the known lack of smaller magnitudes in "dataset 2", it is assumed that the first suggested power-law is valid even though the percentage of data is low. The power-law and rollover point does, however, not fit as well as the examples shown in chapter 2.2.1, from Guthrie and Evans (2004) and Dahl et al. (2013). A larger and more complete dataset is needed to get a clearer relationship between frequency and magnitude in the county.

Some anomalies are seen around 44600 m^2 to 46700 m^2. The plot shape is an almost straight vertical line, with close magnitude values. This deviation from the general shape of the curve could indicate wrong values for the landslide area, as this had a subjective interpretation during mapping. These polygons were then investigated again. Some of them were found to have occurred in the same path as another slide in a previous weather event, possibly influencing the interpretation of the different landslide events, and increasing the chance that an error has been repeated during mapping. Other landslides were influenced by other factors, as hitting mitigation measures and passing roads. As pointed out by Dai et al. (2003), interpretation from aerial photos depends not only on the skills of the observer. It also depends on both the quality of the photos and the conversion of information from the aerial photo to the base map. There are, therefore, several possible reasons for these anomalies, and an increase of data for the analysis might also have had an impact on the shape of the curve.

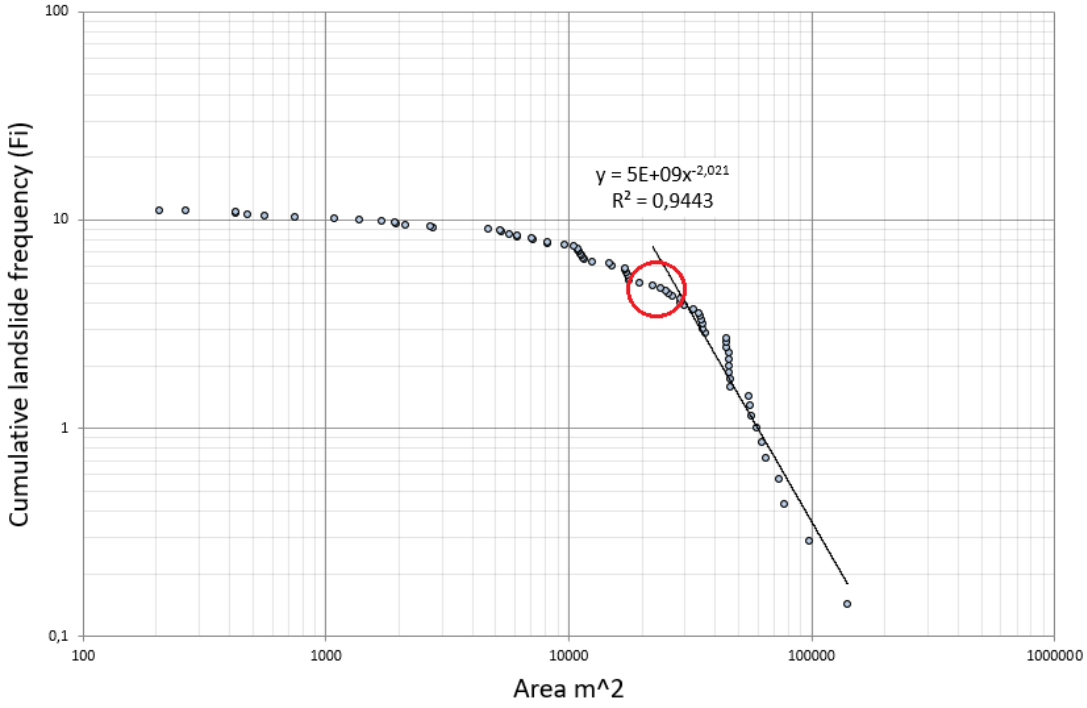

Figure 7.11: FM curve with the proposed trend line, and a possible rollover point within the red circle.

"Dataset 2" was split into the different landslide typologies in figure 6.16, to investigate any differences in characteristics between them. As debris flows greatly dominated "dataset 2", and have a great variety in magnitudes, they are also dominating the curve. They also represent the largest magnitudes in the dataset. Debris slides represent the smallest magnitudes, as expected, with two larger contributions of 1691 m^2 and 8245 m^2. Other factors possibly influenced both of these. The first of these occurred in a road cut, sliding down from one road to another, which

could influence the size and reach. The second large landslide slid out into a river and was likely influenced by water erosion due to the increased amount of water in the river in addition to the river cut.

Because “Dagmar” (2011) dominates “dataset 2”, it will represent most of the landslides in the frequency-magnitude analysis (figure 6.17). The data from the four winter storms are seen to represent the larger values. The two other weather events, occurring in March and October in 2014, have all landslide magnitudes below 10 000 m^2. Both of the latter weather events had a high percentage of registrations from unknown contributors, including a good amount of text in the comment column. Both events lacked aerial photos, which lead to many landslides not being mapped. Many comments, however, mentions “small landslides”. Considering the lack of media support during mapping for these two events, it is likely many of the landslide events during these two weather events were smaller landslides, and not as news-worthy as the larger landslides during the storms. Most landslides in the media were either landslides that hit houses or roads, and others were briefly mentioned. Some of the landslides in the database were however described as “large”, or of unknown size, and a larger sample size is needed to get a good representation of the weather events. For the three first events (“Berit” (2011), “Dagmar” (2011), “Hilde” (2013)) which all had aerial photos, many landslides were not visible, and it was assumed these were of small magnitude. There is therefore likely a lack in smaller magnitudes for these three events as well. “Synne” (2015) also lacked aerial photos, but the comments have descriptions of unknown sizes, and there is also here a need for a larger sample size to find a good representation of magnitudes from this event.

As mentioned in chapter 4.2, another data set was used as a supportive source during the mapping of landslides in ArcMap. This dataset consisted of polygons drawn by other students (Bakken, 2017; Bugge, 2017), and was divided into the different weather events. As the basis for the mapping was the date of occurrence, many polygons were not used as they had an approximate time interval and could not be dated precisely. Some of these occurred outside the period 2011-2017, and these were therefore excluded. Many of the remaining polygons could not be linked to a data point in the national landslide database and were therefore not included in “dataset 2”. However, 22 of the polygons with approximate time were inside the 2011-2017 period, 10 from Bugge (2017) and 12 from Bakken (2017), in addition to the 31 polygons used for the mapping in “dataset 2”. These were therefore put together in another frequency-

magnitude plot, to provide a larger dataset for the county (figure 7.12). The other dataset is seen to contribute in a variety of magnitudes, especially smaller, lifting the flattened side of the curve.

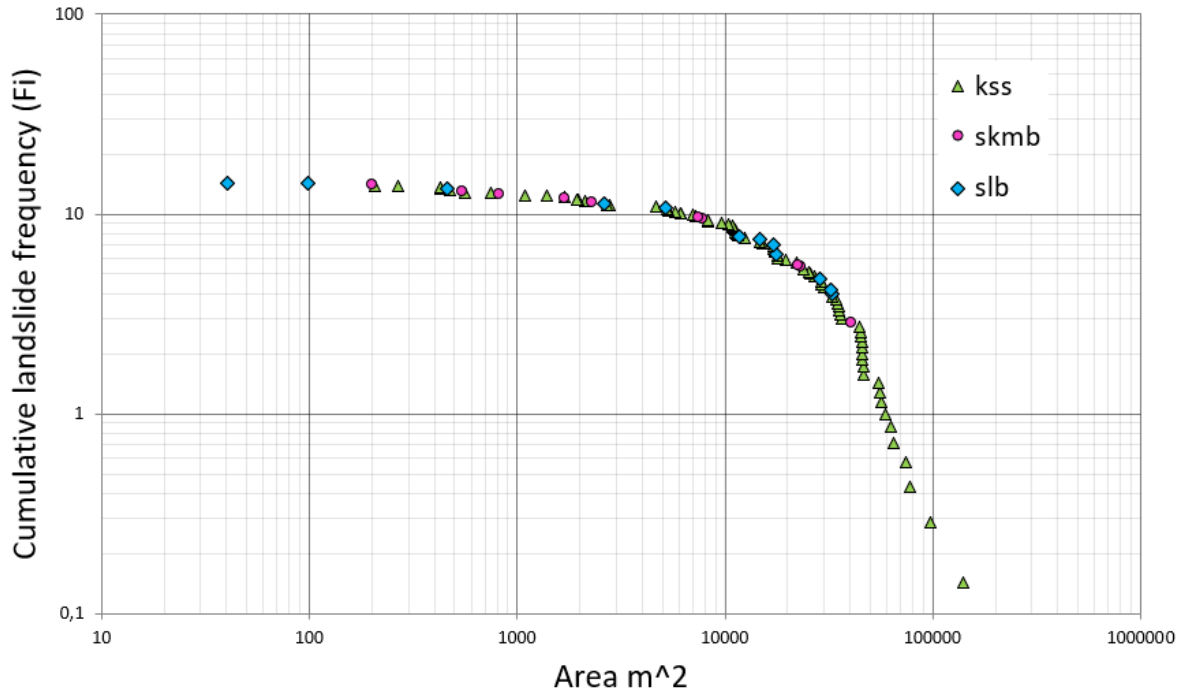

Figure 7.12: All landslides mapped in Hordaland occurring between 2011 and 2017. Some data were excluded due to possibly being outside the period. Landslides from "dataset 2" named kss in green, data from Bugge (2017) named skmb in pink, and data from Bakken (2017) named slb in blue.

A power-law relationship was found here as well (equation 6). This curve is seen below in figure 7.13, with a similar shape as "dataset 2".

$$Y = 7\text{E} + 09x^{-2,062} \qquad R^2 = 0{,}9547 \tag{6}$$

This equation describes 40% of the data and also describe landslides with magnitudes above 20 000m^2. The trend line is slightly steeper than for "dataset 2" alone, and the two other datasets (Bakken, 2017; Bugge, 2017) contributed with mostly smaller magnitudes, therefore increasing the frequency of these as expected. There is, however, still an underestimation of smaller magnitudes, and the curve is still flattened out on the left side. It is likely these other datasets also lacks smaller magnitudes by the same causes as "dataset 2". The point of rollover is placed similarly as for "dataset 2", although the curve is still gradual as it moves away from the power-law.

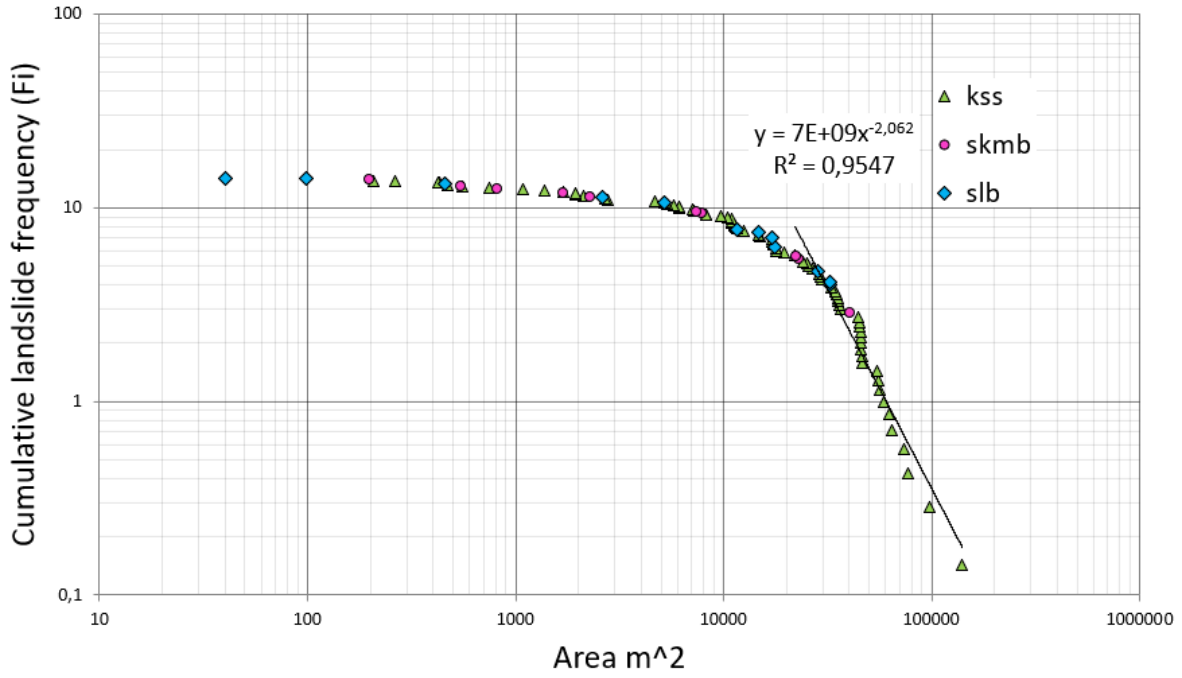

Figure 7.13: All landslides mapped in Hordaland occurring between 2011 and 2017. A trend line is suggested, representing 40% of the data. Landslides from "dataset 2" named kss in green, data from Bugge (2017) named skmb in pink, and data from Bakken (2017) named slb in blue.

7.5 Threshold analysis

The analysis of threshold performance shows that many landslides occurred below the minimum threshold. Dividing the landslide into the six weather events, figure 6.20 shows that only storms are present in the green warning level (1). This is initially surprising as all these storms seemingly caused significant precipitation and initiated several landslides. This indicated an error either in measurements of precipitation, in the model used to simulate the data or the threshold used.

The thresholds used in Norway are continually under adjustment, as the data basis is improved (Boje et al., 2014). Several sources of error are, however well known, both regarding the observed data and the simulated data, especially the observation of precipitation (Boje et al., 2014; Boje, 2017). The model is based on interpolated grids, leading to underestimation of the daily values and lower thresholds than in reality. The model itself is also a simplified version of reality, which causes systematic errors. The simulation of the thaw- and melt processes will, therefore, be simplified because of the use of these daily values (Boje et al., 2014; Boje, 2017). Another source of error is the time frame used to split the precipitation between days (from 07:00 am to 07:00 am), which can cause an issue if the precipitation and/or snowmelt triggering

the landslide is split over these two days. This split will result in lower variables than what is a reality (Boje et al., 2014; Boje, 2017).

The measurement of precipitation is often underestimated, falling victim to large errors and biases (Wolff et al., 2015; Kochendorfer et al., 2017). Measurements of rain can be greatly underestimated if it is windy during the rainfall, such as during storms (Pollock et al., 2018). Snowfall can be underestimated to an even higher degree. This underestimation is due to two factors; the fall speed and the turbulence around the precipitation gauge (Wolff et al., 2015; Kochendorfer et al., 2017), which can cause the precipitation to be deflected and therefore not measured. This effect increases with higher wind speeds, decreasing the measured precipitation (Kochendorfer et al., 2017). All of the landslides within the green level occurred during the storms "Berit" (2011), "Dagmar" (2011), "Hilde" (2013) and "Synne" (2015), which all included strong winds.

Accuracy in measurements also depends on the classification of the thresholds for the different types of precipitation. When temperature thresholds are used to define precipitation types, the amount can be misclassified (Kochendorfer et al., 2017). In Norway, the temperature is used to determine the kind of precipitation that occurs (Engeset, 2016). The snow model, based on the HBV-model, uses daily precipitation and daily temperature to estimate the relative water supply and relative soil water content. The precipitation is classified as rain if the mean air temperature is above 2,0^{o}C, as sleet between 2,0 and -0,5^{o}C, and as snow if it is below -0,5^{o}C. The hydrological model is very sensitive to low temperatures around these thresholds (Boje et al., 2014). If these inputs were to be influenced by these measurement and model errors, the calculated water supply to the soil could be too low. Before and during the storms the temperature in xgeo is seen to stay around these thresholds, giving large variations in precipitation types. The exception is in the eastern mountain plateau where the temperature is slightly lower, and the outermost coastline in the west where the temperature is slightly higher. The temperature and rainfall increase during the storms, before the temperature drops after or at the end of the storms. All of the storms occurred during November and December, and especially "Dagmar" (2011) and "Synne" (2015) experienced increased snowfall before the event. "Berit" (2011) seemed to rather have an increase of snow during the event, mostly in the highlands, but the landslides mapped has a larger level of uncertainty due to its close temporal proximity to "Dagmar". The landslides showing 0% relative water supply all occurred during

these three winter storms. Winter conditions like these storms are a known difficulty in the work with hydrometeorological thresholds (S. Boje, personal communication).

7.6 Evaluation of warning levels

A quantitative evaluation of the warning levels issued was initially attempted to perform in ArcMap but was not possible due to technical issues. A qualitative evaluation of the warning levels issued was then attempted by counting the point data ("dataset 1"). However, after discussions with supervisor Graziella Devoli, a qualitative evaluation was determined to be more difficult to achieve than first assumed. The evaluation used in the landslide forecasting and warning service is qualitative and more complex than just counting the number of landslides and takes more factors into account. Simply counting landslides that occurred in Hordaland during the events will therefore not give any valuable result in evaluating the warning level issued. The evaluation of the warning levels is, therefore considered incomplete. However, the number of landslides and their spatial occurrence in accordance with the warning levels are still valuable information to NVE.

7.7 Comparison of Hordaland and Sogn og Fjordane

The results of the mapping were compared with results from the adjacent county Sogn og Fjordane (Mongstad, 2018). The two counties are both situated at the west coast and experience similar weather and topographical conditions. The landslides mapped in Sogn og Fjordane are mapped in the same methodology as in this work, and he experienced many of the same issues. The final number of polygons mapped is similar, 56 landslide events mapped in Sogn og Fjordane, and 78 mapped in Hordaland. Both datasets consist of very few debris slides. For Hordaland, the mean area of debris avalanches (14.385 m^2) is larger compared to Mongstad (2018), which have a mean value of 12.251 m^2.

In comparison to Mongstad (2018), Hordaland seems more prone to debris flows, whereas Sogn og Fjordane seems more prone to both debris flows and debris avalanches. However, as mentioned in chapter 7.3.3, some debris avalanches in "dataset 2" might be wrongly classified as debris slides in Hordaland. In terms of mean values, debris flows in Hordaland is seen to have longer runout (1169 m) than those in Sogn og Fjordane (774 m). Debris slides are also

seen to have slightly longer runouts, with a mean value of 50 m in Hordaland and 42 m in Sogn og Fjordane. The debris avalanches have a longer runout in Sogn og Fjordane (526 m), compared to Hordaland (338 m). Slope angles are similar for the two counties and shown to mostly occur between 30-50^{o} for both debris flows and debris avalanches for Sogn og Fjordane. In Hordaland, debris flows mostly occur between 30-45^{o}, and debris avalanches 25-35^{o}. All six weather events in this work were present in the dataset from Mongstad (2018), and landslide data from these are included in the comparisons below.

7.7.1 Frequency-magnitude analysis comparison with Sogn og Fjordane

Figure 7.14 shows the frequency-magnitude analysis for Hordaland (red triangles) together with the data from Sogn og Fjordane (blue squares; Mongstad, 2018). Both curves follow the expected shape with the lower frequency for lower magnitudes. The data cannot be combined into one graph representing both counties. As mentioned in chapter 2.2.1, the relationship cannot be applied in other regions with differences in size and relief (Hungr et al., 2008). Because of the influence of the local scale of the slopes, the plot will then under- or overestimate the magnitudes. The landslides in Hordaland are mapped during extreme weather events, and the landslides in Sogn og Fjordane are mapped year-round, which might be a possible influence on the data. However, the adjacent regions are both situated on the west coast, with steep slopes and similar weather patterns. Several of the landslides are also mapped for the same weather events in both counties, showing the similarities in their susceptibility during these events.

Figure 7.15 shows the data for just the weather event “Dagmar” (2011) in both Sogn og Fjordane (Mongstad, 2018) and Hordaland. Sixteen landslides were mapped for “Dagmar” in Sogn og Fjordane, and 54 was mapped for Hordaland. As seen in the graph, Hordaland has several larger magnitude landslides mapped, and a wide specter of magnitudes, while Sogn og Fjordane has most landslides at a more intermediate level of magnitude. The event “Dagmar” also largely dominate the dataset from Mongstad (2018) with a 28% contribution.

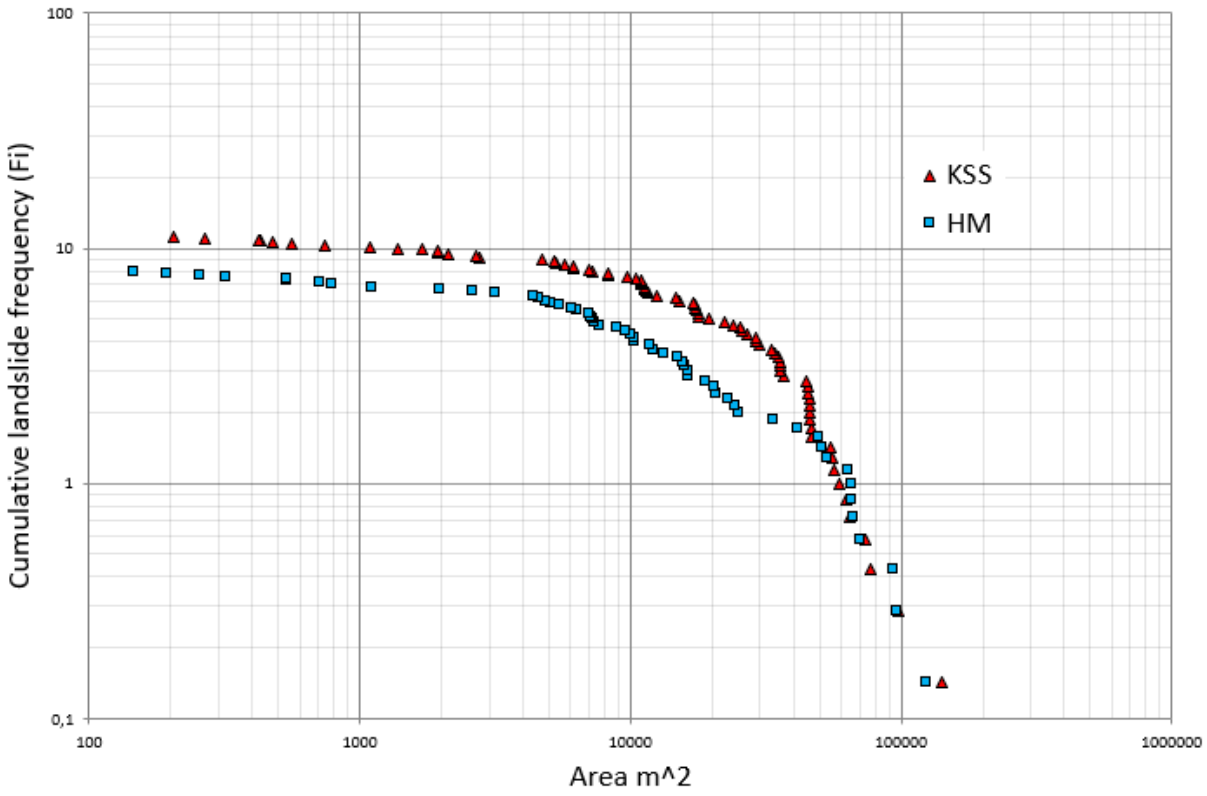

Figure 7.14: Comparison of landslides mapped in Hordaland (KSS) and Sogn and Fjordane (HM). The data from Sogn og Fjordane is modified from Mongstad (2018).

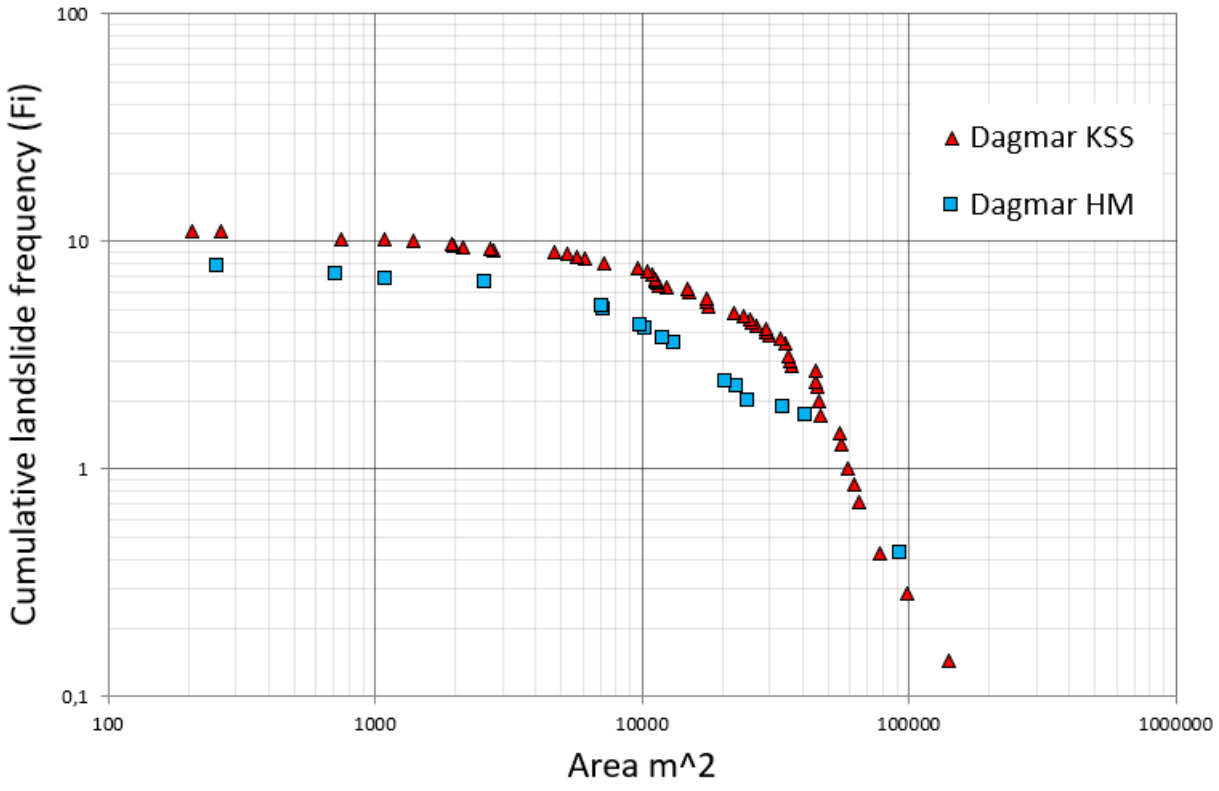

Figure 7.15: Comparison of landslides mapped from "Dagmar" (2011) in Hordaland (KSS) and Sogn and Fjordane (HM). The data from Sogn og Fjordane is modified from Mongstad (2018).

7.7.2 Threshold analysis comparison with Sogn og Fjordane

It was of interest to also compare the result of the threshold analysis to the result of Mongstad (2018). The results from this work and Mongstad (2018) is plotted in figure 7.16. The colors are adjusted to differentiate the datasets. “Dataset 2” is represented by red triangles, and blue squares represent the dataset from Mongstad (2018). The plot shows similar patterns in the datasets, with many landslides, plotted within the green warning level. Both plots show clustering in the lower right corner and several landslides with 0% relative water supply. The similarities in these patterns indicate that it is likely that the data from both counties are affected by similar factors.

The data from the six weather events for both counties are plotted separately in figure 7.17 for comparison. Triangles and squares still represent the datasets, but here with the representative event colors. The dataset from Mongstad (2018) also show landslides from the same three storms along the x-axis of the threshold graph.

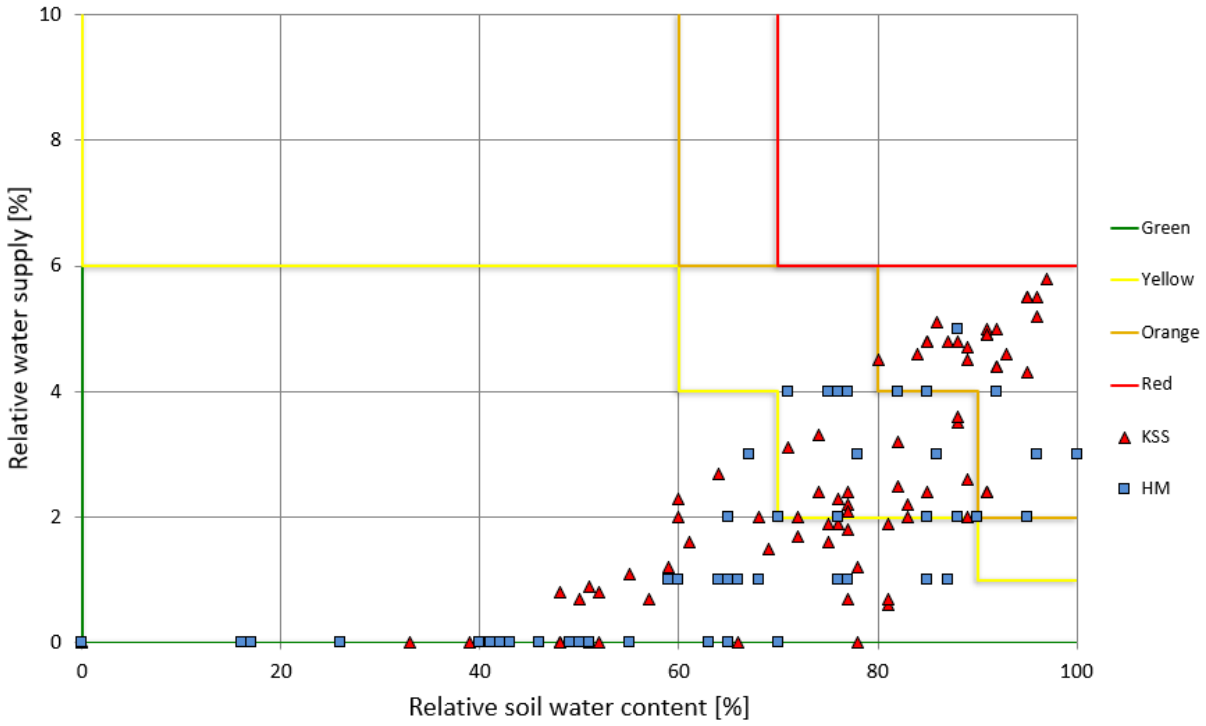

Figure 7.16: Threshold analysis plot with results from Hordaland and Sogn og Fjordane. “Dataset 2” in red triangles, and data from Mongstad (2018) in blue squares.

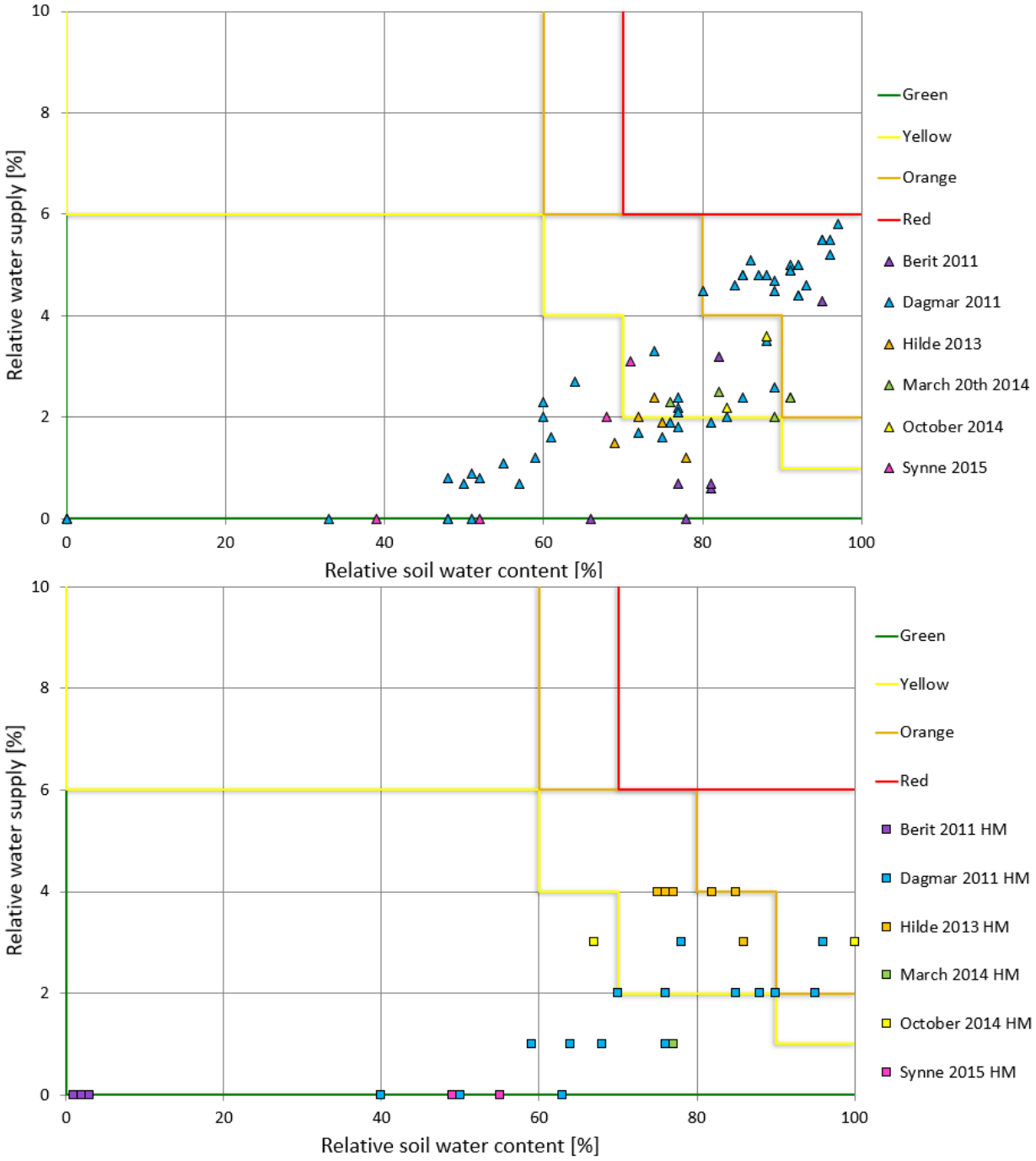

Figure 7.17: ***Top***: *"Dataset 2" divided into the six weather events.* ***Bottom***: *Data from Mongstad (2018) divided into the same weather events. The points have the representative colors for the weather events.*

8 Conclusion

Due to its topography, annual precipitation levels, and the location at the west coast, Hordaland is susceptible to weather-induced landslides. It was, therefore, a goal for this work to create an improved landslide dataset, by collecting and mapping the extension (area, m^2) of landslides which occurred during specific weather events. The mapped area could be used in a frequency-magnitude analysis, important in landslide hazard assessment.

A qualitative rainfall analysis was performed at the beginning of the work, to identify weather events, which led to multiple landslides. This analysis resulted in 20 weather events with precipitation above 100 mm, occurring in the period of interest 2011-2017. For six of these weather events, landslides could be mapped. The national landslide database contained 205 landslides that occurred during these events. In order to map the landslide extension, landslide data in the form of points were downloaded from the national landslide database. The spatial distribution of the point data was combined with different maps, and the landslides seemed to occur according to topography rather than the highest precipitation levels. There is clear favoritism in the database along the roads and railways, as well as in proximity to buildings and other infrastructure. The landforms alpine relief and glacially scoured low mountains and valleys are seen to dominate greatly, with 94% of the landslide point data.

The mapping of landslide extension was performed using different sources such as aerial photos, lidar imagery, pictures, news, google earth pro, google maps, as well as polygons previously drawn by other students. Due to a lack of, and variable quality of, aerial photos and lidar imagery, as well as variable quality in the national landslide database, only 78 polygons could be mapped for the six weather events investigated. The analysis of these 78 landslides shows that the typologies are dominated by debris flows, followed by debris avalanches and debris slides. Debris slides were likely underestimated, due to low visibility in the aerial photos and lack of photos. The landslide characteristics showed a wide variety of slope angles, and debris flows are seen to have longer runouts (up to 140.359 m). Most landslides seem to occur in the soil class «thin or no cover», followed by «moraine material».

The area mapped with the polygons allowed for a frequency-magnitude analysis, which showed the expected curve with a rollover point at 25.000 m^2, indicating an underestimation of values

below this magnitude. As this underestimation was also observed during the mapping, this is believed to be the main reason. An attempt to evaluate the warnings issued during the events was done, but this analysis turned incomplete, due to technical issues, and difficulty performing a qualitative analysis. A threshold analysis was performed using the observed values in the initiation areas of the landslides mapped, of relative water supply and relative soil water saturation. The analysis shows that many observed landslide events fall below the minimum thresholds, with relative water supply values too low, indicating a bad performance of the thresholds. This could be caused by either an error in the GWB-model, the interpolation, or measuring errors in the gauge stations due to wind or other factors.

It was desirable to compare my results to the adjacent county of Sogn og Fjordane, due to its proximity at the western coast and similar topography. Although several characteristics were similar in terms of typical slope angles, landforms, and soil types, some differences were found. Hordaland seems more prone to debris flows, as opposed to Sogn og Fjordane which seems more prone to both debris flows and debris avalanches. When comparing the frequency-magnitude graph, they show similarities, but as the sample sizes are different, the frequency seems lower for Sogn og Fjordane. The results for the threshold analysis is very similar, showing the same low values for the relative water supply, a known problem at NVE, but not previously quantified. This implies that there is indeed an issue with the threshold, whether its the model, or measurements, that needs to be further investigated.

The goal of mapping the magnitudes of weather-induced landslides occurring in Hordaland county and finding their frequencies was achieved. The choice of performing the rainfall analysis to find extreme weather events proved to be useful to identify weather events which induced many landslides. The findings are valuable to the landslide early warning system, in terms of the landslide occurrence in the county. However, only 78 landslides (75 of 205, 36%) could be mapped, and there is an underestimation of smaller landslide magnitudes due to limitations in aerial photos, lidar imagery, pictures available and other sources. This problem shows the need for more aerial photos and lidar imagery, in addition to better quality of these. Regardless, the improved dataset for the region is a valuable result for the project at NVE.

Future work

Possible future work:

- To start the analysis with a systematic and quantitative identification of rainfall events that triggered landslides. This would create a more solid foundation for the rest of the work. This was assumed not to be possible but later learned to be possible for work like this. A quantitative analysis with specific criteria is easier to reproduce in other works and compare results as well.
- Systematic mapping of landslides triggered by these weather events, including smaller landslide events. This would lead to a more accurate picture of their frequency of occurrence, including both those with small impact, and those outside populated areas.
- Aerial photos taken after significant weather events. Landslide analysis is dependent on aerial photos, and these need to be taken more frequently. The areas of interest did not have any photos after 2014, making the interpretations almost impossible in the last years of interest. Good quality aerial photos taken more frequently will improve the basis for analysis, and further improve mapping capabilities of future work.
- Frequency-magnitude analyses and similar statistics in other regions. A similar frequency-magnitude analysis has been performed in Sogn og Fjordane county, using the same period. The results differed between the counties, and cannot be used to represent other counties in Norway. Therefore similar analyses are necessary for other counties as well, to investigate typical landslide occurrence.
- A systematic review of threshold performance in different regions is necessary. The results in the threshold analysis from both counties Hordaland and Sogn og Fjordane were too low compared to the threshold used in the region. More analysis is needed to improve threshold performance.
- Improve terminology and explanations in the database to increase data quality for further work. Accurately classifying typology will increase success in mapping the landslide extent after the occurrence. Photos could also be included in the database, to increase documentation quality, before the landslide deposit is cleared from roads or railways.

References

Amundsen, B. (2009). "Fakta fra NORKLIMA: Flere skred i fremtidens klima." Norges forskningsråd, Klimaendringer og konsekvenser for Norge – NORKLIMA(1).

Andreassen, L. M., H. Elvehøy, B. Kjøllmoen, R. V. Engeset and N. Haakensen (2005). "Glacier mass-balance and length variation in Norway." Annals of Glaciology, 42, 317-325.

Antinao, J. L. and L. M. Farfán (2013). "Occurrence of landslides during the approach of tropical cyclone Juliette (2001) to Baja California Sur, Mexico." Atmósfera, 26(2), 183-208. DOI: 10.1016/s0187-6236(13)71071-3.

Bakken, S. L. (2017). Validation of the NGU susceptibility model for debris avalanches and small to medium sized debris flows. Master thesis, University of Oslo. Available from https://www.duo.uio.no/handle/10852/57973.

Bargel, T. H., Å. T. Fergus, Graziella Devoli, K. Orvedal, I. Peereboom, E. K. Øydvin, K. Stalsberg, K. Sletten, L. Fischer, L. Rubensdotter and R. Eilertsen (2011). Plan for skredfarekartlegging. Delrapport jordskred og flomskred. Report no. 16. The Norwegian Water and Energy Directorate, Oslo, Norway.

Barstad, I. and S. Grønås (2005). Southwesterly flows over southern Norway - mesoscale sensitivity to large-scale wind direction and speed. In: Tellus A: Dynamic Meteorology and Oceanography. UK, Blackwell Munksgaard. Page 136–152.

Baum, R. L. and J. W. Godt (2009). "Early warning of rainfall-induced shallow landslides and debris flows in the USA." Landslides, 7(3), 259-272. DOI: 10.1007/s10346-009-0177-0.

Bazin, S. (2012). "SafeLand: Living with landslide risk in Europe: Assessment, effects of global change, and risk management strategies. 7th Framework Programme Cooperation Theme 6 Environment (including climate change) Sub-Activity 6.1.3 Natural Hazards." Guidelines for landslide monitoring and early warning systems in Europe, Design and required technology(Deliverable 4.8), 153 pp.

Beldring, S., K. Engeland and L. A. Roald (2003). "Estimation of parameters in a distributed precipitation-runoff model for Norway." Hydrol. Earth Syst. Sci., 7, 304–316. DOI: https://doi.org/10.5194/hess-7-304-2003.

Bell, R., J. Cepeda and G. Devoli (2014). "Landslide susceptibility modeling at catchment level for improvement of the landslide early warning system in Norway." Proceeding 3rd World Landslide Forum, 2–6 June 2014, Beijing.

Boje, S. (2017). Hydrometeorologiske terskler for jordskredfare på Sørlandet og Østlandet. Report no. 64. The Norwegian Water and Energy Directorate, Oslo, Norway.

Boje, S., H. Colleuille and G. Devoli (2014). Terskelstudier for utløsning av jordskred i Norge. Report no. 43. The Norwegian Water and Energy Directorate, Oslo, Norway.

Brardinoni, F. and M. Church (2004). "Representing the landslide magnitude–frequency relation: Capilano River basin, British Columbia." Earth Surface Processes and Landforms, 29(1), 115-124. DOI: 10.1002/esp.1029.

Bryhni, I. and Thorsnæs, G. (2014, 22.02.2017). "Hordaland: natur. [Internet]" Store norske leksikon. Retrieved 07.11, 2018, from https://www.snl.no/Hordaland/natur.

Bugge, S. K. M. (2017). Connections between precipitation, stream flow and landslide occurrence in Hordaland county. Master thesis, University of Oslo. Available from https://www.duo.uio.no/handle/10852/58216.

Bøyum, G. (2011). Rapport etter ekstremværhendelsen Berit 25-26. november 2011. Norwegian Meteorological Institute, Oslo, Norway. Available from https://www.met.no/sokeresultat/_/attachment/inline/36685518-4c85-495a-b0c3-1cff9d6bd236:ffeee9e4556fb8463370772567d3dc2341d15ea0/ekstremv%C3%A6rrapport_berit.pdf.

Caine, N. (1980). "The Rainfall Intensity: Duration Control of Shallow Landslides and Debris Flows." Geografiska Annaler. Series A, Physical Geography, Vol. 62, No. 1/2, pp. 23-27.

Calvello, M. (2017). "Early warning strategies to cope with landslide risk." Riv. Ital. di Geot., 2, 63–91, 2, 63–91. DOI: https://doi.org/10.19199/2017.2.0557-1405.063.

Calvello, M., R. N. d'Orsi, L. Piciullo, N. Paes, M. Magalhaes and W. A. Lacerda (2015). "The Rio de Janeiro early warning system for rainfall-induced landslides: Analysis of performance for the years 2010–2013." International Journal of Disaster Risk Reduction, 12, 3-15. DOI: 10.1016/j.ijdrr.2014.10.005.

Cepeda, J. M. (2013a). Calibration of thresholds for Northern Norway. Report no. 20120997-01-TN. The Norwegian Geotechnical Institute, Oslo, Norway.

Cepeda, J. M. (2013b). Calibration of thresholds for Eastern Norway. Report no. 20120997-02-TN. The Norwegian Geotechnical Institute, Oslo, Norway.

Cepeda, J. M. and D. Devoli (2008). Rainfall thresholds for landslide triggering following volcanic ash eruptions and earthquakes. Geophysical Research Abstracts 10, EGU2008-A-03879.

Cepeda, J. and R. Bell (2014). Susceptibility map for debris flows, debris slides and soil slides in Western Norway. Report no. 20130802-01-TN. The Norwegian Geotechnical Institute, Oslo, Norway.

Cepeda, J. M., F. Sandersen, L. Ehlers, R. Bell and D. De Luca (2012). Probabilistic estimation of thresholds for rapid soil-slides and -flows in Norway. Report no. 20110253-00-4-R. The Norwegian Geotechnical Institute, Oslo, Norway.

Colleuille, H. and I. K. Engen (2009). Utredning om overvåking og varsling av løsmasse- og snøskredfare på regionalt nivå. Report no. 16. The Norwegian Water and Energy Directorate, Oslo, Norway.

Colleuille, H., L. E. Haugen and S. Beldring (2010). A forecast analysis tool for extreme hydrological conditions in Norway. Sixth world FRIEND conference, Marokko.

Colleuille, H., S. Boje, G. Devoli, I. K. Krøgli, I. K. Engen, M. Sund, T. Skaslien, T. Humstad, M. Frekhaug and P. Wiréhn (2017). Jordskredvarslingen: Nasjonal varslingstjeneste for jord-, sørpe- og flomskredfare. Report no. 75. The Norwegian Water and Energy Directorate, Oslo, Norway.

Corominas, J. (1996). "The angle of reach as a mobility index for small and large landslides." Canadian Geotechnical Journal, 33, 260-271.

Corominas, J. and J. Moya (2008). "A review of assessing landslide frequency for hazard zoning purposes." Engineering Geology, 102(3-4), 193-213. DOI: 10.1016/j.enggeo.2008.03.018.

Corominas, J., C. van Westen, P. Frattini, L. Cascini, J. P. Malet, S. Fotopoulou, F. Catani, M. Van Den Eeckhaut, O. Mavrouli, F. Agliardi, K. Pitilakis, M. G. Winter, M. Pastor, S. Ferlisi, V. Tofani, J. Hervás and J. T. Smith (2013). "Recommendations for the quantitative analysis of landslide risk." Bulletin of Engineering Geology and the Environment. DOI: 10.1007/s10064-013-0538-8.

Crozier, M. J. (2010). "Deciphering the effect of climate change on landslide activity: A review." Geomorphology, 124(3-4), 260-267. DOI: 10.1016/j.geomorph.2010.04.009.

Cruden, D. M. and D. J. Varnes (1996). Landslide types and processes. Landslides - Investigation and Mitigation. pp. 36–75. National Academy Press, Washington DC.

D'Orsi, R. N. (2012). "Landslide risk reduction measures by the Rio de Janeiro city government. Improving the assessment of disaster risks to strengthen financial resilience." Special Joint G20 Publication, Government of Mexico and World Bank,open publication 2012;77–91.

Dahl, M.-P. J., L. E. Mortensen, N. H. Jensen and A. Veihe (2013). "Magnitude–frequency characteristics and preparatory factors for spatial debris-slide distribution in the northern Faroe Islands." Geomorphology, 188, 3-11. DOI: 10.1016/j.geomorph.2012.09.015.

Dai, F. C., C. F. Lee and S. J. Wang (2003). "Characterization of rainfall-induced landslides." International Journal of Remote Sensing, 24(23), 4817-4834. DOI: 10.1080/01431160131000082424.

Dannevig, P. (2009, 10. april 2019). "Hordaland: klima. [Internet]" Store norske leksikon. Retrieved 07.11, 2018, from https://www.snl.no/Hordaland/klima.

Davis, J. (2002). Analysis of directional data. Chapter 5: Spatial Analysis. In: Statistics and data analysis in geology, John Wiley & Sons, Inc. Third edition. Page 316-330.

Devoli ,G. (2017). Jordskred og flomskred. Faktaark, The Norwegian Water and Energy Directorate, Oslo, Norway. Available from http://publikasjoner.nve.no/faktaark/2013/faktaark2013_05.pdf.

Devoli, G., F. V. De Blasio, A. Elverhøi and K. Høeg (2008). "Statistical Analysis of Landslide Events in Central America and their Run-out Distance." Geotechnical and Geological Engineering, 27(1), 23-42. DOI: 10.1007/s10706-008-9209-0.

Devoli, G., L. Jørandli, K. Engeland and L. M. Tallaksen (2017). Large-Scale Synoptic Weather Types and Precipitation Responsible for Landslides in Southern Norway. Proceedings of World Landslide Forum, Ljubljana, Slovenia, Springer. **4,** pp. 159-167. edited by: Matjaž Mikoš, Nicola Casagli, Yueping Yin, Kyoji Sassa. DOI: https://doi.org/10.1007/978-3-319-53485-5_17.

Devoli, G., D. Tiranti, R. Cremonini, M. Sund and S. Boje (2018). "Comparison of landslide forecasting services in Piedmont (Italy) and Norway, illustrated by events in late spring 2013." Natural Hazards and Earth System Sciences, 18(5), 1351-1372. DOI: 10.5194/nhess-18-1351-2018.

Devoli, G., R. Bell and J. Cepeda (2019). Susceptibility map at catchment level, to be used in landslide forecasting, Norway. Report no. 1. The Norwegian Water and Energy Directorate, Oslo.

Di Biagio, E. and O. Kjekstad (2007). Early Warning, Instrumentation and Monitoring Landslides. Proc. 2nd in Regional Training Course, Reclaim II, Phuket, Thailand. pp. 18–21.

DSB (2014). Veileder til helhetlig risiko- og sårbarhetsanalyse i kommunen. Direktoratet for samfunnssikkerhet og beredskap, Tønsberg, Norway. Available from https://www.dsb.no/globalassets/dokumenter/veiledere-handboker-og-informasjonsmateriell/veiledere/veileder-til-helhetlig-risiko-og-sarbarhetsanalyse-i-kommunen.pdf.

Dyrrdal, A. V., K. Isaksen and H. O. Hygen (2011). Past changes in frequency, intensity, and spatial occurrence of meteorological triggering variables relevant for natural hazards in Norway. Report no. 3. Norwegian Meteorological Institute, Oslo, Norway.

Ekker, R., K. Kværne, A. Os, T. Humstad, A. Wartiainen, V. Eide and R. K. Hansen (2013). regObs - public database for submitting and sharing observations. Proceeding International Snow Science Workshop Grenoble, Chamonix Mont-Blanc. pp. 5 pp. Available from http://arc.lib.montana.edu/snow-science/objects/ISSW13_paper_P5-42.pdf (last access: November 2018).

Engeset, R. (2016). Hvordan lages vær- og snødata for seNorge.no og XGEO.no?, The Norwegian Water and Energy Directorate, Oslo, Norway. Available from https://www.nve.no/Media/4813/weatherandsnowdatav2no.pdf (Accessed in November 2018).

Erikstad, L., R. Halvorsen, R. Moen, T. Thorsnes, T. Andersen, H. B. Blom, A. Elvebakk, R. Elven, G. Gaarder, B. P. Mortensen and F. Ødegaard (2009). "Landformvariasjon (terrengformvariasjon og landformer)." Naturtyper i Norge, 1-91.

Etzelmüller, B., B. Romstad and J. J. Fjellanger (2007). "Automatic regional classification of topography in Norway." Norwegian Journal of Geology, 87, 167-180.

Fischer, L., Rubensdotter, L., Sletten, K., Stalsberg, K., Melchiorre, C., Horton, P., Jaboyedoff, M. (2012). Debris flow modelling for susceptibility mapping at regional to national scale In: Landslides and Engineered Slopes: Protecting Society through Improved Understanding. edited by: Eberhardt, E., Froese, C., Turner, K., and Leroueil, S.,. London, Taylor & Francis Group, CRC Press. Page 723–729.

Fischer, L., Rubensdotter, L., and Stalsberg, K. (2014). Aktsomhetskart jord- og flomskred: Metodeutvikling og landsdekkende modellering. Report no. 2014.019. Geological Survey of Norway, Trondheim, Norway. Available from http://www.ngu.no/upload/Publikasjoner/Rapporter/2014/2014_019.pdf

Flentje, P., D. David Stirling and R. Chowdhury (2011). "Landslide Inventory, Susceptibility, Frequency and Hazard zoning in the Wollongong and wider Sydney Basin Area." Australian Geomechanics, 46, 41-50.

Frauenfelder, R., A. Solheim, K. Isaksen, C. Jaedicke, B. Romstad, A. V. Dyrrdal, R. Gangstø, A. Harbitz, C. B. Harbitz, J. E. Haugen, H. O. Hygen, H. Haakenstad, K. Isaksen, Á. Jónsson, R. Klæboe, J. Ludvigsen, N. K. Meyer, T. Rauken, K. Sverdrup-Thygeson and A. Aaheim (2013). Impacts of extreme weather events on infrastructure in Norway (InfraRisk) - Sluttrapport til NFR-prosjekt 200689. Report no. 20091808-01-R. The Norwegian Geotechnical Institute, Oslo, Norway.

Furseth, A. (2006). Skredulykker i Norge. Oslo, Norway, Tun Forlag AS. First edition.

Førland, E. J., H. Amundsen and G. K. Hovelsrud (2007). Utviklingen av naturulykker som følge av klimaendringer. Report no. 2007:03. pp. 71. CICERO, Oslo, Norway.

Gariano, S. L. and F. Guzzetti (2016). "Landslides in a changing climate." Earth-Science Reviews, 162, 227-252. DOI: 10.1016/j.earscirev.2016.08.011.

Gariano, S. L., M. T. Brunetti, G. Iovine, M. Melillo, S. Peruccacci, O. Terranova, C. Vennari and F. Guzzetti (2015). "Calibration and validation of rainfall thresholds for shallow landslide forecasting in Sicily, southern Italy." Geomorphology, 228, 653–665.

Gjengstø, A. and I. V. Malvik (2014). Erfaringer fra ekstremværet Hilde, november 2013. Report no. 8. The Norwegian Water and Resources Directorate, Oslo, Norway.

Glade, T. and F. Nadim (2013). "Early warning systems for natural hazards and risks." Natural Hazards, 70(3), 1669-1671. DOI: 10.1007/s11069-013-1000-8.

Gregersen, O. F. and F. Sandersen (1989). Landslide: Extent and economic significance in Norway. Proceedings of the 28th Int. Geo. Congress: Symp. on Landslides, Balkema, Rotterdam. pp. 133–139.

Guthrie, R. H. and S. G. Evans (2004). "Magnitude and frequency of landslides triggered by a storm event, Loughborough Inlet, British Columbia." Natural Hazards and Earth System Sciences, 4, 475-483.

Guzzetti, F. (2005). Landslide hazard and risk assessment Concepts, methods and tools for the detection and mapping of landslides, for landslide susceptibility zonation and hazard assessment, and for landslide risk evaluation. PhD Thesis, University of Bonn.

Guzzetti, F., B. D. Malamud, D. L. Turcotte and P. Reichenbach (2002). "Power-law correlations of landslide areas in central Italy." Earth and Planetary Science Letters, 195, 169–183.

Guzzetti, F., S. Peruccacci, M. Rossi and C. P. Stark (2007a). "Rainfall thresholds for the initiation of landslides in central and southern Europe." Meteorology and Atmospheric Physics, 98(3-4), 239-267. DOI: 10.1007/s00703-007-0262-7.

Guzzetti, F., S. Peruccacci, M. Rossi and C. P. Stark (2007b). "The rainfall intensity–duration control of shallow landslides and debris flows: an update." Landslides, 5(1), 3-17. DOI: 10.1007/s10346-007-0112-1.

Guzzetti, F., A. C. Mondini, M. Cardinali, F. Fiorucci, M. Santangelo and K.-T. Chang (2012). "Landslide inventory maps: New tools for an old problem." Earth-Science Reviews, 112(1-2), 42-66. DOI: 10.1016/j.earscirev.2012.02.001.

Hanssen-Bauer, I., E. J. Førland, I. Haddeland, H. Hisdal, S. Mayer, A. Nesje, J. E. Ø. Nilsen, S. Sandven, A. B. Sandø, A. Sorteberg and B. Ådlandsvik (2017a). Climate in Norway 2100, a knowledge base for climate adaptation, NCCS report, 1. Report no. 1. The Norwegian Centre for Climate Services (NCCS), Oslo, Norway. Available from http://www.miljodirektoratet.no/Documents/publikasjoner/M741/M741.pdf.

Hanssen-Bauer, I., Førland, E. J., Haddeland, I., Hisdal, H., Mayer, S., Nesje, A., Nilsen, J. E.Ø., Sandven, S., Sandø, A. B., Sorteberg, A., and Ådlandsvik, B. (2017b). Klimaprofiler for fylker: Et kunnskapsgrunnlag for klimatilpasning. Report no. 3. pp. Page 40-47. The Norwegian Centre for Climate Services (NCCS), Oslo, Norway. Available from https://cms.met.no/site/2/klimaservicesenteret/rapporter-og-publikasjoner/_attachment/12110?_ts=15ddfbccf32.

Haque, U., P. F. da Silva, G. Devoli, J. Pilz, B. Zhao, A. Khaloua, W. Wilopo, P. Andersen, P. Lu, J. Lee, T. Yamamoto, D. Keellings, W. Jian-Hong and G. E. Glass (2019). "The human cost of global warming: Deadly landslides and their triggers (1995–2014)." Science of The Total Environment, 682, 673-684. DOI: 10.1016/j.scitotenv.2019.03.415.

Highland, L. M. and P. Bobrowsky (2008). The Landslide Handbook— A Guide to Understanding Landslides. Reston, Virginia, U.S. Geological Survey Circular 1325. pp. 129.

Hisdal, H., H. Bjordal, H. Colleuille, R. Engeset, G. Helgås, M. M. Odberg, A. Sivle and K. Steinvik (2017). Evaluering av snø- og jordskredvarslingen. Report no. 38. The Norwegian Water and Energy Directorate, Oslo, Norway.

Holmqvist, E. (2016). Flommen i Rogaland og Agder desember 2015. Report no. 5. The Norwegian Water and Resources Directorate, Oslo, Norway.

Hov, Ø., U. Cubasch, E. Fischer, P. Höppe, T. Iversen, N. G. Kvamstø, Z. W. Kundzewicz, D. Rezacova, D. Rios, F. D. Santos, B. Schädler, O. Veisz, C. Zerefos, R. Benestad, J. Murlis, M. Donat, G. C. Leckebusch and U. Ulbrich (2013). Extreme Weather Events in Europe: preparing for climate change adaptation. Norwegian Meteorological Institute, Oslo, Norway. Available from http://real.mtak.hu/8366/1/EASAC_EWWG_Extreme_weather_report.pdf.

Hungr, O., S. G. Evans and J. Hazzard (1999). "Magnitude and frequency of rock falls and rock slides along the main transportation corridors of southwestern British Columbia." Canadian Geotechnical Journal, 36, 224–238.

Hungr, O., S. G. Evans, M. J. Bovis and J. N. Hutchinson (2001). "A review of the classification of landslides of the flow type." Environmental & Engineering Geoscience, 7(3), 221-238. DOI: 10.2113/gseegeosci.7.3.221.

Hungr, O., S. McDougall, M. Wise and M. Cullen (2008). "Magnitude–frequency relationships of debris flows and debris avalanches in relation to slope relief." Geomorphology, 96(3-4), 355-365. DOI: 10.1016/j.geomorph.2007.03.020.

Hungr, O., S. Leroueil and L. Picarelli (2014). "The Varnes classification of landslide types, an update." Landslides, 11(2), 167-194. DOI: 10.1007/s10346-013-0436-y.

Hutchinson, J. N. (1988). "General report: morphological and geotechnical parameters of landslides in relation to geology and hydrogeology." Proceedings 5th International Symposium on Landslides, Lausanne, vol. I, pp. 3-35.

Innes, J. L. (1983). "Debris flows." Prog. Phys. Geog., 7, 469–501.

Meteorologisk institutt (2018a, 22.08.2018). "Ekstremværvarsel. [Internet]" Meteorologisk institutt. Retrieved 11.11.2018, from https://www.met.no/vaer-og-klima/ekstremvaervarsler-og-andre-farevarsler/hva-er-et-ekstremvaervarsel.

Meteorologisk institutt (2018b, 23.11.2018). "Norske ekstremvær får navn. [Internet]" Meteorologisk institutt. Retrieved 11.11.2018, from https://www.met.no/vaer-og-

klima/ekstremvaervarsler-og-andre-farevarsler/hva-er-et-ekstremvaervarsel/norske-ekstremvaer-far-navn.

Intrieri, E., G. Gigli, N. Casagli and F. Nadim (2013). "Brief communication "Landslide Early Warning System: toolbox and general concepts&quot." Natural Hazards and Earth System Sciences, 13(1), 85-90. DOI: 10.5194/nhess-13-85-2013.

Jaedicke, C., A. Solheim, L. H. Blikra, K. Stalsberg, A. Sorteberg, A. Aaheim, K. Kronholm, D. Vikhamar-Schuler, K. Isaksen, K. Sletten, K. Kristensen, I. Barstad, C. Melchiorre, Ø. A. Høydal and H. Mestl (2008). "Spatial and temporal variations of Norwegian geohazards in a changing climate, the GeoExtreme Project." Nat. Hazards Earth Syst. Sci., 8, 893–904.

Jaedicke, C., Lied, K., and Kronholm, K. (2009). "Integrated database for rapid mass movements in Norway." Nat. Hazards Earth Syst. Sci., 9, 469–479. DOI: https://doi.org/10.5194/nhess-9-469-2009.

Jakob , M. (2005). Debris-flow hazard analysis In: Jakob M, Hungr O (eds) Debris-flow hazards and related phenomena. Berlin Heidelberg, Springer. Page 411–438.

Jakob, M., Owen, T., Simpson, T. (2012). "A regional real-time debris-flow warning system for the District of North Vancouver, Canada." Landslides, 9(2), 165-178. DOI: 10.1007/s10346-011-0282-8.

Jensen, O. A., G. Graziella Devoli, B. K. Rustad, A. Verhage, M. Viklund, J. O. Larsen and L. L. Kristensen (2015). Terminologi for naturfarer. Naturfareprosjektet: Delprosjekt 1 Naturskadestrategi. Report no. 90. pp. 30. The Norwegian Water and Energy Directorate, Oslo, Norway.

Johnsen, E. R. (2013). Modern forms of communicating avalanche danger – A Norwegian case. Proceeding at International Snow Science Workshop Grenoble, Chamonix Mont-Blanc. pp. 5 pp. Available from http://arc.lib.montana.edu/snow-science/objects/ISSW13_paper_O5-20.pdf.

Johnson, K. A. and N. Sitar (1989). "Hydrologic conditions leading to debris-flow initiation." Canadian Geotechnical Journal, 27, 789-801.

Jørandli, L. (2016). Landslide occurrence as a response to large-scale synoptic weather types, precipitation and soil saturation in southern Norway. Master thesis, University of Oslo. Available from https://www.duo.uio.no/handle/10852/52171.

Kochendorfer, J., R. Rasmussen, M. Wolff, B. Baker, M. E. Hall, T. Meyers, S. Landolt, A. Jachcik, K. Isaksen, R. Brækkan and R. Leeper (2017). "The quantification and correction of wind-induced precipitation measurement errors." Hydrology and Earth System Sciences, 21(4), 1973-1989. DOI: 10.5194/hess-21-1973-2017.

Kronholm, K. and K. Stalsberg (2009). "Klimaendringer gir endringer i skred hyppigheten." Norges forskningsråd, Klimaendringer og konsekvenser for Norge – NORKLIMA(3), 34-36.

Krøgli, I. K., G. Devoli, H. Colleuille, S. Boje, M. Sund and I. K. Engen (2018). "The Norwegian forecasting and warning service for rainfall- and snowmelt-induced landslides." Natural Hazards and Earth System Sciences, 18(5), 1427-1450. DOI: 10.5194/nhess-18-1427-2018.

Lacerda, W. A. (2007). "Landslide initiation in saprolite and colluvium in southern Brazil: field and laboratory observations." Geomorphology 87:104–119.

Lagomarsino, D., S. Segoni, R. Fanti and F. Catani (2013). "Updating and tuning a regional scale landslide early warning system." Landslides, 10, 91-97.

Lagomarsino, D., S. Segoni, A. Rosi, G. Rossi, A. Battistini, F. Catani and N. Casagli (2015). "Quantitative comparison between two different methodologies to define rainfall thresholds for landslide forecasting." Natural Hazards and Earth System Sciences, 15(10), 2413-2423. DOI: 10.5194/nhess-15-2413-2015.

Mangerud, J. (1976). Fra istid til nåtid In: Hordaland og Bergen. Oslo, Norway, Gyldendal Norsk Forlag. Page 111-151.

Maskrey, A. (1997). "National and Local Capabilities for Early Warning." International Decade for Natural Disaster Reduction IDNDR Early Warning Programme.

Meyer, N. K., Dyrrdal, A. V., Frauenfelder, R., Etzelmüller, B., Nadim, F. (2012). "Hydrometeorological threshold conditions for debris flow initiation in Norway." Natural Hazards and Earth System Sciences, 12(10), 3059-3073. DOI: 10.5194/nhess-12-3059-2012.

Michoud, C., S. Bazin, L. H. Blikra, M. H. Derron and M. Jaboyedoff (2013). "Experiences from site-specific landslide early warning systems." Natural Hazards and Earth System Sciences, 13(10), 2659-2673. DOI: 10.5194/nhess-13-2659-2013.

Mongstad, H. (2018). Landslide magnitude-frequency analysis to better define warning criteria for warning levels in Sogn og Fjordane, Norway. Master thesis, University of Oslo. Available from https://www.duo.uio.no/handle/10852/64422.

Morss, R. E., Wilhelmi, Olga V., Meehl, Gerald A., Dilling, Lisa (2011). "Improving Societal Outcomes of Extreme Weather in a Changing Climate: An Integrated Perspective." Annual Review of Environment and Resources, 36(1), 1-25. DOI: 10.1146/annurev-environ-060809-100145.

Müller, M., Homleid, Mariken, Ivarsson, Karl-Ivar, Køltzow, Morten A. Ø, Lindskog, Magnus, Midtbø, Knut Helge, Andrae, Ulf, Aspelien, Trygve, Berggren, Lars, Bjørge, Dag, Dahlgren, Per, Kristiansen, Jørn, Randriamampianina, Roger, Ridal, Martin, Vignes, Ole (2017). "AROME-MetCoOp: A Nordic Convective-Scale Operational Weather Prediction Model." Weather and Forecasting, 32(2), 609-627. DOI: 10.1175/waf-d-16-0099.1.

Myrabø, S., M. Viklund, K. Øvrelid, E.K.Øydvin, G. Petkovic, T. Humstad, K. Aunaas, V. Thakur and B. K. Dolva (2016). NIFS final report 2012–2016, The Natural Hazards program. Report no. 92. The Norwegian Water and Energy Directorate, OSlo, Norway. Available from http://www.naturfare.no/_attachment/1659339/binary/1154523.

Nadim, F., J. Cepeda, F. Sandersen, C. Jaedicke and H. Heyerdahl (2009). "Prediction of rainfall-induced landslides through empirical and numerical models." Proceedings of the First ItalianWorkshop on Landslides (IWL 2009), Naples, Italy, 8–10 June, 206—215.

NPRA (2012). Då Dagmar kom på julebesøk til Hardanger, The Norwegian Public Roads Administration, Oslo, Norway. Available from https://www.vegvesen.no/_attachment/389194/binary/666880?fast_title=Uv%C3%A6r+og+hendelser.pdf.

NVE (2017a, 12.04.2019). "Glaciers. [Internet]" The Norwegian Water Resources and Energy Directorate. Retrieved 09.11.2018, from https://www.nve.no/hydrology/glaciers/.

NVE (2017b). "Midtre Folgefonna. [Internet]" The Norwegian Water Resources and Energy Directorate. Retrieved 09.11.2018, from http://glacier.nve.no/Glacier/viewer/CI/en/nve/ClimateIndicatorInfo/3119?name=Midtre%20Folgefonna.

NVE (2017c, 09.02.2017). "Skredhendelser. [Internet]" The Norwegian Water Resources and Energy Directorate. Retrieved 07.09.2018, from https://www.nve.no/flaum-og-skred/kartlegging/skred-og-flaumhendingar/skredhendelser/.

Pelletier, J. D., B. D. Malamud, T. Blodgett and D. L. Turcotte (1997). "Scale-invariance of soil moisture variability and its implications for the frequency-size distribution of landslides." Engineering Geology, 48, 254–268.

Piciullo, L., M.-P. Dahl, G. Devoli, H. Colleuille and M. Calvello (2017). "Adapting the EDuMaP method to test the performance of the Norwegian early warning system for weather-induced landslides." Natural Hazards and Earth System Sciences, 17(6), 817-831. DOI: 10.5194/nhess-17-817-2017.

Piciullo, L., M. Calvello and José M. Cepeda (2018). "Territorial early warning systems for rainfall-induced landslides." Earth-Science Reviews, 179, 228-247. DOI: 10.1016/j.earscirev.2018.02.013.

Pollock, M. D., G. O'Donnell, P. Quinn, M. Dutton, A. Black, M. E. Wilkinson, M. Colli, M. Stagnaro, L. G. Lanza, E. Lewis, C. G. Kilsby and P. E. O'Connell (2018). "Quantifying and Mitigating Wind-Induced Undercatch in Rainfall Measurements." Water Resources Research, 54(6), 3863-3875. DOI: 10.1029/2017wr022421.

Puschmann, O. (2005). Nasjonalt referansesystem for landskap. Beskrivelse av Norges 45 landskapsregioner. pp. 66-101. Norsk institutt for jord- og skogkartlegging, Ås, Norway.

Qarinur, M. (2015). "Landslide runout distance prediction based on mechanism and cause of soil or rock mass movement." Journal of the Civil Engineering Forum, 1, 29-36.

Rosi, A., D. Lagomarsino, G. Rossi, A. Segoni, A. Battistini and N. Casagli (2015). "Updating EWS rainfall thresholds for the triggering of landslides." Nat. Hazards, doi:10.1007/s11069-015-1717-7.

Sandersen, F., S. Bakkehøi, E. Erik Hestnes and K. Lied (1996). The influence of meteorological factors on the initiation of debris flows, rockfalls, rockslides and rockmass stability. Proc. of the VII International Symposium on Landslides, Trondheim, Norway, Balkema, Rotterdam. **1,** pp. 97–114.

Sandøy, G., L. Rubensdotter and G. Devoli (2017). Trekantformede jordskred – Studie av fem skredhendelser i Norge. Report no. 2017.017. Geological Survey of Norway, Trondheim, Norway.

Schanche, S. (2014). Sikkerhet mot skred i bratt terreng: Kartlegging av skredfare i arealplanlegging og byggesak. Report no. 8. The Norwegian Water and Resources Directorate, Oslo, Norway.

Schwarze, P., G. Devoli, E. Namork, P. S. Ottesen, A. Soleng and S. Øverland (2018). Klimaendringar og helse. In: Folkehelserapporten: Helsetilstanden i Norge 2018. Norwegian Institute of Public Health. Available from https://www.fhi.no/nettpub/hin/miljo/klima-og-helse/.

Segoni, S., G. Rossi, A. Rosi and F. Catani (2014). "Landslides triggered by rainfall: A semi-automated procedure to define consistent intensity–duration thresholds." Computers & Geosciences, 63, 123-131. DOI: 10.1016/j.cageo.2013.10.009.

Segoni, S., A. Battistini, G. Rossi, A. Rosi, D. Lagomarsino, F. Catani, S. Moretti and N. Casagli (2015). "Technical Note: An operational landslide early warning system at regional scale based on space–time-variable rainfall thresholds." Natural Hazards and Earth System Sciences, 15(4), 853-861. DOI: 10.5194/nhess-15-853-2015.

Segoni, S., L. Piciullo and S. L. Gariano (2018). "A review of the recent literature on rainfall thresholds for landslide occurrence." Landslides, 15(8), 1483-1501. DOI: 10.1007/s10346-018-0966-4.

Seneviratne, S. I., N. Nicholls, D. Easterling, C. M. Goodess, S. Kanae, J. Kossin, Y. Luo, J. Marengo, K. McInnes, M. Rahimi, M. Reichstein, A. Sorteberg, C. Vera and X. Zhang (2012). Changes in climate extremes and their impact on the natural physical environment. In: Managing the Risks of Extreme Events and Disasters to Advance Climate Change Adaptation. A Special Report of Working Groups I and II of the Intergovernmental Panel on Climate Change (ICPP). Cambridge, UK, and New York, NY, USA, Cambridge University Press. Page 109–230.

Smith, K. (2013). Environmental hazards assessing risk and reducing disaster. New York, U.S., Routledge. Sixth edition.

Sokalska, E., G. Devoli, I. Solberg, L. Hansen and V. Thakur (2015). Kvalitetskontroll, analyse og forslag til oppdatering av historiske kvikkleireskred og andre leirskred registrert i Nasjonal skredhendelsesdatabase (NSDB). Report no. 65. pp. 79. The Norwegian Water and Energy Directorate, Oslo, Norway.

Solheim, A. (2017). Naturfarer, risiko og tilpasning. Presentation, The Norwegian Geotechnical Institute, Oslo, Norway. Available from http://www.geografisk.no/wp-content/uploads/2017/01/Solheim-Norsk-Geografisk-Selskap-januar-2017.pdf.

Staley, D. M., J. W. Kean, S. H. Cannon, K. M. Schmidt and J. L. Laber (2012). "Objective definition of rainfall intensity–duration thresholds for the initiation of post-fire debris flows in southern California." Landslides, 10(5), 547-562. DOI: 10.1007/s10346-012-0341-9.

Stark, C. P. and N. Hovius (2001). "The characterization of landslide size distributions." Geophysical Research Letters, 28(6), 1091-1094. DOI: 10.1029/2000gl008527.

Statistisk sentralbyrå (2018, 03.12.2018). "Tettsteders befolkning og areal. [Internet]" Statistisk sentralbyrå. Retrieved 04.05, 2019, from https://www.ssb.no/befolkning/statistikker/beftett/aar.

Stoffel, M., D. Tiranti and C. Huggel (2014). "Climate change impacts on mass movements--case studies from the European Alps." Sci Total Environ, 493, 1255-1266. DOI: 10.1016/j.scitotenv.2014.02.102.

Stähli, M., M. Sättele, C. Huggel, B. W. McArdell, P. Lehmann, A. Van Herwijnen, A. Berne, M. Schleiss, A. Ferrari, A. Kos, D. Or and S. M. Springman (2015). "Monitoring and prediction in early warning systems for rapid mass movements." Natural Hazards and Earth System Sciences, 15(4), 905-917. DOI: 10.5194/nhess-15-905-2015.

Tacher, L. and C. Bonnard (2007). Hydromechanical modelling of a large landslide considering climate change conditions. In: McInnes, R., Jakeways, J., Fairbank, H., Mathie, E. (Eds.), Landslides and Climate Change: Challenges and Solutions. Proceedings of the International Conference on Landslides and Climate Change, Ventnor, Taylor & Francis. pp. 131–141. DOI: 10.1201/NOE0415443180.ch17.

Thiebes, B. and T. Glade (2016). Landslide early warning systems – fundamental concepts and innovative applications. International Symposium on Landslides, Naples, Italy. Available from https://www.researchgate.net/profile/Benni_Thiebes/publication/296319407_Landslide_early_warning_systems_-_fundamental_concepts_and_innovative_applications/links/56d4330408aedf315fb7111d/Landslide-early-warning-systems-fundamental-concepts-and-innovative-applications.pdf.

Thiebes, B., T. Glade and R. Bell (2012). Landslide analysis and integrative early warning – Local and regional case studies. Proc. 11th International Symposium on Landslides, CRC Press. pp. 1915–1921. DOI: 10.13140/RG.2.1.1229.7844.

Thorsnæs, G. (2015, 13.04.2018). "Hardangerfjorden. [Internet]" Store norske leksikon. Retrieved 10.11.2018, from https://snl.no/Hardangerfjorden.

UNISDR (2006). Developing Early Warning Systems: a checklist. EWC III 3rd international Conference on Early warning, From Concept to action, Bonn, Germany. Available from http://www.unisdr.org/2006/ppew/info-resources/ewc3/checklist/English.pdf.

UNISDR (2009). Terminology on Disaster Risk Reduction. Available from http://www.unisdr.org/we/inform/terminology.

Uni Research Klima (2017). "Klimaendringer i Hordaland. [Internet]" Uni Research Klima. Retrieved 07.11, 2018, from http://uni.no/nb/uni-klima/klimaeffekter-pa-natur-og-samfunn/klimaendringer-i-hordaland/.

Varnes, D. J. (1978). Slope movement types and processes In: Schuster RL, Krizek RJ (eds) Landslides, analysis and control, special report 176. Washington, DC., Transportation research board, National Academy of Sciences. Page 11–33.

Vorren, O. T. and J. Mangerud (2007). Istider kommer og går In: Landet blir til. Norges Geologi. Trondheim, Norway, Norsk Geologisk Forening. Second edition. Page 478-531.

Wang, X. L., Y. Feng, G. P. Compo, V. R. Swail, F. W. Zwiers, R. J. Allan and P. D. Sardeshmukh (2012). "Trends and low frequency variability of extra-tropical cyclone activity in the ensemble of twentieth century reanalysis." Climate Dynamics, 40(11-12), 2775-2800. DOI: 10.1007/s00382-012-1450-9.

White, I. D., D. N. Mottershead and J. J. Harrison (1996). Environmental systems. London, Chapman & Hall. Second edition. pp. 616.

Wieczorek, G. F. and T. Glade (2005). Climatic factors influencing occurrence of debris flows In: Debris-flow Hazards and Related Phenomena. Page 325-362.

Wilson, R. C. and A. S. Jayko (1997). Preliminary Maps Showing Rainfall Thresholds for Debris-Flow Activity, San Francisco Bay Region, California. Report no. 97-745 F. U.S. Geological survey.

Wolff, M. A., K. Isaksen, A. Petersen-Øverleir, K. Ødemark, T. Reitan and R. Brækkan (2015). "Derivation of a new continuous adjustment function for correcting wind-induced loss of solid precipitation: results of a Norwegian field study." Hydrology and Earth System Sciences, 19(2), 951-967. DOI: 10.5194/hess-19-951-2015.

Øydvin, E. K. (2011). Plan for skredfarekartlegging - Status og prioriteringer innen oversiktskartlegging og detaljert skredfarekartlegging i NVEs regi. Report no. 14. The Norwegian Water and Resources Directorate, Oslo, Norway.

Appendix

Appendix 1: Dataset 2

Part of the attribute table for the 78 polygons mapped, with the polygons used from the other students.

OBJECT ID	Related ID	NLDB ID	NLDB duplicate	Type	Location name	Extreme event	Date
23	116	5756		Debris flow	Fresvik	Berit 2011	27.11.2011
78		521		Debris flow	Ulvik - bruravik	Berit 2011	27.11.2011
79	50	1800		Debris flow	Veg til Djønno	Berit 2011	27.11.2011
80		5671		Debris flow	Holmane	Berit 2011	27.11.2011
87	260, 259	6916		Debris flow	Skjelvik	Berit 2011	27.11.2011
88		850		Debris flow	Kinsarvik	Berit 2011	27.11.2011
89		8069	513	Debris flow	Bugjelet	Berit 2011	27.11.2011
90		9122		Debris flow	Kyskredo	Berit 2011	27.11.2011
1	13, 249	2517	2304	Debris flow	Aga	Dagmar 2011	26.12.2011
5	247	8171		Debris flow	Aga	Dagmar 2011	26.12.2011
6	16	2467	7933	Debris flow	Kråkevik	Dagmar 2011	26.12.2011
7	17	7167	7933	Debris flow	Kråkevik	Dagmar 2011	26.12.2011
8	64	8756		Debris slide	Kråkevik	Dagmar 2011	26.12.2011
9	68	7204		Debris slide	Bleie	Dagmar 2011	26.12.2011
10	20	9075		Debris avalanche	Fossåna	Dagmar 2011	26.12.2011
13	211,24,208	3980	678	Debris flow	Måge	Dagmar 2011	26.12.2011
14	26	7052		Debris flow	Eikhamrane	Dagmar 2011	26.12.2011
15	84	3675		Debris flow	Eitrheimtunnelen Nord 2	Dagmar 2011	26.12.2011
16	30, 259	4401		Debris flow	Skjelvik	Dagmar 2011	26.12.2011
20	112	6952	8170	Debris avalanche	Skjelvik	Dagmar 2011	26.12.2011
21	113	1242		Debris flow	Skjelvik	Dagmar 2011	26.12.2011
22	114	6186		Debris flow	Fresvik	Dagmar 2011	26.12.2011

24	141	5055	5413,7168	Debris flow	Lofthus	Dagmar 2011	26.12.2011
25	162	5920		Debris flow	Kinsarvik	Dagmar 2011	26.12.2011
26	177	1865		Debris flow	Berget	Dagmar 2011	26.12.2011
27	65	7964		Debris flow	Kråkevik	Dagmar 2011	26.12.2011
29	9	6413		Debris flow	Eidfjord	Dagmar 2011	26.12.2011
30		5126	9137, 2620	Debris flow	Digranes sør	Dagmar 2011	26.12.2011
32		7243		Debris slide	Brattespe	Dagmar 2011	26.12.2011
33		5685		Debris flow	Bratetspe	Dagmar 2011	26.12.2011
34	122	5907		Debris avalanche	Espe-Børve	Dagmar 2011	26.12.2011
35		3846		Debris flow	Espe	Dagmar 2011	26.12.2011
36		8835		Debris flow	Sekse	Dagmar 2011	26.12.2011
37		8977		Debris flow	Espe-Børve	Dagmar 2011	26.12.2011
38		5474		Debris flow	Espe-Børve	Dagmar 2011	26.12.2011
39		535		Debris flow	Urheim	Dagmar 2011	26.12.2011
40		6063		Debris flow	Bugjelet	Dagmar 2011	26.12.2011
42		1280		Debris flow	Brimnes	Dagmar 2011	26.12.2011
43		8034		Debris flow	Erdal	Dagmar 2011	26.12.2011
45		4035		Debris flow	Skarsenden	Dagmar 2011	26.12.2011
46		2868		Debris flow	Kyskredo	Dagmar 2011	26.12.2011
47		1222		Debris flow	Tveito rasteplass	Dagmar 2011	26.12.2011
48		4447		Debris flow	Austrepollen	Dagmar 2011	27.12.2011
49		3140		Debris flow	Sundal	Dagmar 2011	26.12.2011
50		518		Debris flow	Haukanesberget	Dagmar 2011	26.12.2011
51		7156		Debris flow	Nesthusbekken Kvam	Dagmar 2011	27.12.2011
52		5884		Debris flow	Seters bru	Dagmar 2011	26.12.2011
54		3032		Debris flow	Nordalen	Dagmar 2011	26.12.2011
55		3439	131	Debris flow	Langeland	Dagmar 2011	26.12.2011
56		3439	131	Debris avalanche	Langeland	Dagmar 2011	26.12.2011
58		3481		Debris flow	Mestadstranda	Dagmar 2011	26.12.2011
60		7093	1815	Debris flow	Mestad	Dagmar 2011	26.12.2011
62		22		Debris flow	Fadnestreet	Dagmar 2011	26.12.2011
64		2632		Debris flow	Bulken - Evanger	Dagmar 2011	26.12.2011
65		8313		Debris avalanche	Bulken - Evanger	Dagmar 2011	26.12.2011
66	137	5124	5018	Debris flow	Sekse/Hovland	Dagmar 2011	26.12.2011
68				Debris flow	Fossåna	Dagmar 2011	26.12.2011
69		3507		Debris flow	Eitrheimtunnelen	Dagmar 2011	26.12.2011
91				Debris flow	Byrkjenes	Dagmar 2011	26.12.2011
92				Debris flow	Byrkjenes	Dagmar 2011	26.12.2011
93	134	6120		Debris flow	Sekse/ULLENSVANG (flaum)	Dagmar 2011	26.12.2011

94	133	2661		Debris flow	Sekse/ULLENSVANG (flaum)	Dagmar 2011	26.12.2011
70		5102		Debris flow	Forvoskaret	Hilde 2013	15.11.2013
71		2289		Debris flow	Tungegrovi	Hilde 2013	15.11.2013
72		3804		Debris flow	Skjerstølen	Hilde 2013	16.11.2013
73		6133		Debris flow	Vannjolo	Hilde 2013	15.11.2013
96		5476		Debris slide	Flyane, Straume bru	Hilde 2013	15.11.2013
82		2722		Debris avalanche	Roe	20 mars 2014	20.03.2014
83		3895	145, 7231	Debris slide	Honveshagen	20 mars 2014	20.03.2014
84		4050		Debris slide	Rv 13 ved Granvinsvatnet	20 mars 2014	20.03.2014
85		2873		Debris avalanche	Hausnes	20 mars 2014	20.03.2014
86		5040	7227	Debris slide	Vallandsvegen	20 mars 2014	20.03.2014
74		3743		Debris flow	Kambabekken, Klyvevegen, Kvam herad	October 2014	28.10.2014
99		5229		Debris slide	Odda	October 2014	28.10.2014
75		120	2887	Debris flow	Raudskredbekken	Synne 2015	05.12.2015
76		5607	5875	Debris flow	Eitrheimselva	Synne 2015	05.12.2015
77		6127		Debris flow	Tveitnes	Synne 2015	05.12.2015
98		7977		Debris flow	Jordalsvegen	Synne 2015	05.12.2015

Appendix 2: List of sources used to map the polygons

The different sources used during the drawing of polygons.

ID	Aerial photo before	Aerial photo after	Lidar image before	Lidar image after	Other source	Uncertain
1	Vestlandet nord 2006	Hardangervidda 2013	X	Ullensvang 2011	Photo/news	God
5	Vestlandet nord 2006	Hardangervidda 2013	X	Ullensvang 2011	Photo	God
6	Vestlandet nord 2006	Hardangervidda 2013	X	Ullensvang 2011	Photo/news	God
7	Vestlandet nord 2006	Hardangervidda 2013	X	Ullensvang 2011		God
8	Vestlandet nord 2006	Hardangervidda 2013	X	Ullensvang 2011		God
9	Vestlandet nord 2006	Hardangervidda 2013	X	Ullensvang 2011		God
10	Vestlandet nord 2006	Hardangervidda 2013	X	Ullensvang 2011	Photo/news	God
13	Odda 2010	Hardangervidda 2013	X	Ullensvang 2011		God
14	Odda 2010	Hardangervidda 2013	X	Ullensvang 2011	Photo	God
15	Odda 2010	Hardangervidda 2013	(Hordaland 2008)	Odda 2011		God
16	Odda 2010	Hardanger-Voss 2012	X	Odda 2011	Photo	God
20	Odda 2010	Hardanger-Voss 2012	X	Odda 2011	Photo/news	God
21	Odda 2010	Hardanger-Voss 2012	X	Odda 2011	Photo/news	God
22	Vestlandet nord 2006	Hardanger-Voss 2012	X	Ullensvang 2011	Photo	God
23	Odda 2010 + Vestlandet nord 2006	Hardanger-Voss 2012	X	Ullensvang 2011		Medium
24	Vestlandet nord 2006	Hardanger-Voss 2012	X	X		God
25	Vestlandet nord 2006	Hardangervidda 2013 + Hardanger-Voss 2012	X	Kinsarvik 2011		Medium
26	Vestlandet nord 2006 + Indre Sogn 2007	Hardangervidda 2013 + Hardanger-Voss 2012	X	Kinsarvik 2011		God
27	Vestlandet nord 2006	Hardangervidda 2013	X	Ullensvang 2011		God
29	Hardangerjøkulen 2008	Hardangervidda 2013	(Hordaland indre 2009)	Eidfjord_Ulvik_Granvin 2014		God
30	Odda 2010	Hardangervidda 2013	X	Odda 2011		God
31	Odda 2010	Hardangervidda 2013	X	Odda 2011		God
32	Vestlandet nord 2006	Hardanger-Voss 2012	X	Ullensvang 2011	Photo/news	God
33	Vestlandet nord 2006	Hardanger-Voss 2012	X	Ullensvang 2011		Medium
34	Vestlandet nord 2006	Hardanger-Voss 2012	X	Ullensvang 2011		Medium
35	Vestlandet nord 2006	Hardanger-Voss 2012	X	Ullensvang 2011		God
36	Vestlandet nord 2006	Hardanger-Voss 2012	X	Ullensvang 2011	Photo	God
37	Vestlandet nord 2006	Hardanger-Voss 2012	X	Ullensvang 2011		Medium
38	Vestlandet nord 2006	Hardanger-Voss 2012	X	Ullensvang 2011		Medium
39	Vestlandet nord 2006	Hardanger-Voss 2012	X	Kinsarvik 2011		God
40	Indre Sogn 2007	Hardangervidda 2013 + Eidfjord-Ulvik-Granvin 2014	(Hordaland indre 2009)	Eidfjord_Ulvik_Granvin 2014		Medium
42	Indre Sogn 2007	Eidfjord-Ulvik-Granvin 2014	(Hordaland indre 2009)	Eidfjord_Ulvik_Granvin 2014		Medium

43	Indre Sogn 2007	Eidfjord-Ulvik-Granvin 2014	(Hordaland indre 2009)	Eidfjord_Ulvik_Granvin 2014		Medium
44	Indre Sogn 2007	Eidfjord-Ulvik-Granvin 2014	(Hordaland indre 2009)	Eidfjord_Ulvik_Granvin 2014		God
45	Indre Sogn 2007	Hardangervidda 2013	(Hordaland indre 2009)	Eidfjord_Ulvik_Granvin 2014		God
46	Indre Sogn 2007	Hardanger-Voss 2012	(Hordaland indre 2009)	Eidfjord_Ulvik_Granvin 2014		Medium
47	Hardangerjøkulen 2008	Hardanger-Voss 2012	(Hordaland indre 2009)	Eidfjord_Ulvik_Granvin 2014		God
48	Vestlandet nord 2006	Hardangervidda 2013	(Hordaland indre 2009)	Etne-Kvinnherad 2013		God
49	Vestlandet nord 2006	Etne Kvinnherad 2013	(Hordaland indre 2009)	Etne-Kvinnherad 2013		Medium
50	Indre Sogn 2007	Hardanger-Voss 2012	(Hordaland indre 2009)	(Eidfjord_Ulvik_Granvin 2014)		Medium
51	Kvam 2010	Vestlandet 2013	X	Kvam 2011		God
52	Nordhordaland 2011	Vestlandet 2013 + Nordhordaland 2015	Modalen 2011	X		God
54	Voss og Vaksdal 2008	Vestlandet 2013 + Nordhordaland 2015	Modalen 2011	X		God
55	Voss og Vaksdal 2008	Vestlandet 2013	Vaksdal 2011	X		God
56	Voss og Vaksdal 2008	Vestlandet 2013	X	(Voss 2012)		God
58	Voss og Vaksdal 2008	Vestlandet 2013	X	Voss 2012		Medium
60	Voss og Vaksdal 2008	Vestlandet 2013	X	Voss 2012		God
61	Voss og Vaksdal 2008	Vestlandet 2013	X	Voss 2012		God
62	Voss og Vaksdal 2008	Vestlandet 2013	Voss Vaksdal 2010	Voss 2012		Medium
64	Voss og Vaksdal 2008	Vestlandet 2013	Voss Vaksdal 2010	NDH Voss 5 pkt 2016	Photo/news	God
65	Voss og Vaksdal 2008	Vestlandet 2013	Voss og Vaksdal 2010	NDH Voss 5 pkt 2016		God
66	Vestlandet nord 2006	Hardanger-Voss 2012	Voss og Vaksdal 2010	Ullensvang 2011	Photo/report	Lav
68	Vestlandet nord 2006	Hardanger-Voss 2012	X	Ullensvang 2011	Photo/news	God
69	Odda 2010	Hardangervidda 2013	X	(Odda 2011)		Medium
70	Voss og Vaksdal 2008	Voss Fusa Samnanger 2016	Voss 2012	X		Lav
71	Voss og Vaksdal 2008	Voss Fusa Samnanger 2016	Voss 2012	X		Lav
72	Voss og Vaksdal 2008	Voss Fusa Samnanger 2016	Voss 2012	X		Lav?
73	Voss 2012	Voss Fusa Samnanger 2016	Voss Vaksdal 2010	NDH Voss 2 pkt 2016 + NDH Voss 5 pkt 2016		Medium
74	Hardangervidda 2013	X	Kvam 2011	X		Medium
75	Hardangervidda 2013	X	X	X	Photo/news/Regobs	God
76	Hardangervidda 2013	X	X	X	Photo	Medium
77	Vestlandet 2013	X	Etne-Kvinnherad 2013	X		Lav
78	Indre Sogn 2007	Hardanger-Voss 2012	Hordaland indre 2009	Eidfjord_Ulvik_Granvin 2014		Medium
79	Indre Sogn 2007	Hardanger-Voss 2012	Ulvik 2011	Eidfjord_Ulvik_Granvin 2014		Medium
80	Odda 2010	Hardangervidda 2013	Odda 2011	X		Medium
82	Hardangervidda 2013	Voss Fusa Samnanger 2016	Voss Vaksdal 2010	NDH Voss 5pkt 2016	Photo/news/Regobs	God
83	Hardangervidda 2013	Voss Fusa Samnanger 2016	Voss Vaksdal 2010	NDH Voss 5pkt 2016	Photo/news/Regobs	God
84	Hardangervidda 2013	Eidfjord-Ulvik-Granvin 2014	Hordaland indre 2009	Eidfjord_Ulvik_Granvin 2014	Regobs	God
85	Hardangervidda 2013	Eidfjord-Ulvik-Granvin 2014	Hordaland indre 2009	Eidfjord_Ulvik_Granvin 2014	Photo/news/Regobs	God
86	Vestlandet 2013	X	Kvam 2011	X	Photo/news/Regobs	God
87	Odda 2010	Hardanger-Voss 2012	X	Odda 2011		Medium

88	Vestlandet nord 2006	Hardangervidda 2013 + Hardanger-Voss 2012	X	Kinsarvik 2011		Medium
89	Indre Sogn 2007	Hardangervidda 2013 + Eidfjord-Ulvik-Granvin 2014	(Hordaland indre 2009)	Eidfjord_Ulvik_Granvin 2014		Medium
90	Indre Sogn 2007	Hardanger-Voss 2012	(Hordaland indre 2009)	Eidfjord_Ulvik_Granvin 2014		Medium
91	Odda 2010	Hardangervidda 2013	Odda 2011	X	Photo	God
92	Odda 2010	Hardangervidda 2013	Odda 2011	X		God
93	Vestlandet nord 2006	Hardanger-Voss 2012	Ullensvang 2011	X		Medium
94	Vestlandet nord 2006	Hardanger-Voss 2012	Ullensvang 2011	X		Medium
95	Indre Sogn 2007	Hardanger-Voss 2012	(Hordaland indre 2009	Eidfjord_Ulvik_Granvin 2014		Medium
96	Voss og Vaksdal 2008	Voss Fusa Samnanger 2016	Voss 2012	X		Medium
98	Hardangervidda 2013	Voss Fusa Samnanger 2016	Voss_Vaksdal 2011	NDH Voss 5 pkt 2016	Photo/news	God
99	Hardangervidda 2013	X	Odda 2011	Flaum Opo Odda 2014	Photo/news/Regobs	God

Appendix 3: Aerial photos

Aerial photos taken in the three years after the events.

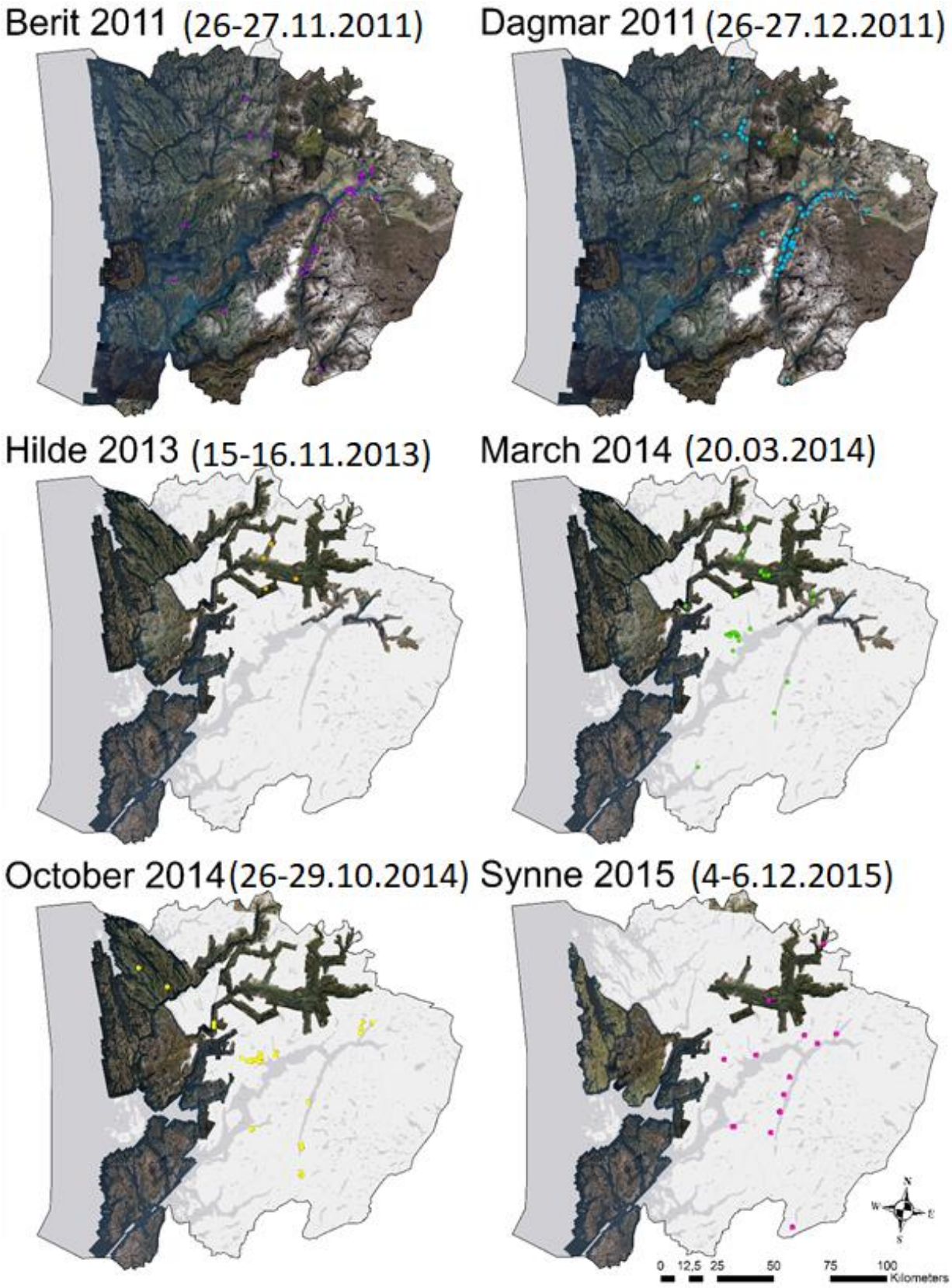

Appendix 4: Lidar images

Lidar images taken in the next three years after the events.

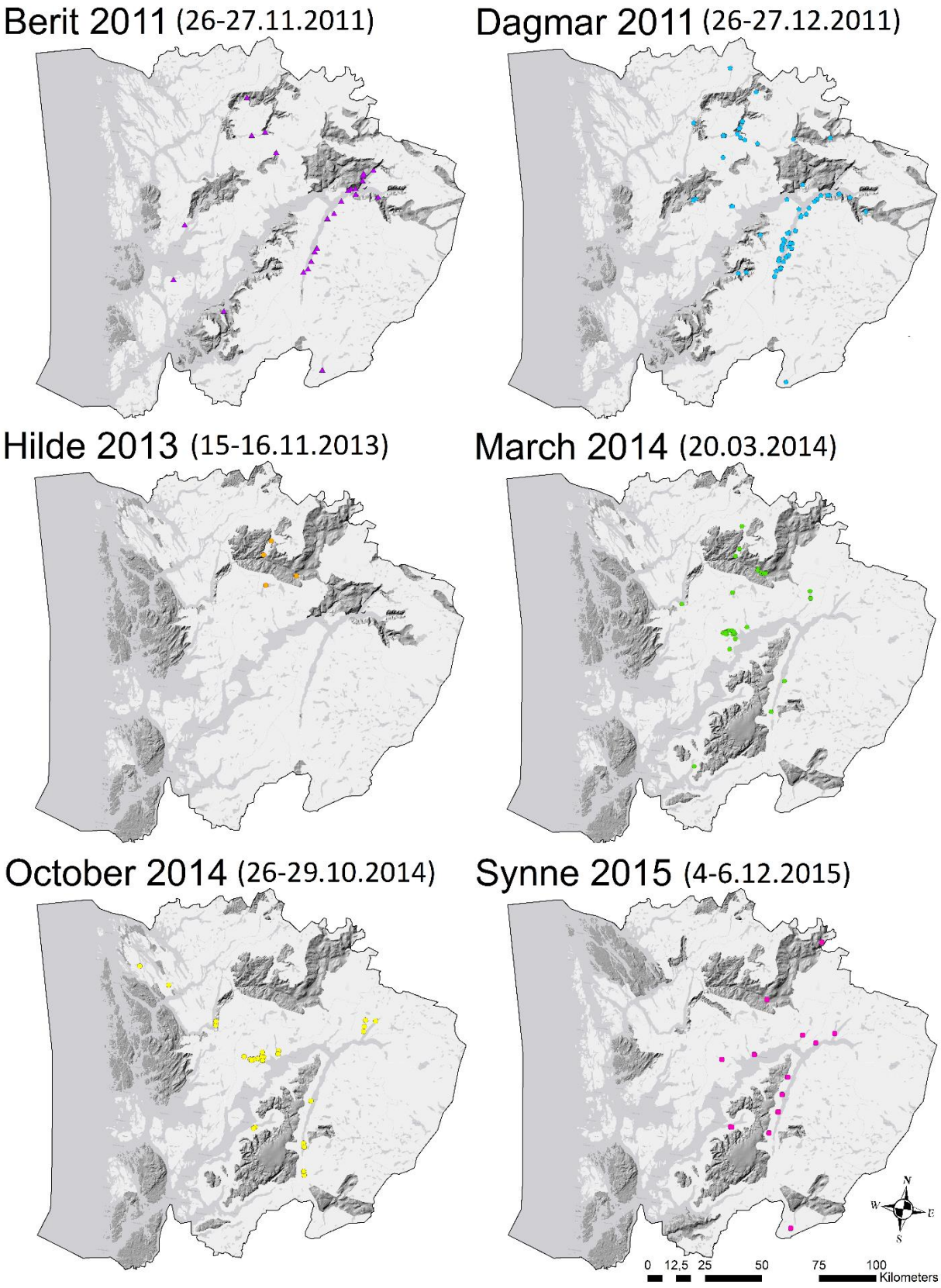

Appendix 5: Spatial distribution of landslides

Landslide data from all the rainfall events in separate maps, showing the spatial distribution of each rainfall event.

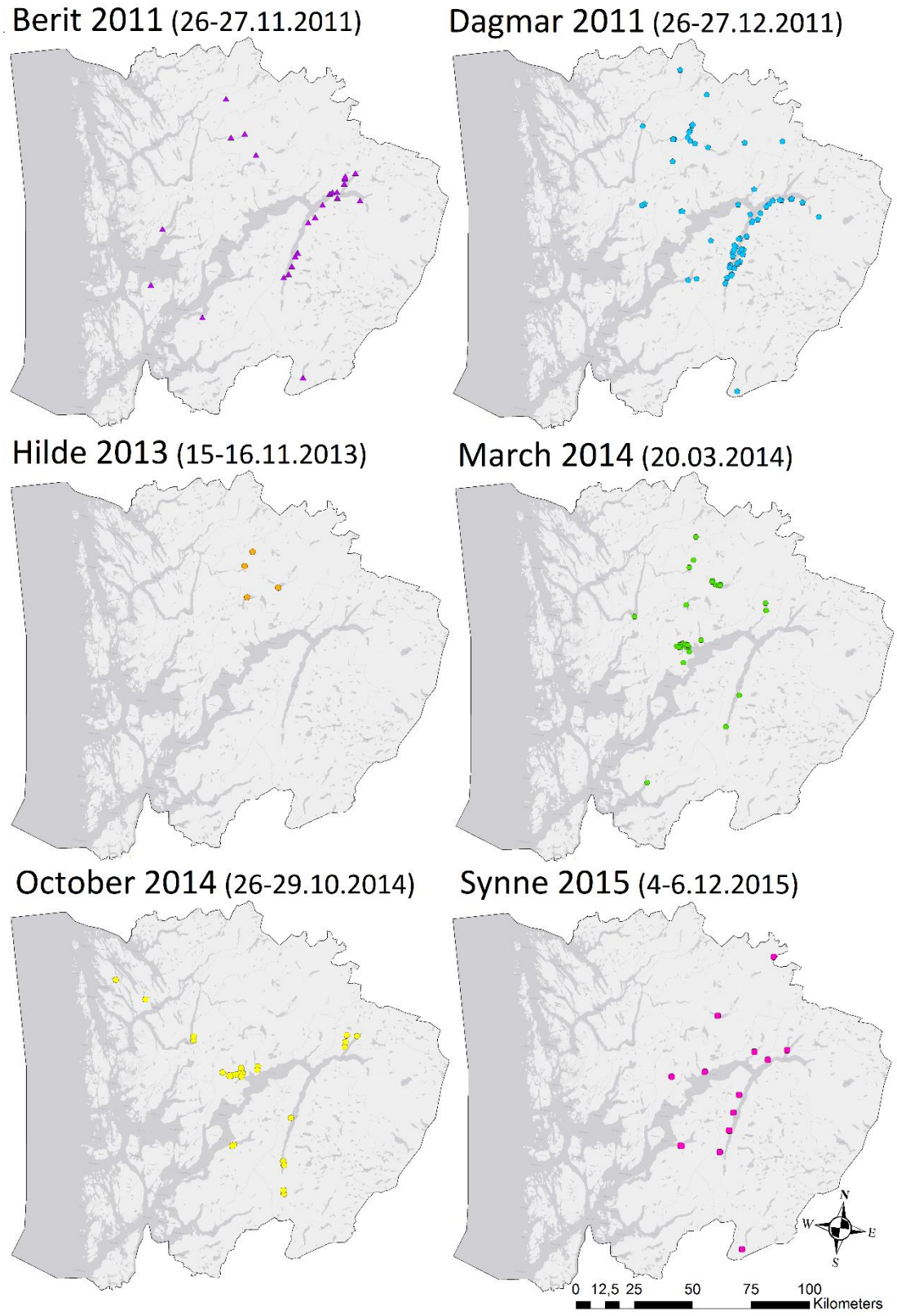

Appendix 6: Terrain parameters and landslide dimensions

Part of the attribute table for the 78 polygons mapped, including calculated parameters as height at initiation point, elevation range, slope angles, landslide area, runout length and H/L ratio.

Extreme event	Date event	Location name	OBJECT ID	Typology	Height at initiation point (masl)	Elevation range (m)	Slope angle at initiation point	Area (m^2)	Runout length (m)	H/L
Berit 2011	27.11.2011	Ulvik - bruravik	78	Debris flow	493,89	492,19	33,51	11016,37	726,33	0,6776534
Berit 2011	27.11.2011	Veg til Djønno	79	Debris flow	592,59	592,59	24,76	17775,57	1050,20	0,564273448
Berit 2011	27.11.2011	Holmane	80	Debris flow	1008,79	624,39	28,71	17172,36	884,70	0,705775962
Berit 2011	27.11.2011	Skjelvik	87	Debris flow	1079,59	1069,09	45,28	46057,04	1476,90	0,723881086
Berit 2011	27.11.2011	Kinsarvik	88	Debris flow	101,59	904,70	44,13	17210,04	1429,29	0,632971632
Berit 2011	27.11.2011	Bugjelet	89	Debris flow	403,20	633,00	35,64	45699,75	1733,70	0,365115086
Berit 2011	27.11.2011	Kyskredo	90	Debris flow	946,20	944,60	34,42	35008,10	1461,26	0,646428433
Berit 2011	27.11.2011	Fresvik	23	Debris flow	714,50	714,50	30,79	19548,49	1469,81	0,486117253
Dagmar 2011	26.12.2011	Aga	1	Debris flow	920,00	918,50	30,58	98056,85	1816,74	0,505575922
Dagmar 2011	26.12.2011	Aga	5	Debris flow	852,50	696,30	36,33	55716,41	1317,48	0,528508974
Dagmar 2011	26.12.2011	Kråkevik	6	Debris flow	727,20	725,50	26,17	25341,29	1679,42	0,431994386
Dagmar 2011	26.12.2011	Kråkevik	7	Debris flow	724,70	584,00	29,12	17419,97	1604,58	0,363958179
Dagmar 2011	26.12.2011	Kråkevik	8	Debris slide	295,00	19,39	26,22	206,19	40,36	0,480673786
Dagmar 2011	26.12.2011	Bleie	9	Debris slide	85,09	21,79	23,68	265,45	50,74	0,429641294
Dagmar 2011	26.12.2011	Fossåna	10	Debris avalanche	565,00	563,6	48,79	35889,63	582,63	0,967337762
Dagmar 2011	26.12.2011	Måge	13	Debris flow	796,79	796,29	34,49	62559,46	1274,65	0,624720502
Dagmar 2011	26.12.2011	Eikhamrane	14	Debris flow	947,90	946,00	44,30	44936,83	1339,05	0,706471024
Dagmar 2011	26.12.2011	Eitrheimtunnelen Nord 2	15	Debris flow	282,89	266,39	41,37	2776,88	332,42	0,801395806
Dagmar 2011	26.12.2011	Skjelvik	16	Debris flow	1079,59	1069,09	45,28	46606,41	1483,99	0,720422628
Dagmar 2011	26.12.2011	Skjelvik	20	Debris avalanche	261,39	261,39	32,33	29062,85	499,52	0,523302358
Dagmar 2011	26.12.2011	Skjelvik	21	Debris flow	728,00	588,10	48,40	24016,46	1069,88	0,549687821

Dagmar 2011	26.12.2011	Fresvik	22	Debris flow	539,70	539,70	39,80	10932,36	1237,73	0,43604018
Dagmar 2011	26.12.2011	Lofthus	24	Debris flow	85,40	85,20	24,21	1953,64	199,14	0,427839718
Dagmar 2011	26.12.2011	Kinsarvik	25	Debris flow	908,40	904,70	44,13	17775,85	1429,29	0,632971632
Dagmar 2011	26.12.2011	Berget	26	Debris flow	1014,40	1014,40	42,09	36618,66	1810,53	0,560277943
Dagmar 2011	26.12.2011	Kråkevik	27	Debris flow	1220,19	1220,09	43,77	77441,79	2645,06	0,461274962
Dagmar 2011	26.12.2011	Eidfjord	29	Debris flow	783,59	774,29	37,54	28983,83	1370,51	0,564972146
Dagmar 2011	26.12.2011	Digranes sør	30	Debris flow	1291,69	1290,89	22,14	64787,17	2403,39	0,537116303
Dagmar 2011	26.12.2011	Brattespe	32	Debris slide	77,69	33,49	23,57	746,00	77,65	0,431423003
Dagmar 2011	26.12.2011	Bratetspe	33	Debris flow	130,60	69,70	20,28	1085,93	185,57	0,375599529
Dagmar 2011	26.12.2011	Espe-Børve	34	Debris avalanche	902,00	268,20	26,51	11411,36	346,56	0,773892002
Dagmar 2011	26.12.2011	Espe	35	Debris flow	79,19	78,49	24,18	1383,18	262,43	0,299127375
Dagmar 2011	26.12.2011	Sekse	36	Debris flow	477,70	474,60	32,47	15058,66	1123,25	0,422523937
Dagmar 2011	26.12.2011	Espe-Børve	37	Debris flow	721,90	721,10	40,87	29872,22	1562,26	0,461574914
Dagmar 2011	26.12.2011	Espe-Børve	38	Debris flow	244,50	218,70	32,47	6134,84	548,10	0,39901478
Dagmar 2011	26.12.2011	Urheim	39	Debris flow	142,10	142,10	17,68	4685,20	528,31	0,268970881
Dagmar 2011	26.12.2011	Bugjelet	40	Debris flow	634,40	633,00	35,64	45723,05	1733,70	0,365115086
Dagmar 2011	26.12.2011	Brimnes	42	Debris flow	323,79	322,79	44,27	10458,96	522,86	0,617373652
Dagmar 2011	26.12.2011	Erdal	43	Debris flow	608,00	607,60	40,34	26768,27	853,29	0,71206741
Dagmar 2011	26.12.2011	Skarsenden	45	Debris flow	922,79	922,19	43,88	44637,80	1216,31	0,758194858
Dagmar 2011	26.12.2011	Kyskredo	46	Debris flow	946,20	944,60	34,42	35621,30	1461,26	0,646428433
Dagmar 2011	26.12.2011	Tveito rasteplass	47	Debris flow	812,29	644,39	43,37	12455,79	704,04	0,915288895
Dagmar 2011	26.12.2011	Sundal	49	Debris flow	438,79	435,49	33,42	11282,63	561,79	0,775200676
Dagmar 2011	26.12.2011	Haukanesberget	50	Debris flow	325,60	318,10	44,16	1933,29	247,83	1,283541162
Dagmar 2011	26.12.2011	Seters bru	52	Debris flow	1000,59	883,69	22,55	140359,81	2076,72	0,42552678
Dagmar 2011	26.12.2011	Nordalen	54	Debris flow	865,70	356,70	42,16	11230,93	567,85	0,628158866
Dagmar 2011	26.12.2011	Langeland	55	Debris flow	554,09	464,69	35,88	11623,54	539,18	0,861864264
Dagmar 2011	26.12.2011	Langeland	56	Debris avalanche	387,79	298,19	40,36	14786,73	383,51	0,777554664
Dagmar 2011	26.12.2011	Mestadstranda	58	Debris flow	271,29	204,59	43,56	5230,43	254,83	0,802888164
Dagmar 2011	26.12.2011	Mestad	60	Debris flow	771,70	705,20	34,43	32930,65	1827,02	0,38598374
Dagmar 2011	26.12.2011	Fadnestreet	62	Debris flow	510,79	486,69	32,13	59251,05	1520,74	0,32004155
Dagmar 2011	26.12.2011	Bulken - Evanger	64	Debris flow	246,50	233,90	37,17	17446,40	678,59	0,344685303
Dagmar 2011	26.12.2011	Bulken - Evanger	65	Debris avalanche	180,30	155,00	31,37	7178,72	261,12	0,593596828
Dagmar 2011	26.12.2011	Sekse/Hovland	66	Debris flow	923,20	923,20	39,02	55102,25	1911,54	0,482961388
Dagmar 2011	26.12.2011	Fossåna	68	Debris flow	848,59	845,29	39,58	25723,32	1244,65	0,679146729
Dagmar 2011	26.12.2011	Eitrheimtunnelen	69	Debris flow	186,60	184,60	40,95	2131,51	234,42	0,787475497
Dagmar 2011	26.12.2011	Byrkjenes	91	Debris flow	743,70	743,70	25,96	34271,62	1266,56	0,587181035
Dagmar 2011	26.12.2011	Byrkjenes	92	Debris flow	868,00	868,00	36,89	22189,83	1329,60	0,652827918
Dagmar 2011	26.12.2011	Sekse/ULLENSVANG (flaum)	93	Debris flow	564,70	77,50	33,17	2696,12	189,14	0,409749392
Dagmar 2011	26.12.2011	Sekse/ULLENSVANG (flaum)	94	Debris flow	571,09	163,79	31,63	5723,79	347,92	0,470797849

Dagmar 2011	27.12.2011	Austrepollen	48	Debris flow	640,90	640,80	42,74	45633,41	1473,21	0,434968555
Dagmar 2011	27.12.2011	Nesthusbekken Kvam	51	Debris flow	320,10	319,50	20,12	9664,35	670,43	0,476559829
Hilde 2013	15.11.2013	Forvoskaret	70	Debris flow	608,20	549,00	21,62	35477,69	2288,26	0,239920294
Hilde 2013	15.11.2013	Tungegrovi	71	Debris flow	294,00	234,09	19,57	7053,69	465,06	0,503375905
Hilde 2013	15.11.2013	Vannjolo	73	Debris flow	707,09	661,59	33,26	74036,36	3225,42	0,205120566
Hilde 2013	15.11.2013	Flyane, Straume bru	96	Debris slide	136,80	39,20	48,66	474,23	49,67	0,78920887
Hilde 2013	16.11.2013	Skjerstølen	72	Debris flow	704,20	116,20	8,820	8240,15	519,42	0,223711086
20 mars 2014	20.03.2014	Roe	82	Debris avalanche	113,69	20,00	32,51	558,74	59,36	0,336927224
20 mars 2014	20.03.2014	Honveshagen	83	Debris slide	79,80	32,20	36,26	1691,29	50,10	0,642714662
20 mars 2014	20.03.2014	Rv 13 ved Granvinsvatnet	84	Debris slide	54,79	22,29	38,71	428,15	32,73	0,681332088
20 mars 2014	20.03.2014	Hausnes	85	Debris avalanche	126,09	83,50	25,01	5326,63	239,49	0,348657564
20 mars 2014	20.03.2014	Vallandsvegen	86	Debris slide	36,09	8,89	33,63	425,50	29,78	0,298858217
October 2014	28.10.2014	Kambabekken, Klyvevegen, Kvam herad	74	Debris flow	272,50	272,10	25,44	6153,30	429,62	0,633350403
October 2014	28.10.2014	Odda	99	Debris slide	45,09	31,49	26,01	8245,77	75,94	0,414801134
Synne 2015	05.12.2015	Raudskredbekken	75	Debris flow	947,90	946,00	44,30	44936,83	1339,05	0,706471024
Synne 2015	05.12.2015	Eitrheimselva	76	Debris flow	879,59	879,49	24,13	56619,63	2179,84	0,403469968
Synne 2015	05.12.2015	Tveitnes	77	Debris flow	879,29	879,29	34,24	46712,32	1740,45	0,505214162
Synne 2015	05.12.2015	Jordalsvegen	98	Debris flow	692,79	460,99	36,04	10924,52	627,06	0,735176833

Appendix 7: Dataset 2

List of mapped landslides including geologic information, sources used and comments.

Extreme event	Date event	Location name	NLDB ID	OBJECT ID	LøsmNavn	BerggNavn	Bildekilde	Support map	Other source	Comments
Berit 2011	27.11.2011	Fresvik	5756	23	Bart fjell	Vulkanske bergarter (uspesifisert)	Aerial photo	Lidar		Debris flow in creek
Berit 2011	27.11.2011	Ulvik - bruravik	521	78	Skredmateriale, sammenhengende dekke, stedvis med stor mektighet	Vulkanske bergarter (uspesifisert)	Aerial photo	Lidar		In old path
Berit 2011	27.11.2011	Veg til Djønno	1800	79	Bart fjell	Granitt, granodioritt	Aerial photo	Lidar		Possibly in river, unknown starting point
Berit 2011	27.11.2011	Holmane	5671	80	Bart fjell	Granitt, granodioritt	Aerial photo	Lidar		In creek/old track?
Berit 2011	27.11.2011	Skjelvik	6916	87	Bart fjell	Vulkanske bergarter (uspesifisert)	Aerial photo	Lidar		Slide in the same path as nr 16 Dagmar 2011
Berit 2011	27.11.2011	Kinsarvik	850	88	Bart fjell	Vulkanske bergarter (uspesifisert)	Aerial photo	Lidar		Slide in the same path as nr 25 Dagmar 2011
Berit 2011	27.11.2011	Bugjelet	8069	89	Bart fjell	Diorittisk til granittisk gneis, migmatitt	Aerial photo	Lidar		Debris flow down creek
Berit 2011	27.11.2011	Kyskredo	9122	90	Bart fjell	Diorittisk til granittisk gneis, migmatitt	Aerial photo	Lidar		Debris slide in old path
Dagmar 2011	26.12.2011	Aga	2517	1	Bart fjell	Glimmergneis, glimmerskifer, metasandstein, amfibolitt	Aerial photo	Lidar	Photo News	Spread out in several directions, also related ID 249
Dagmar 2011	26.12.2011	Aga	8171	5	Bart fjell	Kvartsitt	Aerial photo	Lidar	Photo	Stopped by physical mitigation measure, containment of water caused flood
Dagmar 2011	26.12.2011	Kråkevik	2467	6	Bart fjell	Kvartsitt	Aerial photo	Lidar	Photo News	Joined 7

Dagmar 2011	26.12.2011	Kråkevik	7167	7	Bart fjell	Kvartsitt	Aerial photo	Lidar		Joined 6
Dagmar 2011	26.12.2011	Kråkevik	8756	8	Bart fjell	Kvartsitt	Aerial photo	Lidar		Small local slide on property
Dagmar 2011	26.12.2011	Bleie	7204	9	Morenemateriale, usammenhengende eller tynt dekke over berggrunnen	Kvartsitt	Aerial photo			Small local slide on property
Dagmar 2011	26.12.2011	Fossåna	9075	10	Bart fjell	Vulkanske bergarter (uspesifisert)	Aerial photo	Lidar	Photo News	Large slide blocked road. Mentioned in news
Dagmar 2011	26.12.2011	Måge	3980	13	Bart fjell	Vulkanske bergarter (uspesifisert)	Aerial photo	Lidar		Several joined into one and hit road
Dagmar 2011	26.12.2011	Eikhamrane	7052	14	Bart fjell	Vulkanske bergarter (uspesifisert)	Aerial photo	Lidar	Photo	Debris flow in old path
Dagmar 2011	26.12.2011	Eitrheimtunnelen Nord 2	3675	15	Bart fjell	Øyegneis, granitt, foliert granitt	Aerial photo	Lidar		Debris flow down to road, probably cleared, fan visible below
Dagmar 2011	26.12.2011	Skjelvik	4401	16	Bart fjell	Vulkanske bergarter (uspesifisert)	Aerial photo	Lidar	Photo	Debris flow with several possible source areas
Dagmar 2011	26.12.2011	Skjelvik	6952	20	Bart fjell	Vulkanske bergarter (uspesifisert)	Aerial photo	Lidar	Photo News	Share a deposit with 21
Dagmar 2011	26.12.2011	Skjelvik	1242	21	Bart fjell	Vulkanske bergarter (uspesifisert)	Aerial photo	Lidar	Photo News	Share a deposit with 20
Dagmar 2011	26.12.2011	Fresvik	6186	22	Morenemateriale, usammenhengende eller tynt dekke over berggrunnen	Vulkanske bergarter (uspesifisert)	Aerial photo	Lidar	Photo	Debris flow in creek
Dagmar 2011	26.12.2011	Lofthus	5055	24	Skredmateriale, sammenhengende dekke, stedvis med stor mektighet	Ryolitt, ryodacitt, dacitt, keratofyr	Aerial photo			Short debris flow in river hitting road
Dagmar 2011	26.12.2011	Kinsarvik	5920	25	Bart fjell	Vulkanske bergarter (uspesifisert)	Aerial photo	Lidar		Uncertain starting point
Dagmar 2011	26.12.2011	Berget	1865	26	Bart fjell	Granitt, granodioritt	Aerial photo	Lidar		Crossed road several times
Dagmar 2011	26.12.2011	Kråkevik	7964	27	Bart fjell	Glimmergneis, glimmerskifer, metasandstein, amfibolitt	Aerial photo	Lidar		Crossed road

Dagmar 2011	26.12.2011	Eidfjord	6413	29	Bart fjell	Diorittisk til granittisk gneis, migmatitt	Aerial photo	Lidar		Crossed road
Dagmar 2011	26.12.2011	Digranes sør	5126	30	Bart fjell	Øyegneis, granitt, foliert granitt	Aerial photo	Lidar		One slide, but splits up damaging road in two places
Dagmar 2011	26.12.2011	Brattespe	7243	32	Morenemateriale, sammenhengende dekke, stedvis med stor mektighet	Basalt	Aerial photo	Lidar	Photo News	Small debris slide on property
Dagmar 2011	26.12.2011	Bratetspe	5685	33	Morenemateriale, sammenhengende dekke, stedvis med stor mektighet	Basalt	Aerial photo	Lidar		Debris flow in creek, road slid out
Dagmar 2011	26.12.2011	Espe-Børve	5907	34	Bart fjell	Kvartsitt	Aerial photo	Lidar		Debris slide or avalanche, removed debris
Dagmar 2011	26.12.2011	Espe	3846	35	Morenemateriale, usammenhengende eller tynt dekke over berggrunnen	Glimmergneis, glimmerskifer, metasandstein, amfibolitt	Aerial photo	Lidar		Small debris flow in creek
Dagmar 2011	26.12.2011	Sekse	8835	36	Morenemateriale, usammenhengende eller tynt dekke over berggrunnen	Glimmergneis, glimmerskifer, metasandstein, amfibolitt	Aerial photo	Lidar	Photo	Debris flow in river
Dagmar 2011	26.12.2011	Espe-Børve	8977	37	Morenemateriale, usammenhengende eller tynt dekke over berggrunnen	Glimmergneis, glimmerskifer, metasandstein, amfibolitt	Aerial photo	Lidar		Debris flow in river, source unknown, decided by lidar
Dagmar 2011	26.12.2011	Espe-Børve	5474	38	Morenemateriale, usammenhengende eller tynt dekke over berggrunnen	Glimmergneis, glimmerskifer, metasandstein, amfibolitt	Aerial photo	Lidar		Debris flow in river, source unknown, decided by lidar
Dagmar 2011	26.12.2011	Urheim	535	39	Skredmateriale, sammenhengende dekke, stedvis med stor mektighet	Vulkanske bergarter (uspesifisert)	Aerial photo	Lidar		Debris flow in creek
Dagmar 2011	26.12.2011	Bugjelet	6063	40	Bart fjell	Diorittisk til granittisk gneis, migmatitt	Aerial photo	Lidar		Debris flow down creek
Dagmar 2011	26.12.2011	Brimnes	1280	42	Bart fjell	Diorittisk til granittisk gneis, migmatitt	Aerial photo	Lidar		Debris flow in creek
Dagmar 2011	26.12.2011	Erdal	8034	43	Bart fjell	Diorittisk til granittisk gneis, migmatitt	Aerial photo	Lidar		Uncertain due to another slide before aerial photo
Dagmar 2011	26.12.2011	Skarsenden	4035	45	Bart fjell	Diorittisk til granittisk gneis, migmatitt	Aerial photo	Lidar		Debris slide in old path, passed over road on physical mitigation measure
Dagmar 2011	26.12.2011	Kyskredo	2868	46	Bart fjell	Diorittisk til granittisk gneis, migmatitt	Aerial photo	Lidar		Debris slide in old path

Dagmar 2011	26.12.2011	Tveito rasteplass	1222	47	Bart fjell	Diorittisk til granittisk gneis, migmatitt	Aerial photo	Lidar		Debris flow in creek
Dagmar 2011	26.12.2011	Sundal	3140	49	Bart fjell	Diorittisk til granittisk gneis, migmatitt	Aerial photo	Lidar		Largely mapped by lidar due to shadows, might start higher
Dagmar 2011	26.12.2011	Haukanesberget	518	50	Bart fjell	Kvartsdioritt, tonalitt, trondhjemitt	Aerial photo			Debris flow in old path
Dagmar 2011	26.12.2011	Seters bru	5884	52	Bart fjell	Diorittisk til granittisk gneis, migmatitt	Aerial photo	Lidar		Large debris flow damaging road
Dagmar 2011	26.12.2011	Nordalen	3032	54	Bart fjell	Fyllitt, glimmerskifer	Aerial photo	Lidar		Old path/creek
Dagmar 2011	26.12.2011	Langeland	3439	55	Bart fjell	Fyllitt, glimmerskifer	Aerial photo	Lidar		River overflowed, debris over edge
Dagmar 2011	26.12.2011	Langeland	3439	56	Bart fjell	Glimmergneis, glimmerskifer, metasandstein, amfibolitt	Aerial photo	Lidar		Met overflowed river
Dagmar 2011	26.12.2011	Mestadstranda	3481	58	Bart fjell	Metasandstein, glimmerskifer	Aerial photo	Lidar		Mostly Lidar mapped, in creek/path
Dagmar 2011	26.12.2011	Mestad	7093	60	Bart fjell	Granitt, granodioritt	Aerial photo	Lidar		Debris flow in creek
Dagmar 2011	26.12.2011	Fadnestreet	22	62	Bart fjell	Metasandstein, glimmerskifer	Aerial photo	Lidar		Mostly Lidar mapped
Dagmar 2011	26.12.2011	Bulken - Evanger	2632	64	Forvitringsmateriale, ikke inndelt etter mektighet	Kvartsdioritt, tonalitt, trondhjemitt	Aerial photo	Lidar	Photo News	Hit railway
Dagmar 2011	26.12.2011	Bulken - Evanger	8313	65	Forvitringsmateriale, ikke inndelt etter mektighet	Kvartsdioritt, tonalitt, trondhjemitt	Aerial photo	Lidar		Hit railway, in creek
Dagmar 2011	26.12.2011	Sekse/Hovland	5124	66	Skredmateriale, sammenhengende dekke, stedvis med stor mektighet	Gabbro, amfibolitt	Aerial photo	Lidar	Photo	Wrong date? 27.11.2011 Used in SVV report on Dagmar
Dagmar 2011	26.12.2011	Fossåna		68	Bart fjell	Vulkanske bergarter (uspesifisert)	Aerial photo	Lidar	Photo News	Not registered, caught by mitigation measure, mentioned in news
Dagmar 2011	26.12.2011	Eitrheimtunnelen	3507	69	Bart fjell	Øyegneis, granitt, foliert granitt	Aerial photo			Debris flow down to road, probably cleared, fan visible below

Dagmar 2011	26.12.2011	Byrkjenes		91	Bart fjell	Øyegneis, granitt, foliert granitt	Aerial photo	Lidar	Photo	Not registered, pictured in NVE faktaark with date
Dagmar 2011	26.12.2011	Byrkjenes		92	Bart fjell	Øyegneis, granitt, foliert granitt	Aerial photo	Lidar		Not registered, pictured in NVE faktaark with date
Dagmar 2011	26.12.2011	Sekse/ULLENSVANG (flaum)	6120	93	Morenemateriale, usammenhengende eller tynt dekke over berggrunnen	Gabbro, amfibolitt	Aerial photo	Lidar		Small slide, low accuracy
Dagmar 2011	26.12.2011	Sekse/ULLENSVANG (flaum)	2661	94	Morenemateriale, usammenhengende eller tynt dekke over berggrunnen	Gabbro, amfibolitt	Aerial photo	Lidar		Small slide, low accuracy
Dagmar 2011	27.12.2011	Austrepollen	4447	48	Bart fjell	Diorittisk til granittisk gneis, migmatitt	Aerial photo	Lidar		Debris flow in old path
Dagmar 2011	27.12.2011	Nesthusbekken Kvam	7156	51	Forvitringsmateriale, ikke inndelt etter mektighet	Grønnstein, amfibolitt	Aerial photo	Lidar		Debris flow in creek, unknown source area
Hilde 2013	15.11.2013	Forvoskaret	5102	70	Bart fjell	Kvartsitt	Aerial photo	Lidar		Unknown starting point, point far away but name in polygon location
Hilde 2013	15.11.2013	Tungegrovi	2289	71	Morenemateriale, usammenhengende eller tynt dekke over berggrunnen	Diorittisk til granittisk gneis, migmatitt	Aerial photo	Lidar		Unknown location name, probably in creek
Hilde 2013	15.11.2013	Vannjolo	6133	73	Morenemateriale, usammenhengende eller tynt dekke over berggrunnen	Granitt, granodioritt	Aerial photo	Lidar		Debris flow in creek
Hilde 2013	15.11.2013	Flyane, Straume bru	5476	96	Bart fjell	Glimmergneis, glimmerskifer, metasandstein, amfibolitt	Aerial photo			Only one visible
Hilde 2013	16.11.2013	Skjerstølen	3804	72	Morenemateriale, usammenhengende eller tynt dekke over berggrunnen	Fyllitt, glimmerskifer	Aerial photo	Lidar		Small debris flow in creek
20 mars 2014	20.03.2014	Roe	2722	82	Forvitringsmateriale, ikke inndelt etter mektighet	Fyllitt, glimmerskifer	Aerial photo	Lidar	Photo Regobs	Debris slide/avalanche in removed forest area
20 mars 2014	20.03.2014	Honveshagen	3895	83	Forvitringsmateriale, ikke inndelt etter mektighet	Fyllitt, glimmerskifer	Aerial photo	Lidar	Photo Regobs	Slid down from upper road
20 mars 2014	20.03.2014	Rv 13 ved Granvinsvatnet	4050	84	Skredmateriale, sammenhengende dekke, stedvis med stor mektighet	Metasandstein, glimmerskifer	Aerial photo	Lidar	Regobs	20-30 m slide down to road
20 mars 2014	20.03.2014	Hausnes	2873	85	Forvitringsmateriale, ikke inndelt etter mektighet	Fyllitt, glimmerskifer	Aerial photo	Lidar	Photo News Regobs	In newspaper

20 mars 2014	20.03.2014	Vallandsvegen	5040	86	Forvitringsmateriale, ikke inndelt etter mektighet	Grønnstein, amfibolitt	Newsp aper		Photo News Regobs	Slide inbetween houses
October 2014	28.10.2014	Kambabekken, Klyvevegen, Kvam herad	3743	74	Bart fjell	Glimmergneis, glimmerskifer, metasandstein, amfibolitt	Aerial photo	Lidar		Debris flow in creek, mostly mapped from lidar, unknown which tractor path
October 2014	28.10.2014	Odda	5229	99	Breelvavsetning (Glasifluvial avsetning)	Vulkanske bergarter (uspesifisert)		Lidar	Photo News Regobs	Debris slide in river, many other smaller
Synne 2015	05.12.2015	Raudskredbekken	120	75	Bart fjell	Vulkanske bergarter (uspesifisert)	Aerial photo	Lidar	Photo News Regobs	In previous nr 14 track, picture in news
Synne 2015	05.12.2015	Eitrheimselva	5607	76	Bart fjell	Diorittisk til granittisk gneis, migmatitt	Aerial photo	Lidar	Photo	Described as in river, old path, might be double with 5875
Synne 2015	05.12.2015	Tveitnes	6127	77	Bart fjell	Diorittisk til granittisk gneis, migmatitt	Aerial photo	Lidar		In old path? Unknown starting point
Synne 2015	05.12.2015	Jordalsvegen	7977	98	Bart fjell	Anortositt	Aerial photo	Lidar	Photo News	Unknown starting point and contribution, hit mitigation measure

Appendix 8: List of frequency-magnitude values

Extreme event	Date event	Stedsnavn	Typology	OBJECTID	Magnitude (m^2)	Individual landslide frequency (fi)	Annual landslide frequency (Fi)
Dagmar 2011	26.12.2011	Seters bru	Debris flow	52	140359,8105	0,142857143	0,142857143
Dagmar 2011	26.12.2011	Aga	Debris flow	1	98056,8559	0,142857143	0,285714286
Dagmar 2011	26.12.2011	Kråkevik	Debris flow	27	77441,7964	0,142857143	0,428571429
Hilde 2013	15.11.2013	Vannjolo	Debris flow	73	74036,36788	0,142857143	0,571428571
Dagmar 2011	26.12.2011	Digranes sør	Debris flow	30	64787,1777	0,142857143	0,714285714
Dagmar 2011	26.12.2011	Måge	Debris flow	13	62559,46621	0,142857143	0,857142857
Dagmar 2011	26.12.2011	Fadnestreet	Debris flow	62	59251,05142	0,142857143	1
Synne 2015	05.12.2015	Eitrheimselva	Debris flow	76	56619,63262	0,142857143	1,142857143
Dagmar 2011	26.12.2011	Aga	Debris flow	5	55716,41339	0,142857143	1,285714286
Dagmar 2011	26.12.2011	Sekse/Hovland	Debris flow	66	55102,2568	0,142857143	1,428571429
Synne 2015	05.12.2015	Tveitnes	Debris flow	77	46712,32205	0,142857143	1,571428571
Dagmar 2011	26.12.2011	Skjelvik	Debris flow	16	46606,41342	0,142857143	1,714285714
Berit 2011	27.11.2011	Skjelvik	Debris flow	87	46057,04997	0,142857143	1,857142857
Dagmar 2011	26.12.2011	Bugjelet	Debris flow	40	45723,05217	0,142857143	2
Berit 2011	27.11.2011	Bugjelet	Debris flow	89	45699,75132	0,142857143	2,142857143
Dagmar 2011	27.12.2011	Austrepollen	Debris flow	48	45633,4115	0,142857143	2,285714286
Dagmar 2011	26.12.2011	Eikhamrane	Debris flow	14	44936,83707	0,142857143	2,428571429
Synne 2015	05.12.2015	Raudskredbekken	Debris flow	75	44936,83707	0,142857143	2,571428571
Dagmar 2011	26.12.2011	Skarsenden	Debris flow	45	44637,80506	0,142857143	2,714285714
Dagmar 2011	26.12.2011	Berget	Debris flow	26	36618,66683	0,142857143	2,857142857
Dagmar 2011	26.12.2011	Fossåna	Debris avalanche	10	35889,63309	0,142857143	3
Dagmar 2011	26.12.2011	Kyskredo	Debris flow	46	35621,30333	0,142857143	3,142857143
Hilde 2013	15.11.2013	Forvoskaret	Debris flow	70	35477,69832	0,142857143	3,285714286
Berit 2011	27.11.2011	Kyskredo	Debris flow	90	35008,10961	0,142857143	3,428571429
Dagmar 2011	26.12.2011	Byrkjenes	Debris flow	91	34271,62369	0,142857143	3,571428571
Dagmar 2011	26.12.2011	Mestad	Debris flow	60	32930,6564	0,142857143	3,714285714

Dagmar 2011	26.12.2011	Espe-Børve	Debris flow	37	29872,22699	0,142857143	3,857142857
Dagmar 2011	26.12.2011	Skjelvik	Debris avalanche	20	29062,85258	0,142857143	4
Dagmar 2011	26.12.2011	Eidfjord	Debris flow	29	28983,83021	0,142857143	4,142857143
Dagmar 2011	26.12.2011	Erdal	Debris flow	43	26768,27172	0,142857143	4,285714286
Dagmar 2011	26.12.2011	Fossåna	Debris flow	68	25723,32187	0,142857143	4,428571429
Dagmar 2011	26.12.2011	Kråkevik	Debris flow	6	25341,29953	0,142857143	4,571428571
Dagmar 2011	26.12.2011	Skjelvik	Debris flow	21	24016,46473	0,142857143	4,714285714
Dagmar 2011	26.12.2011	Byrkjenes	Debris flow	92	22189,83559	0,142857143	4,857142857
Berit 2011	27.11.2011	Fresvik	Debris flow	23	19548,49465	0,142857143	5
Dagmar 2011	26.12.2011	Kinsarvik	Debris flow	25	17775,85532	0,142857143	5,142857143
Berit 2011	27.11.2011	Veg til Djønno	Debris flow	79	17775,5731	0,142857143	5,285714286
Dagmar 2011	26.12.2011	Bulken - Evanger	Debris flow	64	17446,40229	0,142857143	5,428571429
Dagmar 2011	26.12.2011	Kråkevik	Debris flow	7	17419,97356	0,142857143	5,571428571
Berit 2011	27.11.2011	Kinsarvik	Debris flow	88	17210,04339	0,142857143	5,714285714
Berit 2011	27.11.2011	Holmane	Debris flow	80	17172,36999	0,142857143	5,857142857
Dagmar 2011	26.12.2011	Sekse	Debris flow	36	15058,66391	0,142857143	6
Dagmar 2011	26.12.2011	Langeland	Debris avalanche	56	14786,73193	0,142857143	6,142857143
Dagmar 2011	26.12.2011	Tveito rasteplass	Debris flow	47	12455,79356	0,142857143	6,285714286
Dagmar 2011	26.12.2011	Langeland	Debris flow	55	11623,54776	0,142857143	6,428571429
Dagmar 2011	26.12.2011	Espe-Børve	Debris avalanche	34	11411,36758	0,142857143	6,571428571
Dagmar 2011	26.12.2011	Sundal	Debris flow	49	11282,63079	0,142857143	6,714285714
Dagmar 2011	26.12.2011	Nordalen	Debris flow	54	11230,9333	0,142857143	6,857142857
Berit 2011	27.11.2011	Ulvik - bruravik	Debris flow	78	11016,37275	0,142857143	7
Dagmar 2011	26.12.2011	Fresvik	Debris flow	22	10932,36175	0,142857143	7,142857143
Synne 2015	05.12.2015	Jordalsvegen	Debris flow	98	10924,52647	0,142857143	7,285714286
Dagmar 2011	26.12.2011	Brimnes	Debris flow	42	10458,96832	0,142857143	7,428571429
Dagmar 2011	27.12.2011	Nesthusbekken Kvam	Debris flow	51	9664,351993	0,142857143	7,571428571
October 2014	28.10.2014	Odda	Debris slide	99	8245,77538	0,142857143	7,714285714
Hilde 2013	16.11.2013	Skjerstølen	Debris flow	72	8240,150882	0,142857143	7,857142857
Dagmar 2011	26.12.2011	Bulken - Evanger	Debris avalanche	65	7178,720995	0,142857143	8
Hilde 2013	15.11.2013	Tungegrovi	Debris flow	71	7053,695063	0,142857143	8,142857143
October 2014	28.10.2014	Kambabekken, Klyvevegen, Kvam herad	Debris flow	74	6153,303699	0,142857143	8,285714286
Dagmar 2011	26.12.2011	Espe-Børve	Debris flow	38	6134,849319	0,142857143	8,428571429
Dagmar 2011	26.12.2011	Sekse/ULLENSVANG (flaum)	Debris flow	94	5723,799884	0,142857143	8,571428571
20 mars 2014	20.03.2014	Hausnes	Debris avalanche	85	5326,630985	0,142857143	8,714285714
Dagmar 2011	26.12.2011	Mestadstranda	Debris flow	58	5230,437185	0,142857143	8,857142857
Dagmar 2011	26.12.2011	Urheim	Debris flow	39	4685,205845	0,142857143	9
Dagmar 2011	26.12.2011	Eitrheimtunnelen Nord 2	Debris flow	15	2776,885057	0,142857143	9,142857143

Dagmar 2011	26.12.2011	Sekse/ULLENSVANG (flaum)	Debris flow	93	2696,127183	0,142857143	9,285714286
Dagmar 2011	26.12.2011	Eitrheimtunnelen	Debris flow	69	2131,51762	0,142857143	9,428571429
Dagmar 2011	26.12.2011	Lofthus	Debris flow	24	1953,6469	0,142857143	9,571428571
Dagmar 2011	26.12.2011	Haukanesberget	Debris flow	50	1933,295559	0,142857143	9,714285714
20 mars 2014	20.03.2014	Honveshagen	Debris slide	83	1691,296925	0,142857143	9,857142857
Dagmar 2011	26.12.2011	Espe	Debris flow	35	1383,184833	0,142857143	10
Dagmar 2011	26.12.2011	Bratetspe	Debris flow	33	1085,937735	0,142857143	10,14285714
Dagmar 2011	26.12.2011	Brattespe	Debris slide	32	746,0077335	0,142857143	10,28571429
20 mars 2014	20.03.2014	Roe	Debris avalanche	82	558,744614	0,142857143	10,42857143
Hilde 2013	15.11.2013	Flyane, Straume bru	Debris slide	96	474,2338279	0,142857143	10,57142857
20 mars 2014	20.03.2014	Rv 13 ved Granvinsvatnet	Debris slide	84	428,1518438	0,142857143	10,71428571
20 mars 2014	20.03.2014	Vallandsvegen	Debris slide	86	425,5062442	0,142857143	10,85714286
Dagmar 2011	26.12.2011	Bleie	Debris slide	9	265,4514304	0,142857143	11
Dagmar 2011	26.12.2011	Kråkevik	Debris slide	8	206,1969464	0,142857143	11,14285714

Appendix 9: Values of soil water used in threshold analysis

OBJECTID	SDB	Extreme_event	Date_event	Time of day	Accuracy time	Dato hentet fra	Relative water supply (%)	Relative water supply range	Relative soil water content (%)	Relative water content range
88	850	Berit 2011	27.11.2011	06:37:00	Eksakt	26.11.2011	5,30	4-6%	113,00	>90%
80	5671	Berit 2011	27.11.2011	05:30:00	Eksakt	26.11.2011	3,20	2-4%	82,00	80-90%
89	8069	Berit 2011	27.11.2011	06:19:00	Eksakt	26.11.2011	4,30	4-6%	95,00	>90%
90	9122	Berit 2011	27.11.2011	05:20:00	Eksakt	26.11.2011	0,00	0 %	66,00	60-70%
78	521	Berit 2011	27.11.2011	08:00:00	30 min	27.11.2011	0,60	<2%	81,00	80-90%
79	1800	Berit 2011	27.11.2011	08:00:00	30 min	27.11.2011	0,70	<2%	81,00	80-90%
23	5756	Berit 2011	27.11.2011	12:06:00	Eksakt	27.11.2011	0,70	<2%	77,00	70-80%
87	6916	Berit 2011	27.11.2011	11:48:00	Eksakt	27.11.2011	0,00	0 %	78,00	70-80%
50	518	Dagmar 2011	26.12.2011	02:00:00	30 min	25.12.2011	1,70	<2%	72,00	70-80%
39	535	Dagmar 2011	26.12.2011	01:32:00	Eksakt	25.12.2011	2,10	2-4%	77,00	70-80%
21	1242	Dagmar 2011	26.12.2011	02:00:00	30 min	25.12.2011	0,90	<2%	51,00	<60%
26	1865	Dagmar 2011	26.12.2011	01:05:50	Eksakt	25.12.2011	0,80	<2%	48,00	<60%
54	3032	Dagmar 2011	26.12.2011	02:00:00	30 min	25.12.2011	1,20	<2%	59,00	<60%
49	3140	Dagmar 2011	26.12.2011	06:00:00	30 min	25.12.2011	1,60	<2%	75,00	70-80%
69	3507	Dagmar 2011	26.12.2011	01:01:30	Eksakt	25.12.2011	No Data	No Data	0,00	<60%
16	4401	Dagmar 2011	26.12.2011	05:22:00	Eksakt	25.12.2011	0,00	0 %	51,00	<60%
24	5055	Dagmar 2011	26.12.2011	01:33:50	Eksakt	25.12.2011	1,80	<2%	77,00	70-80%
66	5124	Dagmar 2011	26.12.2011	05:44:00	Reg annen dato	25.12.2011	4,80	4-6%	88,00	80-90%
30	5126	Dagmar 2011	26.12.2011	01:03:00	Eksakt	25.12.2011	0,80	<2%	52,00	<60%
25	5920	Dagmar 2011	26.12.2011	01:25:20	Eksakt	25.12.2011	1,10	<2%	55,00	<60%
22	6186	Dagmar 2011	26.12.2011	06:30:00	Eksakt	25.12.2011	2,30	2-4%	60,00	60-70%
20	6952	Dagmar 2011	26.12.2011	06:47:00	Eksakt	25.12.2011	2,20	2-4%	77,00	70-80%
60	7093	Dagmar 2011	26.12.2011	02:00:00	30 min	25.12.2011	0,70	<2%	50,00	<60%

43	8034	Dagmar 2011	26.12.2011	01:02:30	Eksakt	25.12.2011	0,70	<2%	57,00	<60%
62	22	Dagmar 2011	26.12.2011	19:00:00	30 min	26.12.2011	1,90	<2%	76,00	70-80%
47	1222	Dagmar 2011	26.12.2011		Ukjent nar pa dagen	26.12.2011	5,10	4-6%	86,00	80-90%
42	1280	Dagmar 2011	26.12.2011		Ukjent nar pa dagen	26.12.2011	No Data	No Data	0,00	<60%
6	2467	Dagmar 2011	26.12.2011	18:00:00	30 min	26.12.2011	4,80	4-6%	85,00	80-90%
1	2517	Dagmar 2011	26.12.2011	18:00:00	30 min	26.12.2011	4,90	4-6%	91,00	>90%
64	2632	Dagmar 2011	26.12.2011		Ukjent nar pa dagen	26.12.2011	2,40	2-4%	77,00	70-80%
94	2661	Dagmar 2011	26.12.2011		5 år	26.12.2011	5,50	4-6%	95,00	>90%
46	2868	Dagmar 2011	26.12.2011	09:51:00	Eksakt	26.12.2011	0,00	0 %	48,00	<60%
55	3439	Dagmar 2011	26.12.2011	18:00:00	30 min	26.12.2011	2,00	<2%	60,00	60-70%
56	3439	Dagmar 2011	26.12.2011	18:00:00	30 min	26.12.2011	2,00	<2%	83,00	80-90%
58	3481	Dagmar 2011	26.12.2011		Ukjent nar pa dagen	26.12.2011	2,40	2-4%	85,00	80-90%
15	3675	Dagmar 2011	26.12.2011		Ukjent nar pa dagen	26.12.2011	No Data	No Data	0,00	<60%
35	3846	Dagmar 2011	26.12.2011	11:49:00	Eksakt	26.12.2011	5,00	4-6%	92,00	>90%
13	3980	Dagmar 2011	26.12.2011	18:00:00	30 min	26.12.2011	4,50	4-6%	80,00	70-80%
45	4035	Dagmar 2011	26.12.2011		Ukjent nar pa dagen	26.12.2011	0,00	0 %	48,00	<60%
38	5474	Dagmar 2011	26.12.2011	11:53:00	Ukjent nar pa dagen	26.12.2011	5,20	4-6%	96,00	>90%
33	5685	Dagmar 2011	26.12.2011		Ukjent nar pa dagen	26.12.2011	4,40	4-6%	92,00	>90%
52	5884	Dagmar 2011	26.12.2011		Ukjent nar pa dagen	26.12.2011	1,60	<2%	61,00	60-70%
34	5907	Dagmar 2011	26.12.2011		Ukjent nar pa dagen	26.12.2011	4,90	4-6%	91,00	>90%
40	6063	Dagmar 2011	26.12.2011	09:53:00	Eksakt	26.12.2011	5,50	4-6%	96,00	>90%
93	6120	Dagmar 2011	26.12.2011		5 år	26.12.2011	5,50	4-6%	95,00	>90%
29	6413	Dagmar 2011	26.12.2011	09:29:00	Eksakt	26.12.2011	4,80	4-6%	87,00	80-90%
14	7052	Dagmar 2011	26.12.2011	19:44:00	Eksakt	26.12.2011	4,50	4-6%	89,00	80-90%
7	7167	Dagmar 2011	26.12.2011	18:00:00	30 min	26.12.2011	4,80	4-6%	85,00	80-90%
9	7204	Dagmar 2011	26.12.2011		1 dag	26.12.2011	4,70	4-6%	89,00	80-90%
32	7243	Dagmar 2011	26.12.2011		1 dag	26.12.2011	4,40	4-6%	92,00	>90%
27	7964	Dagmar 2011	26.12.2011	18:00:00	30 min	26.12.2011	0,00	0 %	33,00	<60%
5	8171	Dagmar 2011	26.12.2011		1 dag	26.12.2011	4,90	4-6%	91,00	>90%
65	8313	Dagmar 2011	26.12.2011		Ukjent nar pa dagen	26.12.2011	2,60	2-4%	89,00	80-90%
8	8756	Dagmar 2011	26.12.2011	19:00:00	1 time	26.12.2011	5,00	4-6%	91,00	>90%
36	8835	Dagmar 2011	26.12.2011		5 år	26.12.2011	5,50	4-6%	107,00	>90%
37	8977	Dagmar 2011	26.12.2011	10:59:00	Ukjent nar pa dagen	26.12.2011	5,80	4-6%	97,00	>90%
10	9075	Dagmar 2011	26.12.2011	11:06:00	Eksakt	26.12.2011	4,60	4-6%	93,00	>90%
68		Dagmar 2011	26.12.2011		Ukjent nar pa dagen	26.12.2011	4,60	4-6%	84,00	80-90%
91		Dagmar 2011	26.12.2011		Ukjent nar pa dagen	26.12.2011	3,30	2-4%	74,00	70-80%
92		Dagmar 2011	26.12.2011		Ukjent nar pa dagen	26.12.2011	3,50	2-4%	88,00	80-90%
48	4447	Dagmar 2011	27.12.2011	10:18:00	Eksakt	27.12.2011	2,70	2-4%	64,00	60-70%
51	7156	Dagmar 2011	27.12.2011		1 dag	27.12.2011	1,90	<2%	81,00	80-90%

71	2289	Hilde 2013	15.11.2013	19:30:00	Eksakt	15.11.2013	2,00	<2%	72,00	70-80%
70	5102	Hilde 2013	15.11.2013	19:25:00	Eksakt	15.11.2013	2,40	2-4%	74,00	70-80%
96	5476	Hilde 2013	15.11.2013	19:00:00	30 min	15.11.2013	1,50	<2%	69,00	60-70%
73	6133	Hilde 2013	15.11.2013	17:00:00	30 min	15.11.2013	1,90	<2%	75,00	70-80%
72	3804	Hilde 2013	16.11.2013	19:20:00	Eksakt	16.11.2013	1,20	<2%	78,00	70-80%
82	2722	20 mars 2014	20.03.2014	18:00:00	12 timer	20.03.2014	2,00	<2%	89,00	80-90%
85	2873	20 mars 2014	20.03.2014	12:00:00	12 timer	20.03.2014	2,40	2-4%	91,00	>90
83	3895	20 mars 2014	20.03.2014	21:35:00	Eksakt	20.03.2014	2,30	2-4%	76,00	70-80%
84	4050	20 mars 2014	20.03.2014	17:00:00	Eksakt	20.03.2014	2,40	2-4%	91,00	>90%
86	5040	20 mars 2014	20.03.2014	16:50:00	Eksakt	20.03.2014	2,50	2-4%	82,00	80-90%
74	3743	October 2014	28.10.2014	17:00:00	1 time	28.10.2014	2,20	2-4%	83,00	80-90%
99	5229	October 2014	28.10.2014		1 dag	28.10.2014	3,60	2-4%	88,00	80-90%
75	120	Synne 2015	05.12.2015	06:00:00	4 timer	04.12.2015	3,10	2-4%	71,00	70-80%
76	5607	Synne 2015	05.12.2015	07:34:00	1 time	04.12.2015	0,00	0 %	39,00	<60%
77	6127	Synne 2015	05.12.2015	05:39:00	Eksakt	04.12.2015	2,00	<2%	68,00	60-70%
98	7977	Synne 2015	05.12.2015	06:00:00	12 timer	05.12.2015	0,00	0 %	52,00	<60%

Appendix 10: Poster for Geofaredagen 2018

Poster presented at Geofaredagen in Lillestrøm 2018.

Regional mapping and frequency-magnitude analysis of debris avalanches and debris flows in Hordaland, Norway

Kamilla Skåre Sandboe[1], Graziella Devoli[2], Karianne Staalesen Lilleøren[1]
1 Department of Geosciences, University of Oslo, Norway 2 Hydrology Department, Norwegian Water Resources and Energy Directorate, Oslo, Norway

INTRODUCTION

The possible occurrence of rainfall- and snowmelt induced landslides (i.e. debris flows, debris avalanches and slush flows) (figure 1), is forecasted at the Norwegian landslide forecasting and warning service at NVE. The service sends out warnings of expected landslides in different weather conditions (Krøgli et al., 2018). The service works with four levels of warning, green, yellow, orange and red (figure 2). The levels are divided based on the expected number of landslides within the warning zone, but do not include specific expected landslide magnitude.

Knowing the typical and most frequent magnitude in a certain area is essential in landslide hazard analyses. For example, it provides information about which damage extension to expect after we send a warning. This will help to organize a more effective mitigative effort, or assist emergency response actions. With an increase in number of weather-induced landslides from increased precipitation and snow melt due to climate change, the need for knowing the expected magnitude will also increase.

FIGURE 1: Debris flow and debris avalanche come together hitting houses and the road in several locations during Dagmar 2011

FIGURE 2: The four warning levels and their colors

OBJECTIVES

The main aim of the study is to perform a frequency-magnitude analysis in weather induced landslides occurred in the period 2011-2017 in Hordaland (figure 3) and to evaluate the performance of the warning system during the mapped cases.

METHOD

- ANALYSIS OF RAINFALL EVENTS

The first analysis was done identifying all rainfall and snowmelt events that triggered landslides in the area. This was done by analyzing precipitation data at xgeo.no, and cross checking with reported landslides at the national database (figure 4). A list of significant rainfall events that triggered landslides was prepared (figure 5).

STUDY AREA

FIGURE 3: The study area is Hordaland county, located at the west coast of Norway. The county has high annual precipitation and steep mountainsides along its fjords, and two of Norway's largest glaciers. Most of the precipitation is convective or orographic. The area is very prone to weather-induced landslides.

FIGURE 4: Notes of rainfall events of interest during the work. The events marked in green were mapped, the events marked in red did not have enough confirmatory sources to be mapped.

THE EVENTS

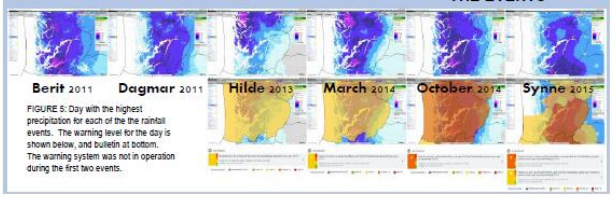

FIGURE 5: Day with the highest precipitation for each of the the rainfall events. The warning level for the day is shown below, and bulletin at bottom. The warning system was not in operation during the first two events.

- MAPPING OF LANDSLIDES

Based on the first analysis, polygons were drawn for landslides which occurred during these major rainfall events, focusing on the events with more than two landslides registered (figure 6 and 7).

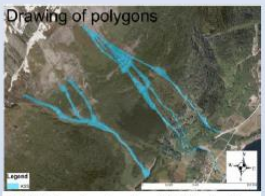

FIGURE 6: Two of the polygons drawn for landslides, here ID 1 and 5 which occurred during the extreme weather Dagmar 2011.

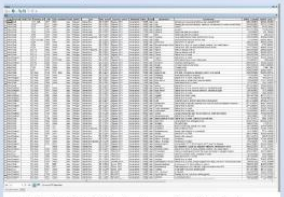

FIGURE 7: Attribute table for the polygons, with their location, type, size, map scale, uncertainty, NLDB ID and additional comments.

- ADDITIONAL SOURCES FOR THE MAPPING

Additional sources were used to map the landslides (figure 8, 9, 10). Landslides mentioned in the news are often the ones causing trouble for the population, or have hit roads, railways, infrastructure or residences.

FIGURE 8: Fjordaland avis covering a debris avalanche in Husnes, Hordaland, which hit a residence.

FIGURE 9: Picture taken by Aart Verhage on a field trip to Sørfjorden, Hordaland. The debris avalanche have the ID 10 in the attribute table.

FIGURE 10: Picture taken by SVV, the location found on google maps and the point location registered in the NLDB.

- OBSTACLES DURING MAPPING

Several obstacles were experienced during the mapping (figure 11, 12, 13).

FIGURE 11: Shadows on an aerial photo, making it impossible to map the landslide from this source

FIGURE 12: Slide is not visible in aerial photo, and picture available in newspaper does not show extent.

FIGURE 13: All the point data marked in turquois blue do not have a supporting aerial photo to map. A previous photo is used as background.

RESULTS SO FAR

Rainfall events have been analysed in Hordaland county in the period of 2011-2017, and the magnitude of landslides could be mapped for only 79 of them occurring in 6 major rainfall events (figure 14).
A total number of 205 point data were investigated. The number of polygons for each event, possible double registrations, and number of point data not mapped are shown in table 1.

Event	# point reg	# polygons drawn	# possible doubles	# events not mapped
Berit 2011	28	9	2	15
Dagmar 2011	85	54	11	25
Hilde 2013	5	5	0	0
March 2014	35	5	4	26
October 2014	35	2	0	33
Synne 2015	17	4	3	10

Table 1: Number of registered landslides and polygons mapped/not mapped.

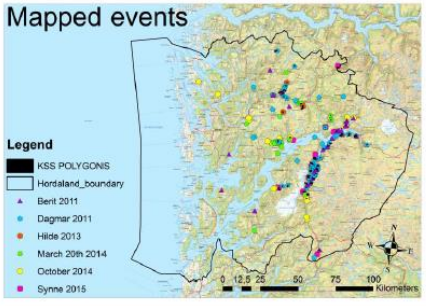

FIGURE 14: Point data from the national landslide database divided into the different weather events and color coded.

Mapped polygons from all the events investigated. The size has been significantly increased to be visible in the county map.

FIGURE 15: An example of FM curve obtained in Sogn og Fjordane by the previous master thesis of Mongstad, 2018. A similar curve will be prepare for Hordaland.

FUTURE WORK

1. Magnitude frequency
A frequency-magnitude curve will be made for the events, showing the relationship between the frequency and magnitude of the slides (figure 15).

2. Evaluation of warning levels
The accuracy of the warnings sent out for each of the weather events will be evaluated.

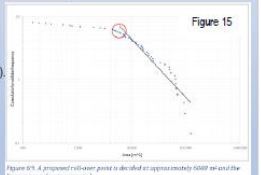

REFERENCES
Krøgli,I.K., Devoli, G., Colleuille, H., Boje,S., Sund,M. and Engen,I.K. (2018): The Norwegian forecasting and warning service for rainfall- and snowmelt-induced landslides, Nat. Hazards Earth Syst. Sci., 19, 1427-1450, https://doi.org/10.5194/nhess-18-1427-2018.

Mongstad H., 2018. Landslide frequency-magnitude analysis to better define warning levels criteria in Sogn og Fjordane (Norway). MS thesis, Department of Geosciences, University of Oslo, Oslo, Norway. June 2018.

Contact information: kamillss@student.geo.uio.no

Appendix 11: Poster for EGU 2019

Poster presented at the European Geoscience Union General Assembly in Vienna 2019.